FHWA-WFL/TD-12-003 MARCH 2012

DEEP PATCH REPAIR

Phase 1: Analysis and Design

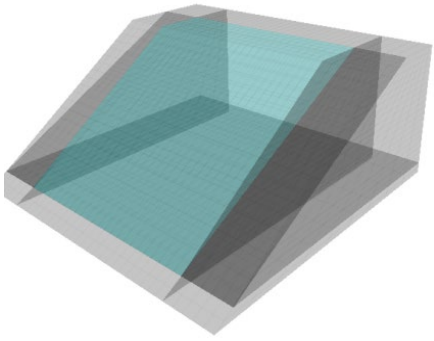

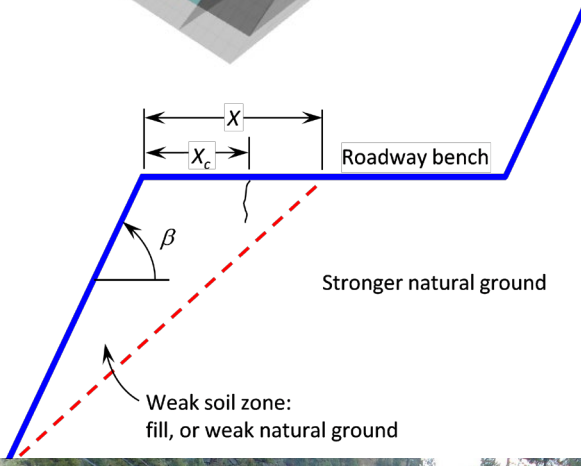

Federal Highway Administration
U.S. Department of Transportation

Technical Report Documentation Page

1. Report No.	2. Government Accession No.	3. Recipient's Catalog No.
FHWA-WFL/TD-12-003		

4. Title and Subtitle	5. Report Date
Deep Patch Repair, Phase I: Analysis and Design	March 2012
	6. Performing Organization Code

7. Author(s)	8. Performing Organization Report No.
Eli Cuelho, Steve Perkins and Michelle Akin	

9. Performing Organization Name and Address	10. Work Unit No. (TRAIS)
Western Transportation Institute PO Box 174250 Montana State University – Bozeman Bozeman, Montana 59717-4250	11. Contract or Grant No.

12. Sponsoring Agency Name and Address	13. Type of Report and Period Covered
Federal Highway Administration Western Federal Lands Highway Division 610 East 5th St. Vancouver, WA 98661-3801	Final Report September 2010- March 2012
	14. Sponsoring Agency Code HFL-17

15. Supplementary Notes

COTR: Brian Collins, FHWA-WFLHD, Advisory Panel Members: Rich Barrows and Malcolm Ulrich, FHWA-WFLHD. This project was funded under the FHWA Federal Lands Highway Coordinated Technology Implementation Program (CTIP).

16. Abstract

A repair technique known as a deep patch has been widely used in the western U.S. to address settlement and shallow failures in both fill and natural slopes. While deep patches have been used for over 20 years, there has been little information documented about their performance, design, and construction. The objective of this research was to evaluate the deep patch slope repair methodology by analytical methods and field observations for the purpose of developing a simple design method suitable for use by Federal Lands Highway and Forest Service personnel. Literature was reviewed, current design methodologies were documented and site visits were conducted to better understand how the deep patch methodology has been used in the past, to evaluate the performance of in-service deep patch sites and to help authenticate the newly proposed design method. An analytical study was conducted to model the effects of various slope configurations, failure mechanisms, deep patch design geometries, and type of geosynthetics using 2D and 3D computer modeling software. The effects of depth and vertical spacing of the reinforcement on the performance of the deep patch was analyzed in addition to the geometry of the reinforcement at the face of the slope. From these efforts, a new design procedure was developed.

17. Key Words	18. Distribution Statement
deep patch, geosynthetics, design, finite element analysis, limit equilibrium, numerical analysis, case studies	No restriction. This document is available to the public from the sponsoring agency at the website http://www.wfl.fhwa.dot.gov/programs/td/publications

19. Security Classif. (of this report)	20. Security Classif. (of this page)	21. No. of Pages	22. Price
Unclassified	Unclassified	254	$0.00

March 2012

Report Number: FHWA-WFL/TD-12-003

DEEP PATCH REPAIR

Phase 1: Analysis and Design

Federal Highway Administration
U.S. Department of Transportation

TABLE OF CONTENTS

FOREWORD

NOTICE

This document is disseminated under the sponsorship of the U.S. Department of Transportation in the interest of information exchange. The U.S. Government assumes no liability for the use of the information contained in this document. This report does not constitute a standard, specification, or regulation.

The U.S. Government does not endorse products or manufacturers. Trademarks or manufacturers' names appear in this report only because they are considered essential to the objective of the document.

QUALITY ASSURANCE STATEMENT

The Federal Highway Administration (FHWA) provides high-quality information to serve Government, industry, and the public in a manner that promotes public understanding. Standards and policies are used to ensure and maximize the quality, objectivity, utility, and integrity of its information. FHWA periodically reviews quality issues and adjusts its programs and processes to ensure continuous quality improvement.

EXECUTIVE SUMMARY

A repair technique known as a deep patch has been widely used in the western U.S. to address settlement and shallow failures in both fill and natural slopes. A deep patch typically involves a 3 to 6-ft deep excavation that is backfilled with well compacted granular material and incorporates one or more layers of geosynthetic reinforcement. Most deep patches have been constructed to address distresses induced by settlement and shallow slumping within poorly performing sidecast embankments and natural slopes consisting of weak soils overlying stronger soils. While deep patches have been used for over 20 years, there has been little information documented about their performance, design, and construction.

The objective of this research was to evaluate the deep patch embankment repair application by analytical methods and field observations for the purpose of developing a simple design method suitable for use by Federal Lands Highway and Forest Service personnel. As a first step, a review of literature was conducted to determine the current state of practice for deep patch design and construction techniques. Interviews of personnel involved in deep patch design and construction were also conducted to obtain current information about design practices. Additional literature pertaining to other geosynthetic-reinforced soil applications also provided insight to the deep patch method.

Several site visits were made to visually inspect the performance of existing deep patch installations, and to document site characteristics of road distresses commonly addressed by the deep patch repair technique. Sites were located in national forests in Washington and Oregon. A total of 48 individual sites on 11 roads within four forests were visited during two separate site visits in fall 2010 and spring 2011. With the exception of a single site in the Siuslaw National Forest the deep patch repairs that were visited were performing well.

A significant portion of this project involved conducting an analytical study to evaluate features believed to be of importance to the performance and design of deep patch slope instability repair, with the ultimate goal of incorporating findings into a design method. These features included:

1. reinforcement vertical spacing,
2. depth of the deep patch reinforced mass,
3. reinforcement strength/stiffness,
4. mode of failure, including rotational and wedge-type failures,
5. anchoring at the lateral ends of the patch,
6. uniaxial versus biaxial reinforcement materials, and
7. geometry of the deep patch section at the slope face.

These features were examined by the use of two analytical methods, namely a limit equilibrium slope stability program for reinforced slopes and a finite difference numerical method for both two-dimensional and three-dimensional slopes. A detailed evaluation of the limit equilibrium method used to analyze slopes repaired by the deep patch method was conducted, and shows the need for advanced analytical methods (i.e., numerical methods) to account for the features presented above. A finite-difference, numerical method was used in this project to examine these features. From this analysis, a design method that incorporates these features was developed.

The geometry of a deep patch repair was modeled by assuming a slope below the road consists of a wedge-shaped zone of weaker soil within which slope failure has occurred. This zone of soil may be fill soil created by a cut and cast operation or a region of native soil that is weaker than the underlying and adjacent native soil. In either case, the wedge was assumed to rest on a steep slope consisting of soils of greater strength than the material within the wedge. Failure by 1) rotational movement within the weak soil wedge, and 2) sliding along the interface between the weak and stronger soils (wedge-type failure), was considered.

To ensure the accuracy and validity of the results, the suitability of two analysis methods (the limit equilibrium method and the numerical finite difference method) was evaluated. The slope stability programs ReSSA and FLAC/Slope, respectively, were used to make these comparisons. For unreinforced slopes on the verge of rotational failure, ReSSA and FLAC/Slope produced identical factors of safety. They differed slightly in their estimates of the location of the failure surface, with FLAC/Slope usually estimating larger values of X_c (the distance from the crest of the slope to the furthest point of surface distress, e.g., a crack) than ReSSA. Further comparisons using a reinforced slope showed significant advantages of using FLAC/Slope for modeling deep patch performance. The limit equilibrium method was unable to differentiate the performance between a deep patch with a single layer of strong reinforcement near the top of the slope and a deep patch with multiple layers of weaker reinforcement within a zone of depth at the top of the slope. The limit equilibrium method provides no information on material movement in the failure state and cannot be used to judge the effectiveness of a given deep patch configuration. In contrast, results generated by FLAC/Slope provide a visual representation of the modes of failure and patterns of material movement at failure (in the form of shear strain rate contour plots and velocity vector plots). Results from various deep patch configurations with different depths and number of layers of reinforcement were compared by examining shear strain rate contour plots and velocity vector plots. Visual comparisons provided a means to qualitatively rank the cases from best to worst. Acceptable deep patch configurations were identified as those associated with 1) improved factors of safety, 2) estimated soil movement at failure limited to the face of the weak soil slope, and 3) a failure surface that did not extend up into the roadway bench.

FLAC/Slope was used to analyze slope configurations, based on two slope angles (β = 34 and 39 degrees), for both rotational and wedge-type failures, to make recommendations for reinforcement configurations and determine required tensile strengths that resulted in acceptable performance. The five main steps in this methodology were to 1) determine the soil strength parameters using ReSSA, 2) determine X_c using FLAC/Slope, 3) analyze several deep patch configurations, 4) examine velocity vector plots and shear strain rate contour plots to determine acceptable performance threshold, and 5) suggest "best" deep patch reinforcement configuration.

Two additional aspects of the deep patch methodology were also examined: 1) the effect of biaxial versus uniaxial geogrids on the behavior of deep patches and the need for anchoring the ends of the reinforcement, and 2) the performance of negative batter deep patches. A three-dimensional analysis program (FLAC3D) was used to evaluate the effect of biaxial versus uniaxial geogrids. For a reinforcement spacing of 1 ft, the biaxial reinforcement resulted in considerable improvement and prevented material movement along and below the roadway bench for all cases examined. The uniaxial reinforcement resulted in improvement but also in unacceptable movement along the roadway bench. The performance of negative batter deep patches was investigated using FLAC/Slope for two slope geometries with various soil types (strengths) and failure mechanisms. The results indicated that negative batter deep patches were sometimes acceptable, and in some cases possibly required a deeper repair.

The deep patch design methodology created as part of this research effort is based on the analytical work using limit equilibrium and numerical methods-based slope stability software. The method is specific to addressing shallow rotational or wedge failures in the fill and/or weak material of road embankments by providing stability through geosynthetic reinforced soil layers in the upper part of the embankment beneath the road surface. Three general steps were outlined as part of the deep patch design process: 1) site selection based on field data, 2) field data collection, and 3) using field data as design inputs to determine the depth, width, number of layers, layer spacing and tensile strength of the reinforcement in the deep patch. Specifically, the design charts rely on field measurements of X_c, X, β and L, where X_c is between 3 and 15 feet, X is between 3 and 30 feet, and β is between 34 and 39 degrees. Selection of the most efficient design is based on a synthesis of the information collected from these steps; however, the most economical approach will also depend on several external factors such as cost and availability of construction materials, topography, site layout, anticipated traffic levels, etc.

1 INTRODUCTION

A repair technique known as a deep patch has been widely used in the western U.S. to address settlement and shallow failures in both fill and natural slopes. A deep patch typically involves a 3 to 6-ft deep excavation that is backfilled with well compacted granular material and incorporates one or more layers of geosynthetic reinforcement (Figure 1). Most deep patches have been constructed to address distresses induced by settlement and shallow slumping within poorly performing sidecast embankments and natural slopes consisting of weak soils overlying stronger soils. While deep patches have been used for over 20 years, there has been little information documented about their performance, design, and construction.

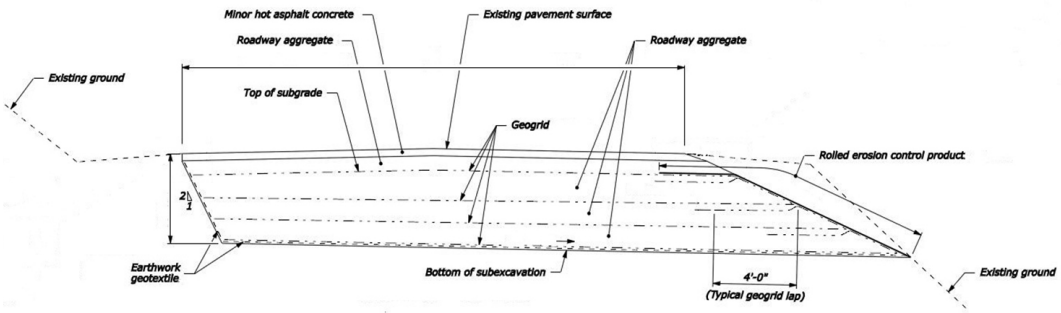

Figure 1: Schematic of a typical deep patch repair.

A common method that was historically used to construct low-volume roads in mountainous regions was to cut into the uphill side of the road and cast the material onto the downhill side (known as cut and cast, cut and fill, partial bench, or sidecast construction technique). This technique typically utilizes balanced cut and fill quantities. These sidecast fills were frequently constructed with minimal or no compaction effort. This commonly leads to settlement and creep of the fill soil, which in turn leads to roadway surface distresses such as cracks and subsidence (Figure 2 and Figure 3). Inadequate drainage, consolidation of the soil, and decomposition of vegetation within the fill also contribute to settlement. Furthermore, sidecast embankment materials are typically placed on natural slopes that have not been cleared of vegetation. The decay of vegetation within the interface between the fill and natural slope may lead to a weak plane upon which slip and failure occurs.

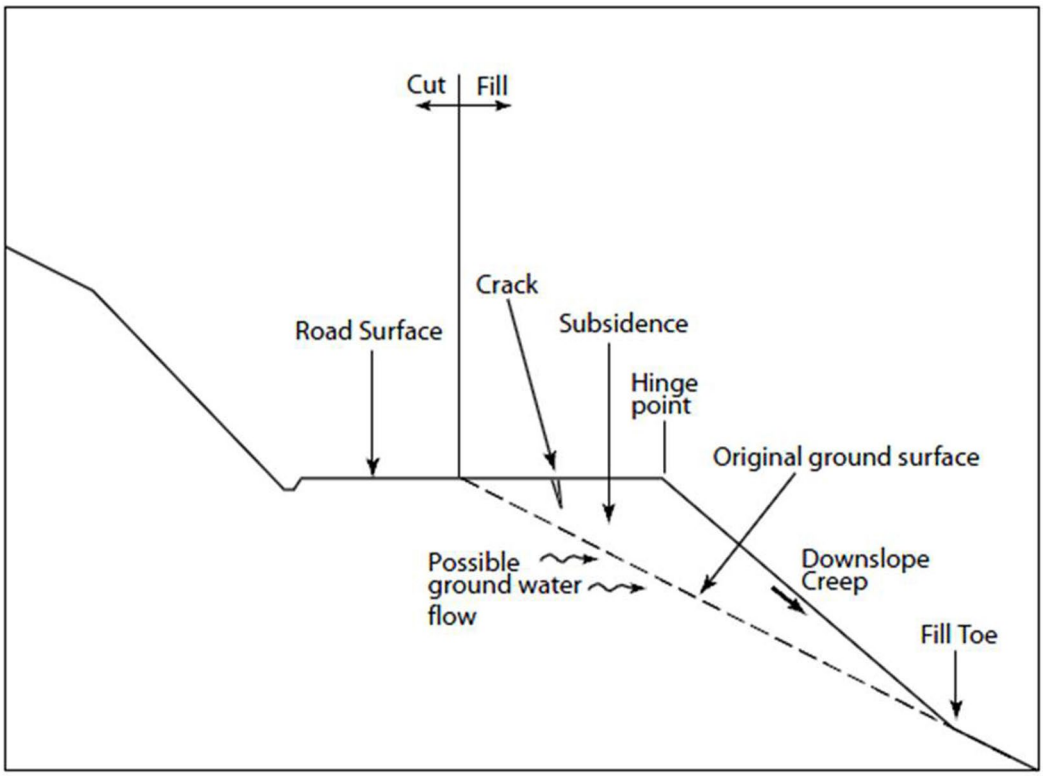

Figure 2: Cross section of typical sidecast road embankment fill (Musser and Denning, 2005).

Figure 3: Common fill slope distress on sidecast constructed road.

The deep patch repair method was developed in the 1980s, but did not appear in literature for several years. This method is intended for use on failed slopes consisting primarily of non-cohesive soils. The first documented deep patch in the Mount Hood National Forest was constructed around 1988, although there were several earlier projects that utilized chain link fencing for reinforcing layers (personal communication with Cliff Denning on January 6, 2011). Deep patches were also constructed in the mid to late 1980s in the Willamette National Forest. In 1999 Powell et al., reported no subsidence of any of about 50 deep patches constructed over the previous eight years in the Mount Hood National Forest in Oregon.

The majority of deep patches have been constructed to fix problems associated with settlement within sidecast embankments. However, there are several cases of deep patches used in areas with larger-scale movements and more severe distresses. In these instances, the deep patch was often selected as an affordable treatment to slow down movement and reduce distresses, not with the expectation that the rehabilitation will fix the problem (Musser and Denning, 2005; personal communication with Cliff Denning on January 6, 2011). In general, the design philosophy for a deep patch repair is that the role of the deep patch is to confine the likelihood of failure to the face of the weak soil slope and to prevent failure from extending up into the roadway bench. This implies that a satisfactory factor of safety exists for potential failure surfaces extending up into the roadway bench while a substandard factor of safety may exist for regions of the slope well below the bench and extending to the slope face.

1.1 OBJECTIVE

The objective of this research was to evaluate the deep patch slope repair application by analytical methods and field observations for the purpose of developing a simple design method suitable for use by Federal Lands Highway and Forest Service personnel. Literature was reviewed, current design methodologies were documented and site visits were conducted to better understand how the deep patch methodology has been used in the past, to evaluate the performance of in-service deep patch sites and to help validate the newly proposed design method. An analytical study was conducted to model the effects of various slope configurations, deep patch design geometries, and type of geosynthetics using 2-D and 3-D computer modeling software. The effects of depth and vertical spacing of the reinforcement on the performance of the deep patch was analyzed in addition to the geometry of the reinforcement at the face of the slope. From these efforts, a design procedure was developed.

1.2 BACKGROUND AND LITERATURE REVIEW

A review of literature was conducted to determine the current state of practice for deep patch design and construction techniques. Interviews of personnel involved in deep patch design and construction were also conducted to obtain current information about design practices. Additional literature pertaining to other geosynthetic-reinforced soil applications also provided insight to the deep patch method.

1.2.1 Design and Construction

In 1994, Mohney et al. presented the deep patch repair technique as a simple, cost-effective alternative for repair of sidecast fill settlement. This is the oldest document found about the deep patch method and is limited to a single layer of geosynthetic. A simple design procedure is presented for two cases. For cases of settlement without impending sliding of the sidecast embankment, a simple analysis indicates the width of the geosynthetic inside the "failure" surface (towards the cut side of the slope—the portion of the geosynthetic anchored by the stable part of the slope) should be at least as wide as the portion of the geosynthetic outside the "failure" surface (towards the cast side of the slope). For cases where the sidecast embankment is susceptible to sliding downslope, a limit equilibrium slope stability analysis with an assumed circular failure surface (e.g., modified Bishop method) is also recommended. The analysis begins with the assumption that the factor of safety equals one and back-calculating the soil parameters (friction angle and cohesion, ϕ and c) for the unreinforced case. Continuing the analysis with a layer of geosynthetic provides a resisting moment and increased factor of safety. In this study, it is shown that use of a single layer of sufficiently strong reinforcement may provide a satisfactory factor of safety when evaluated using limit equilibrium methods, but may result in unsatisfactory performance when viewed by more sophisticated numerical methods that model deformations within the slope.

Interviews conducted in 2000 and reported by Musser and Denning (2005) indicated professional judgment and computer models (e.g., XSTABL) are common methods for designing deep patches. Musser and Denning developed design charts based on a simplified wedge analysis that can be used for typical Forest Service roads, but the methodology used to develop the graphs is not well-documented. The design charts incorporate a factor of safety of 1.2 and provide the depth and required reinforcement for deep patches for the following site conditions:

- fill slope angles of 1.5H:1V and 1.25H:1V
- cohesionless soil
- soil strength friction angles of 25, 30, and 35 degrees

However, according to Cliff Denning and several individuals currently involved in deep patch design, the design charts are probably not widely used. Interviews were

conducted to determine the current state of the practice regarding deep patch design and were consistent with the findings of Musser and Denning (2005). In general, deep patch design is often based on familiarity and previous experience within an agency, and is sometimes carried out with the use of limit equilibrium slope stability computer programs (personal communication with individuals from Western Federal Lands Highway Division, Gifford Pinchot National Forest, Mount Hood National Forest, Siuslaw National Forest, Willamette National Forest, and Klamath National Forest). In this report, it is demonstrated that limit equilibrium slope stability programs may be used to analyze a reasonable deep patch repair configuration. To establish a reasonable repair configuration, however, requires additional guidelines. These guidelines have been historically based on previous experience within an agency. In this report, advanced computer modeling is used to establish easy to follow guidelines that are intended to supplement existing experience.

Deep patches constructed on Forest Service roads are usually constructed with moderate sized equipment. According to various individuals familiar with deep patches (primarily Western Federal Lands Highway Division and the Forest Service, although employees of other agencies as well) the following construction aspects should be adhered to, which are consistent with good geotechnical practices:

- Granular soil is recommended for backfill within the deep patch reinforced zone. If the existing material is suitable it is the most cost-effective. Some national forests routinely use pit run or crushed rock because it is widely available (e.g., Mount Hood National Forest).
- Good compaction is important. Inadequate compaction may have been a contributing factor to the original failure.
- Good drainage is needed. Again, most failures of sidecast embankments occurred during periods of heavy precipitation or high groundwater. Therefore, inclusion of drainage elements can greatly improve the performance of the deep patch and reduce the chance of subsequent failure. Good drainage in the ditch line of the cut slope is especially needed and can be accomplished with a culvert installed during construction of the deep patch.
- Finally, geosynthetics should be pulled taut in the direction of greater strength oriented perpendicular to the direction of traffic. The geosynthetics should also be sufficiently embedded beyond the failure surface to prevent pullout failure.
- It is suggested that deep patches are constructed as either half-width or full-width because deep patches at in-between sizes are more difficult to build due to the lack of available space for equipment and traffic during construction.

Two specific issues concerning construction of deep patches that are not adequately addressed in the current literature include: 1) keeping the road open to traffic during construction, and 2) facing design and details. Deep patches have primarily been used on remote, low-volume roads where alternate routes are not readily accessible for vehicles during construction. Thus, keeping a lane open for traffic is often necessary. This is more easily accomplished when the width of the deep patch does not extend all the way

to the cut slope side of the road. For full-width repairs, traffic can be accommodated by staging construction in half-width phases and moving one-way traffic alternately across the side that has compacted fill over the geosynthetic (personal communication with Brian Collins, 2011).

Construction of deep patches on very steep slopes without a shoulder can be difficult. One technique that may be utilized involves constructing the face of the geosynthetic at a negative batter—this reduces the width of excavation at the deepest portion (Figure 4). There are several case histories of walls with negative batter (Barrett and Ruckman, 2007) and it is expected that negative batter will be compatible with deep patches utilizing closely-spaced geosynthetics. Several different deep patches with negative batter geometries were modeled in this study (Chapter 8).

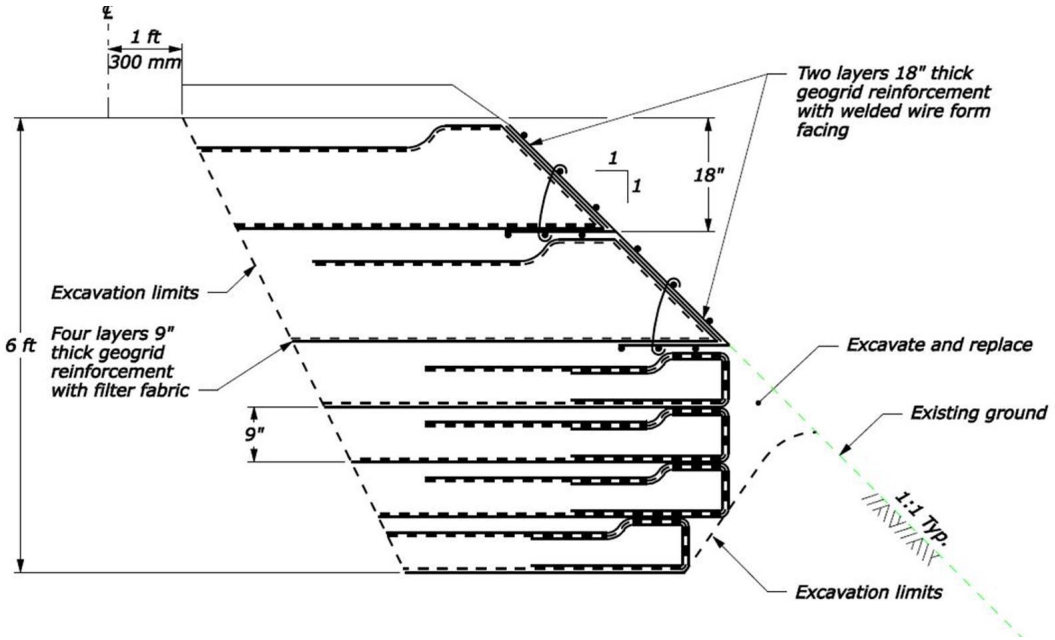

Figure 4: Example of a deep patch with negative batter.

1.2.2 Experimental Studies

Laboratory tests were performed by Wu and Helwany (2001) to compare the performance of the US Forest Service deep patch method to a similarly constructed unreinforced alternative. The objective was to learn whether the reinforcement played a significant role or if adequate performance could be achieved with compaction alone. The laboratory tests utilized a 6-ft deep cohesionless gravelly sand road base material (ϕ=40°) compacted in 12 6-in lifts to approximately 95 percent of standard Proctor. Three additional lifts were placed as surcharge. The constructed slope was about 2H:1V.

Settlement was simulated by lowering a section of the base of the testing apparatus incrementally (but not uniformly) until a total displacement of 11 in. was achieved over 160 minutes. The apparatus was 3 ft wide and modeled plane strain conditions. The unreinforced version was tested in addition to a reinforced alternative with five layers of geotextile installed at 1-ft spacing. Instrumentation recorded the normal and shear stresses along the base and strain within three of the layers of geotextile. The location and depth of cracks were measured with a grid mounted on the side of the apparatus.

There was a significant difference between the unreinforced and reinforced experiments. In the unreinforced test, a crack that initiated at the first displacement increment essentially split the soil in half by the end. The crack was 6 ft deep and 1 ft wide at the surface. Smaller cracks formed in the reinforced section—all above the movable section of the base; the worst one was 10 in deep at the end of the test. The load cells also showed a significant difference in the stress distribution at the base of the soil among the two experiments (Figure 5). In the unreinforced experiment the area near the boundary between the stationary and movable sections of the base experienced a significant increase in stress towards the end of the test. This was not seen in the reinforced test. Strain gages bonded to the geotextile showed strains were largest in the upper layer of reinforcement, especially near the stationary/movable sections boundary, and smaller at lower levels, where the maximum strain was closer to the face of the slope. Based on data from the strain gages and load cells, Wu and Helwany (2001) suggested the geosynthetic contributed to a cantilever effect of the fill and would reduce the potential for subsequent failure after construction of a deep patch. The experiments also demonstrated the effectiveness of deep patches is primarily due to the presence of the reinforcement, and that fill replacement and compaction alone will not stabilize the road surface if additional movement is expected.

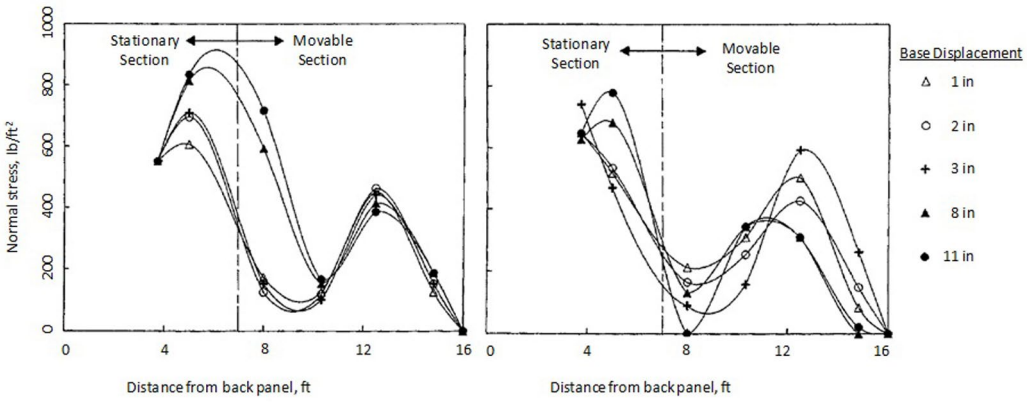

Figure 5: Distribution of normal stress along base panel in unreinforced (left) and reinforced (right) tests (modified from Wu and Helwany, 2001 to show English units).

Helwany (1994) describes results from similar laboratory tests as reported in Wu and Helwany (2001) with a modified design called the CTI (Colorado Transportation Institute) deep patch technique. The geometry has a vertical reinforced wrapped face in the upper portion (directly below the theoretical road surface) and the lower portion has wrapped reinforcement layers constructed at a negative batter behind fill soil. The slope of the negative batter was 1H:2.25V and the slope of the fill was 1.25H:1V. A diagram of the CTI deep patch geometry in the testing apparatus is shown in Figure 6. One advantage of the CTI deep patch geometry is the roadway can be widened by about 4 ft. The only crack that formed was behind the reinforced section along the back wall of the apparatus. By the end of the test the crack was 1 in wide and 7 ft deep. In this experiment the load cells were placed at different locations. They were nearly all within the stationary section; only one load cell located 8 ft from the back panel was within the movable section. The magnitude of the normal stress at the base was almost twice as large as that from tests with the traditional geometry (Figure 7—note the change in scale of the vertical axis). The strain gages showed about half as much strain on the upper layer of reinforcement and twice as much in the lower region, although the gage layout was not consistent between the two geometries.

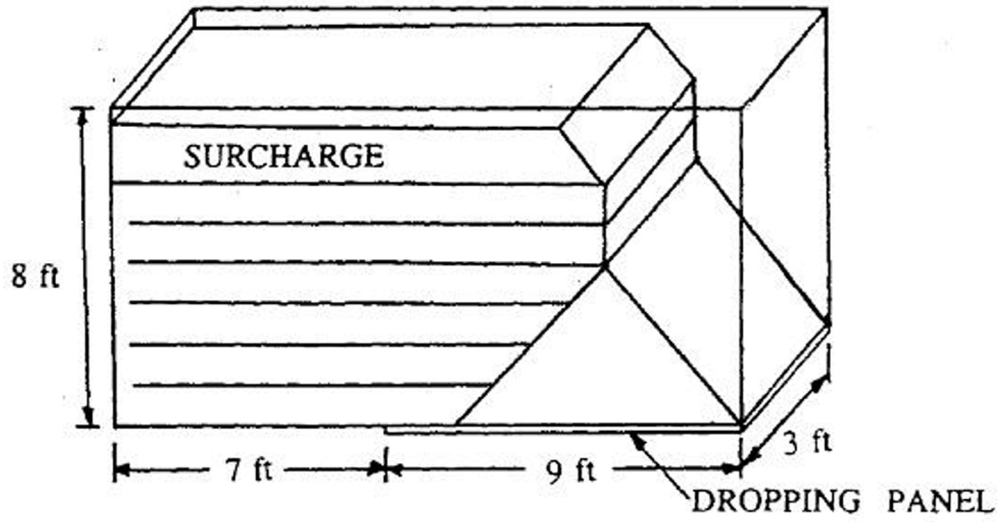

Figure 6: Schematic diagram of CTI deep patch technique in full-scale model testing apparatus (from Helwany, 1994).

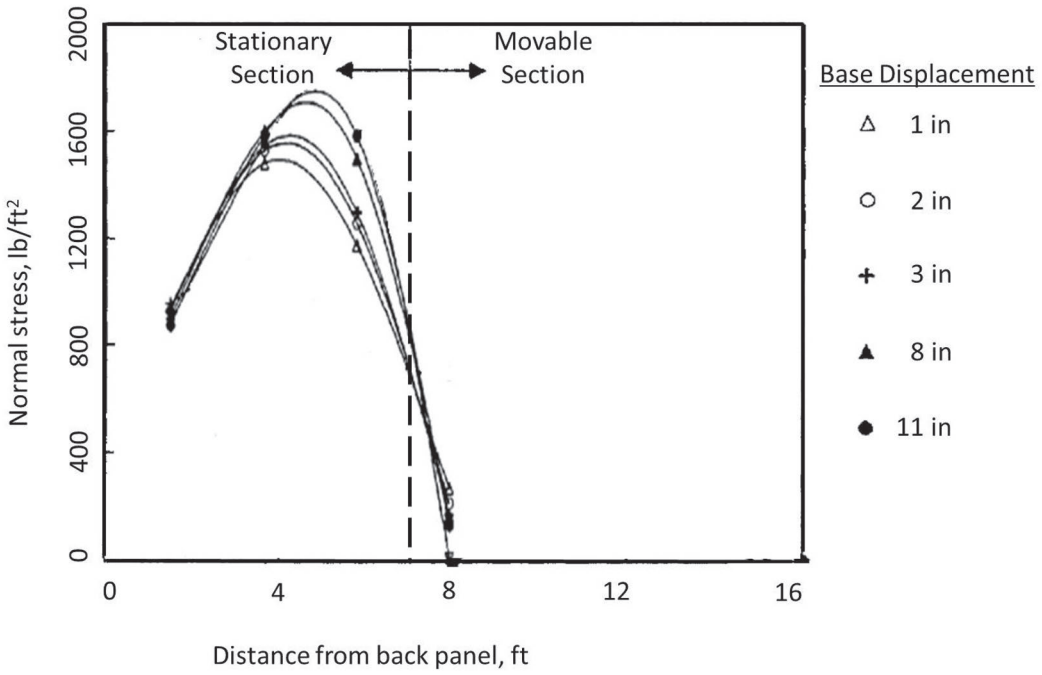

Figure 7: Distribution of normal stress along base panel in CTI deep patch test (modified from Helwany, 1994 to more closely match Figure 5).

The CTI deep patch technique was constructed in Silverthorne, CO in October 1993 (Helwany, 1994). The location was not reported, but personal correspondence with the principal investigator (Dr. Jonathan Wu of the University of Colorado—Denver) reported that a few years after construction "the repaired slope had 'merged' well into the environment" and the widened road bench was the only feature that allowed him to identify the site.

1.2.3 Role of Reinforcement

While there is little information specifically referring to deep patches in the literature, the use of geosynthetics for reinforcement of soil slopes is common (Holtz and Schuster, 1996). A comprehensive report on reinforced soil slopes and embankments for highway applications has design charts and other information about geogrid reinforcement (Mitchell and Villet, 1987). However, the design charts are for cases in which the entire depth of soil within the embankment is reinforced with geogrids, instead of just the upper portion as with deep patches. Regardless, several studies have investigated the importance of various properties relevant to deep patches, such as reinforcement spacing and stiffness. A discussion of the relative importance of these properties for geosynthetic reinforced soil structures follows.

Numerical models with consecutive runs of increased height of MSE walls by Vulova and Leshchinsky (2003) conclusively showed reinforcement spacing was a primary factor in wall behavior. The numerical investigation determined the critical wall height for various combinations of different soil types, reinforcement spacing geometries, and reinforcement stiffnesses. The critical wall height was the maximum wall height associated with a stable configuration (e.g., no defined failure surface or nonlinear cumulative displacement). Failure was categorized as "external" when a sliding wedge developed behind the reinforced mass (within the backfill soil) and "deep seated" when the failure surface proceeded through the foundation soil. Smaller reinforcement spacing (8 to 16 in compared to 2 to 3.3 ft) generated greater internal stability causing the reinforced soil to move as a coherent mass (similar to a conventional gravity retaining wall) and was associated with external failure modes. All other parameters being equal —including identical reinforcement strength and stiffness— smaller spacing was also associated with greater critical wall heights. Smaller spacing could also make up for lower strength soil (ϕ of 35° instead of 45°) by allowing a similar critical wall height. Thus, "reinforcement spacing was identified as a major factor controlling all aspects of wall behavior" (Vulova and Leshchinksy, 2003).

Design inputs for the MSE Walls modeled by Vulova and Leschinksy (2003) simulated a relatively stiff reinforcement (elastic modulus of 68,500 lb/ft), strong soil–reinforcement interaction, and reinforcement tensile yield strength of 13,700 lb/ft. A few cases were modified by reducing the stiffness by a factor of ten to investigate the effect of reinforcement stiffness. The decreased stiffness resulted in lower critical wall heights and more internal instability (failure developed within the structure instead of external or deep seated)—similar to the results from increased spacing of stiffer reinforcement (Vulova and Leschinsky, 2003).

Actual reinforcement loads in geosynthetic reinforced soil structures tend to be significantly less than loads predicted by design methods (Yang et al., 2010; Bussert and Cavanaugh, 2010; VanBuskirk, 2010). Numerical simulations by Yang et al. (2010) showed mobilization of reinforcement tensile capacity was low until the average soil shear stress approached peak strength. Results from computational modeling showed reinforcement tensile strength mobilization is nonlinearly related to the mobilization of soil shear strength. Bussert and Cavanaugh (2010) show that superposition of the resistance provided individually by the soil and geogrid does not adequately capture the composite behavior that develops when geosynthetics are used in soil structures.

The current design method for MSE walls does not reflect the composite behavior of soil with closely-spaced reinforcement and thus underestimates the importance of reinforcement spacing (VanBuskirk, 2010). However, the recent deployment of the FHWA Geosynthetic Reinforced Soil Integrated Bridge System (GRS–IBS) highlights the current state-of-knowledge of this composite behavior by promoting soil structures

with closely-spaced reinforcement (Wu et al., 2006; Adams et al., 2011a). The relationship between reinforcement spacing and reinforcement strength is also not proportional. Reduced reinforcement spacing has a greater effect on the strength of the composite soil-geosynthetic structure than increased reinforcement strength. All GRS–IBS constructed to date have used a woven polypropylene geotextile. If a geogrid is desired for future projects Adams et al. (2011b) recommend a biaxial geogrid be used to eliminate construction placement errors.

2 CASE STUDIES

Several site visits were made to visually inspect the performance of existing deep patch installations, and to document site characteristics of road distresses commonly addressed by the deep patch repair technique. Sites were located in national forests in Washington and Oregon.

Assessments generally included a visual survey of the road surface and adjacent cut and fill slopes to determine the stability of the area repaired using the deep patch method. In most cases, photographs were taken to document the general site topography, specific features, and any distresses. When possible, the review also attempted to determine slope angles, soil type, road width, geosynthetic type, drainage features, vegetation, and presence of water. Measurements of the distance from the slope hinge point to the furthest point of cracking distress (X_c) were taken, knowing that this parameter was of particular interest in designing deep patches. However, measurements of X, the distance from the slope hinge point to the weak/strong interface, were not taken in the field because it is difficult to estimate this parameter without extensive topographic and/or geologic information. Methods of estimating this parameter are provided in Chapter 9.

A total of 48 individual sites on 11 roads within four forests were visited during two separate site visits during November 2010 and May 2011, as shown in Figure 8. Information gathered during these visits is summarized in each of the sections that follow.

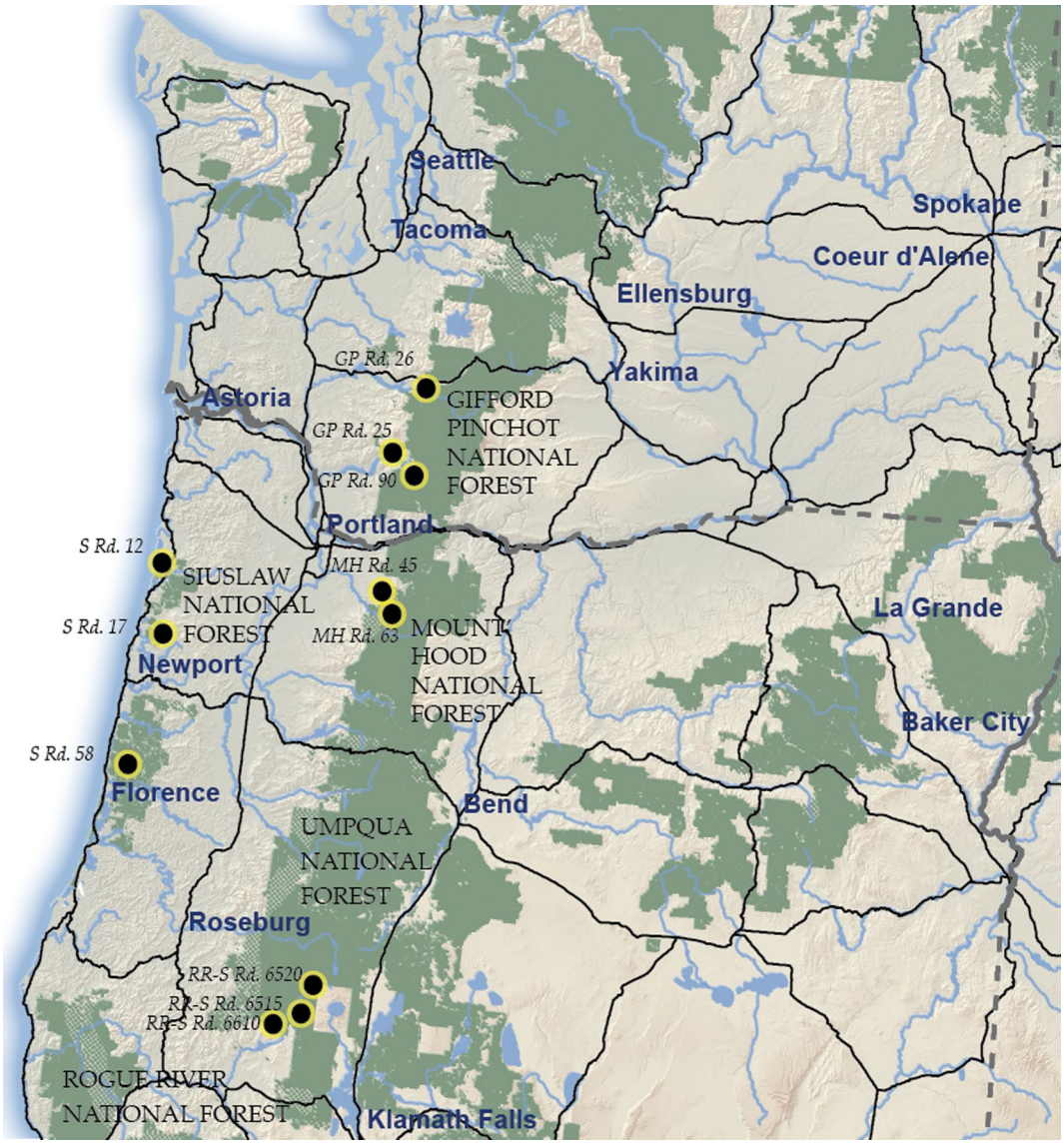

Figure 8: Map of site visits.

2.1 GIFFORD PINCHOT NATIONAL FOREST

2.1.1 Road 26, MP 1.1

Slope instability in the area was generally associated with heavy precipitation that occurred in 1996. According to a Western Federal Lands Highway Division (WFLHD) memo[1], slopes in this area, near Mount Saint Helens, are composed predominantly of pumice, ash and tuffaceous units decomposed to silts and clays. Distresses were evident

[1] Geotechnical memorandum (GM9-99), Project: WA FS ERFO 96-22(13), September 1999

as a vertical drop of the roadway surface of about 18 inches (Figure 9a) over about 66 feet of roadway. In 2000, the USFS repaired and graded over the failed section, until a more substantial repair could be made. A deep patch repair strategy was selected because other alternatives (road realignment or full slide correction) were too costly. Based on an analysis using XSTABL (Ver. 5) and following the USFS Reinforced Deep Patch guidelines, a deep patch design that varied from 4 feet deep near the ends to 8 feet deep near the center of the deep patch was constructed in summer 2001 (Figure 9b). The number of layers of geosynthetic reinforcement varied between 4 and 8 layers depending on the depth. Layers were 1 foot thick. A schematic of the geogrid reinforced section is shown in Figure 10.

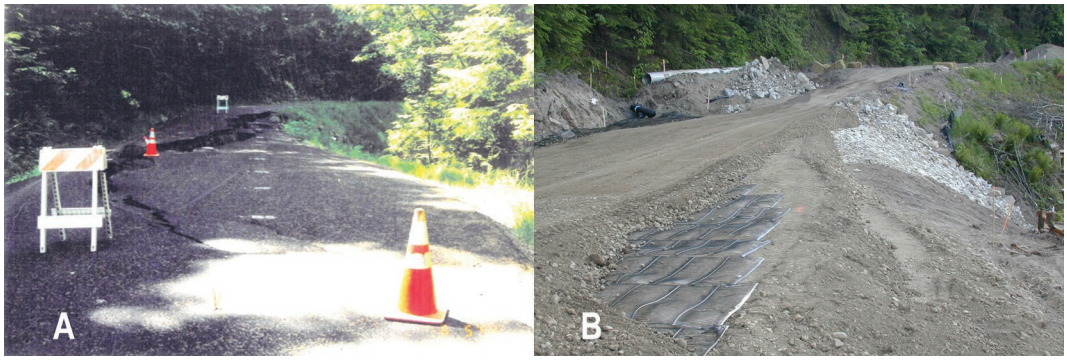

Figure 9: Gifford Pinchot, Road 26, MP 1.1: a) preconstruction photo, b) construction photo.

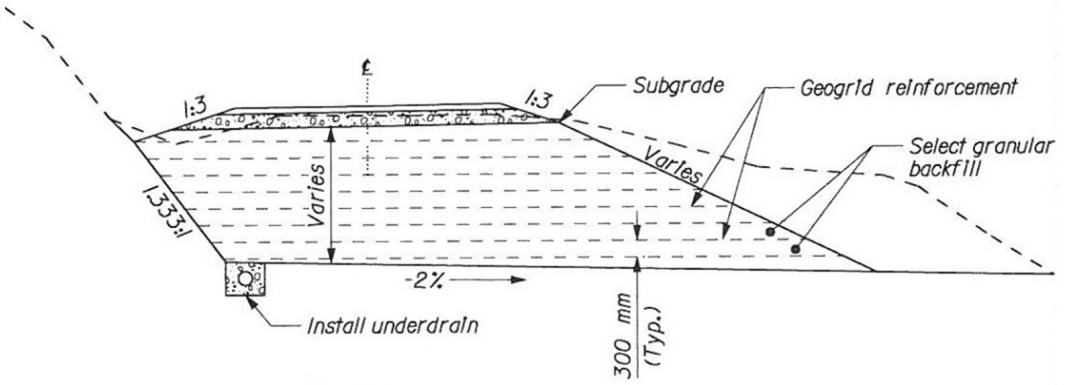

Figure 10: Typical geogrid reinforced section at Gifford Pinchot, Road 26.

Site visits in November 2010 generally revealed that the deep patch was performing well with no noticeable distresses in the paved surface or surrounding embankments. Drainage culverts were open and no standing water was present on the cut side of the slope. Geosynthetics extracted from the site were uniaxial (possibly Tensar UXMESA3, but equivalent to Tensar UX1400HS) having an ultimate tensile strength of about 4800 lbs/ft. The reinforced fill consisted of 4-in minus pit run material. A soil sample

from the cut slope indicated that the soils consisted of about 20 percent fines, and classified as a clayey sand with gravel. Figure 11 shows several photos of the site when visited in November 2010.

Figure 11: Photos of Road 26, Gifford Pinchot National Forest, MP 1.1 a) distant view of site from lower road, b) layout of site from end of repair, c) road surface, d) road surfacewith fill slope, e) fill slope showing drainage features and protective stone facing, and f) road surface with cut slope.

2.1.2 Road 25

Deep patch repairs were constructed on Road 25 in the Gifford Pinchot forest in 2007. These repairs mainly consisted of a relatively shallow excavation in the affected area where a single layer of uniaxial woven geogrid (Figure 12) was used as reinforcement at the bottom of the subbase (schematic shown in Figure 13). Crushed aggregates were used in the subbase and base course layers and the surface was paved with hot mix asphalt. The geosynthetic extended from the termination of the excavation to the slope face. Side slopes were reconstructed at 1.5H:1V. Excavation widths (orthogonal to the direction of traffic) varied from site to site (between 23.5 and 31.5 feet at the bottom of the excavation) as tabulated in Table 1. For the most part, the widths of the asphalt patches extended past the centerline by 2 to 3 feet. One exception was the full width deep patch located at MP 10.032. The topography at that location was such that the geometry of the road resembled an embankment (all fill) rather than the traditional sidecast construction. Site visits in December 2010 by WFLHD staff showed that the sites were performing well after 3 years in service. Photos in Figure 14 provide a representative view of each of the sites.

Figure 12: Photo of uniaxial geogrid used on Road 25 repairs in the Gifford Pinchot forest.

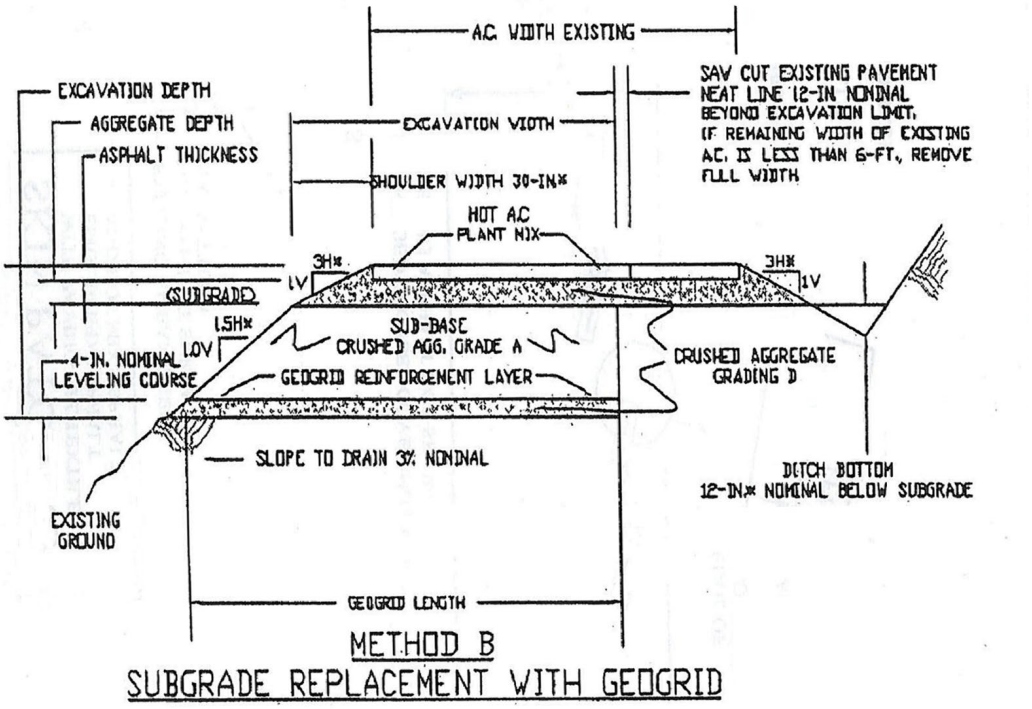

Figure 13: Generic schematic of deep patch repair and site-specific dimension information for sites on Road 25, Gifford Pinchot National Forest.

Table 1: Deep Patch Dimensions on Road 25, Gifford Pinchot National Forest

MP	Length (ft)	Width* (ft)	Depth (ft)
9.150	250	27	5
8.228	65	25.5	4
9.252	200	25	3
10.032	70	31.5	6
10.898	125	27	5
11.509	250	23	3

*width of the bottom of the excavation

Figure 14: Photos of Road 25, Gifford Pinchot National Forest deep patch repairs at a) MP 9.158, b) MP 9.228, c) MP 9.252, d) MP 10.032, e) MP 10.898, and f) MP 11.509.

2.1.3 Road 90

A thorough review of multiple sites on Road 90 (also known as Lewis River Road) was conducted by Golder & Associates in late 2009 for WFLHD[2]. Their investigations consisted of geotechnical borings, inclinometer readings, geologic mapping, soil testing, visual distress surveys, soil tests and more. Brief site visits were also made by WTI in May 2011

[2] Geotechnical Investigation Report, Task Order T-09-002, WFLHD Project No. WA PFH 16(1), WFLHD Geotechnical Report No. GR15-10, September 2010.

to seven locations along this road where deep patch repair was recommended as a possible treatment to the distresses found as part of Golder & Associates' investigations (mileposts 0.1, 5.5, 6.3, 10.1, 11.9, 14.1, and 17.8). These distresses have not yet been repaired and the project is still under development by WFLHD. General information about these sites is summarized in Table 2. Length of the distresses and maximum X_c was determined from site visits by WTI, while the proposed length, width, depth and number of layers for the deep patch repairs was obtained from the Golder & Associates report. A couple of notable differences between WTI's and Golder and Associates' site investigations are listed below. Photos of the distresses and general site layout at each of these seven sites are shown in Figure 15 through Figure 21.

- The cracking at milepost 5.5 was most severe at one end where the deep patch was recommended, but distresses did extend significantly beyond that point as evident from the difference in distress length and proposed repair length.
- Many of the distresses originally recorded by Golder & Associates at milepost 17.8 were obscured by a recent pavement overlay, which explains the difference between the distress length and proposed repair length.

Table 2: Details for Potential Deep Patch Sites on Road 90 in Gifford Pinchot National Forest

MP	Distress Length (ft)	Maximum X_c (ft)	Proposed Length (ft)	Proposed Width (ft)	Proposed Depth (ft)	Proposed Layers
0.1	30	6	40	15	6	3
5.5	120	16	50	25	6	3
6.3	60	19	80	25	6	3
10.1	100	6	200	15	6	3
11.9	80	21	110	15	6	3
14.1	60	18.5	60	25	6	3
17.8	75	11	300	20	6	3

Figure 15: Photos of distresses at milepost 0.1, Road 90, Gifford Pinchot National Forest.

Figure 16: Photos of distresses at milepost 5.5, Road 90, Gifford Pinchot National Forest.

Figure 17: Photos of distresses at milepost 6.3, Road 90, Gifford Pinchot National Forest.

Figure 18: Photos of distresses at milepost 10.1, Road 90, Gifford Pinchot National Forest.

Figure 19: Photos of distresses at milepost 11.9, Road 90, Gifford Pinchot National Forest.

Figure 20: Photos of distresses at milepost 14.1, Road 90, Gifford Pinchot National Forest.

Figure 21: Photos of distresses at milepost 17.8, Road 90, Gifford Pinchot National Forest.

2.2 MOUNT HOOD NATIONAL FOREST

2.2.1 Road 45

Road 45 in the Mount Hood National Forest contained five deep patch repairs that were constructed in 2004 at milepost 5.25, 5.45, 5.85 and 6.76 (two sites at 6.76), and a 815-foot long area at milepost 28.2 scheduled for future repair. The repaired sites were generally constructed as shown in Figure 22, built at a 1:1 slope using pit run and a woven geogrid (Type 2000) at 2-foot spacing. Depths and widths of the deep patches varied between the five sites as tabulated in Table 3. The geogrids were wrapped at the face. The surface of the roadway was left unpaved, and was topped with 9 inches of gravel surfacing. Site visits in May 2011 by WTI staff showed that the sites were performing well after about 7 years in service. More extensive investigations were made at mileposts 5.85 and 6.76 since they were shallower deep patches; however, all installations on Road 45 were performing well. Photos in Figure 23 provide a representative view of these sites.

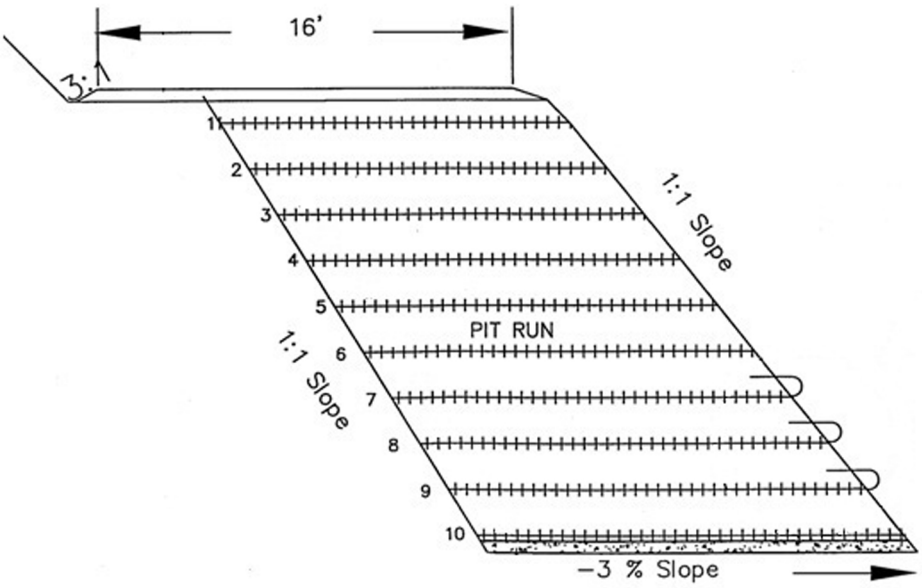

Figure 22: General layout of deep patches on Road 45 in Mount Hood National Forest.

Table 3: Dimensions and Details for Deep Patches on Road 45 in Mount Hood National Forest

MP	Length (ft)	Width (ft)	Depth (ft)	No. of Layers
5.25a	140	10	20	10
5.25b*	50	8	6	3
5.45	155	12	18	9
5.85	130	12	8	4
6.76a	20	10	8	4
6.76b	140	10	8	4

*immediately adjacent to the deep patch at 5.25a

Figure 23: Photos of Road 45, Mount Hood National Forest, deep patch repairs at MP 5.85 (a, b, c) and MP 6.76 (d, e, f).

Multiple distresses at milepost 28.2 on Road 45 had not yet been repaired. An area 815 feet long was to receive one of five treatments: Method BF, C1, BV, C2 or A, as illustrated in Figure 24. A plan view of the site is shown in Figure 25. Photos of the site are shown in Figure 26. Surface distresses were generally arc shaped, some having vertical displacements of 2 to 3 inches. Some cracks extended all the way across the road to the inside edge of the pavement. A summary of the scheduled repairs at this site is provided in Table 4.

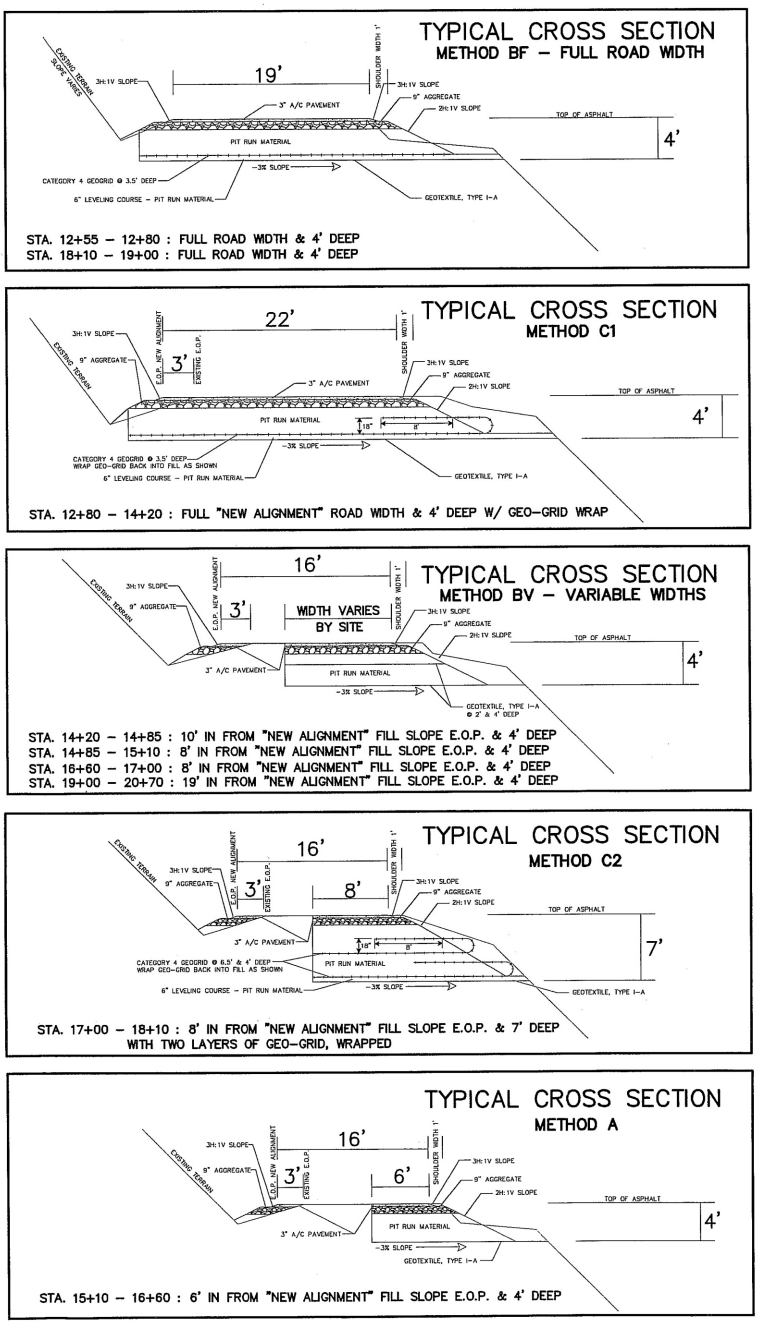

Figure 24: Cross sections of five scheduled repair methods on Road 45, Mount Hood National Forest, MP 28.2.

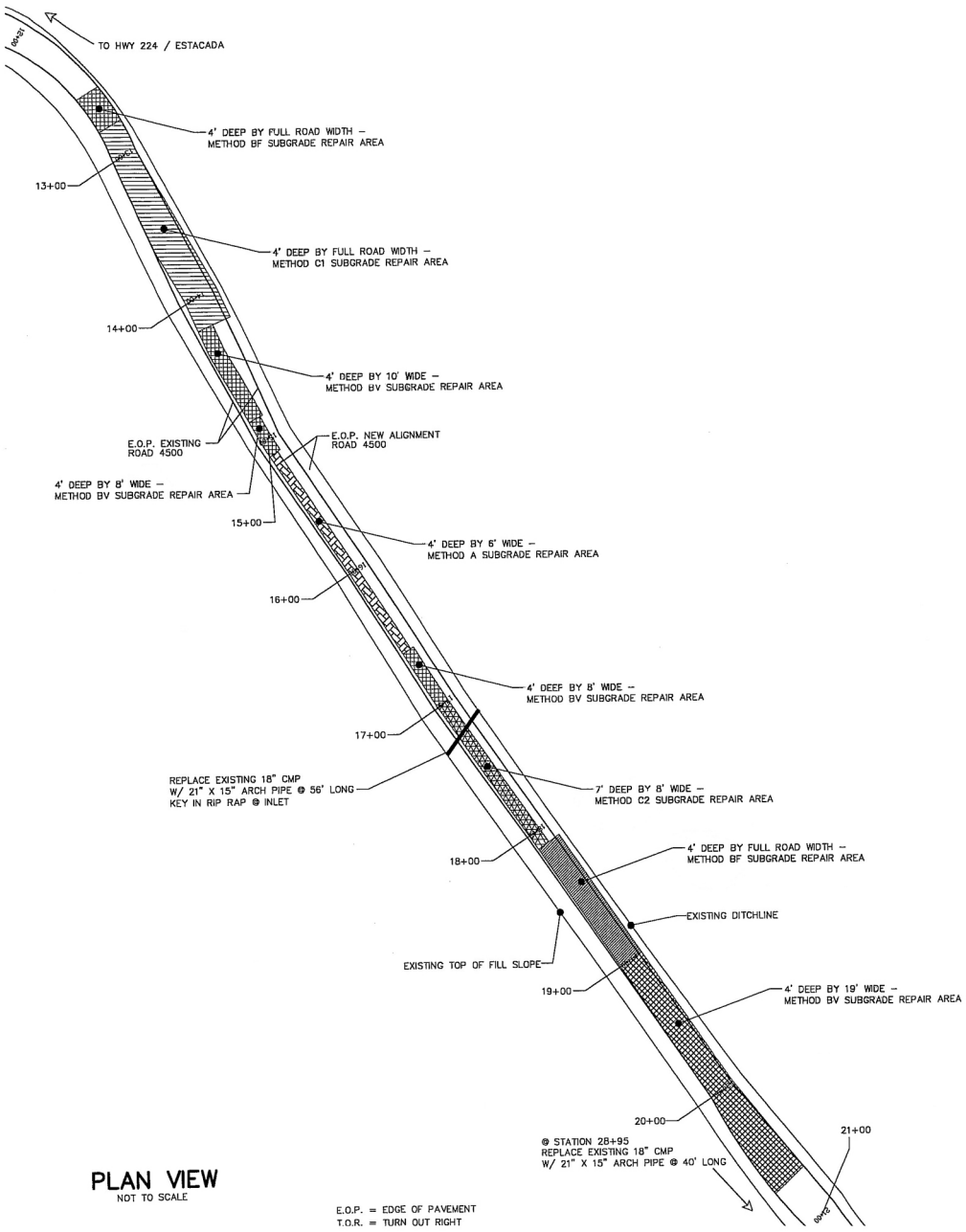

Figure 25: Plan view of scheduled repairs on Road 45, Mount Hood National Forest, MP 28.2.

Figure 26: Photos of distresses on Road 45, Mount Hood National Forest, MP 28.2 a) close-up of differential settlement at crack interface, b) crack extending to inside shoulder, c) close-up of crack at inside shoulder, d) general view of road surface distresses, e) surface cracking and f) general view of surface distresses.

Table 4: Details for Potential Deep Patch Sites on Road 45 in Mount Hood National Forest

Beg. Station	Repair Method	Proposed Length (ft)	Proposed Width (ft)	Proposed Depth (ft)	Proposed Layers
12+55	BF	25	full	4	1
12+80	C1	140	full	4	1
14+20	BV	65	10	4	2
14+85	BV	25	8	4	2
15+10	A	150	6	4	1
16+60	BV	40	8	4	2
17+00	C2	110	8	7	2
18+10	BF	90	full	4	1
19+00	BV	170	19	4	2

2.2.2 Road 63

Twenty-five separate deep patch repairs were constructed in 2005 on Road 63 in the Mount Hood National Forest. A summary of all of the repaired sites on Road 63 is provided in Table 5. Most deep patches were 4 or 6 feet deep having 2 to 3 layers of reinforcement (Type 2000) at about 2-foot spacing. Photos were taken at six sites by WTI staff during a site visit in May 2011 to evaluate the performance of deep patch repairs (Figure 27). All of the sites were performing well with no distresses in the paved road surface or roadside embankment. Six of these sites were constructed by excavating 7 feet down and reinforcing the roadway with four layers of geosynthetics (Type 6000 geogrid) oriented in alternating patterns parallel and perpendicular to the road (referred to as the "herring bone configuration"). Four of these types of repairs were located in areas that were relatively flat and resembled small embankments rather than the traditional cut and cast construction.

Table 5: Dimensions and Details for Deep Patches on Road 63 in Mount Hood National Forest

Beg. Station	Length (ft)	Width[a] (ft)	Depth (ft)	No. of Layers
20+15	45	12	6	3
20+60	85	24	3, 6[b]	1, 3
30+35	35	6	4	2[c]
35+20	90	24	4	2
38+50	60	12	3	1[c]
51+00	50	12	6	3
56+40	90	16	4	2
58+10	30	12	4	2
58+40	60	24	4	2
59+00	30	12	4	2
60+75	60	12	4	2
61+35	55	12	6	3
80+68	77	10	4	2
81+45	30	15	4	2
90+55	12	33[d]	7	4[e]
91+43	12	33[d]	7	4[e]
97+70	30	33[d]	7	4[e]
100+65	55	33[d]	7	4[e]
109+52	28	12	6	3
111+60	230	24	4	2
115+96	34	24	7	4[e]
118+80	25	24	7	4[e]
163+60	35	10	6	3
187+40	110	12	6	3
200+00	150	15	3	1

[a]width of the road surface
[b]3 feet deep on inner lane, 6 feet deep on outer lane
[c]seperator geotextile(Type1-A) used
[d]24-feet of road surface + 9 feet of shoulder work
[e]herring bone configuration

Figure 27: Photos of deep patch repairs on Road 63, Mount Hood National Forest, at a) Sta. 20+15, b) Sta. 30+35, c) Sta. 80+68, d) Sta. 115+96, and e) Sta. 187+40.

2.3 SIUSLAW NATIONAL FOREST

Twenty individual sites were visited on three roads (Road 58, Road 17 and Road 12) in the Siuslaw National Forest to assess existing deep patch repairs (9 sites) as well as review sites that are scheduled for deep patch repair (11 sites). The subsections below summarize these visits.

2.3.1 Road 58

According to a Western Federal Lands Highway Division memo[3], slopes in this area were damaged as a result of heavy rainfall during December 1995 and February 1996, which elevated the ground water table and saturated the ground. Two separate slumps occurred at this site affecting about 120 feet of the road. Vertical displacement of the slumped areas was significant, as shown in Figure 28. The depth of the slump was difficult to determine due to heavy vegetation, but was estimated to extend to the bottom of the draw. Soil samples from the cut slope taken during site visits in 2010 indicated that soils were mostly coarse grained sand with fines and traces of gravel and organic matter. Exposed areas of the cut slopes partially consisted of sandstone and mudstone (Figure 29). A deep patch 13.5 feet deep, 20 feet wide and 120 feet long (including some taper on both ends) was used to repair the area. A typical section of the repair is shown in Figure 30. A uniaxial, integrally-formed geogrid spaced at 1.5-foot layers was used for reinforcement. An 8-inch perforated pipe underdrain system was also installed as part of the repair.

Figure 28: Photo of slope failures on Road 58, MP 29.65, Siuslaw National Forest.

[3] FHWA Western Federal Lands Highway Division, Emergency Relief for Federally Owned Roads (ERFO)Siuslaw National Forest Geotechnical Recommendations (GM 21-96), October 1, 1996.

Figure 29: Exposed soil of cut face, Road 58, MP 29.65, Siuslaw National Forest.

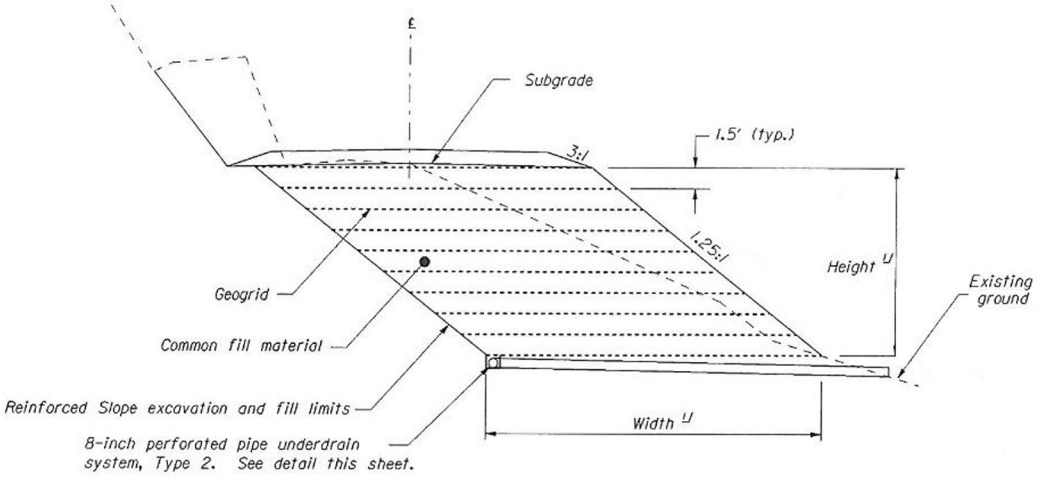

Figure 30: Cross-section of deep patch repair on Road 58, MP 29.65, Siuslaw National Forest.

A site visit by WTI in November 2010 indicated that the deep patch area was performing well after 14 years of service. The road surface is unpaved and no surface distresses indicating differential settlement were noted during the site visit. Photos taken during the site visit are presented in Figure 31.

Figure 31: Photos of deep patch repairs on Road 58, Siuslaw National Forest a) layout of site from end of repair, b) layout of site looking from other end, c) fill slope showing stone facing, and d) close-up of deep patch showing exposed geogrid.

2.3.2 Road 17

On Road 17 in the Siuslaw National Forest, twelve sites were repaired using the deep patch method in 2004-05, and five sites are scheduled for repair in the near future. The dimensions and construction details for the repaired areas are summarized in Table 6. A typical geometry for these repairs is provided in Figure 32 and Figure 33 for Methods B and C, respectively. A Type 4 geogrid was specified for these repairs, having a minimum required ultimate tensile strength of 4110 lb/ft and a required aperture size between 0.75 and 3 inches. Eight of the 13 repaired sites were located by WTI staff during the May 2011 visit. All of the repaired sections, with the exception of the site located at MP 7.92, were performing very well. Selected photos of repaired sites located at mileposts 9.14, 9.39 and 9.65 are provided in Figure 34. Even though the deep patches were performing

well, in some locations (e.g., MP 9.39, Figure 34) cracking had developed near the end of the repaired area indicating that if perhaps the deep patch extended further, these distresses could be mitigated.

Table 6: Dimensions and Details for Deep Patch Repairs on Road 17 in Siuslaw National Forest

Beg. MP	Year Built	Length (ft)	Depth (ft)	Width (ft)	No. of Layers	Facing Type[a]	Found[b]
0.72	2004	215	4	16	1	B	Y
0.87	2004	100	4	18	1	B	Y
0.89	2004	105	4	8	2	C	Y
0.93	2004	70	4	8	2	C	N
0.98	2004	90	4	8	3	C	Y
1.06	2004	60	3	9	1	B	N
2.19	2004	60	4	15	2	C	N
6.48	2004	140	1	13	1	B	N
7.92	2005	70	5	27	2	C	Y
9.14	2005	105	4	19	1	B	Y
9.39	2005	80	4	15	1	B	Y
9.65	2005	160	6	28	1	B	Y

[a] Facing Type B = Single Geogrid reinforcement layer having 1.5H:1V slope at face
Facing Type C = Two Geogrid reinforcement layers with vertical wrapped face

[b] found during May 2011 site visit by WTI (Y=Yes, N=No)

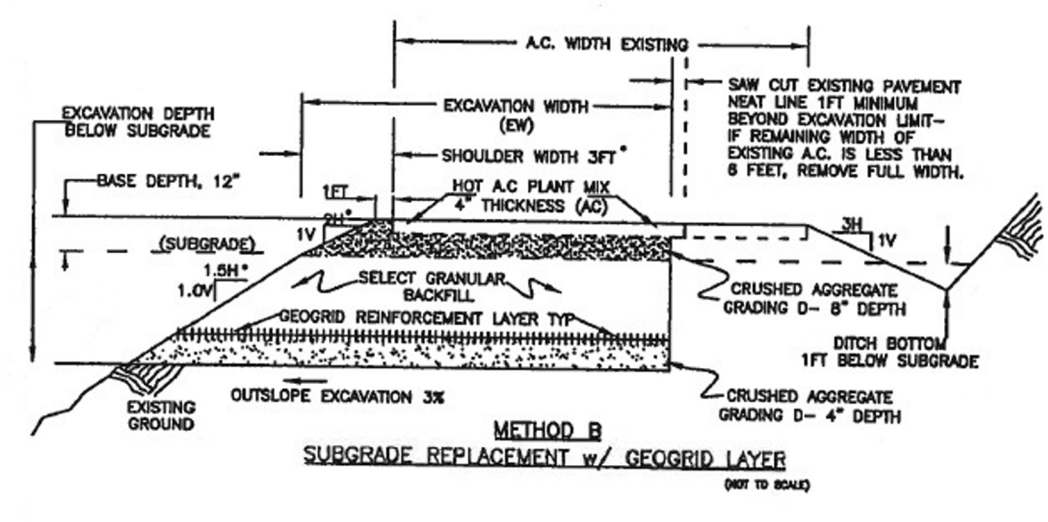

Figure 32: Cross-section of Method B deep patch repair on Road 17, Siuslaw National Forest.

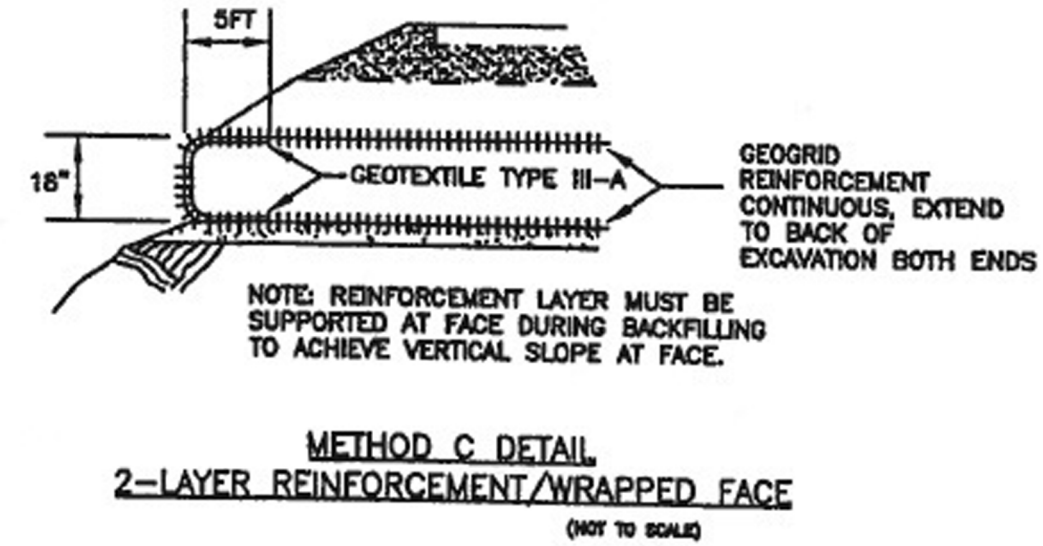

Figure 33: Cross-section of Method C deep patch repair on Road 17, Siuslaw National Forest.

Figure 34: Selected photos of repaired sites on Road 17, Siuslaw National Forest: a) MP 9.14, b) MP 9.39, c) adjacent distresses near repair at MP 9.39, d) MP 9.65.

The deep patch located at milepost 7.92 on Road 17 was not performing well. This deep patch was built in 2005 using Method C (refer to Figure 33), was 5 feet deep, and contained two layers of biaxial woven geogrid. A welded wire basket was used to maintain a vertical orientation of the geogrid wrapped face. Soils extracted from the cut slope adjacent to this deep patch were characterized as poorly graded sand with silt, gravel and organics. Poor performance was characterized by multiple longitudinal cracks (~ 1 inch wide) along approximately 50 feet of the roadway and some holes opening as part of the horizontal movement of the slope near the shoulder (a little over 2 feet deep), as shown in Figure 35. Vertical displacement from either side of the crack was minimal. A plan view of this deep patch that shows the location and layout of this site is provided in Figure 36. Without a more substantial site investigation, it was difficult to determine the cause of these distresses.

Figure 35: Photos of deep patch repairs at milepost 7.92 on Road 17, Siuslaw National Forest showing a) layout of site from end of repair, b) layout of site looking from other end, c) fill slope showing vertical facing, d) welded wire mesh to provide vertical support of slope face, e) close-up of vertical wire mesh showing geosynthetic reinforcement and separation geotextile, and f) hole near outside edge of pavement.

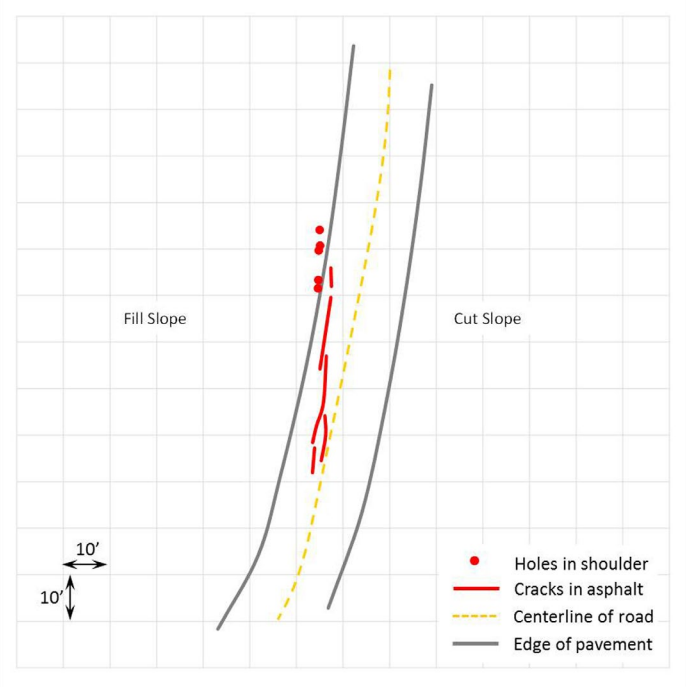

Figure 36: Plan view of distresses at milepost 7.92, Road 17, Siuslaw National Forest.

Five sites on Road 17 selected for future deep patch repair were also visited by WTI staff (MP 10.885, MP 13.664, MP 13.851, MP 14.244 and MP 14.413). General information about these sites is summarized in Table 7. Length and maximum X_c was determined from site visits by WTI, while the preliminary proposed width and number of layers for the deep patch repairs was provided by geotechnical engineers in Siuslaw National Forest. Fill slopes were generally very steep (1:1 or greater) and shoulders were narrow to non-existent and the road width was about 16 feet. Photos of the distresses and general site layout at each of these five sites are shown in Figure 37 through Figure 41.

Table 7: Details for Potential Deep Patch Sites on Road 17 in Siuslaw National Forest

MP	Length (ft)	Max X_c (ft)	Proposed Width (ft)	Proposed Layers
10.885	80	8	full	1
13.664	55	8	full	2
13.851	150	8.5	full	2
14.244	70	6	10	1
14.413	115	10.5	full	1

Figure 37: Photos of distresses at milepost 10.885, Road 17, Siuslaw National Forest.

Figure 38: Photos of distresses at milepost 13.664, Road 17, Siuslaw National Forest.

Figure 39: Photos of distresses at milepost 13.851, Road 17, Siuslaw National Forest.

Figure 40: Photos of distresses at milepost 14.244, Road 17, Siuslaw National Forest.

Figure 41: Photos of distresses at milepost 14.413, Road 17, Siuslaw National Forest.

2.3.3 Road 12

Twenty-seven sites on Road 12 in the Siuslaw National Forest were identified for repair by the Forest Service using Method A (subgrade replacement), Method B (subgrade replacement with geogrid) or Method C (subgrade replacement with double-layer of reinforcement and wrapped face). Five sites that were medium to high severity with recommended repair types of Method B or C deep patch were visited by WTI staff in May 2011. Of these five sites, only two were repaired with Method B (mileposts 2.9 and 4.929) during summer 2011 because of funding constraints. General information about these sites is summarized in Table 8. Length and maximum X_c was provided by geotechnical engineers in Siuslaw National Forest and verified by WTI staff during their site visit. Fill slopes were generally very steep (1:1 or greater) and shoulders were narrow to non-existent and the road width was about 20 feet. Photos of the distresses and general site layout at each of these two sites are shown in Figure 42 and Figure 43.

Table 8: Dimensions and Details for Scheduled Deep Patch Repairs on Road 12, Siuslaw National Forest

MP	Distress Length (ft)	Max X_c (ft)	Proposed Length (ft)	Proposed Width (ft)	Proposed Layers	Proposed Depth (ft)
2.900	160	13	162	29	3	3
4.929a	40	12	45	34	3	3
4.929b	20	6	24	18	3	3

Figure 42: Photos of distresses at milepost 2.9, Road 12, Siuslaw National Forest.

Figure 43: Photos of distresses at milepost 4.929, Road 12, Siuslaw National Forest.

2.4 ROGUE RIVER-SISKIYOU NATIONAL FOREST

Three deep patch repair sites in the Rogue River-Siskiyou National forest were visited by WTI staff in November 2010. Original failures on these roads were likely a result of heavy precipitation. Details of the site reconnaissance were taken from a geotechnical memorandum from Western Federal Lands Highway Division[4]. The deep patches were constructed in 2001 on Road 6610, Road 6515 and Road 6520, known as sites 3, 5 and 12, respectively. All three sites were unpaved. Details associated with these sites are summarized in Table 9, and typical cross-sections for the sites are shown in Figure 44. Uniaxial geogrid samples were extracted from all of these sites having an estimated tensile capacity of about 3,700 to 4,000 lb/ft. Soil samples taken from the cut slopes generally indicated that the soils in this area were silty sands. Overall, the deep patch repairs were performing very well, and drainage at these sites was good. Photos from the site visits are provided in Figure 45 through Figure 47.

[4] FHWA Western Federal Lands Highway Division Geotechnical Memorandum, Prospect Area Roads, Rogue River National Forest, OR ERFO 97-19(3); Geotechnical Design Recommendations.

Table 9: Dimensions and Details for Deep Patch Repairs in Rogue River-Siskiyou National Forest

Site	Year Built	Crack Length (ft)	Scarp Depth (ft)	Repair Width (ft)	Repair Length (ft)	Repair Depth (ft)	No. of Layers
3	2001	108	1.3	16	180	6.9	8
5	2001	108	3.9	32	98	6.9	7
12	2001	Unknown	2	16	131	6.9	8

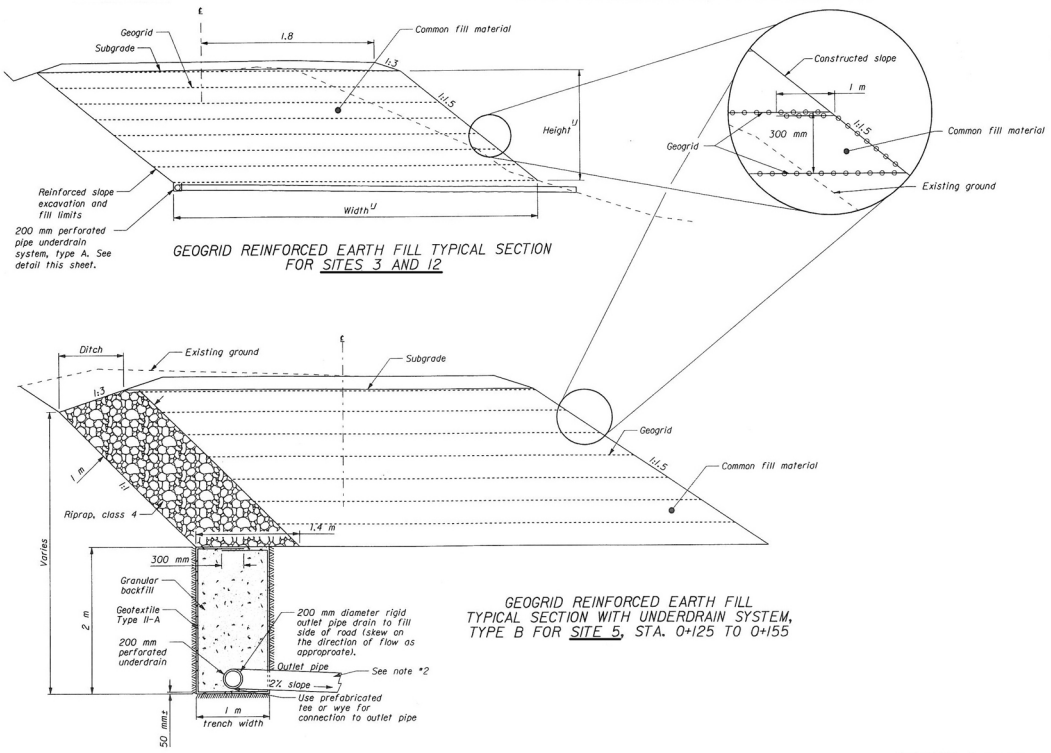

Figure 44: Cross-section of deep patch repairs at Sites 3, 5 and 12, Rogue River-Siskiyou National Forest.

Figure 45: Photos of deep patch repairs at Site 3 on Road 6610, Rogue River-Siskiyou National Forest showing a) layout of site and road surface, b) layout of site and embankment, c) layout of site and embankment from the other end, d) geogrid reinforcement in embankment.

Figure 46: Photos of deep patch repairs at Site 5 on Road 6515, Rogue River-Siskiyou National Forest showing a) general layout of site and road surface, b) layout of site from other direction (note geogrid in foreground that was unearthed by grader), c) embankment, d) exposed geogrid reinforcement in embankment.

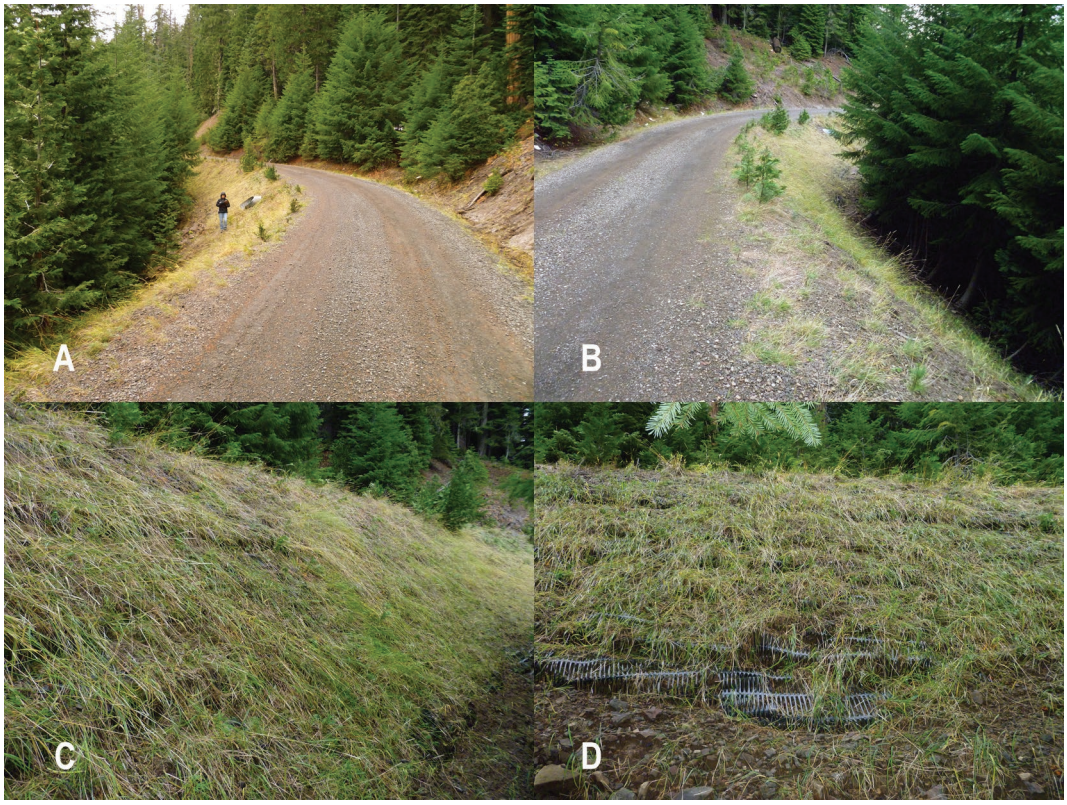

Figure 47: Photos of deep patch repairs at Site 12 on Road 6520, Rogue River-Siskiyou National Forest showing a) general layout of site and road surface, b) layout of site from other direction, c) embankment, d) exposed geogrid reinforcement in embankment.

2.5 SUMMARY OF SITE VISITS

Overall, the 48 deep patch-repaired sites that were visited in November 2010 and May 2011 were performing well, with the exception of the site at milepost 7.92 in the Siuslaw National Forest. Most of the deep patch sites were constructed in the mid-2000s; the oldest site was built in 1996. In terms of their sizes, most were around 4 to 6 feet deep with layers that were, on average, about 2 feet thick. Most repairs were less than 100 feet long with the smallest stand-alone repair at 30 feet and the longest at 250 feet. The important attributes of the deep patch sites visited as part of this effort are summarized in Table 10. Four roads in three forests were visited to better understand preexisting conditions associated with planned deep patch repairs (summarized in Table 11). When possible, an estimate of the effected road length and the maximum X_c were made. Other parameters such as depth, width and number of layers were obtained from planning documentation or local engineers. Maximum X_c values ranged from 6 to 21 feet and the average depth of the proposed repairs was about 5 feet, which usually included about two layers of geosynthetic.

Table 10: Summary of Deep Patch-Repaired Case Studies

National Forest[a]	Road	Milepost/ Station/Site	Year Built	Length (ft)	Depth (ft)	Width (ft)	No. of Layers	Layers Thickness (ft)	Geogrid Type	Facing Slope H:V
GP	26	1.1	2001	200	4-8	full	4-8	1	uniaxial	3:1
GP	25	9.15	2007	250	5	27[b]	1	5	uniaxial	1.5:1
GP	25	8.228	2007	65	4	25.5[b]	1	4	uniaxial	1.5:1
GP	25	9.252	2007	200	3	25[b]	1	3	uniaxial	1.5:1
GP	25	10.032	2007	70	6	31.5[b]	1	6	uniaxial	1.5:1
GP	25	10.898	2007	125	5	27[b]	1	5	uniaxial	1.5:1
GP	25	11.509	2007	250	3	23[b]	1	3	uniaxial	1.5:1
MH	45	5.25a	2004	140	20	10	10	2	biaxial	1:1
MH	45	5.25b	2004	50	6	8	3	2	biaxial	1:1
MH	45	5.45	2004	155	18	12	9	2	biaxial	1:1
MH	45	5.85	2004	130	8	12	4	2	biaxial	1:1
MH	45	6.76a	2004	20	8	10	4	2	biaxial	1:1
MH	45	6.76b	2004	140	8	10	4	2	biaxial	1:1
MH	63	20+15	2005	45	6	12[c]	3	2	biaxial	variable[d]
MH	63	20+60	2005	85	3,6	24[c]	1,3	2	biaxial	variable[d]
MH	63	30+35	2005	35	4	6[c]	2	2	biaxial	variable[d]
MH	63	35+20	2005	90	4	24[c]	2	2	biaxial	variable[d]
MH	63	38+50	2005	60	3	12[c]	1	3	biaxial	variable[d]
MH	63	51+00	2005	50	6	12[c]	3	2	biaxial	variable[d]
MH	63	56+40	2005	90	4	16[c]	2	2	biaxial	variable[d]
MH	63	58+10	2005	30	4	12[c]	2	2	biaxial	variable[d]
MH	63	58+40	2005	60	4	24[c]	2	2	biaxial	variable[d]
MH	63	59+00	2005	30	4	12[c]	2	2	biaxial	variable[d]
MH	63	60+75	2005	60	4	12[c]	2	2	biaxial	variable[d]
MH	63	61+35	2005	55	6	12[c]	3	2	biaxial	variable[d]
MH	63	80+68	2005	77	4	10[c]	2	2	biaxial	variable[d]
MH	63	81+45	2005	30	4	15[c]	2	2	biaxial	variable[d]
MH	63	109+52	2005	28	6	12[c]	3	2	biaxial	variable[d]
MH	63	111+60	2005	230	4	24[c]	2	2	biaxial	variable[d]

[a]GP= Gifford Pinchot, MH= Mount Hood, S= Siuslaw

[b]width of the bottom of the excavation

[c]width of the roadway

[d]slopes were reconstructed to match existing slope angles (variable)

[e]shoulder tapered down to a welded wire basket to create a vertical face

National Forest[a]	Road	Milepost/ Station/Site	Year Built	Length (ft)	Depth (ft)	Width (ft)	No. of Layers	Layers Thickness (ft)	Geogrid Type	Facing Slope H:V
MH	63	187+40	2005	110	6	12[c]	3	2	biaxial	variable[d]
MH	63	200+00	2005	150	3	15[c]	1	3	biaxial	variable[d]
S	58	29.65	1996	120	13.5	20	10	1.5	uniaxial	1.25:1
S	17	0.72	2004	215	4	16[c]	1	4	biaxial	1.5:1
S	17	0.87	2004	100	4	18[c]	1	4	biaxial	1.5:1
S	17	0.89	2004	105	4	8[c]	2	2	biaxial	vertical[e]
S	17	0.93	2004	70	4	8[c]	2	2	biaxial	vertical[e]
S	17	0.98	2004	90	4	8[c]	3	1.3	biaxial	vertical[e]
S	17	1.06	2004	60	3	9[c]	1	3	biaxial	1.5:1
S	17	2.19	2004	60	4	15[c]	2	2	biaxial	vertical[e]
S	17	6.48	2004	140	1	13[c]	1	1	biaxial	1.5:1
S	17	7.92	2005	70	5	27[c]	2	2.5	biaxial	vertical[e]
S	17	9.14	2005	105	4	19[c]	1	4	biaxial	1.5:1
S	17	9.39	2005	80	4	15[c]	1	4	biaxial	1.5:1
S	17	9.65	2005	160	6	28[c]	1	6	biaxial	1.5:1
RR-S	6610	#3	2001	180	6.9	16	8	1	uniaxial	1.5:1
RR-S	6515	#5	2001	98	6.9	32	7	1	uniaxial	1.5:1
RR-S	6520	#12	2001	131	6.9	16	8	1	uniaxial	1.5:1

[a]GP= Gifford Pinchot, MH= Mount Hood, S= Siuslaw, RRS-S= Rogue River- Siskiyou

[b]width of the bottom of the excavation

[c]width of the roadway

[d]slopes were reconstructed to match existing slope angles (variable)

[e]shoulder tapered down to a welded wire basket to create a vertical face

Table 11: Summary of Deep Patch Case Studies Scheduled for Future Repair

National Forest[a]	Road	Milepost/ Station/Site	Maximum X_c	Proposed Length (ft)	Proposed Depth (ft)	Proposed Width (ft)	Proposed No. of Layers	Layer Thickness (ft)
GP	90	0.1	6	40	6	15	3	2
GP	90	5.5	16	50	6	25	3	2
GP	90	6.3	19	80	6	25	3	2
GP	90	10.1	6	200	6	15	3	2
GP	90	11.9	21	110	6	15	3	2
GP	90	14.1	18.5	60	6	25	3	2
GP	90	17.8	11	300	6	20	3	2
MH	45	12+55	NM	25	4	full	1	4
MH	45	12+80	NM	140	4	full	1	4
MH	45	14+20	NM	65	4	10	2	2
MH	45	14+85	NM	25	4	8	2	2
MH	45	15+10	NM	150	4	6	1	4
MH	45	16+60	NM	40	4	8	2	2
MH	45	17+00	NM	110	7	8	2	3.5
MH	45	18+00	NM	90	4	full	1	4
MH	45	19+00	NM	170	4	19	2	2
S	17	10.885	8	80[b]	NP	full	1	NP
S	17	13.664	8	55[b]	NP	full	2	NP
S	17	13.851	8.5	150[b]	NP	full	2	NP
S	17	14.244	6	70[b]	NP	10	1	NP
S	17	14.413	10.5	115[b]	NP	full	1	NP
S	12	2.900	13	162	3	29	3	1
S	12	4.929a	12	45	3	34	3	1
S	12	4.929b	6	24	3	18	3	1

[a]GP= Gifford Pinchot, MH= Mount Hood, S= Siuslaw

[b]measured by WTI staff

NM= Not Measured

NP= Not Provided

Site visits were conducted to monitor performance of past deep patches and understand preexisting conditions of future deep patches. This information was also used to help substantiate design methodology alternatives, as outlined in Chapter 9.

3 ANALYTICAL METHODS

3.1 OBJECTIVE AND APPROACH

A significant portion of this project involved conducting an analytical study to evaluate features believed to be of importance to the performance and design of deep patch slope instability repair, with the ultimate goal of incorporating findings into a design method. These features included:

1. reinforcement vertical spacing,
2. depth of the deep patch reinforced mass,
3. reinforcement strength/stiffness,
4. mode of failure, including rotational and wedge-type failures,
5. anchoring at the lateral ends of the patch,
6. uniaxial versus biaxial reinforcement materials, and
7. geometry of the deep patch section at the slope face.

These features were examined by the use of two analytical methods, namely a limit equilibrium slope stability program for reinforced slopes and a finite difference numerical method for both two-dimensional and three-dimensional slopes. A review of these methods is provided in Section 3.2 and provides justification for the selection of the commercial programs used in this project. These programs are introduced and compared in Section 3.4. A detailed evaluation of the limit equilibrium method used to analyze slopes repaired by the deep patch method is given in Chapter 4 and shows the need for advanced analytical methods (i.e., numerical methods) to account for the features presented above. A finite-difference, numerical method was used in this project to examine these features. Details from this analysis are presented in Chapters 5 through 8. From this analysis, a design method that incorporates these features was developed and is presented in Chapter 9.

The geometry of a deep patch repair was modeled by assuming a wedge-shaped zone of soil within which slope failure has occurred. This zone of soil may be fill soil created by a cut and cast operation or a region of native soil that is weaker than the underlying and adjacent native soil. In either case, the wedge was assumed to rest on a steep slope consisting of soils of greater strength than the material within the wedge. Failure by 1) rotational movement within the weak soil wedge, and 2) sliding along the interface between the weak and stronger soils (wedge-type failure), was both considered. The terminology and parameters that define the geometry of slopes subject to repair by the deep patch method are presented in Section 3.3.

3.2 REVIEW OF ANALYTICAL METHODS

The purpose of this section is to review methods for analyzing the stability of steep slopes containing geosynthetic reinforcement and to make recommendations on methods that will be used in the analytical portion of this project. These methods are reviewed in light of the features of importance to deep patch slope repair, as discussed in Section 3.1.

The two main classes of methods used to analyze the stability of reinforced slopes include limit equilibrium and numerical continuum mechanics methods. Limit equilibrium methods have historically been the most common as they tend to take the least amount of effort and expertise. Numerical continuum mechanics methods are typically finite element or finite difference methods. Limit equilibrium methods tend to be the most restrictive due to the assumptions inherent in the methods. Nevertheless, they are and will remain the most widely used, and are considered robust provided they have been validated against more sophisticated methods backed by field performance data.

Numerical methods offer greater flexibility in terms of modeling the mechanics of the components involved in the system and therefore can offer insight into the importance of the issues listed above. This is particularly important in this project since the mechanisms of failure may be quite different from rotational or internal sliding mechanisms for conventional reinforced slopes. Numerical methods can also be robustly extended to three dimensions, which is important for examining the type of the geosynthetics (biaxial or uniaxial) and anchorage of the geosynthetics. The advantages and disadvantages of these methods are elaborated upon below.

3.2.1 Limit Equilibrium Methods

Limit equilibrium methods are well established for unreinforced earthen slopes and have evolved as the availability of computational resources has increased. Historically, methods based on the analysis of a single sliding wedge, such as the Culmann method, and failure along a circular arc in homogeneous soils, such as Taylor's stability chart method, were used to define a factor of safety against slope failure. These methods were computationally simple but were limited in terms of slope geometry, soil layering and groundwater conditions. The method of slices was introduced to overcome some of these limitations. This method requires a set of assumptions concerning the equilibrium of interslice forces, which has resulted in a number of methods within this analysis category.

Limit equilibrium methods were extended to reinforced slopes in the mid-1980s. The reinforced mass introduces several possible modes of failure, including 1) an internal failure where the failure surface passes through the reinforcing elements, 2) an external failure where the failure surface passes behind and underneath the reinforced mass,

and 3) a compound failure where the surface passes through both the unreinforced and reinforced masses (Elias et al., 2001). Internal instability tends to govern in cases where the vertical spacing of the geosynthetic is large and/or the reinforcement length is short. Failure involving the reinforced mass (i.e., internal and compound) typically is analyzed using a wedge-type failure surface as failure is assumed to develop along block-like masses. External stability is analyzed using an assumed rotational failure mechanism and one of the methods of slices.

The results of a limit equilibrium slope stability analysis are typically expressed in terms of a factor of safety, which is a ratio of the available resisting forces divided by the forces driving failure. Driving forces are derived predominately from the soil's weight within the sliding mass. Forces due to surcharge and groundwater seepage also contribute to driving forces. Resisting forces are due to shear resistance along the failure surfaces and anchoring forces developed in the reinforcement layers when failure surfaces intersect these layers. Geosynthetic reinforcement adds a tensile force that acts about the center of rotation providing a restoring moment to increase the factor of safety, or to force the failure to a more critical circle outside the area of reinforcement.

FHWA sponsored the development of a computer program to analyze and design reinforced slopes and is based on the manual by Christopher et al. (1989). The program was developed using the computer program STABL as its basis. The program (RSS) is in MS-DOS format and is distributed for free by FHWA. This program has been updated to a windows based program (ReSSA 1.0) and uses a program interface based on the program MSEW for reinforced walls. A limited number of copies are distributed by FHWA to federal agencies and state DOTs. The program with further updates is available commercially through ADAMA Engineering as program ReSSA 3.0. The program uses Bishop's method (Bishop, 1955) for circular failure surfaces and Spencer's method (Spencer, 1967) for wedge shaped surfaces. A two-part wedge is used to assess the potential for sliding along each reinforcement layer.

Many other limit equilibrium slope stability programs are available for reinforced slopes and are most likely equally suitable for these problems. Given the developmental history of ReSSA and the accepted use and support for the program by FHWA, this program was used in this project.

3.2.2 Numerical (Finite Element / Finite Difference) Methods

Numerical methods (finite element, FE, and finite difference, FD), allow for the modeling of each component of the reinforced slope system. The geosynthetic is modeled as a distinct component where the material's stiffness and strength can be specified. Interaction between the geosynthetic and surrounding soil is modeled through

interfaces that develop frictional resistance. Soil layers are described in terms of material models that account for both stiffness and strength.

Advantages of numerical methods over limit equilibrium include: 1) the shape and location of the failure surface does not need to be assumed; the FE/FD model locates zones within the soil mass where the applied shear stresses exceed the material's shear strength, which eventually coalesce to form a failure surface; 2) assumptions inherent in common limit equilibrium methods, namely the equilibrium on interslice forces in techniques involving the method of slices, are not required; 3) the FE/FD model gives information on deformations under working stress conditions; and 4) the FE/FD methods can provide information as failure progresses in the slope (Griffiths and Lane, 1999).

Determination of factor of safety is typically accomplished by progressively reducing the soil's strength properties (cohesion and friction angle) by a strength reduction factor, taken as the factor of safety, until failure occurs. Definition of failure in a FE/FD model has been commonly defined in three ways, including 1) meeting some definition of excessive bulging of the slope, 2) exceeding some shear stress level on the failure surface and 3) non-convergence of the solution. While there is no consensus on which definition is most suitable, the third definition appears to be most commonly used. The lack of solution convergence implies that global equilibrium cannot be reached while satisfying the failure criterion of the soil; in other words, the slope mass is sliding excessively along the failure surface such that equilibrium cannot be restored.

San et al. (1994) compared FE and limit equilibrium methods for simple reinforced slopes. Comparison was made between the predicted failure surface and the maximum tensile force developed in the geosynthetic. Reasonable agreement between the two methods was achieved.

Vulova and Leshchinsky (2003) investigated mechanically stabilized earth walls with modular block facing and geosynthetic reinforcement. Failure was by gravity loading as the wall height was increased in the model. The finite difference program FLAC version 3.4, which is a two-dimensional (2D) program, was used for modeling. Material parameters used in the model were taken as typical design values reported in the literature. Variables studied included: geosynthetic spacing, soil strength, reinforcement stiffness, connection strength, secondary reinforcement layers, foundation stiffness, and reinforcement length. FLAC predictions were compared to the AASHTO design method (MSEW). Within MSEW, three methods were used for comparison, namely the L-method, the Demo 82 method and Bishop's method. Reinforcement spacing ranged from 8 in. to 3.3 ft. Four failure modes were identified: external, deep-seated, compound and connection. Reinforcement spacing was a key element in controlling which type of failure mode developed. Increasing spacing changed the failure mode from external or deep-seated to compound and connection mode. Other variables, including soil

strength, reinforcement stiffness and foundation stiffness, also influenced the failure mode. Secondary reinforcement improved performance only when reinforcement spacing was large. The results compared well to the AASHTO method.

Hatami and Bathurst (2005) used the program FLAC (2D) to model a series of large-scale laboratory MSEWs. The focus of the study was on predicting deformations under working stress levels. Details concerning implementation of FLAC were provided. Good agreement was obtained between the FLAC model and measurements from the experimental walls. Huang et al. (2009) examined the influence of the backfill soil constitutive model and concluded that the relatively simple Duncan-Chang hyperbolic model available within FLAC provides predictions well within the level of measurement accuracy and that more sophisticated soil models are not necessarily warranted.

Tanchaisawat et al. (2009) modeled a full-scale reinforced test embankment constructed on soft foundation soil. A 2D FE (Plaxis) and a 3D FD (FLAC) model were used to analyze the embankment. Comparison of vertical and horizontal deformations, excess pore water pressure and reinforcement tensile stress were made. The 3D analysis gave slightly lower values of these measures, while both gave reasonable predictions of observed behaviors.

The above selection of examples illustrates the viability of using FE/FD for prediction of reinforced slope movement and failure. Commercially available programs have been successfully used for these analyses. For this project, the availability of a 3D code was important. FLAC offers both a 2D code meant specifically for slopes and a general 3D code. Given the previous successful use of FLAC for reinforced soils and walls, and its availability in both 2D and 3D, this program was used in this project.

3.3 SLOPE GEOMETRY AND ASSUMED CONDITIONS

A simplified geometry of slopes that have been repaired or require repair by the deep patch method was assumed in order to perform a parametric study with a minimum number of variables such that a design method for deep patch repair could be developed (Figure 48). The geometry depicted in Figure 48 represents a slope resulting from a cut-and-cast construction method, but is shown later in this section to be applicable to natural slopes with a zone of weak soil along the slope face. In reality, the geometry of the cut-and-cast construction technique depends on the topography and geology of the area that was developed. Large stone outcroppings, steep topography, and other natural obstructions, drainages, etc. create a host of possible cross-sections. In order to draw meaningful conclusions, the myriad of possible slope configurations was idealized by a single geometry corresponding to a situation where material from the cut slope is cast directly onto the fill side.

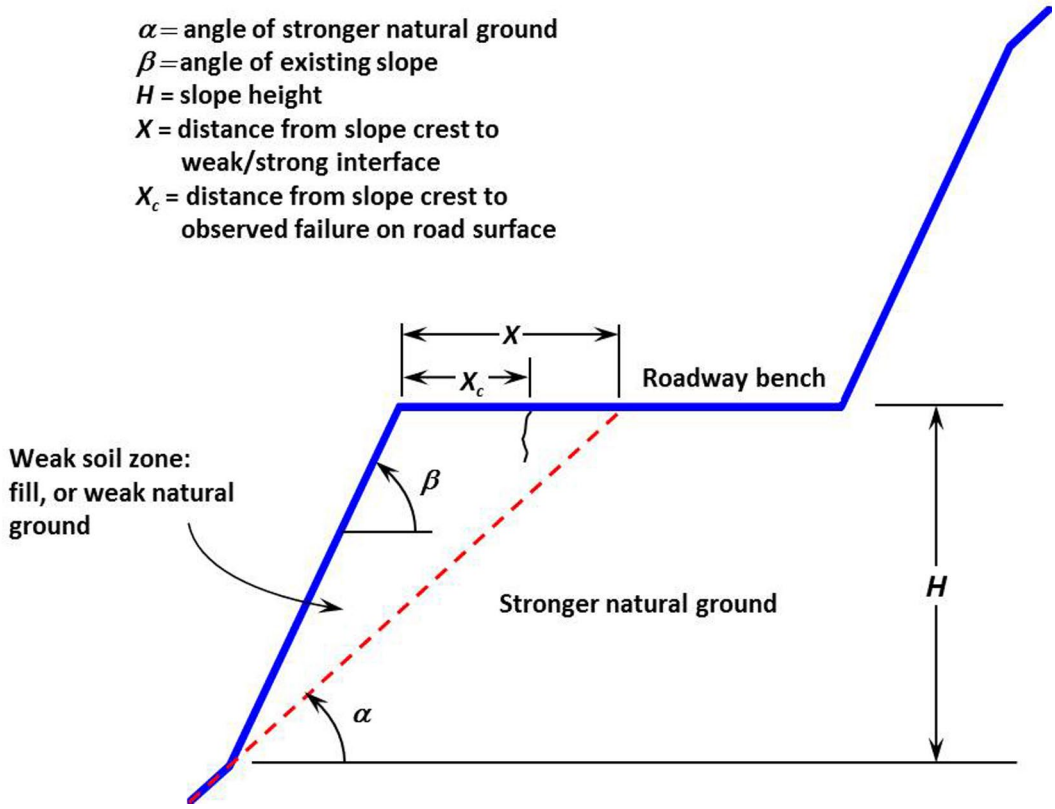

Figure 48: Idealized geometry of deep patch slopes.

In Figure 48, the slope's original and natural grade is given by the slope angle α. The roadway surface that was created by the cut-and-cast operation has an embankment slope defined by the angle β, which is steeper than α. The slope height is defined as H. The parameter X defines the distance from the slope crest to the interface between the fill and native soil. The parameter X_c is the distance from the slope crest to the observed failure surface (shown as a crack in Figure 48) initiating on the top of the slope. The design method developed for deep patch slope repair in this report is dependent on the measurement of both X and X_c. The parameter X_c is a distance that can be directly measured in the field for the failed slope prior to deep patch repair, design and construction, as was illustrated in Chapter 2 for field cases examined as part of this project. The parameter X, however, is more difficult to measure in the field, as previously discussed in Chapter 2. Methods for estimating X are discussed in Chapter 9.

The weak soil shown in Figure 48 is assumed to have strength properties different from and inferior to the surrounding natural ground to confine failure to be within the weak soil zone. For cases where the slope consists entirely of natural ground, the geometry shown in Figure 48 may still be used. In this case, it is assumed that the weak soil zone is simply natural deposits with strength properties weaker than the underlying and

adjacent natural ground. For this case, the parameter X_c is still readily identified from field observations, however the distance X is more difficult to identify. The implications of the uncertainty associated with identifying X are discussed in Chapter 9.

For simplicity, groundwater was not included in the slope and was not considered in the analytical models and design method presented in subsequent chapters. This was necessary to limit the number of variables associated with the slope and to make a parametric study and resulting design method more feasible. Groundwater is an important agent in initial failure of a slope, and slope specific analyses should include this condition. However, the purpose of this study was to develop general recommendations and a simplified design method suitable for use by design engineers and public authorities, and not a site specific analysis tool. As demonstrated in subsequent chapters, failure of unreinforced slopes in the absence of groundwater effects was "simulated" by lowering strength properties of the weak soil zone. Since the influence of a deep patch repair was analyzed for the condition when failure occurs in the unreinforced weak soil zone, the agents leading to failure, including groundwater, are essentially implicit to the resulting findings.

There are two general mechanisms by which slopes have been historically observed to fail. Failure may occur as a rotational failure within the body of the weak zone of soil (defined as fill or weak natural ground) or as a sliding along the interface between this zone of soil and the adjoining strong natural ground (i.e., along the dashed red line extending up to the roadway bench). Historically, analysis methods have developed according to these two broad categories. Rotational failures correspond to classical circular arc slip surfaces and typically occur in situations where the soil within the zone of fill or weak natural ground is homogeneous and the interface between the weak and strong soil zones is reasonably strong. Rotational failures, as demonstrated in this chapter, result in smaller values of X_c. Failures along the interface between weak and strong soil zones (referred to hereafter as wedge-type failures) most likely occur when fill soil is deposited directly on a native slope containing vegetation, where the organic matter decays creating a weak seam. Wedge failures may also occur in entirely natural slopes when a natural seam of weak soil exists. As shown in this chapter, wedge failures generally result in larger values of X_c.

For most of the failed slope field sites examined in this study, it was not possible to directly and conclusively distinguish between rotational and wedge failures. This was mostly due to heavy vegetation, uneven topography, and lack of an obvious toe bulge. In some cases, however, multiple, progressive, arc-shaped cracks were observed at a single location indicating greater likelihood of rotational failures simultaneously occurring in the weaker slope material. Conversely, locations where cracking was more linear in the direction of traffic indicated a greater likelihood of wedge-type failures. Outside of these rarer cases, however, large and small values of X_c were observed, which, together

with the body of knowledge available and results from analyses discussed in subsequent chapters, led to the need to examine both rotational and wedge failures. The design method resulting from these analyses includes results from both failure mechanisms. Knowledge of the distance X_c serves as a possible identifier of the failure mode, meaning the designer is not required to determine the actual failure mode in the field.

3.4 LIMIT EQUILIBRIUM AND FINITE DIFFERENCE MODELING COMPARISONS

The purpose of this section is to compare two analysis methods for failed slopes suitable for a deep patch repair. These two analysis methods correspond to the limit equilibrium method using the slope stability program ReSSA and a numerical finite difference method using the program FLAC/Slope. The programs were used for two slope configurations (Slope I and Slope II) having the basic geometry illustrated in Section 3.3, Figure 48. Values for the parameters shown in this figure are provided in Table 12 for these two slopes. These two configurations were chosen to match commonly encountered failed slopes suitable for a deep patch repair. For these two slope configurations, both rotational and wedge-type failures were analyzed. For rotational failures, ReSSA was compared to FLAC/Slope and produced identical factors of safety. Results indicated that FLAC/Slope tended to produce a slightly different failure surface with larger values of X_c.

FLAC/Slope was used to model wedge-type failures and produced smaller yet similar factors of safety as compared to an equation for sliding of a wedge along a planar failure surface. The smaller factor of safety is due to a more critical failure surface involving the development of a tension crack, which is not taken into account by the sliding wedge equation. Values of X_c were larger for wedge-type failures as compared to rotational failures.

Table 12: Slope Geometry Parameters for Comparative Analyses

Slope Geometry Parameter	Slope I	Slope II
β	34°	39°
α	26.8°	29.8°
H	60 ft	35 ft
X	30 ft	18 ft

These results show the viability of using FLAC/Slope to analyze factors of safety and failure mechanisms in unreinforced slopes. Results from FLAC/Slope expressed in terms of shear strain rate contours and velocity vector plots are shown to provide information on patterns of slope movement and location of failure surfaces. This type of information from FLAC/Slope is used later to judge the effectiveness of various deep patch repair strategies. Details of this summary are found in the following subsections.

3.4.1 Rotational Failure Surfaces

Slope I and Slope II, defined in Table 12, were created and analyzed to compare the factor of safety and location of the failure surface calculated by ReSSA and FLAC/Slope. A schematic of the geometry for Slope I is shown in Figure 49 for ReSSA and FLAC/Slope models. For these models, the strong native soil was given strength properties of ϕ= 50° and c = 0 and a unit weight of γ= 125 lb/ft^3. The relatively high value of friction angle was used to confine failure to the weak soil zone.

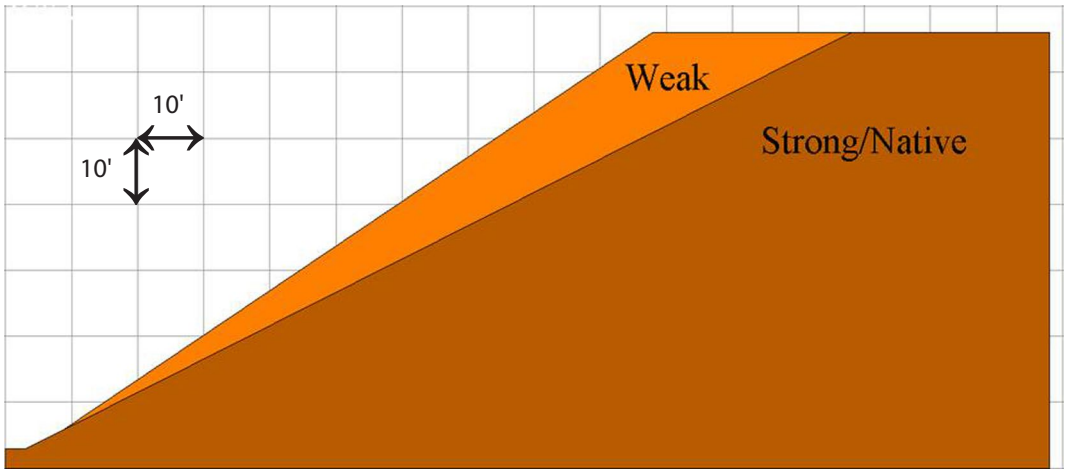

Figure 49: Schematic of Slope I geometry for rotational analyses.

ReSSA was used to analyze the two slopes assuming the weak soil zone was homogeneous and that a circular (rotational) failure surface could develop. The strength properties of the weak soil were chosen to produce a factor of safety (FS) for the critical failure surface of 1.0, representing a failed slope requiring repair. The weak soil in the two slopes was given a relatively small cohesion (refer to Table 13). A small value of cohesion allows the failure surface to develop within the body of the fill and to have a meaningful value of X_c. Slopes with no cohesive strength result in surficial critical failure surfaces and small values of X_c. Slopes with small values of X_c most likely do not require a deep patch repair technique. Based on the cohesion chosen for the weak soil, the friction angle for this soil was then selected to produce a FS = 1.0, with resulting values listed in Table 13. These properties were also used in the FLAC/Slope analyses.

Table 13: Slope Soil Properties for Comparative Analyses of Rotational Failures

Soil Unit	Slope I			Slope II		
	ϕ(°)	c(1b/ft^2)	γ(1b/ft^3)	ϕ(°)	c(1b/ft^2)	γ(1b/ft^3)
Weak	23.1	116	125	23.0	110	125
Strong/Native	50	0	125	50	0	125

The location of the critical failure surfaces from the ReSSA analyses for Slopes I and II are shown in Figure 50. The values of X_c as determined from the analyses are 5.43 ft and 4.77 ft for Slopes I and II, respectively. The combined results from the ReSSA and FLAC/Slope analyses are shown in Figure 51. The FLAC/Slope results are expressed as shear strain rate contours, which denote the rate of development of shear strain at the point where failure occurs in the slope. The greatest values of shear strain rate illustrate the location of the failure surface through the material. On these diagrams, the slip circle from the ReSSA analyses are shown as a solid black line for comparison. The factors of safety from the FLAC/Slope analyses were also equal to 1.0 for both slopes. The values of X_c determined from the FLAC/Slope analyses were larger than those from ReSSA and equaled 8.1 and 6.5 feet for Slopes I and II, respectively.

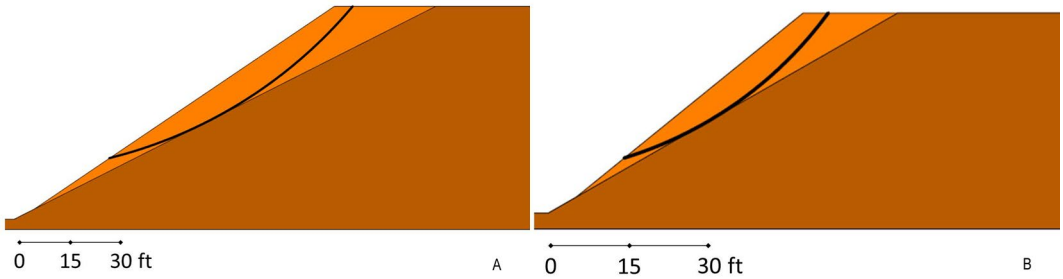

Figure 50: Results of ReSSA unreinforced slope analysis for a) Slope I and b) Slope II.

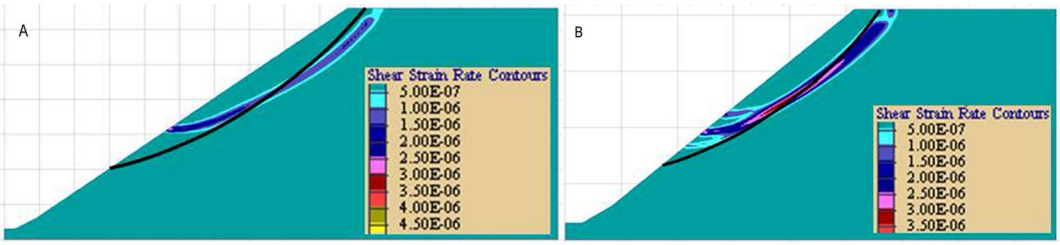

Figure 51: Results of FLAC/Slope unreinforced slope analysis for a) Slope I and b) Slope II.

As part of the FLAC/Slope analysis, velocity is computed at mesh grid points and is determined as the displacement occurring between the last two steps of the equilibrium calculation scheme corresponding to the failure state when instability occurs. Both the magnitude of velocity and its direction is determined at the mesh grid points such that a velocity vector can be drawn. When velocity vectors for all grid points are drawn on a cross section of the slope, the pattern of motion at the onset of slope failure is depicted, as shown in Figure 51 and Figure 52 for Slope I and II. Since velocity is defined as the

difference in displacement between the last two equilibrium time steps, where time is an arbitrary measure depending on the numerical scheme, velocity vectors are not meant to provide information on the actual magnitude of movement but rather on the pattern of movement. Velocity vector plots are useful for visualizing material movement within the slope that is involved in the failure process. From Figure 51 and Figure 52, it is seen that soil movement, as denoted by velocity vectors, occurs within the zone delineated by the failure surface shown by shear strain rate contours. Material outside this zone is stable and is not part of the slope failure. Velocity vector plots are used later to judge the effectiveness of various deep patch slope repair simulations.

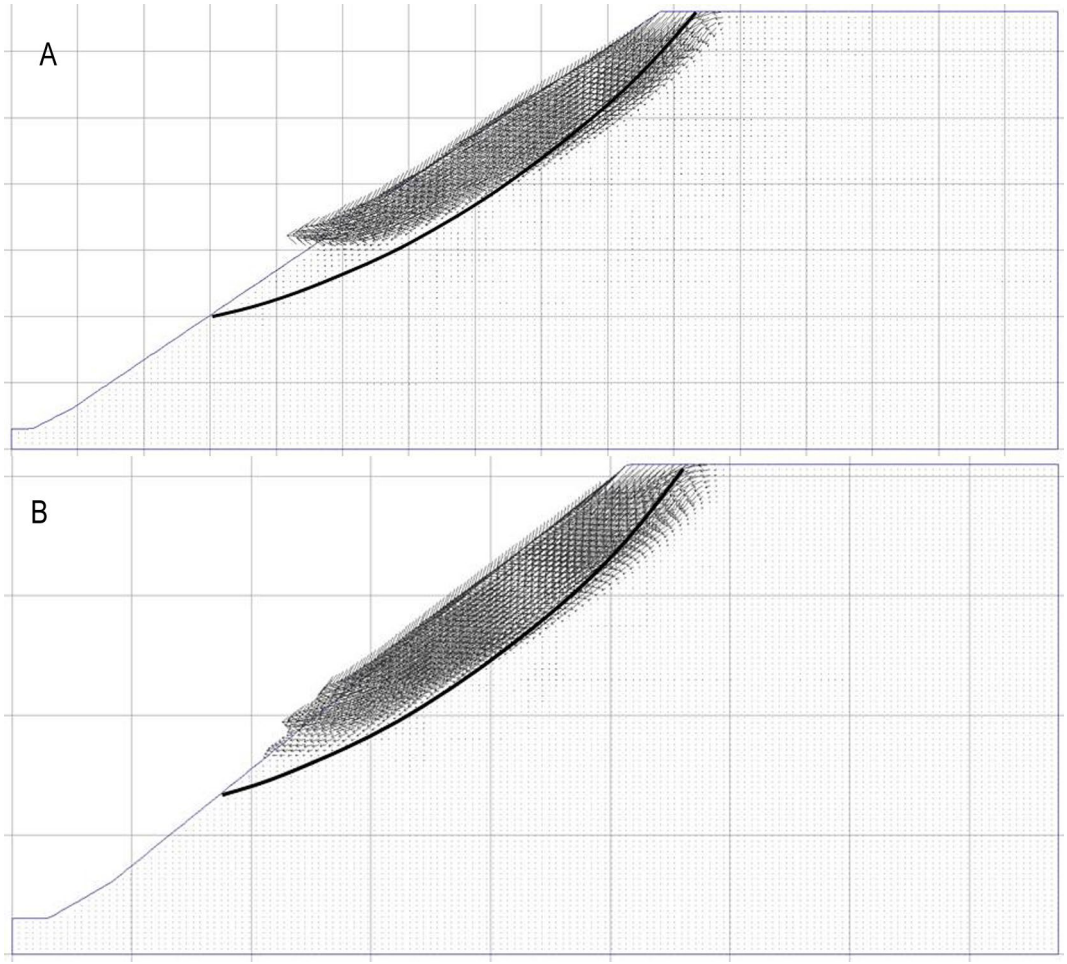

Figure 52: Velocity vector results from FLAC/Slope unreinforced slope analysis for a) Slope I and b) Slope II.

3.4.2 Wedge Failure Surfaces

The factor of safety for wedge-type failures from limit equilibrium methods is most easily evaluated using a simple closed-form equation for sliding of a soil wedge along an inclined plane. In terms of the geometry defined in Figure 48, this equation is given by:

$$FS = \frac{2c \sin \beta}{H\gamma \sin \alpha \sin (\beta - \alpha)} \qquad \textbf{Equation 1}$$

where the material along the weak soil-strong native soil interface is assumed to have a friction angle of zero and a cohesion c. For the Slope I and II geometries defined in the above section, Equation 1 was used to determine the cohesion necessary to obtain a FS = 1.0. Values of c = 380 and 277 lb/ft^2 were obtained for Slopes I and II, respectively.

FLAC/Slope was used to model wedge-type failures by creating a separate soil layer within the weak soil body along the interface with the strong native soil as illustrated in Figure 53 for the Slope I geometry. For these analyses, the weak soil, slip plane and strong native soil layers were given the strength properties presented in Table 15. Figure 54 shows results of the FLAC/Slope analyses in terms of shear strain rate and illustrates that failure predominately occurs within the slip plane soil and terminates at the top as a vertical tension crack. From these analyses, values of X_c of 14.0 and 8.1 ft were obtained for Slopes I and II and are larger than those seen for rotational failures. The factors of safety from these analyses were 0.94 and 0.93 for Slopes I and II, respectively. The lower factors of safety as compared to the sliding wedge equation are due to FLAC/Slope finding the most critical failure surface, which initiates as a tension crack and an early release along the slope face for Slope I, and is more critical than one which follows the entire interface boundary.

Table 14: Slope Soil Properties for Comparative Analyses of Wedge Failures

Soil Unit	Slope I			Slope II		
	ϕ(°)	c(1b/ft^2)	γ(1b/ft^3)	ϕ(°)	c(1b/ft^2)	γ(1b/ft^3)
Weak	32	200	125	32	200	125
Slip Plane	0	380	125	0	277	125
Strong/Native	50	0	125	50	0	125

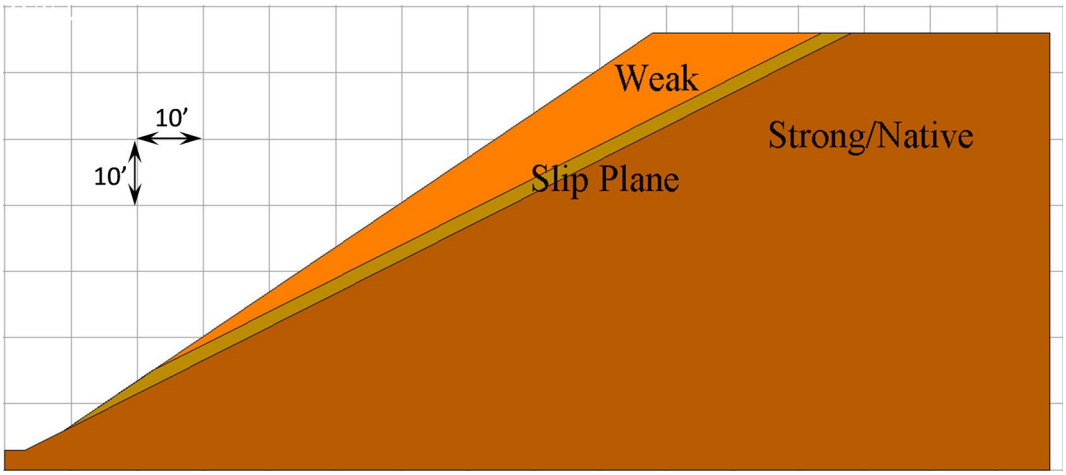

Figure 53: Schematic of unreinforced embankment geometry for Slope I for wedge analyses in FLAC/Slope.

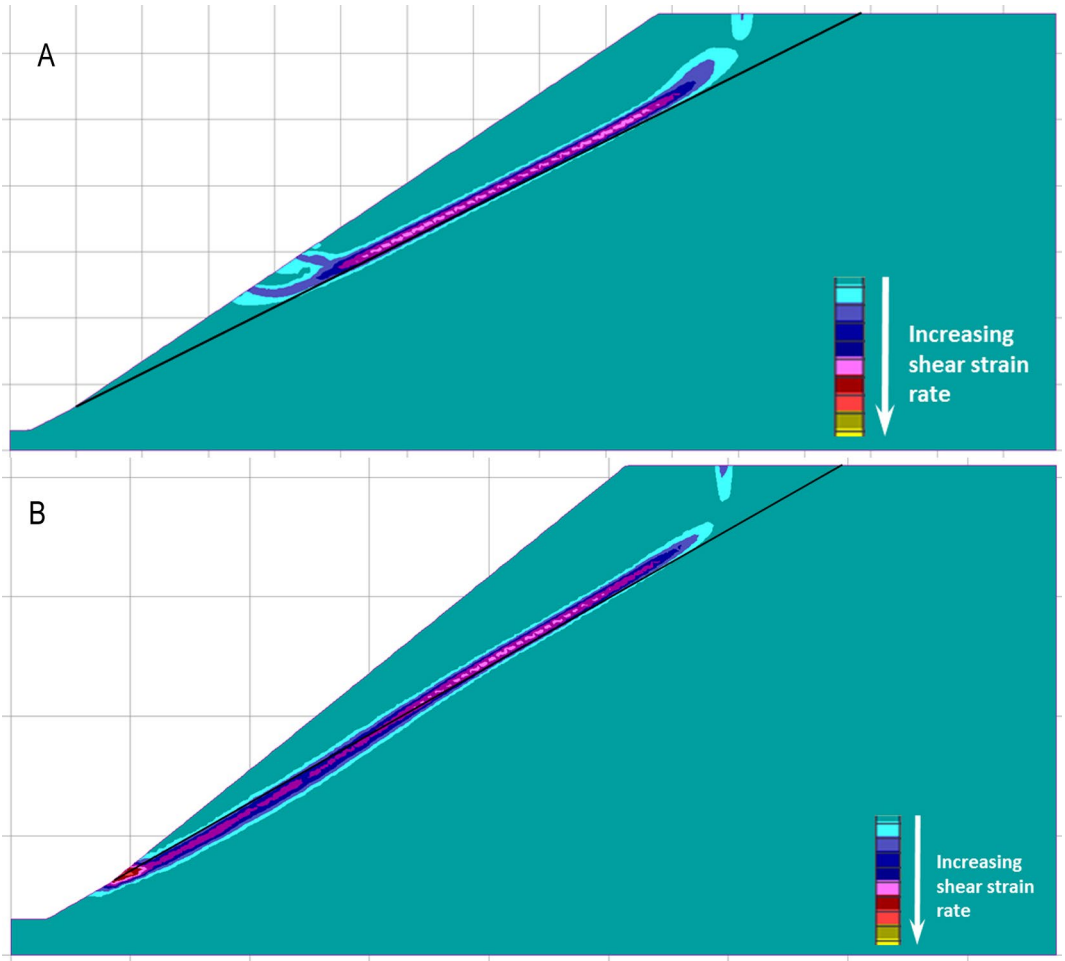

Figure 54: Results of FLAC/slope unreinforced wedge slope analyses for a) Slope I and b) Slope II.

4 LIMIT EQUILIBRIUM ANALYSES

The purpose of this section is to further examine the operation of a limit equilibrium slope stability method for the evaluation of slopes suitable for repair by the deep patch method. As explained in Section 3.2, the commercial program ReSSA was used. The program was used to evaluate both unreinforced and reinforced slopes.

Unreinforced slopes were analyzed for a number of cases using various combinations of slope geometry. Values of slope geometry parameters (Table 15) were chosen to represent the typical range of conditions for failed slopes suitable for deep patch repair, and were selected in consultation with the project sponsor. The parameters shown in Table 15 correspond to those defined illustrated in Figure 48.

Table 15: Range of Values for Slope Geometry Parameters

Slope Geometry Parameter	Range of Values
β	34° and 39°
α	20 – 38°
H	10 – 60 ft
X	3 – 30 ft

Unreinforced slopes were evaluated to examine the conditions under which failure occurs. In particular, the strength properties (friction angle and cohesion) of the weak soil for rotational failures or the slip-plane soil for wedge failures necessary to achieve a factor of safety of 1.0 were determined. For rotational failures, various combinations of friction angle and cohesion for the weak soil producing a factor of safety of 1.0 were used. For each case, values of X_c were documented for the critical slip circle. Resulting values of X_c were plotted against the distance X for the slope. Large values of X_c correspond to situations where a large amount of soil mass is involved in the failure process. It is shown in subsequent chapters that larger values of X_c for the unreinforced slope result in greater reinforcement requirements for the deep patch repair. Furthermore, large values of X_c for rotational failures were possible only when unrealistically low values of friction angle and correspondingly moderate values of cohesion were combined. Most deep patch applications are not currently used for failure in these types of soils. Large values of X_c may result, however, from wedge-type failures. This pointed to the need to analyze the deep patch method for both rotational and wedge-type failures and supports the arguments made in Section 3.3 for examining both.

The limit equilibrium method was also used to evaluate failed slopes reinforced by the deep patch method and resulted in two principal findings. First, reinforcement added to the top layers of the slope can increase the factor of safety to an acceptable level when slip circles are required to initiate along the roadway bench and thereby intercept the reinforcement. This does not prevent, however, failure circles with unacceptable factors of safety from developing below the lowest layer of reinforcement. This supports the

design philosophy that claims the role of the deep patch is to confine failure to the face of the weak soil slope, and to prevent failure from extending up into the roadway bench.

The second principal finding was that within the context of limit equilibrium analyses, the above requirement could be accomplished with a single layer of strong reinforcement close to the top of the slope. This result is an artifact of the mechanics associated with limit equilibrium slope stability analyses and defies good engineering judgment. Furthermore, it is shown that limit equilibrium cannot distinguish between a single layer of strong reinforcement close to the top of the slope and tightly spaced layers of weaker reinforcement contained within a zone of depth at the top of the slope. For both situations, it is shown that an adequate factor of safety is obtained for slip circles extending to the roadway bench and that substandard factors of safety are seen for slip circles initiating along the slope face. No information is available on the movement of soil within the reinforced zone and below the roadway bench. The limit equilibrium method does not provide information on the movement of soil as failure occurs and cannot be used to determine whether soil within the area of the roadway bench experiences excessive movement for a given reinforcement configuration. As such, it is shown that the limit equilibrium method is limited in terms of its ability to determine the influence of reinforcement depth and spacing. These findings and conclusions are detailed in the following sections of this chapter.

4.1 UNREINFORCED SLOPES

Geometric parameters X and H (as defined in Figure 48) were varied to create representative cross sections having values of α within the range noted in Table 15. Cases were developed for slopes with values of β equal to 34° and 39°. Unit weight of the fill soil was also varied between 115 and 135 lb/ft^3. For each slope configuration, different combinations of the weak soil's strength properties (ϕ and c) were chosen to create critical slip circles for rotational failures having a FS=1.0. For a given slope configuration, this resulted in critical slip circles having different entrance points given by the distance X_c. All failure surfaces corresponded to circular arcs within the weak soil zone. In total, 277 cases were examined.

Values of X and X_c were selected as the best parameters to demonstrate the relationship between the geometry of a particular slope configuration (represented by X) and the extent or size of the sliding mass (represented by X_c). For greater values of X and X_c, more weak soil mass is involved in the failure process. It is shown later that these combinations impose greater reinforcement requirements for a deep patch repair. A plot of values of X versus X_c for all the cases examined for $\beta = 34°$ and 39° is shown in Figure 55. Only cases corresponding to X and X_c greater than 3 ft are of interest, which is depicted in these figures by the dotted horizontal and vertical lines. The dashed angled line represents a boundary drawn to contain the points obtained during the analysis.

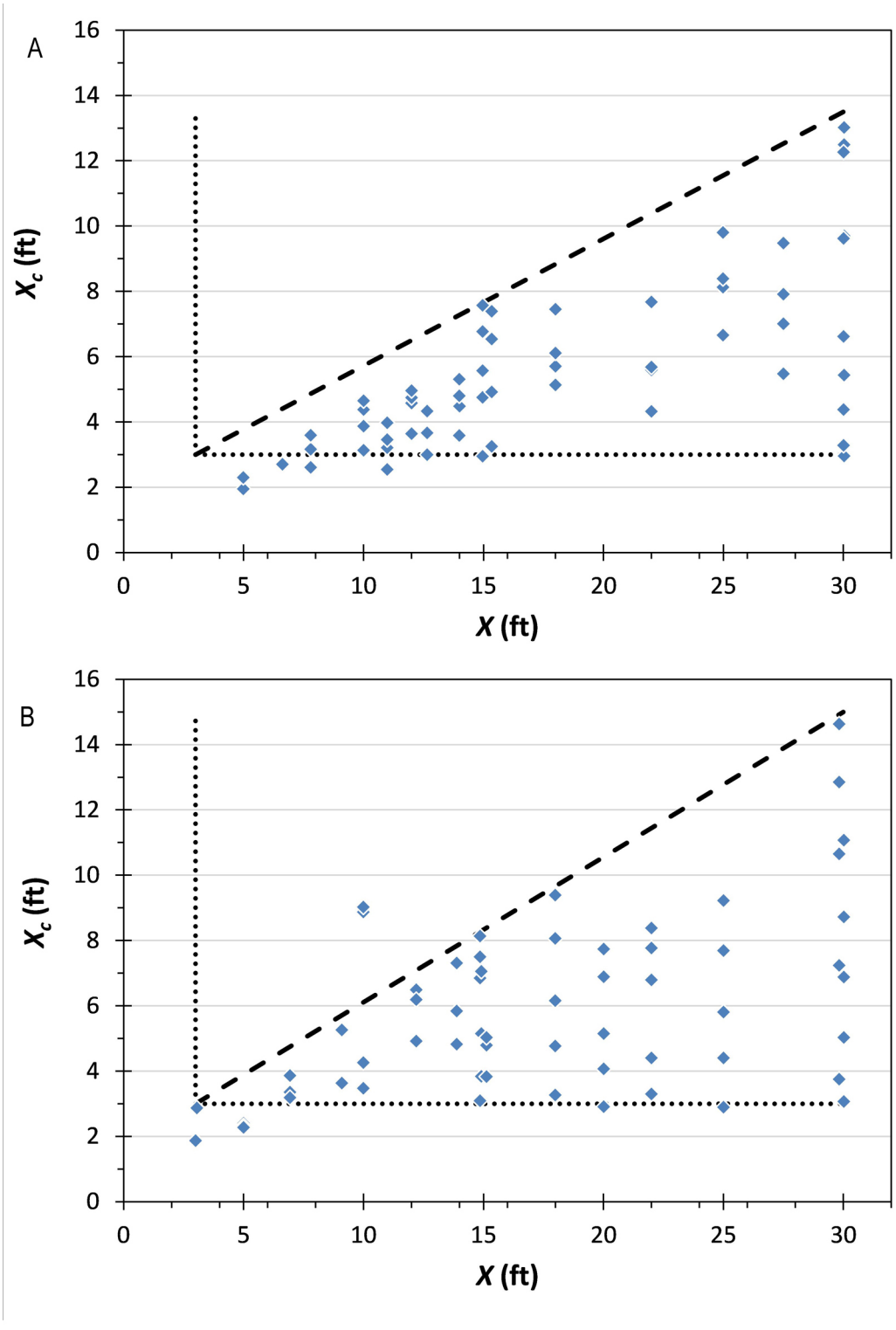

Figure 55: Unreinforced slopes, ReSSA analyses for a) β = 34° and b) β= 39°.

In general, for points approaching the angled limit line (dashed), unreinforced slopes failed under a combination of decreasing ϕ and increasing c. Points shown in the upper right side of the diagrams were possible only for values of ϕ at or close to zero and with moderate values of c. For rotational failures, large values of X_c are only possible when ϕ is at or close to zero and c is adjusted accordingly to produce a FS=1.0. This combination of strength properties is considered unrealistic for most slopes for which a deep patch repair is applicable. Current experience does not extend to deep patch repairs used for purely cohesive slopes. Deep patch repair has typically been used for situations where the weak soil contains sufficient granular soil to show an effective friction angle of no less than about 15°.

Figure 56 shows the same plots but for cases where ϕ is greater than 15°. From these diagrams, it can be seen that cases of rotational failure tend to be confined to values of X_c less than approximately 6 to 7 ft. In Section 3.3, it was shown that wedge-type failures produce larger values of X_c as compared to rotational failures, therefore, failures involving X_c values greater than about 6 to 7 ft are most likely due to a wedge-type failure and not a rotational failure. A mixture of wedge-type failures and rotational failures, however, appears possible for other regions of the diagram. Both mechanisms of failure were evaluated using a numerical method (FLAC/Slope) to model the slope. This information was used to develop a design method to determine the depth of the reinforced mass, reinforcement spacing, and reinforcement strength.

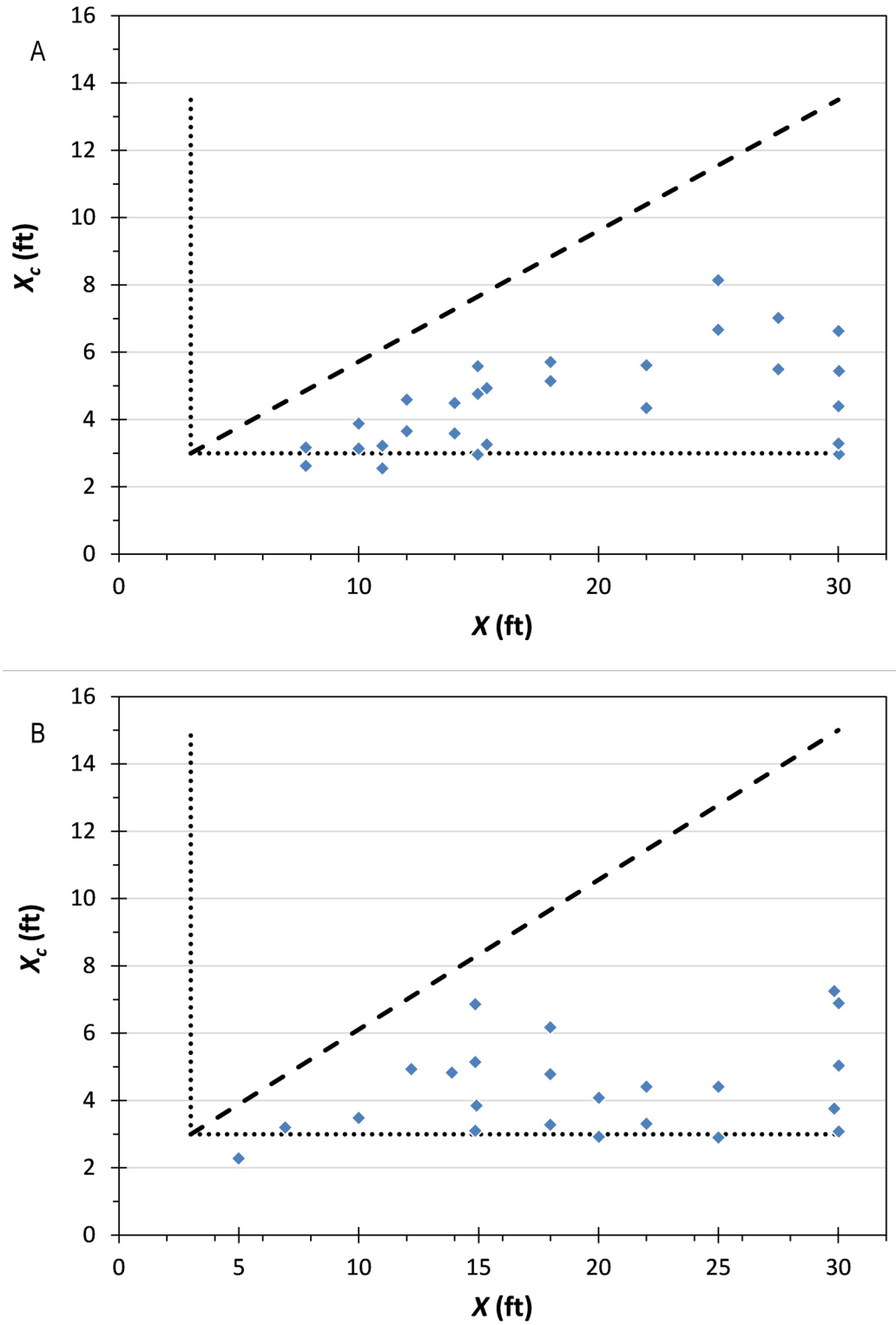

Figure 56: Unreinforced slopes, ReSSA analyses, ϕ>15°, for a) $\beta = 34°$ and b) $\beta = 39°$.

4.2 REINFORCED SLOPES

The limit equilibrium slope stability program ReSSA was evaluated to determine whether it was a suitable tool for the analysis of the deep patch repair method based on how well it was able to distinguish between various deep patch reinforcement depths and spacing configurations. Limit equilibrium programs that incorporate reinforcement show benefit by the restoring moment created due to the anchoring of the reinforcement sheet in stable soil and the resulting tensile force acting around the center of rotation, as illustrated in Figure 57. The driving moment (M_D) due to the sliding soil mass is countered in part by a resisting moment created by the product of the reinforcement tensile force (F_R) and the moment arm (H_R).

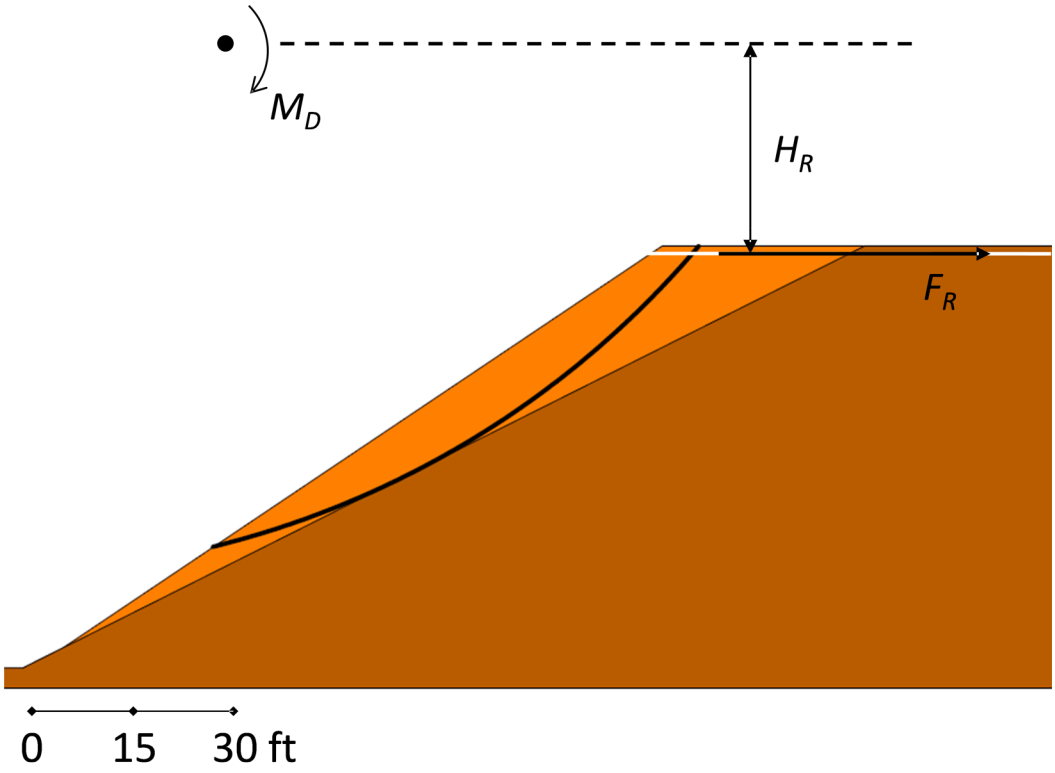

Figure 57: Illustration of reinforcement restoring force in limit equilibrium programs.

To illustrate these mechanisms, Slope I (geometry defined in Section 3.4, Table 12) was modeled with ReSSA using a single layer of reinforcement located at a depth of 1 ft below the roadway bench. The weak soil properties (defined in Table 13 for Slope I) were used in this analysis, which resulted in an X_c of 5.43 ft. For these conditions, the unreinforced slope was at a FS = 1.0 and was considered a failed slope requiring repair. The length of the reinforcement was sufficiently long to prevent pullout. The slope was analyzed with a broad range of circle initiation and termination limits. This resulted in

a FS = 1.04, where the critical slip circle was within the weak soil below the single layer of reinforcement, as shown in Figure 58. This analysis was repeated where the circle initiation limits were confined to the road bench, thereby forcing the critical slip circle to intersect the reinforcement. This resulted in a FS = 1.30, with the critical slip circle shown in Figure 59. Multiple runs were used to determine the tensile strength of the reinforcement (10,000 lb/ft) necessary to yield a FS = 1.30 for this analysis. A FS = 1.30 is considered satisfactory for deep patch repair design.

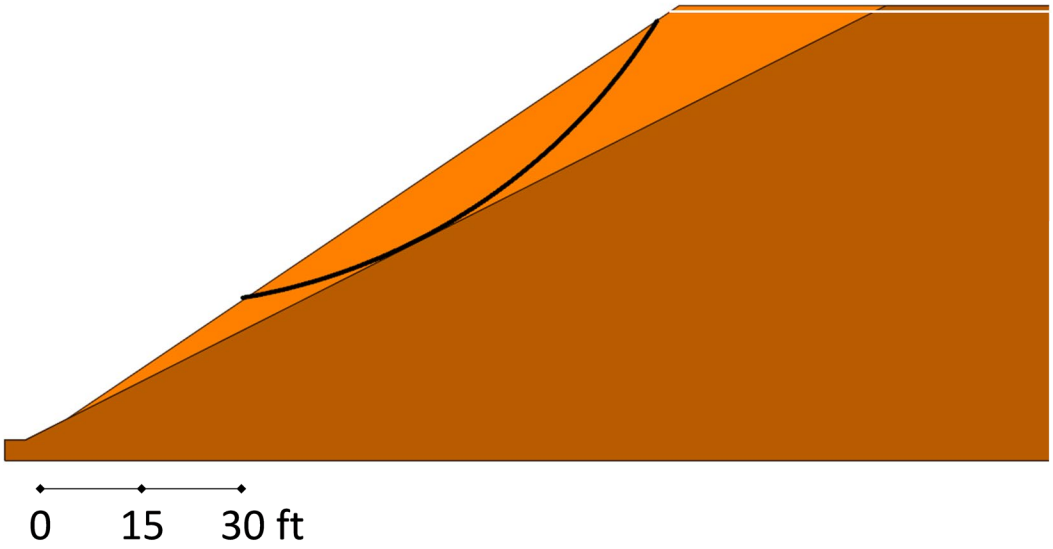

Figure 58: ReSSA analysis, Slope I, β= 34°, single layer of reinforcement, unlimited circle search.

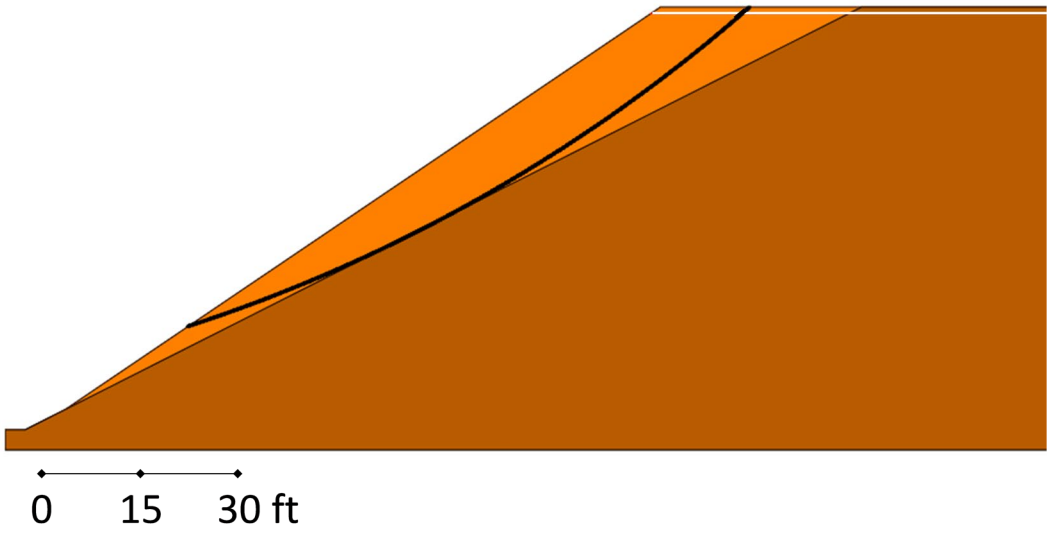

Figure 59: ReSSA analysis, Slope I, β = 34°, single layer of reinforcement, limited circle search.

Additional analyses were made with this slope configuration using the reinforcement depth and spacing configurations shown in Table 16 to test the suitability of limit equilibrium for this application. The tensile strength of the reinforcement for each case was set to provide a total reinforcement force equivalent to the single layer case. A factor of safety was determined for 1) an unlimited circle search, which always resulted in critical slip circles below the lowest level of reinforcement, and 2) a limited search that required the circle initiation to be along the roadway bench. The modest increase in FS for the "limited search" as deeper and more layers of reinforcement are added is due to the increased moment arm when more layers are located at deeper depths, as explained below.

Table 16: Summary of FS for ReSSA analyses of reinforced Slope I

Number of Reinforcement Layers and Depth Below Top of Slope	Tensile Strength of an Individual Layer (lb/ft)	FS Unlimited Search	FS Limited Search
1 @ 1 ft	10,000	1.04	1.30
2 @ 1 and 2 ft	5,000	1.04	1.30
4 @ 1, 2, 3, 4 ft	2,500	1.06	1.31
6 @ 1, 2, 3, 4, 5, 6 ft	1,667	1.07	1.31
1 @ 6 ft	10,000	1.08	1.32

These results illustrate several important points. The deep patch repair method does not provide an overall satisfactory factor of safety for slope failure initiating along the face of the slope and typically below the lowest layer of reinforcement. Improved and satisfactory factors of safety are achieved only for slip circles extending to the roadway bench. This is consistent with the intention of the deep patch repair method which seeks to improve the stability of the roadway surface and not necessarily the stability of the entire slope. In terms of analysis, the goal should therefore be to confine potential slope failure to the face of the weak soil slope and to prevent failure from extending up into the roadway bench. Within the context of using limit equilibrium as an analysis/design tool, this then requires that information from the "limited search" be used to judge the effectiveness of the deep patch.

Furthermore, the results shown in Table 16 show only a modest benefit to increased number of layers of reinforcement and to deeper depths of reinforcement when the total reinforcement force is kept constant. This observation is due to the mechanics associated with a greater moment arm for the reinforcement to act upon. Consequently, within the context of limit equilibrium methods, a single layer of strong reinforcement would be just as suitable as multiple layers of tightly spaced weaker layers of reinforcement. No information can be obtained to make judgments concerning the benefit of deeper

depths of reinforcement and the spacing of the reinforced mass. The limit equilibrium provides no information on material movement in the failure state, only the factor of safety at failure. This is a significant limitation to using limit equilibrium methods for assessing the best reinforcement configuration for deep patch repair methods.

The following chapter examines the stability of these slopes using the finite difference method (FLAC/Slope). This evaluation shows that this method provides information on areas of soil movement at failure and is able to distinguish between various deep patch reinforcement configurations.

5 FINITE DIFFERENCE ANALYSES

In Chapter 3 (Section 3.4), a comparison between a limit equilibrium method (ReSSA) and a finite difference method (FLAC/Slope) was made for unreinforced slopes. This comparison showed the viability of using FLAC/Slope for analyzing failure conditions in steep slopes. Chapter 4 also showed limitations associated with using the limit equilibrium method for the evaluation of the deep patch repair method. The limit equilibrium method was unable to differentiate between a single layer of strong reinforcement at the top of the slope and multiple layers of weaker reinforcement within a zone of depth at the top of the slope. The limit equilibrium method provides no information on material movement in the failure state and cannot be used to judge the effectiveness of a given deep patch configuration. In contrast, results generated by FLAC/Slope (in the form of shear strain rate contour plots and velocity vector plots) provide a visual representation of the modes of failure and patterns of material movement at failure. In this chapter, a methodology to use these results to judge the effectiveness of various deep patch reinforcement configurations is presented.

FLAC/Slope was used to examine some of the same cases evaluated using the limit equilibrium method presented in Chapter 4 in order to evaluate their effectiveness. In particular, the Slope I geometry was evaluated for both rotational and wedge failures for a number of reinforcement configurations, which included different number of reinforcement layers and different reinforcement spacing. Results from these different cases were compared by examining shear strain rate contour plots and velocity vector plots. Visual comparisons provided a means to qualitatively rank the cases from best to worst. This ranking was established by examining shear strain rate contour plots and velocity vector plots within the context of the design philosophy for deep patch slope repair. This philosophy, as established in Chapter 4, claims that the purpose of a deep patch repair is to confine potential slope failure to the face of the weak soil slope and to prevent failure from extending up into the roadway bench. Improved ranking then corresponds to cases where the failure surface (as seen from shear strain rate contour plots) and material movement (as seen from velocity vector plots) is less pronounced and further removed from soil within the reinforced zone and below the roadway bench. Since comparisons of one case to another are based on qualitative visualization of these plots, the approach is subjective and not quantitative. The implications of this subjectivity are shown to be minor in Chapter 6 when a parametric study is performed for a large number of cases and results are summarized. This methodology is illustrated by an example for a specific case where supporting figures showing the performance of the cases are presented.

5.1 REINFORCED SLOPE I – ROTATIONAL FAILURE

Slope models corresponding to the five cases shown in Table 16 and an additional nine cases were analyzed using FLAC/Slope. All 14 cases correspond to the Slope I configuration and are summarized in Table 17. The ranking shown in Table 17 from best (1) to worst (14) was established by the methodology described above and is illustrated by an example in this section.

Table 17: Summary of FLAC/Slope Rotational Failure Analyses (Slope I)

Depth of Reinforced Soil (ft)	Number of Reinforcement Layers	Reinforcement Spacing (ft)	Ranking
6	12	0.5	1
5	10	0.5	2
6	6	1	3
6	4	1.5	4
6	3	2	5
5	5	1	6
5	4	1.25	7
5	3	1.83	8
5	2	2.5	9
4	8	0.5	10
4	4	1	11
6	1	6	12
2	2	1	13
1	1	1	14

The FLAC/Slope models differed from the ReSSA models in that the soil within the area of the reinforcement was given properties corresponding to a good quality compacted granular fill. The soil properties used for the soil layers in this model are provided in Table 18. The tensile strength of the reinforcement was typically set to a high value (4,000 lb/ft) to prevent failure of the reinforcement and to allow for consistent comparisons between the models. FLAC/Slope shows the tensile force mobilized within each reinforcement layer when slope failure occurs and is documented for each configuration examined.

Table 18: Reinforced Slope Soil Properties for FLAC/Slope Analyses of Rotational Failures

Soil Unit	ϕ(°)	c(lb/ft^2)	γ(lb/ft^3)
Fill	23.1	116	125
Reinforced Fill	45	0	125
Native	50	0	125

A velocity vector plot and a shear strain rate contour plot for the case of one layer of reinforcement at a depth of 1 foot are shown in Figure 60a and b, respectively. The velocity vector plot shows the pattern of movement as indicated by the size and direction of the vector arrows. The velocity vector plot shows a portion of the roadway bench being involved in the failure of the slope. The shear strain rate contour plot shows the failure surface extending up into the roadway bench as well as fingering out to the slope face below the reinforcement layer (colors evolving from light blue to red on this type of plot indicates greater shear strain rates). Based on these results, this is an unacceptable design from the standpoint of limiting movement of the roadway bench. It should be noted that the limit equilibrium method (ReSSA) analysis indicated a factor of safety of 1.30 for slip circles initiating along the roadway bench and 1.04 for an unlimited circle search, with a required tensile strength of 10,000 lb/ft for the reinforcement. The factor of safety shown by FLAC/Slope was 1.00 and a force of only 1,782 lb/ft was mobilized (needed) in the reinforcement. Whereas the ReSSA method is based on the method of slices (Bishop's method), FLAC/Slope solves a set of constitutive equations. FLAC/Slope does not allow the user to limit the search for the critical failure surface. Thus, the FLAC/Slope results are more comparable to the unlimited circle search in ReSSA, and not the case where the search was limited to failure surfaces that intersected the road bench.

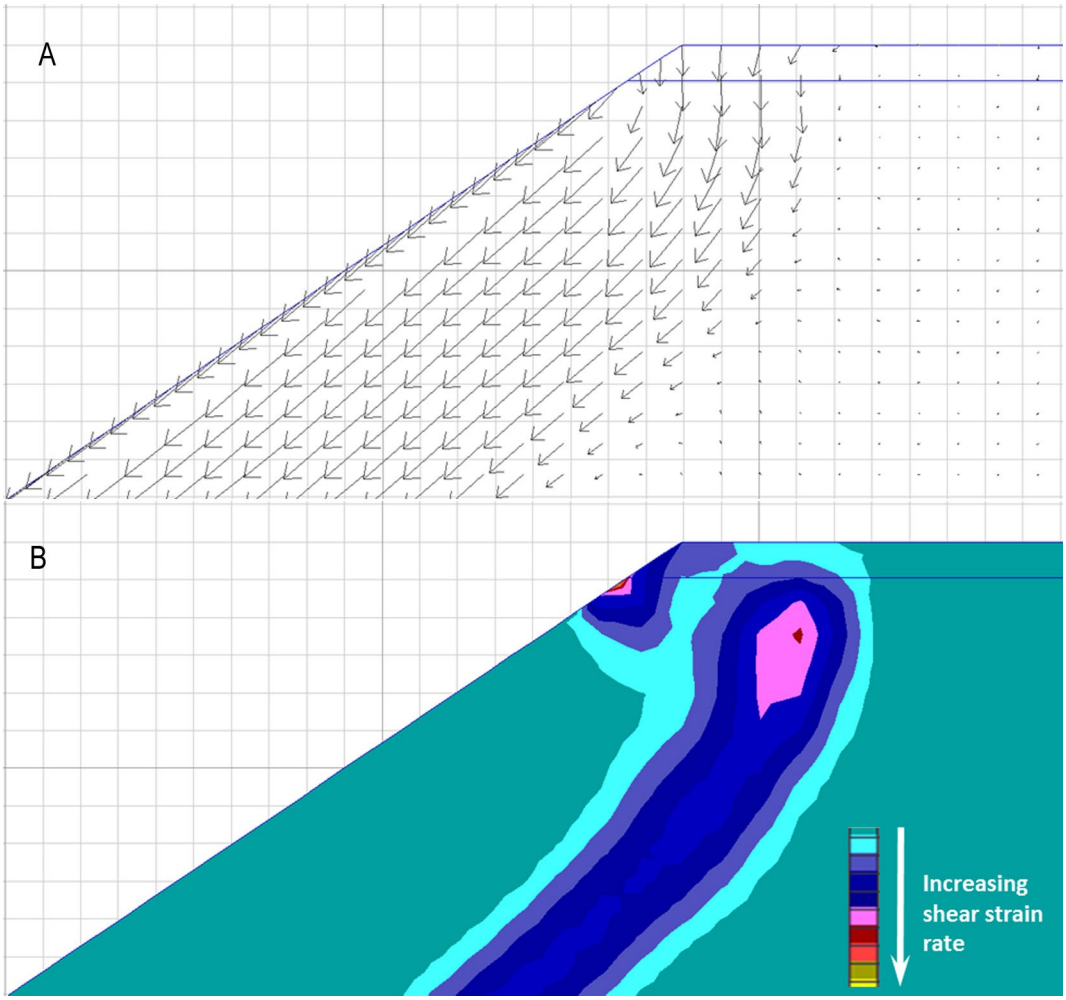

Figure 60: Results of FLAC/Slope analysis for Slope I, rotational failure, 1 layer of reinforcement at 1 ft spacing, a) velocity vector plot and b) shear strain rate contours.

Similar results for the case of 2 layers of reinforcement at a 1 ft spacing are shown in Figure 61. The velocity vector plot shows appreciable movement along the roadway bench while the shear strain rate contour plots tends to show failure occurring in the fill soil below the reinforcement. Results for the case of 4 layers at a 1 ft spacing are shown in Figure 62. Movement along the roadway bench is still seen while the failure surface appears to be confined to the fill below the reinforcement.

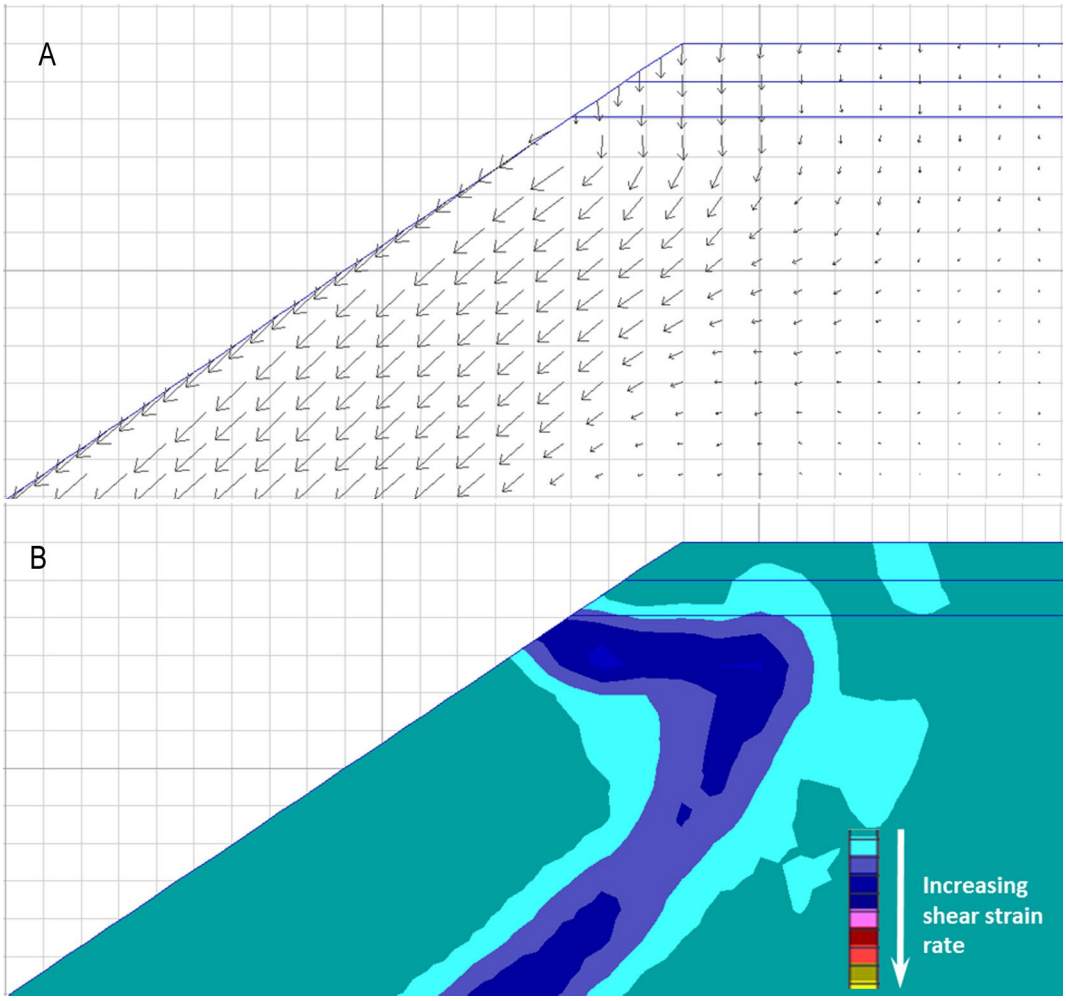

Figure 61: Results of FLAC/Slope analysis for Slope I, rotational failure, 2 layers of reinforcement at 1 ft spacing, a) velocity vector plot and b) shear strain rate contours.

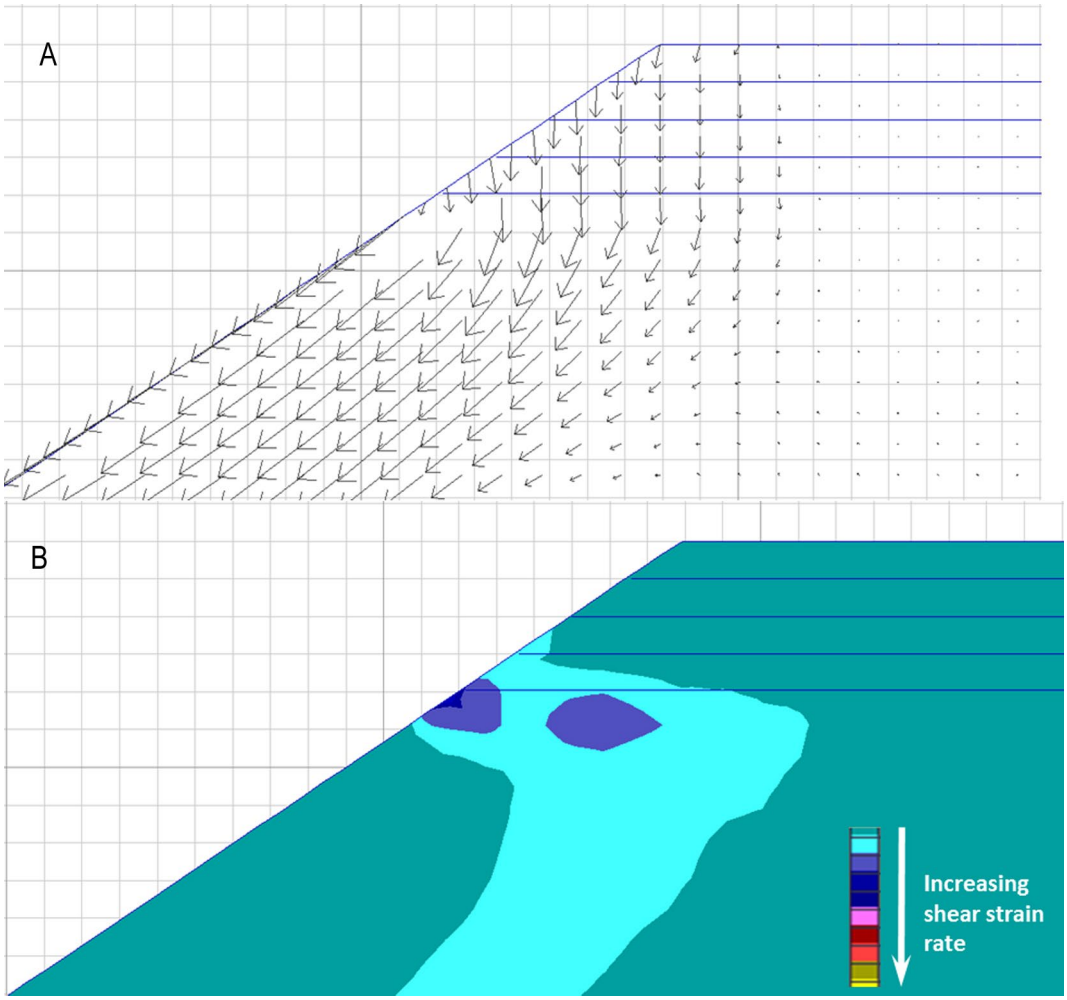

Figure 62: Results of FLAC/Slope analysis for Slope I, rotational failure, 4 layers of reinforcement at 1 ft spacing, a) velocity vector plot and b) shear strain rate contours.

Velocity vector plots and shear strain rate contour plots for the two remaining cases in Table 16, namely 6 layers of reinforcement at a 1 ft spacing and 1 layer of reinforcement at a 6 ft spacing are shown in Figure 63 and Figure 64, respectively. The results shown in Figure 63 indicate minimal deformation along the roadway bench. This deep patch configuration (6 ft deep, 6 layers of reinforcement) is considered acceptable. The case of 1 layer at a depth of 6 ft (Figure 64) shows excessive deformation of the roadway bench and failure surfaces developing both above and below the reinforcement layer and is considered unacceptable.

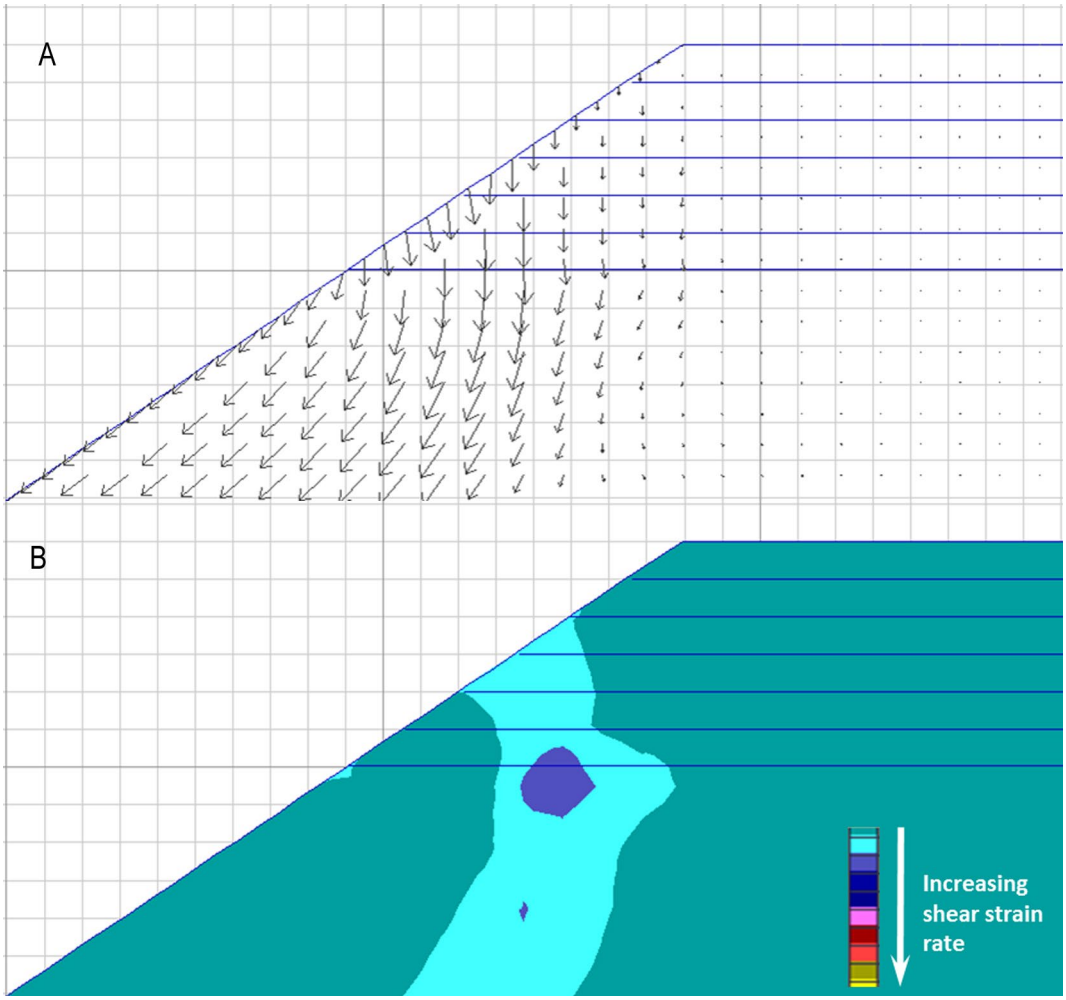

Figure 63: FLAC/Slope analysis, Slope I, rotational failure, 6 layers of reinforcement at 1 ft spacing, velocity vector plot.

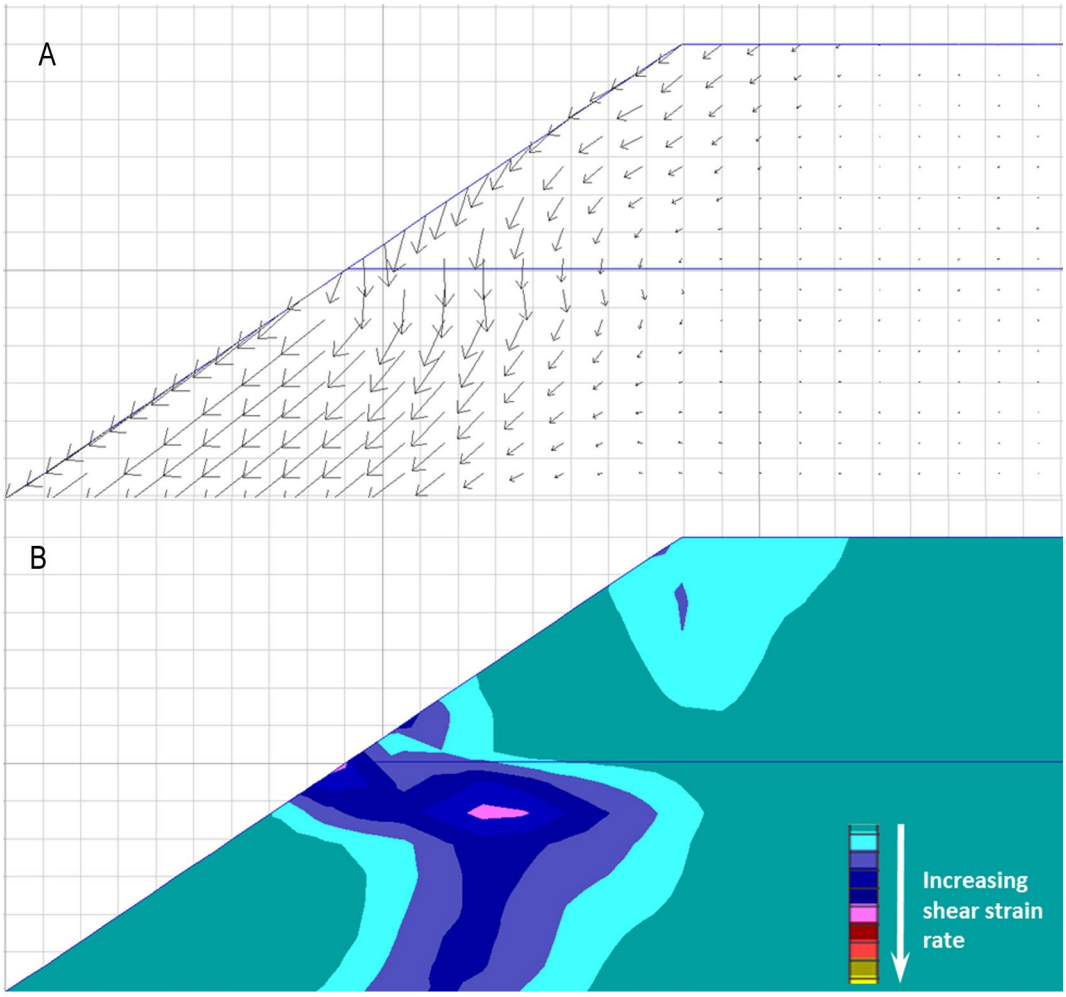

Figure 64: FLAC/Slope analysis, Slope I, rotational failure, 1 layer of reinforcement at 6 ft spacing, velocity vector plot.

The results shown in Figure 60 through Figure 64 illustrate how the velocity vector plots are used to determine an acceptable reinforcement configuration. These results also show some ambiguity in using the shear strain rate contour plots to make this assessment. For instance, Figure 62b) shows the configuration to be acceptable in terms of shear strain rate while Figure 62a) does not. Because the velocity vector results were more consistent than the shear strain rate results, the velocity vector results were primarily used to judge the suitability of various reinforcement configurations; however, when considering two cases showing similar performance in terms of velocity vector plots, shear strain rate contour plots were used as additional information to determine which case was best.

The evaluation of reinforcement requirements for the Slope I configuration was carried out further by considering nine additional cases listed in Table 17. The velocity vector plots for these nine cases and the previous five cases are shown in Appendix A. For cases with a rank of 7 and below, the velocity vector plots showed unacceptable movement of the roadway bench. For the case with a rank of 6, the performance was considered marginally acceptable, and cases with a rank of 5 or less were considered acceptable. As mentioned earlier, the velocity vector plots were the main source of data considered to determine rank. Several cases tended to show unclear differences in the velocity vector plots. In those cases, the shear strain rate contour plots were examined to see if one case showed worse performance by failure surfaces extended up into the roadway surface.

While the selection of performance rank is based on visual observations, the results show some clear bounds for acceptable and unacceptable performance. For instance, cases with a depth of reinforced soil of 4 ft or less are unacceptable, even for a reinforcement spacing of 0.5 ft. When extending the depth of the reinforced soil to 5 ft, the only acceptable cases are those when the spacing is small (1 ft to 0.5 ft). For a 6 ft depth of reinforced mass, performance becomes unacceptable when the reinforcement spacing is greater than 2 ft. These results show that for a given slope configuration, there is a small range of reinforcement configurations that will result in acceptable performance. For this particular slope configuration (i.e., Slope I, as defined in Section 3.4, Table 12) a depth of reinforced soil of 5 to 6 ft is required. When 6 ft is used, the spacing may be as great as 2 ft. When 5 ft is used, the spacing should be kept to 0.5 ft. At the end of this section, the mobilized strength in the reinforcement is examined to provide further information on the best reinforcement layout and required reinforcement strength for this slope configuration.

5.2 REINFORCED SLOPE I – WEDGE FAILURE

The Slope I configuration was analyzed for a wedge-type failure to determine reinforcement requirements. Table 19 shows the properties of the soil layers used in this model. Ten cases were examined with the reinforcement configurations listed in Table 20. Examination of the results led to the ranking of best (1) to worst (10) shown in Table 20. Results of velocity vectors for each case are provided in Appendix B, and are shown in the order of the rank listed. Based on this examination, cases with a rank of 5 or greater are considered unacceptable. The case with a ranking of 4 is considered marginally acceptable. Cases with a rank of 3 or less are considered acceptable.

Table 19: Reinforced Slope Soil Properties for FLAC/Slope Analyses of Wedge Failures (Slope I)

Soil Unit	Slope I		
	$\phi(^\circ)$	c(1b/ft^2)	γ(1b/ft^3)
Weak	32	200	125
Reinforced Fill	40	0	125
Slip Plane	0	380	125
Strong/Native	50	0	125

Table 20: Summary of FLAC/Slope Wedge Failure Analyses (Slope I)

Depth of Reinforced Soil (ft)	Number of Reinforcement Layers	Reinforcement Spacing (ft)	Ranking
8	8	1	1
7	14	0.5	2
8	4	2	3
7	7	1	4
6	12	0.5	5
6	6	1	6
7	4	1.75	7
7	3	2.33	8
6	3	2	9
8	2	4	10

Similar to the results for rotational failures, the analyses for wedge failures clearly show bounds of acceptable and unacceptable performance. For a depth of reinforcement of 6 ft, unacceptable performance is seen when the reinforcement spacing is 1 ft and greater. When reduced to a spacing of 0.5 ft, marginally acceptable performance is seen. For 7 ft of reinforced soil, unacceptable performance is seen when the spacing is 1.75 ft or greater; a 1ft spacing results in marginally acceptable performance, and a 0.5 ft spacing results in acceptable performance. For a depth of reinforcement of 8 ft, acceptable performance is seen for a spacing of 2 ft or less and a 4 ft spacing results in unacceptable performance.

A comparison of the results for wedge failures to those for rotational failures for the same slope configuration shows that wedge failures have greater reinforcement requirements as compared to rotational failures. On average, about two additional feet of reinforced soil is required to remedy wedge-type failures. The values of X_c for the unreinforced slope for wedge and rotational failures for this slope configuration were 14.0 and 8.1 ft,

respectively, indicating that more of the weak soil was involved in the failure process for wedge failures, resulting in a greater demand for the reinforcement. In Chapter 6, it is shown that the parameter X_c can be used to establish the reinforcement requirements for wedge and rotational failures and that specific knowledge of the failure mechanism is not required for design.

5.3 REINFORCEMENT TENSILE STRENGTH REQUIREMENTS

The tensile force mobilized in each reinforcement layer was tabulated for the cases examined in Sections 5.1 and 5.2 for rotational and wedge failures using FLAC/Slope. For a given case, the tensile force varied from layer to layer. Table 21 and Table 22 provide the force mobilized in each reinforcement layer for the cases examined, organized according to rank, for rotational and wedge analyses, respectively. For all but one case, the maximum tensile force occurs in the bottom layer of reinforcement, as indicated by the bold values in Table 21 and Table 22.

For rotational failures, the maximum is as much as 74 % above the average reinforcement tensile force. For wedge failures, the maximum tensile force is as much as 180 % above the average reinforcement tensile force. For both rotational and wedge failures, more difference between the maximum and average reinforcement tensile force values tends to occur for cases where a large number of reinforcement layers are used. Since most designs will use the same geosynthetic type for all layers and be chosen to carry the maximum tensile force expected, there will be greater excess capacity for those cases showing greater differences between the maximum and average reinforcement tensile forces. This is taken into consideration when choosing a "best" reinforcement configuration.

Table 21: Reinforcement Tensile Force Mobilized Per Layer for Rotational Failure (Slope I)

	Tensile Forced Mobilized (lb/ft)													
	Ranked and Configuration (depth/# of layers)													
	1	2	3	4	5	6	7	8	9	10	11	12	13	14
Layer	(6/12)	(5/10)	(6/6)	(6/4)	(6/3)	(5/5)	(5/4)	(5/3)	(5/2)	(4/8)	(4/4)	(6/1)	(2/2)	(1/1)
1	1170	1172	1011	1290	1394	1068	1129	1347	1936	937	1167	**3389**	1131	**1782**
2	1009	1016	1045	1324	1328	1049	1328	1339	**2028**	1015	1053		**1510**	
3	1159	1017	1325	1384	**1898**	1334	1343	**1956**		1019	1342			
4	1046	1047	1327	**2017**		1342	**1512**			1054	**1366**			
5	1320	1060	1044			**1739**				1068				
6	1250	1323	**1950**							**1338**				
7	1071	1073								1098				
8	1335	1336								1256				
9	1341	1363												
10	820	**1736**												
11	1357													
12	**2178**													
Total	15,056	12,143	7702	6015	4620	6532	5312	4642	3964	8785	4928	3889	2641	1782
Avg.	1255	1214	1284	1504	1540	1306	1328	1547	1982	1098	1232	3889	1321	1782

Table 22: Reinforcement Tensile Force Mobilized Per Layer for Wedge Failure (Slope I)

Tensile Forced Mobilized (lb/ft)										
Rank and Configuration (depth/# of layers)										
	1	2	3	4	5	6	7	8	9	10
Layer	(8/8)	(7/14)	(8/4)	(6/12)	(7/7)	(6/6)	(7/4)	(7/3)	(6/3)	(8/2)
1	1337	1146	2203	937	1251	1447	2061	2640	2673	3803
2	1133	1304	1739	1018	1042	1170	1725	2432	1890	**5724**
3	1054	991	2262	1021	1306	1330	1658	**3999**	**3975**	
4	1335	1245	**3613**	1052	1308	1332	**3427**			
5	1093	1027		1064	1317	**1177**				
6	1345	1295		1060	1317	**3702**				
7	1306	1301		1072	**3240**					
8	**3169**	1307		1071						
9		1307		1070						
10		989		1084						
11		1050		1330						
12		1321		**3998**						
13		1317								
14		**3521**								
Total	11,772	19,121	9817	15,777	10,781	10,158	8871	9071	8538	9527
Avg.	1472	1366	2454	1315	1540	1693	2218	3024	2846	4764

The sum of the reinforcement force for all layers in a given case was computed and is plotted in Figure 65 for each case as identified by rank. In general, the results show that more reinforcement tensile force is mobilized for higher ranked configurations, which means that more of the reinforcement is actively engaged in providing stability to the slope. Conversely, for lower ranked configurations (i.e., poorer performance), failure occurred between the reinforcement sheets for wide reinforcement spacing, and below the depth of reinforcement for cases of shallow reinforcement depth, meaning the reinforcement had no opportunity to stabilize the slope. These results are in contrast to those obtained by the limit equilibrium method (ReSSA), which showed that a factor of safety of 1.3 was obtained for rotational failures with slip circles initiating along the roadway bench when the sum of the reinforcement tensile strength was approximately 10,000 lb/ft, regardless of the number of reinforcement layers used (see Table 16, Section 4.2).

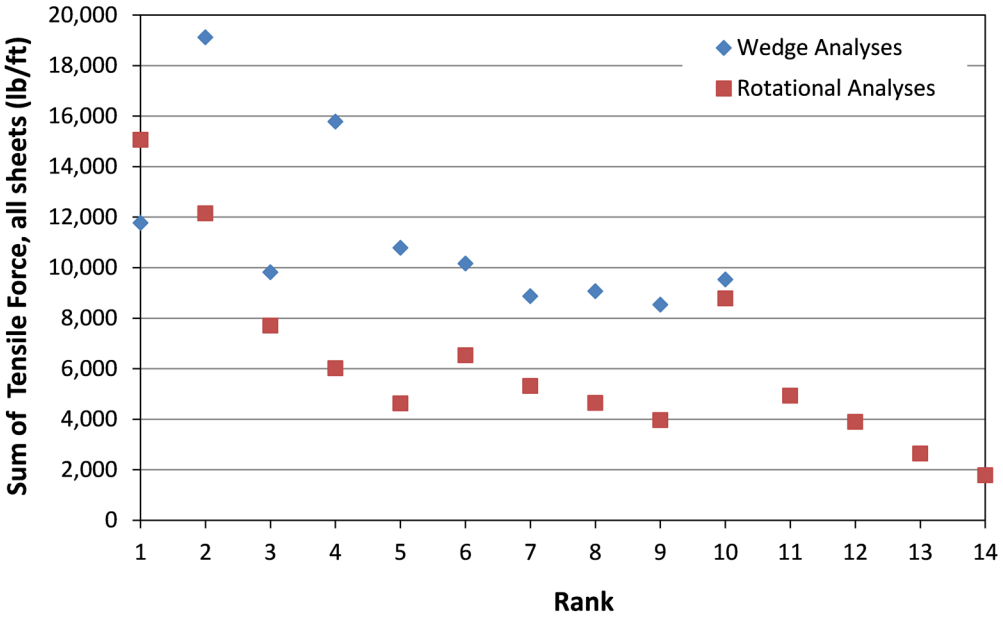

Figure 65: Total reinforcement tensile strength results from FLAC/Slope analyses for Slope I.

The maximum tensile force developed in the reinforcement layers for all cases examined is shown in Figure 66. The results indicate that the maximum tensile force developed in the layers of reinforcement is not significantly different for cases centered around the optimal case even though the number of reinforcement layers is different between these cases. The most economical design will be the one using the fewest layers of reinforcement while having acceptable performance. For rotational failures, cases with a rank of 5 or less were considered acceptable. The case corresponding to rank 5 used 3 layers of reinforcement at a spacing of 2 ft. Cases ranking 1–4 used from 4 to 12 layers of reinforcement. The case corresponding to rank 2 was 1 ft shallower but used 10 layers of reinforcement. The case corresponding to rank 5 is therefore considered the "best" case. The ReSSA analysis for this case showed that 10,000 lb/ft of total reinforcement strength was needed for a FS=1.3. For three layers of reinforcement, the tensile strength of the geosynthetic would therefore need to be 3330 lb/ft; however, the FLAC/Slope analyses showed that only 1,900 lb/ft of strength was needed for this same configuration.

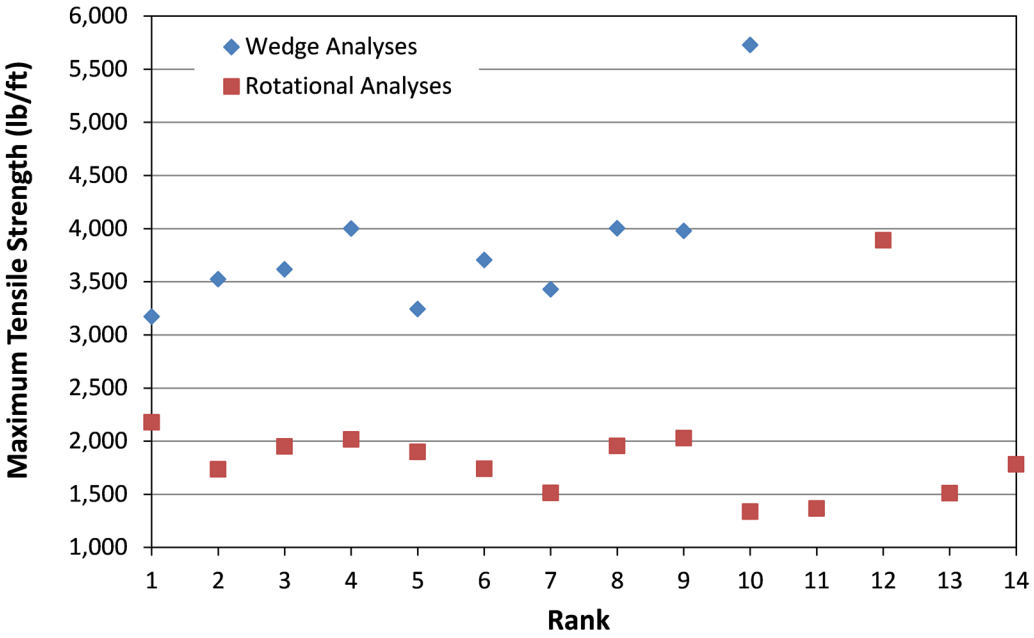

Figure 66: Maximum reinforcement tensile strength results from FLAC/Slope analyses for Slope I.

For wedge failures, cases with a rank of 3 or less were considered acceptable. This case used 4 layers of reinforcement at a spacing of 2 ft. Cases for rank 1 and 2 used 8 and 14 layers of reinforcement and a spacing of 1 and 0.5 ft, respectively. The case corresponding to rank 3 is therefore considered "best". A minimum reinforcement tensile strength of 3,600 lb/ft is required according to the data shown in Table 22.

These results show a discrepancy between information obtained from ReSSA and FLAC/Slope concerning required reinforcement tensile strength. For the case of a rotational failure, ReSSA overestimated the required tensile strength. Had information from ReSSA been used for the wedge failure, it would have shown an underestimate of the required tensile strength. FLAC/Slope shows the maximum tensile force occurring in a single reinforcement sheet, which can be considerably larger than the average tensile force in all the sheets. This is believed to be a reflection of the mechanics of the slope being modeled and how localized shear mechanisms place different requirements on reinforcement sheets at different levels. The limit equilibrium method associated with ReSSA is not sophisticated enough to show these mechanisms; therefore, FLAC/Slope will be used to specify the required reinforcement tensile strength when developing general guidelines for deep patch design and reinforcement configurations.

5.4 TENSILE STRENGTH LIMITATIONS BASED ON PULLOUT

Resistance to tensile forces generated in each layer of the reinforcement is achieved through pullout interaction between the geosynthetic and the confining soil. The length of the reinforcement embedded beyond X_c (L_e) should be sufficiently long to ensure adequate pullout resistance in the stable/native embankment material. Musser and Denning (2005) suggests using L_e at least as long as X_c to provide adequate pullout resistance. Equation 2 (from Equation 4-36, Berg et al., 2009a) that is used to estimate the embedment length of the reinforcement (L_e), requires a minimum embedment length of 3 feet. For the purposes of this project and the development of a new design methodology for deep patches, an embedment length of 10 feet beyond X_c was assumed for geogrids and 15 feet beyond X_c was assumed for geotextiles. This assumption seems to be in line with typical deep patch construction practices where narrow failures (smaller X_c) are constructed across about half the total road width, while wider failures (larger X_c) are constructed as a full-width deep patch. Based on this assumption, Equation 2 was rearranged to solve for the maximum tensile strength that can be attained in the geosynthetic (Equation 3). The relationship of T_{nom} to depth of the deep patch is shown in Figure 67, based on the assumed values listed in Table 23 for geogrids and geotextiles.

$$L_e \geq \frac{T_{nom} FS}{\phi F^* \alpha \sigma'_v R_c C} \geq 3\,ft$$ **Equation 2**

T_nom is the nominal strength of the geogrid reinforcement.

FS is the factor of safety; FS = 1.5 as recommended in Appendix F.7 in Berg et al., 2009b.

ϕ is the resistance factor for soil reinforcement pullout (ϕ= 0.8 for geotextiles orϕ = 0.9 for geogrids; see Table 4.7 in Berg et al., 2009a).

F* is the pullout resistance factor, and can be conservatively estimated as $2/3\tan\phi_{peak}$, where ϕ_{peak} is the peak friction angle of the soil, see Chapter 3 of Berg et al., 2009a.

α is a scale effect correction factor to account for a non-linear stress reduction over the embedded length of the reinforcement (0.6 for geotextiles, 0.8 for geogrids); see Table 3-6 in Berg et al., 2009a.

σ_v' is the effective vertical stress at the interfaces between the soil and the reinforcement. Use σ_v' for the uppermost layer of reinforcement to be conservative.

R_c is a coverage ratio used to relate the force per unit width of discrete reinforcement to the force per unit width required across the entire structure; R_c = 1.0 for full-width reinforcement having 100 percent coverage.

C is the reinforcement effective unit perimeter; C = 2 for strips and grids.

$$T_{nom} = \frac{L_e \phi F^* \alpha \sigma'_v R_c C}{FS}$$ **Equation 3**

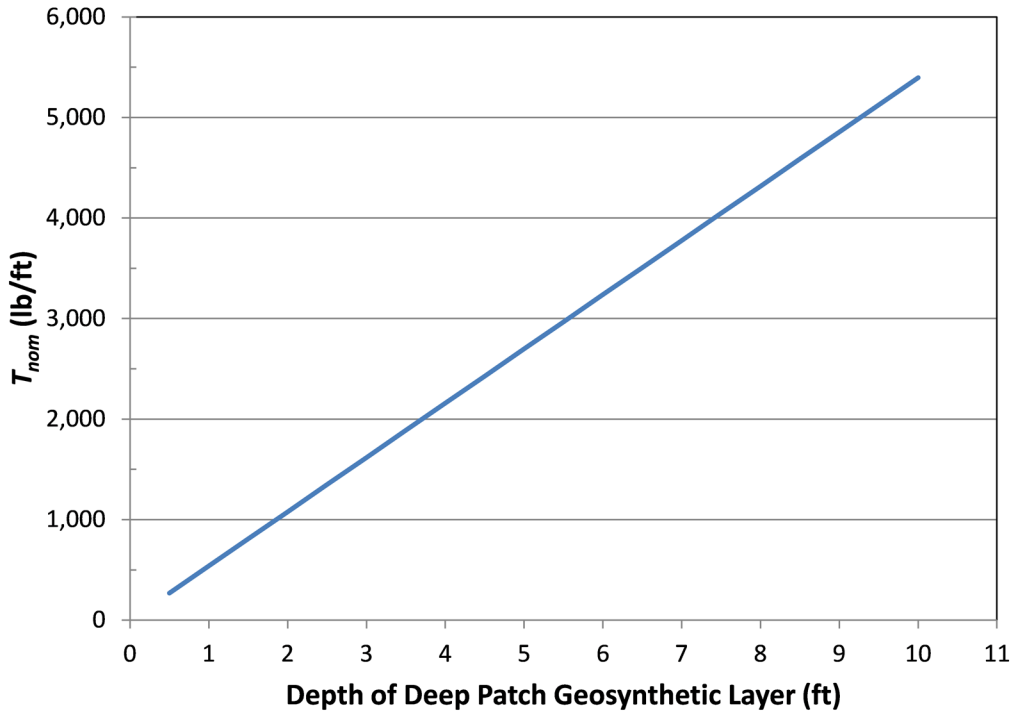

Figure 67: Relationship of nominal tensile strength of the reinforcement and depth of the layer.

Table 23: Definitions of Variables Used in Equation 3 to Generate Figure 67

Variable	Geogrids	Geotextiles
FS	1.5	1.5
L_e	10 ft	15 ft
ϕ	0.9	0.8
$F^*=2/3\tan\phi_{peak}$; $\phi_{peak}=$	34°	34°
α	0.8	0.6
$\sigma_v'=\gamma^*z;\gamma=$	125lb/ft^3	125lb/ft^3
R_c	1.0	1.0
C	2	2

The anticipated tensile forces to be mobilized in each layer of the best deep patch configurations for the Slope I geometry were evaluated to ensure adequate pullout resistance. Specifically, Case 5 based on the rotational analysis (Table 21) and Case 3 based on the wedge analysis (Table 22) were selected because they were the most efficient cases determined from the analysis. Case 5 – rotational was a 6-ft deep patch with 3 layers and Case 3 – wedge was an 8 ft deep patch with 4 layers. A comparison between the anticipated mobilized tensile force, T_{mob}, and the resistance available based on pullout, T_{nom} from Equation 3 or Figure 67, is presented in Table 24. In both cases T_{mob} exceeds T_{nom} in the top layer of reinforcement. The FLAC/Slope models for these two cases were adjusted and reanalyzed using reduced tensile capacities of the geosynthetic to match what is available based on T_{nom}. In comparing the results from both cases, the velocity vectors are not dramatically different from one another and both indicate acceptable performance (see Figure 68 and Figure 69). Therefore, the remaining analyses conducted as part of this research compared the anticipated mobilized tensile force in the geosynthetic to its associated pullout resistance based on a 10-foot embedment length for geogrids or a 15-foot embedment length for geotextiles, to ensure adequate performance.

Table 24: Summary of Tensile Strength Comparisons for Case 5 – Rotational and Case 3- Wedge

Layer Depth (ft)	Case 5 - Rotational		Case 3 - Wedge	
	T_{mob}(lb/ft)	T_{nom}(lb/ft)	T_{mob}(lb/ft)	T_{nom}(lb/ft)
2	1394	1080	2203	1080
4	1328	2158	1739	2158
6	1898	3238	2262	3238
8			3613	4317

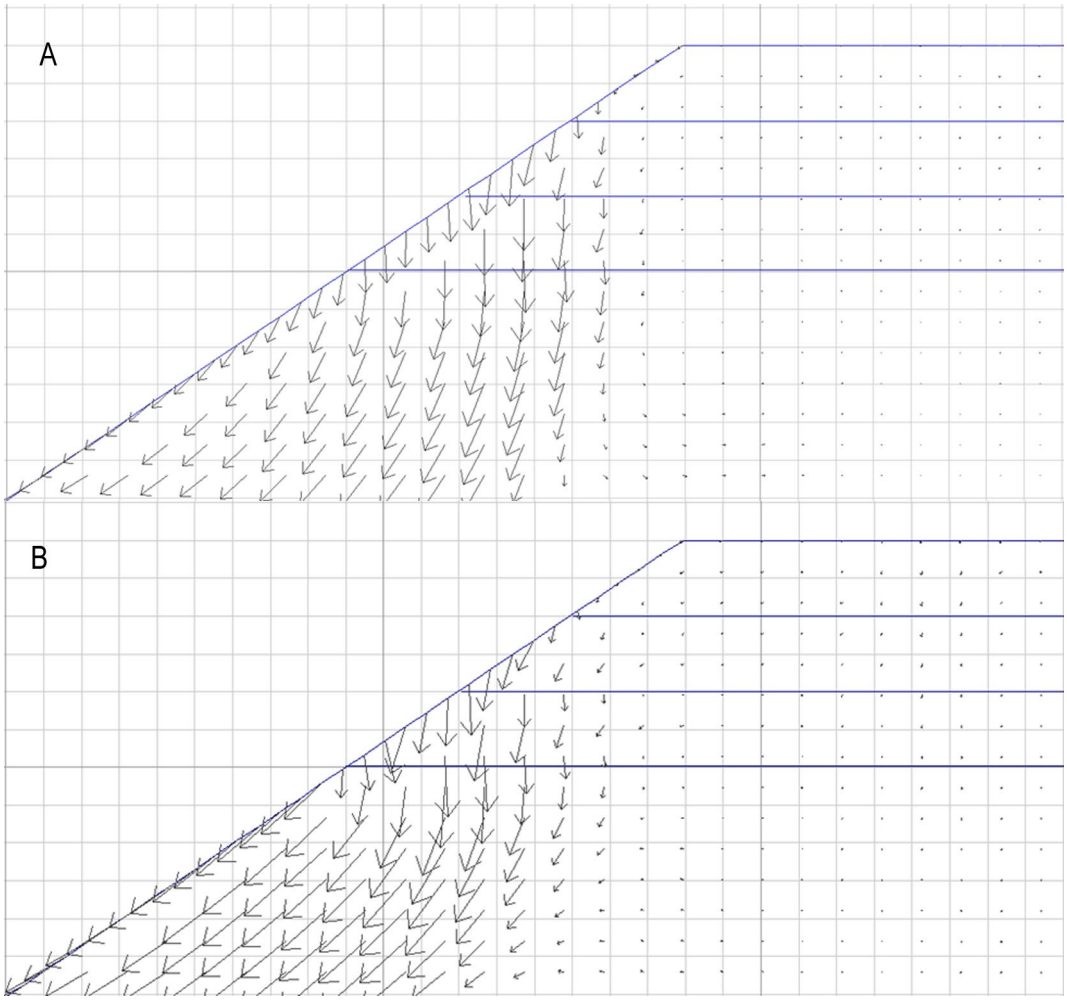

Figure 68: Velocity vector plots for Case 5 – Rotational before and after T_{nom} adjustment: a) original analysis, b) adjusted tensile strength analysis.

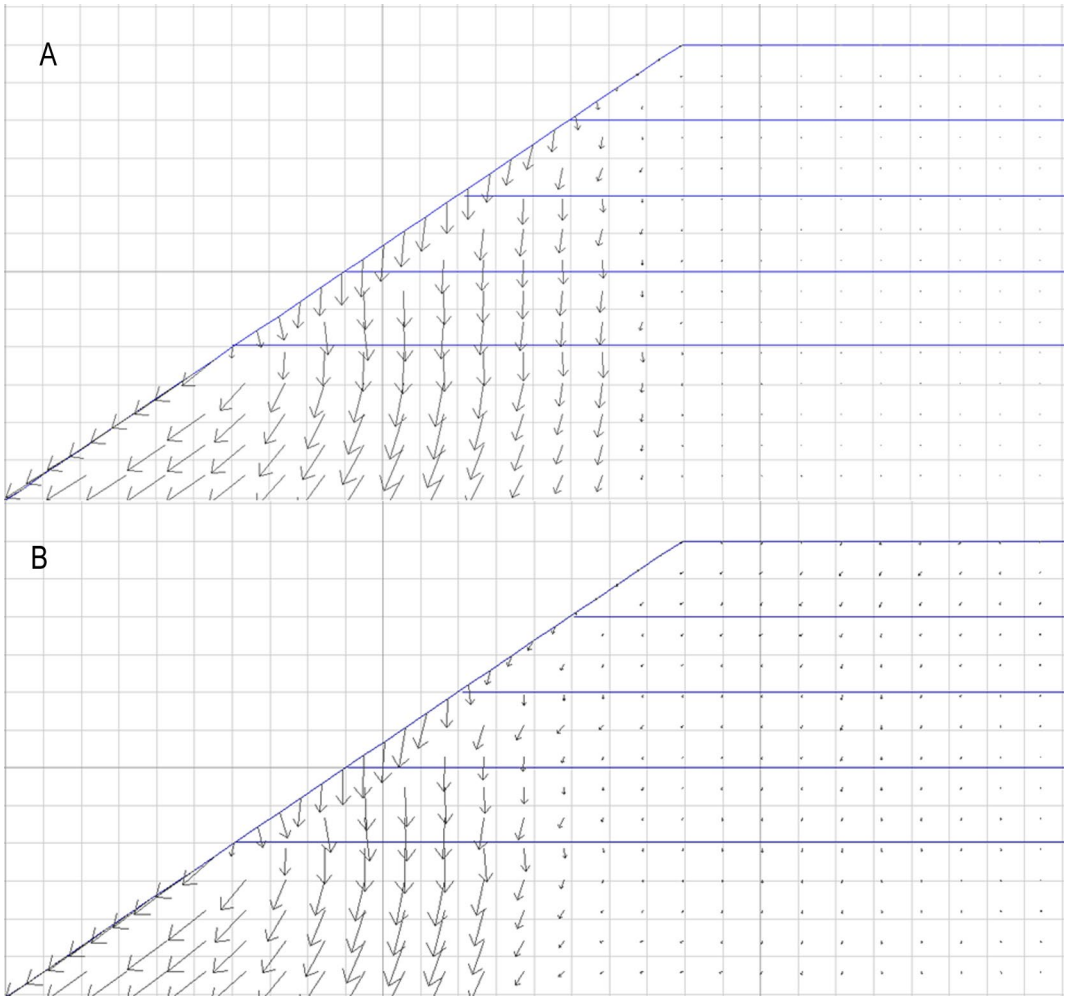

Figure 69: Velocity vector plots for Case 3 – Wedge before and after T_{nom} adjustment: a) original analysis, b) adjusted tensile strength analysis.

5.5 SUMMARY

In this section, the Slope I geometry was analyzed using FLAC/Slope for both rotational and wedge-type failures. Previously in Section 3.3, the performance of FLAC/Slope for unreinforced slopes was examined and shown to produce comparable factors of safety to ReSSA and slightly different failure surfaces. Additional information provided by FLAC/Slope on patterns of material movement at failure (expressed by velocity vector plots) was also illustrated.

For reinforced slopes, Chapter 4 illustrated limitations associated with the limit equilibrium method when used to determine optimal reinforcement configurations for the deep patch repair. With the design philosophy for a deep patch repair being

one where material movement and failure should be confined to material on or below the slope face and not below the roadway bench, velocity vector and shear strain rate contour information from FLAC/Slope was used to examine a number of reinforcement configurations for the Slope I geometry. This examination resulted in acceptable and unacceptable designs based on the number of layers and their performance ranking. An acceptable design was defined as the point where material movement and failure did not extend onto or below the roadway bench. While this decision process was dependent on visual assessments of the vector velocity plots, the methodology resulted in clear bounds in terms of depth of the reinforced mass and number of reinforcement layers of acceptable and unacceptable performance. The examples illustrated in this chapter showed that for a given slope geometry, several reinforcement configurations can result in acceptable performance. This methodology formed the basis for the parametric study described in Chapter 6.

The examination of optimal reinforcement configuration for the Slope I geometry for both rotational and wedge type failures illustrated a greater reinforcement demand for wedge type failures. This is primarily due to the larger amount of weak soil involved in the failure process as seen by larger values of X_c and is taken into account in the design method by developing charts in terms of X_c.

An evaluation of tensile force mobilized in the reinforcement layers for the cases examined showed that the maximum tensile force mobilized is as much as 180 percent above the average tensile force mobilized for all layers. Since most designs will use the same geosynthetic type for all layers and be chosen to carry the maximum tensile force expected, there will be greater excess capacity for those cases showing greater differences between the maximum and average reinforcement tensile forces. This is taken into consideration when a "best" reinforcement configuration is chosen in Chapter 6. The results also showed a discrepancy between FLAC/Slope and ReSSA for required tensile force, and it is argued that FLAC/Slope provides the more realistic reinforcement strength requirement for the deep patch repair configuration. In Chapter 6, mobilized tensile force results from FLAC/Slope are compiled and used for developing design recommendations.

Pullout resistance was evaluated with respect to the anticipated tensile forces generated in each layer of reinforcement. For the specific cases analyzed, it was noted that the tensile forces in the upper layers of reinforcement had exceeded the pullout capacity. The best FLAC/Slope configurations in Chapter 6 will be further evaluated to ensure adequate pullout resistance assuming a 10-foot embedment for geogrids or a 15-foot embedment for geotextiles.

6 PARAMETRIC STUDY USING FLAC/SLOPE

In Chapter 5, FLAC/Slope was used to analyze slope configurations that require a deep patch repair to make recommendations for reinforcement configurations and determine required tensile strengths that resulted in acceptable performance. This methodology can be summarized as follows:

Step 1: Determine soil strength parameters—Use ReSSA for rotational failure mode or Equation 1 for wedge failure mode to determine ϕ and c for an unreinforced slope configuration having a factor of safety of 1.0.

Step 2: Determine X_c—Use FLAC/Slope to determine X_c from shear strain contour plots of unreinforced models for both rotational and wedge failure modes.

Step 3: Analyze several deep patch configurations—Create a number of FLAC/Slope model cases by varying the depth of reinforcement, the number of reinforcement layers and the spacing of the reinforcement while specifying a reinforcement tensile strength that is sufficiently high to prevent yield.

Step 4: Examine results to determine acceptable performance threshold—For each case analyzed, examine velocity vector plots and shear strain rate contour plots from the FLAC/Slope models to determine reinforcement configurations resulting in acceptable performance. Acceptable performance is determined using visual assessments of the slope failure modes (i.e., material movement and failure surfaces). Failure surfaces and gross material movement should be confined to material on and below the slope face and not extending up to the roadway bench or involving material below the bench. For each case examined, document the maximum tensile force developed in the reinforcement.

Step 5: Suggest "best" deep patch reinforcement configuration—Suggest a most efficient reinforcement configuration based on cases giving acceptable performance while minimizing the number of layers necessary to achieve the required tensile strength.

Step 6: Check the "best" deep patch configuration with reinforcement capacities governed by pullout considerations.

This methodology was followed to analyze deep patches on two slope angles (β = 34 and 39 degrees), for both rotational and wedge-type failures. For each slope angle, a number of cases corresponding to different values of slope height H, fill slope angle α and different combinations of fill strength properties leading to different values of X_c were examined. The cases examined are a subset of those analyzed in Section 4.1 for unreinforced slopes at a FS = 1.0 using the limit equilibrium program ReSSA and were selected to represent a distribution of points lying on a diagram of X versus X_c

as previously presented in Figure 55. For each case, the steps described above were followed and are summarized in the following sections in charts that provide information on reinforcement requirements for a given set of slope parameters.

6.1 REINFORCEMENT REQUIREMENTS FOR $\beta = 34°$ SLOPES

The slope geometry and soil parameters for the subset of cases examined for optimal deep patch designs are listed in Table 25 for rotational failures and Table 26 for wedge failures. For the rotational failure analyses on unreinforced slopes evaluated with ReSSA, the ϕ and c listed in Table 25 are for the weak soil properties that result in a FS = 1.0. For the wedge failure analyses, the c listed in Table 26 is for the slip plane soil having a $\phi = 0$ and within which wedge failure occurs. Analysis of the unreinforced slopes for rotational failures produced values of X_c listed previously in Section 4.1. In Section 4.2 it was shown that values of X_c produced by FLAC/Slope differed from those produced by ReSSA. Since FLAC/Slope is being used to determine reinforcement depth, spacing and required tensile strength, values of X_c were visually determined from FLAC/Slope for both rotational and wedge failure analyses for consistency. This was accomplished by analyzing all the cases shown in Table 25 and Table 26 for an unreinforced slope using FLAC/Slope and estimating the value of X_c from shear strain rate contour plots.

As previously described in Section 4.1, values of X and X_c were selected as the best parameters to demonstrate the relationship between the geometry of a particular slope configuration (represented by X) and the extent of the sliding mass (represented by X_c). A plot of values of X versus X_c for all the rotational cases listed in Table 25 for $\beta = 34°$ is shown in Figure 70 with data point labels indicating the depth of the reinforcement followed by the number of equally spaced layers within the reinforced depth. The dotted and dashed lines on this diagram, and the others to follow, are the same as those used previously in Figure 55. These data labels correspond to the reinforcement configuration judged to be "best" in terms of the criteria in Chapter 5. In making this determination, a number of reinforcement configurations were analyzed for each case listed in Table 25 and Table 26. Data points with an asterisk denote cases where a secondary configuration, always involving a shallower reinforcement depth and reduced reinforcement spacing, was equally suitable. The results show a consistent trend of greater reinforcement requirements as X and X_c increase. As discussed previously in Chapter 5, this is due to a greater volume of soil engaged in the failure process as X and X_c increase. It should be noted that in this figure, all cases are included, even those having very low values of friction angle for the weak soil unit. These values have been included since they still tend to support the observed trends.

Table 25: FLAC/Slope Model Parameters for Rotational Failure Analyses, β = 34°

Run	Case	α(°)	H(ft)	ϕ(°)	c(psf)	X(ft)	X_c(ft)
1	5	20	10	3.8	99	12.7	3.3
3	8	26.8	60	15.4	224	30.0	10.1
3	9	26.8	60	23.1	116	30.0	8.1
3	10	26.8	60	28.5	50	30.0	5.1
5	2	25	10	0	85.4	6.6	2.14
6	6	30	60	0	277	15.0	4.9
6	9	30	60	23.1	82	15.0	2.9
7	6	23.1	35	0	341	30.0	9.5
7	7	23.1	35	7.7	250	30.0	8.8
7	8	23.1	35	15.4	163	30.0	9
7	10	23.1	35	25.5	60	30.0	6.5
9	5	27.5	35	0	236	15.3	5.5
9	7	27.5	35	15.4	120	15.3	4.8
9	8	27.5	35	24.5	55	15.3	6.1
11	1	29.9	30	20	55	7.8	3.2
11	2	29.9	30	16	73	7.8	2.6
12	1	30	40	20	72	10.0	3.6
12	2	30	40	16	95	10.0	3.4
13	1	26.2	20	20	55	11.0	3
13	2	26.2	20	16	74	11.0	3.8
14	1	29.3	40	20	80	12.0	3.8
14	2	29.3	40	16	106	12.0	4.2
15	1	27.2	30	20	77	14.0	4.7
15	2	27.2	30	16	103	14.0	4.5
16	1	27.4	40	20	100	18.0	5.4
16	2	27.4	40	16	134	18.0	6.2
17	1	24.3	30	20	93	22.0	5.4
17	2	24.3	30	16	127	22.0	5.9
18	1	27.8	60	20	144	25.0	9.4
18	2	27.8	60	16	194	25.0	8.4
19	1	24.7	40	20	121	27.5	8.6
19	2	24.7	40	16	165	27.5	7.5

Table 26: FLAC/Slope Model Parameters for Wedge Failure Analyses, β= 34°

Run	α(°)	H(ft)	c(psf)	X(ft)	X_c(ft)
1	20	10	92.5	12.7	4.5
3	26.8	60	380	30.0	14.1
5	25	10	74	6.6	2.7
6	30	60	234	15.0	5.9
7	23.1	35	289	30.0	11.5
9	27.5	35	204	15.3	6.7
11	29.9	30	121	7.8	3.1
12	30.0	40	156	10.0	3.8
13	26.2	20	134	11.0	4.8
14	29.3	40	180	12.0	5.1
15	27.2	30	182	14.0	5.6
16	27.4	40	238	18.0	7.4
17	24.3	30	233	22.0	9.3
18	27.8	60	339	25.0	10.4
19	24.7	40	301	27.5	12.2

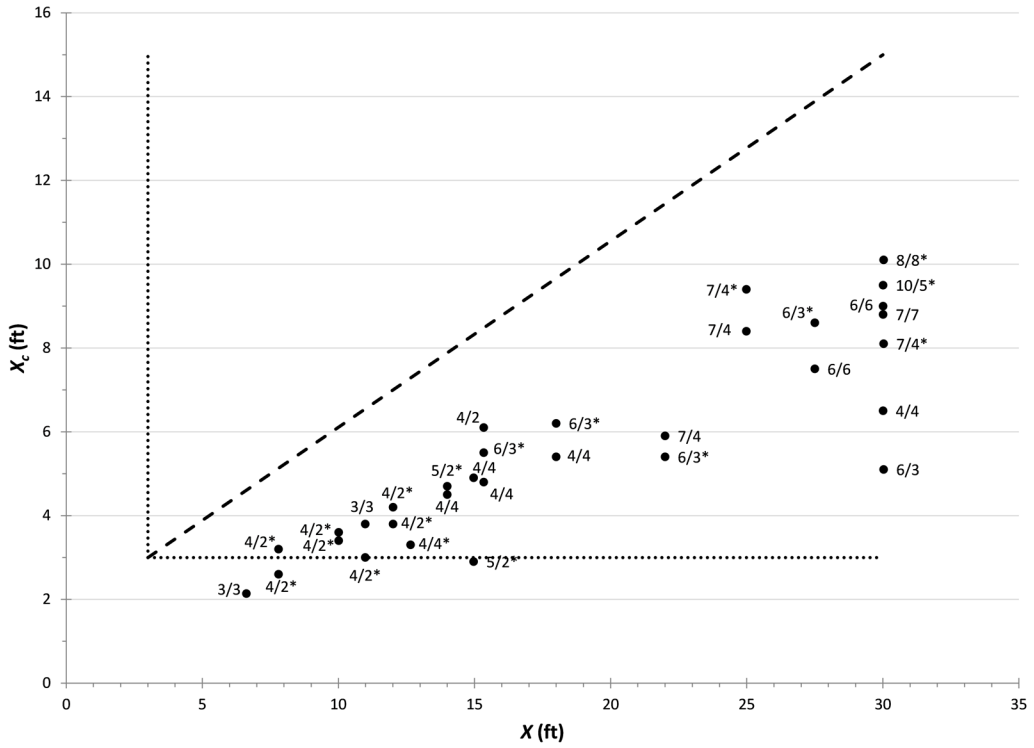

Figure 70: Best deep patch configurations (depth / # of layers) for β = 34°, rotational failure mode.

A similar plot of X versus X_c for the wedge-type failure cases listed in Table 28 is shown in Figure 71. These results indicate that, overall, wedge-type failures produce greater values of X_c for corresponding values of X. In general, the points shown in Figure 71 appear to follow the same trend as that seen in Figure 70 suggesting that a single diagram may be used to represent reinforcement requirements for both rotational and wedge failures. To examine this, points from Figure 70 and Figure 71 where plotted together (Figure 72, where depths are shown near each data point). For this plot, only those cases with a 1 ft reinforcement spacing are included. The results show a reasonably consistent trend of increased depth of reinforcement with increasing X_c and X. This suggests that this diagram can be used to determine required depth of the reinforced mass for a 1 ft reinforcement spacing, which is achieved by drawing lines showing proposed zones of required depth of reinforcement for a reinforced mass with a 1 ft reinforcement spacing. The lines were drawn conservatively; non-conservative outliers are nearly always associated with unrealistically low ϕ soils.

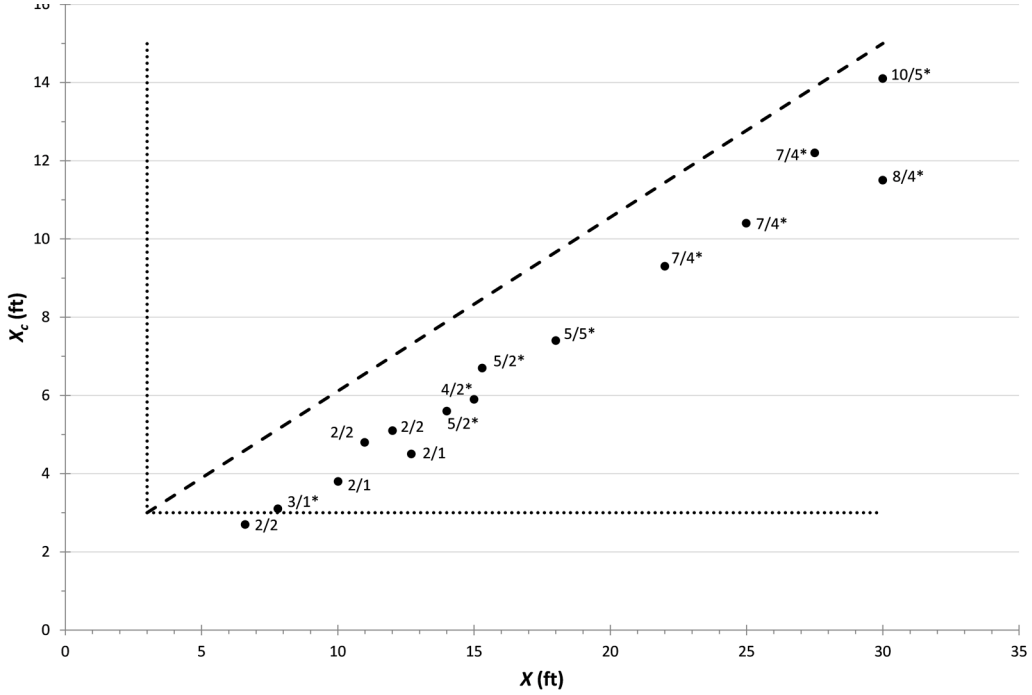

Figure 71: Best deep patch configurations (depth/# of layers) for β = 34°, wedge failure mode.

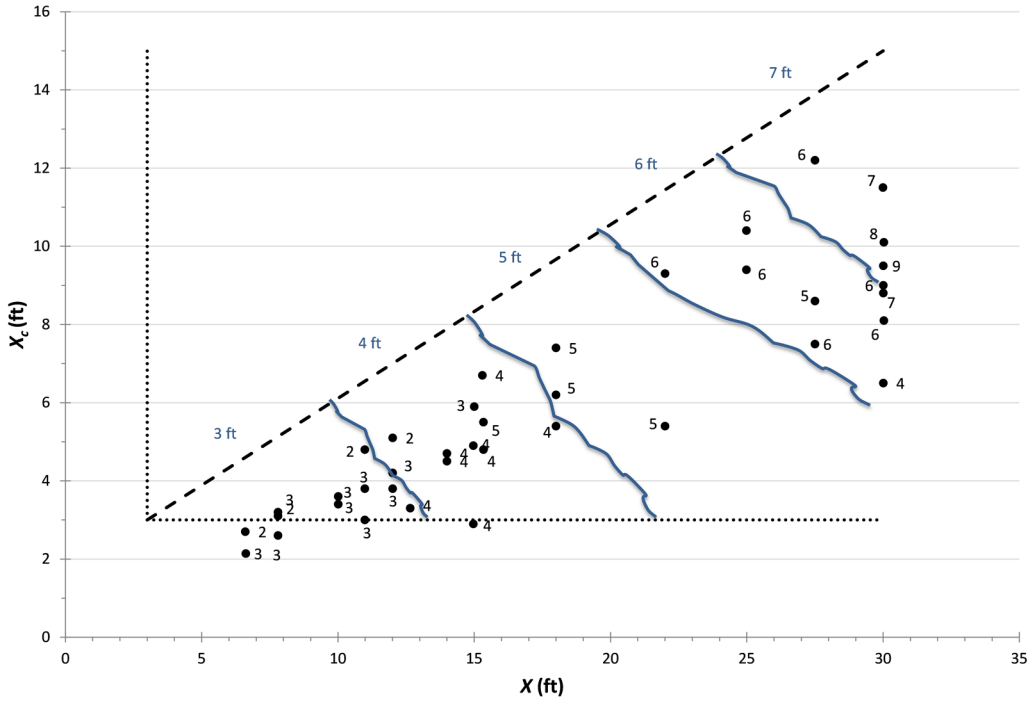

Figure 72: Best deep patch configurations for β = 34°, rotational and wedge failure modes, 1 ft reinforcement spacing only.

Cases in Table 25 and Table 26 (i.e., rotational and wedge-type failures) corresponding to best configurations with a reinforcement spacing greater than 1 ft are shown in Figure 73. The majority of these cases correspond to a 2 ft reinforcement spacing, although several cases have spacing as low as 1.75 ft and a few have 2.5 ft spacing. The trend in this data is not as consistent as that shown in Figure 72 and therefore lines delineating zones of depth of reinforcement are more conservatively chosen. This is most likely due to points of reinforcement spacing other than 2 ft being shown. Given the fewer number of points supporting this trend, it is proposed that this diagram represent required depth of reinforcement when only a 2 ft spacing is used; therefore, the required depths of reinforcement are shown in 2 ft delineations.

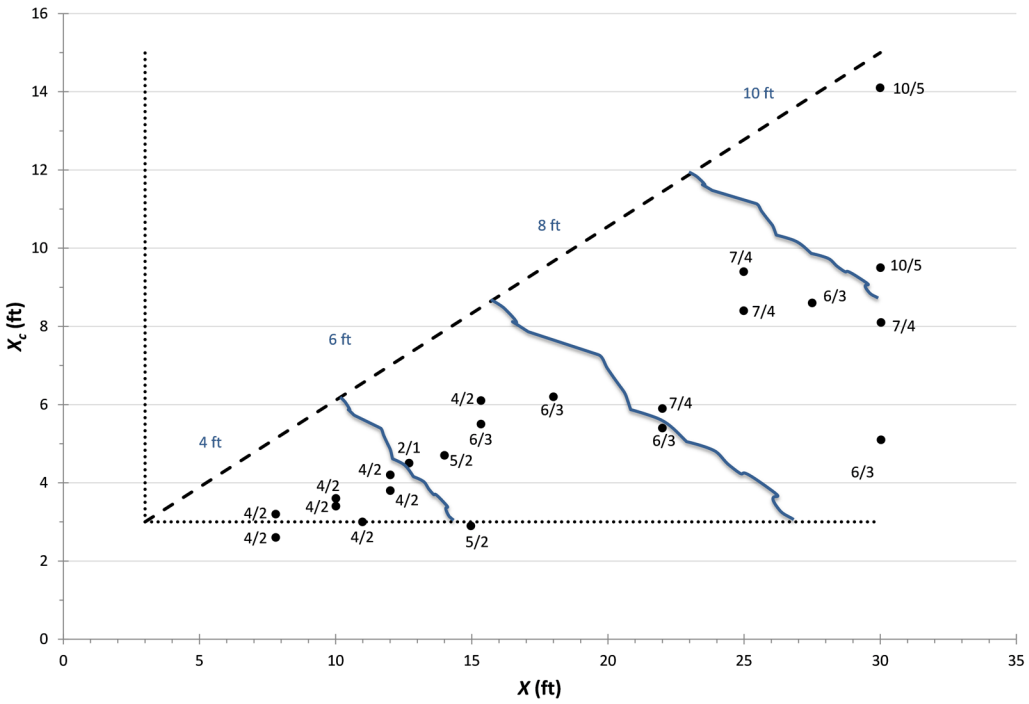

Figure 73: Best deep patch configurations (depth/# layers) for β = 34°, rotational and wedge failure modes, greater than 1 ft reinforcement spacing.

For the cases listed in Table 25 and Table 26 (for rotational and wedge-type failures, respectively), the maximum reinforcement force mobilized in any of the layers was documented for configurations with 1 and 2 ft reinforcement spacing. Assuming this force will represent the required reinforcement strength for all the reinforcement layers used for a particular case (i.e., only one type of geogrid strength will be specified), this value was multiplied by the number of layers used for that case to determine the total

required reinforcement tensile strength for a particular configuration. The maximum mobilized force in a particular layer was the basis for the total required strength in order to ensure all layers of reinforcement had sufficient capacity to avoid rupture. If the average mobilized force was used, then at least one layer would reach capacity and potentially rupture. X and X_c were previously selected as the best parameters to demonstrate the relationship between the geometry of a particular slope configuration (represented by X) and the extent of the sliding mass (represented by X_c). Because of this relationship, X and X_c are also directly related to the amount of reinforcement required (T_{req}). The relationship between X_c and T_{req}, however, showed less scatter so it was plotted with respect to the required reinforcement tensile strength, as shown in Figure 74 for 1 ft reinforcement spacing. Furthermore, measurements of X_c are easier to obtain in the field. A similar plot was made for 2 ft reinforcement spacing, and is shown in Figure 75. As expected, these diagrams show that the total required reinforcement strength increases as X_c increases. A polynomial best fit line is used to approximate the total required tensile strength for a given X_c. The equations for these lines and corresponding R^2 values are shown in each of these figures. This information, coupled with the information presented in Figure 72 and Figure 73, can be used to determine the depth of the deep patch and the required total reinforcement tensile strength for a particular reinforcement configuration.

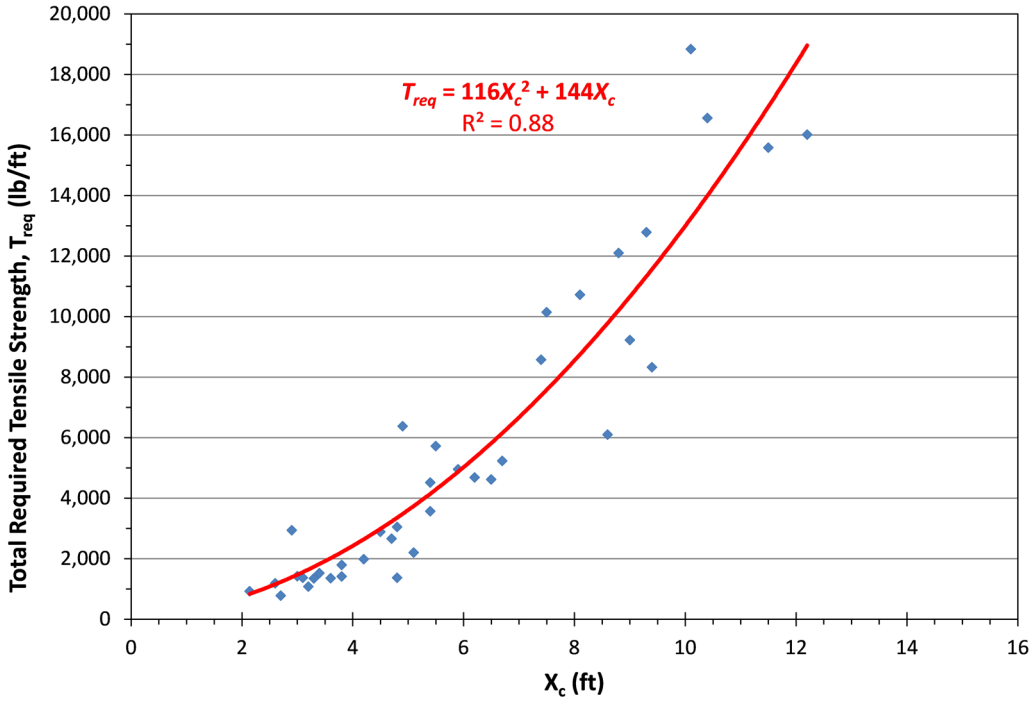

Figure 74: Required total reinforcement tensile strength as a function of X_c for $\beta = 34°$ and 1 ft reinforcement spacing (regression equation only valid for units of ft and lb/ft).

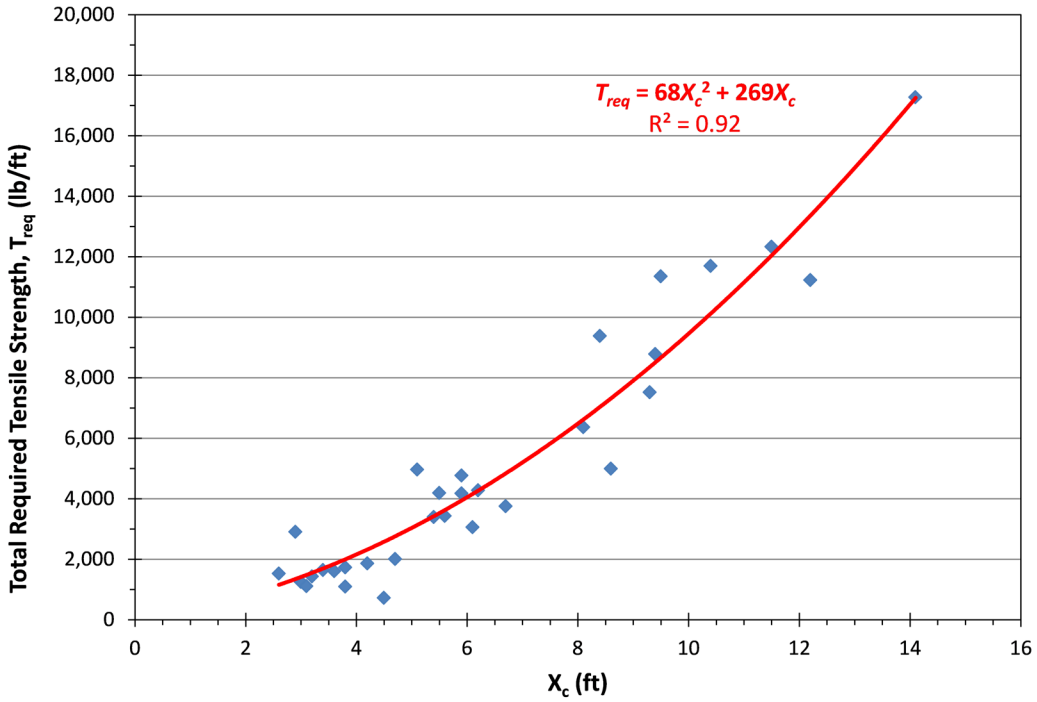

Figure 75: Required total reinforcement tensile strength as a function of X_c for β = 34° and 2 ft reinforcement spacing (regression equation only valid for units of ft and lb/ft).

6.2 REINFORCEMENT REQUIREMENTS FOR β= 39° SLOPES

A parametric study was also performed with a subset of cases for a fill slope angle of β = 39° (cases outlined in Table 27 and Table 28 for rotational and wedge failures modes, respectively). Recall that for these analyses, 1) the ϕ and c for the rotational failure analyses correspond to the unreinforced ReSSA analyses in which FS = 1.0, 2) the slip plane soil in the wedge analyses has ϕ = 0 and c corresponding to FS = 1.0 in Equation 1, and 3) X_c was determined by analyzing the shear strain contour plots from the unreinforced slope analyses in FLAC/Slope.

The "best" configurations are plotted on a diagram of X_c versus X for the rotational failure modes (Figure 76). As before, labels indicating the depth of reinforcement and number of layers are shown for each data point. The reinforcement spacing ranges from 0.5 ft to 2.3 ft with the majority having a spacing of 1 ft. Points with an asterisk denote cases where a secondary case, always involving a shallower reinforcement depth with reduced reinforcement spacing, was equally suitable. Again, the results show greater reinforcement requirements as X_c and X increase. It should be noted that in this figure, all cases are included, even those having very low values of friction angle for the fill. These values have been included because they tend to support the trend observed. Results from the wedge failures (Table 28) are shown in Figure 77. Again, as seen in the β =34° cases, values of X_c are toward the upper limit line for corresponding values of X.

Table 27: FLAC/Slope Model Parameters for Rotational Failure Analyses, $\beta = 39°$.

Run	Case	α(°)	H(ft)	ϕ(°)	c(psf)	X(ft)	X_c(ft)
1	5	20.0	10	9	100	15.1	3.8
3	6	30.0	60	0	525	29.8	12.2
3	7	30.0	60	8	405	29.8	11.7
3	10	30.0	60	33	53	29.8	11.4
5	3	25.0	10	0	118	9.1	3.2
6	6	34.0	60	0	337	14.9	6.3
6	8	34.0	60	18	178	14.9	6.0
6	9	34.0	60	26	105	14.9	5.8
7	6	24.1	30	0	366	30.0	10.2
7	7	24.1	30	10	254	30.0	9.8
7	8	24.1	30	17	180	30.0	8.9
8	1	37.1	35	0	88	3.1	0.7
9	5	33.3	35	0	220	10.0	4.2
9	8	33.3	35	25	72	10.0	4.3
11	2	24.1	20	8	185	20.0	6.4
11	4	24.1	20	21	92	20.0	5.4
12	1	21.9	20	0	265	25.0	8.0
12	3	21.9	20	14	150	25.0	6.7
12	5	21.9	20	25	68	25.0	4.9
13	1	28.2	35	0	265	22.0	8.5
13	3	28.2	35	12.5	160	22.0	8.0
13	4	28.2	35	20	103	22.0	7.5
14	2	29.8	35	6	258	18.0	7.4
14	4	29.8	35	23	110	18.0	6.5
15	2	34.0	20	10	83	5.0	2.1
16	3	34.0	28	18	83	6.9	2.9
17	2	33.0	40	10	190	12.2	5.2
17	3	33.0	40	20	120	12.2	5.1
18	2	32.0	38	10	200	13.9	5.8
18	3	32.0	38	20	125	13.9	6.0

Table 28: FLAC/Slope Model Parameters for Wedge Failure Analyses, $\beta = 39°$.

Run	α(°)	H(ft)	c(psf)	X(ft)	X_c(ft)
1	20.0	10	111	15.1	6.9
3	30.0	60	466	29.8	14.1
5	25.0	10	102	9.1	3.8
6	34.0	60	290	14.9	6.9
7	24.1	30	313	30.0	12.5
8	37.1	35	70	3.1	0.7
9	33.3	35	189	10.0	4.4
11	24.1	20	209	20.0	8.7
12	21.9	20	218	25.0	9.8
13	28.2	35	307	22.0	10.1
14	29.8	35	277	18.0	8.1
15	34.0	20	98	5.0	2.1
16	34.0	28	136	6.9	6.0
17	33.0	40	226	12.2	5.6
18	32.0	38	244	13.9	6.6

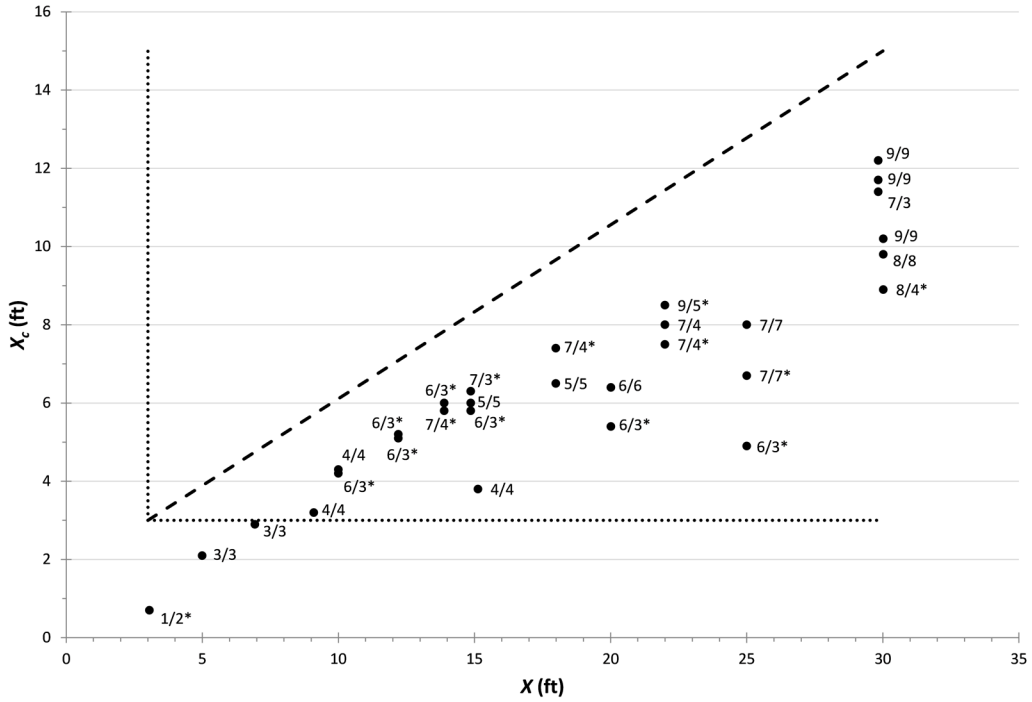

Figure 76: Best deep patch configurations (depth/# of layers) for β = 39°, rotational failure mode.

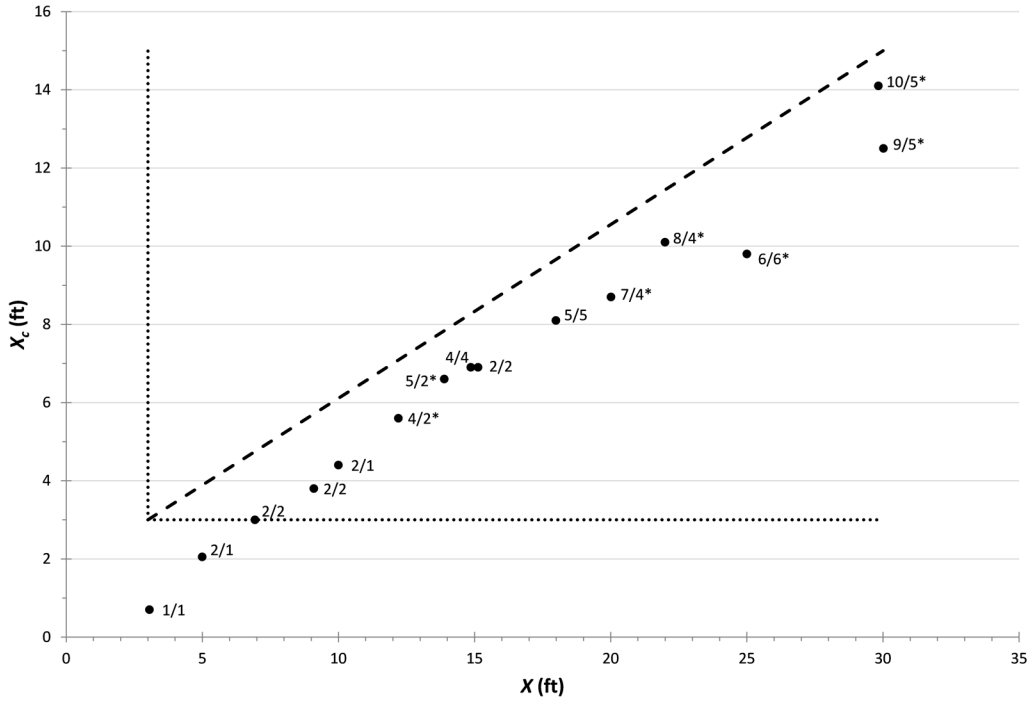

Figure 77: Best deep patch configurations (depth/# of layers) for β = 39°, wedge failure mode.

Similar to before, a plot combining rotational and wedge analyses showing acceptable deep patches with 1 ft reinforcement spacing is presented in Figure 78. Zones of proposed reinforcement depth at 1 ft intervals were conservatively selected. Reinforcement requirements for 2 ft reinforcement spacing are shown in Figure 79. In general, reinforcement requirements are greater for steeper slopes. For β = 34°, the range of proposed reinforcement depths was 3–7 ft (for 1-ft reinforcement spacing) and 4–10 ft (for 2-ft reinforcement spacing). For the steeper β = 39° slopes, the 1-ft spacing range peaked at 9 ft (compared to 7 ft) and the minimum acceptable reinforcement depth at 2-ft spacing was 6 ft (compared to 4 ft).

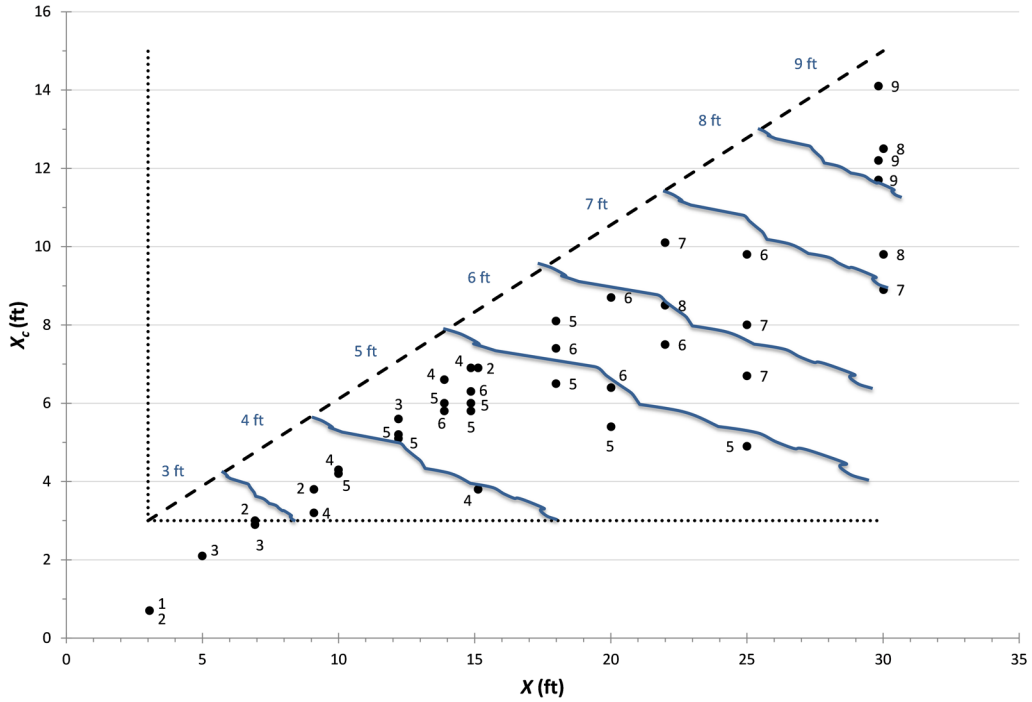

Figure 78: Best deep patch configurations for β= 39°, rotational and wedge failure modes, 1 ft reinforcement spacing only.

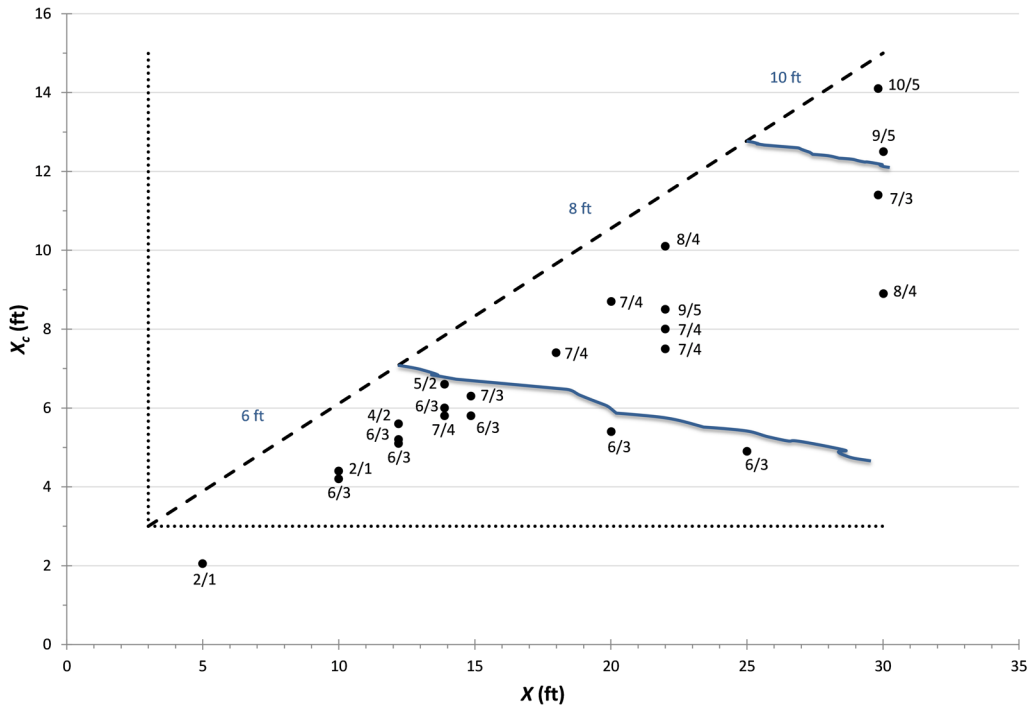

Figure 79: Best deep patch configurations (depth/# layers) for β = 39°, rotational and wedge failure modes, greater than 1 ft reinforcement spacing.

The maximum reinforcement force mobilized in any of the layers was documented for the β = 39° cases listed in Table 27 and Table 28 (for the rotational and wedge-type failures). Again, the maximum mobilized force was multiplied by the number of reinforcement layers to determine T_{req}. As before, X_c is plotted with respect to T_{req} to determine the required total tensile strength of the reinforcement for any X_c, as shown in Figure 80 for 1 ft and Figure 81 for 2 ft reinforcement spacing. The equations for these lines are shown in each of these figures.

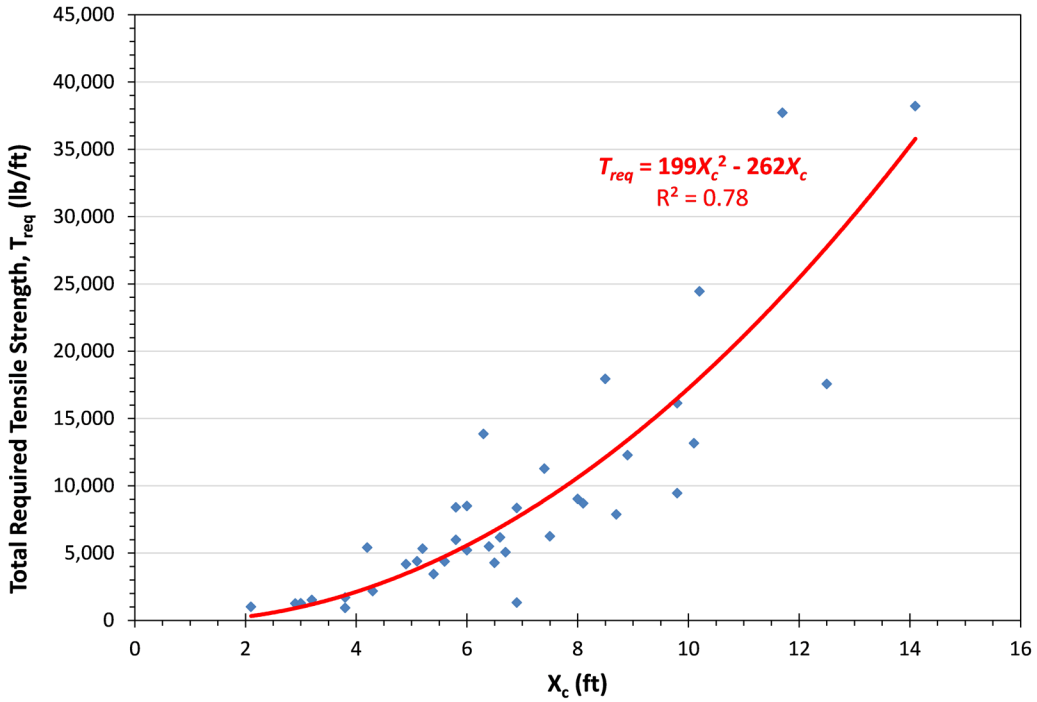

Figure 80: Required total reinforcement tensile strength as a function of X_c for $\beta = 39°$ and 1 ft reinforcement spacing (regression equation only valid for units of ft and lb/ft).

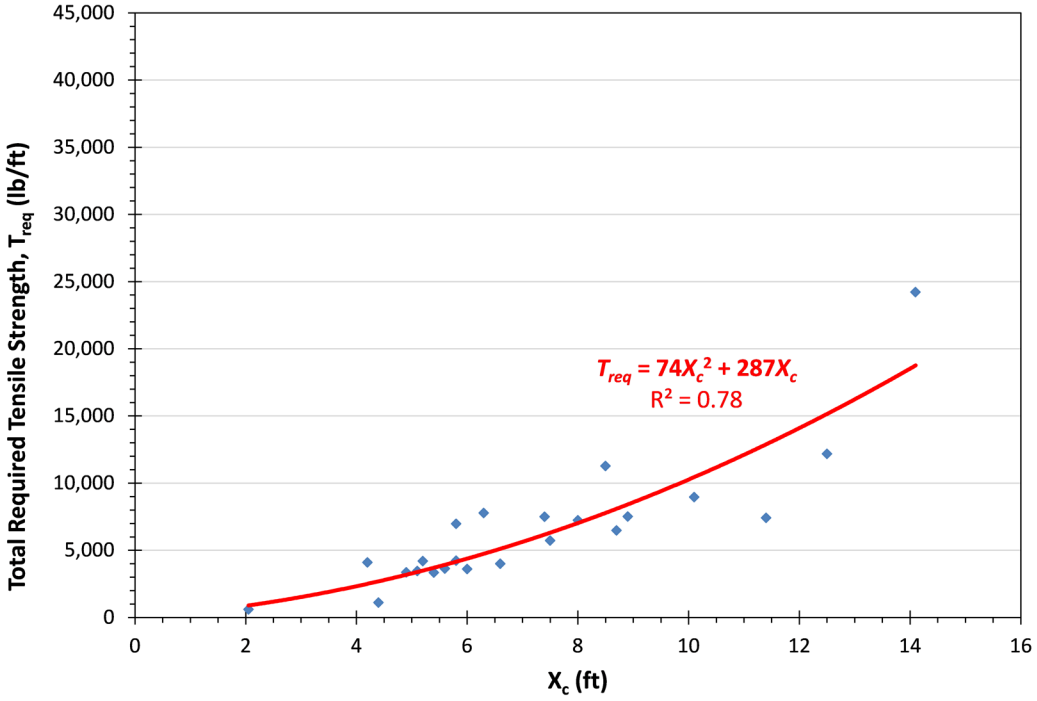

Figure 81: Required total reinforcement tensile strength as a function of X_c for $\beta = 39°$ and 2 ft reinforcement spacing (regression equation only valid for units of ft and lb/ft).

6.3 SUMMARY

In this chapter, a number of cases corresponding to different slope geometries, weak soil strengths, and rotational versus wedge failures were analyzed using the finite difference program FLAC/Slope. Each case was analyzed for a variety of different reinforcement configurations to determine the "best" reinforcement configuration. In general, these results agreed with the findings from Chapter 5, which showed that reinforcement spacing ranging from 0.5 to 2 feet were most effective. From these analyses, results were presented on diagrams of X versus X_c. Presentation of the results in this format allowed the diagram to be divided into regions corresponding to minimum requirements of reinforcement depth and spacing. These diagrams are used to develop a chart based design method, which is presented in Chapter 9. For the cases analyzed, the maximum tensile force mobilized in any of the layers of reinforcement was documented. This individual reinforcement layer force was multiplied by the number of layers of reinforcement for the corresponding configuration, which was plotted against the parameter X_c. The maximum mobilized tensile force was used to determine the total required force to ensure none of the layers would rupture. The resulting diagrams are used as part of the chart based design method to determine the required tensile strength of the reinforcement for the particular design.

7 THREE-DIMENSIONAL FINITE DIFFERENCE ANALYSIS

A three-dimensional analysis program (FLAC3D) was used to evaluate the effect of biaxial versus uniaxial geogrids on the behavior of deep patches and the need for anchoring the ends of the reinforcement. The material elements and model properties used for the geosynthetics, the configuration of the three-dimensional slopes examined, and a summary of these analyses is detailed in this chapter.

7.1 GEOSYNTHETIC ELEMENTS AND PROPERTIES

FLAC3D uses "geogrid" structural elements to model geosynthetics. The elements are 3-noded membrane elements, which develop resistance in tension while having no resistance in bending. The material models available for these elements are isotropic or orthotropic linear elastic models with no failure limit. Interface surfaces are used to model shear resistance developed between the geosynthetic and surrounding soil as relative motion occurs between them.

Biaxial and uniaxial geosynthetics were modeled using isotropic and orthotropic linear-elastic properties, respectively. The use of isotropic properties results in the same elastic modulus in the two principal directions of the geosynthetic. FLAC3D requires the specification of an elastic modulus and a Poisson's ratio when an isotropic elastic material model is selected. The use of orthotropic elastic properties allows for the specification of different elastic moduli in the two material principal directions. In particular, FLAC3D requires the specification of four elastic constants when using orthotropic elasticity given by Equations 4 through 7:

$$c'_{11} = \frac{E'_{x'}}{1 - v_{x'} v_{y'}} \qquad \textbf{Equation 4}$$

$$c'_{22} = \frac{E'_{y'}}{1 - v_{x'} v_{y'}} \qquad \textbf{Equation 5}$$

$$c'_{33} = G \qquad \textbf{Equation 6}$$

$$c'_{12} = \frac{E'_{x'} v_{y'}}{1 - v_{x'} v_{y'}} = \frac{E'_{y'} v_{x'}}{1 - v_{x'} v_{y'}} \qquad \textbf{Equation 7}$$

where:

$E'_{x'}$ and $E'_{y'}$ = elastic moduli in two material principal directions, G = in-plane shear modulus, and $v_{x'}$ and $v_{y'}$ = in plane Poisson's ratios.

To represent a uniaxial material, the in-plane shear modulus and the in-plane Poisson's ratios are set equal to zero. The elastic modulus in the x' direction ($E'_{x'}$) is given a realistic value while the value in the y' direction is assigned a small value ($E'_{y'}$ = 1; a value of zero is inadmissible). Use of these values results in the geosynthetic taking load only in the direction perpendicular to the slope face. With these values, Equations 4 through 7 reduce to:

$$c'_{11}=E'_{x'}$$

$$c'_{22}=E'_{y'}$$

$$c'_{33}=G=0$$

$$c'_{12}=0$$

For the slopes modeled as part of this research project, isotropic and orthotropic properties were assigned the values given in Table 29. The use of v=o for the isotropic geosynthetic discounts any Poisson effect in biaxial loading, which is viewed as conservative and necessary since some geosynthetics exhibit this property. The combination of the elastic modulus and thickness used results in a tensile strength of 4,125 lb/ft at 5 percent strain, which is within the range of commonly available reinforcement geotextiles and geogrids.

Table 29: Isotropic and Orthotropic Properties for Biaxial and Uniaxial Geosynthetics

Geosynthetic Type	Properties
Isotropic	$E(psf) = 25 \times 10^6$
	$v = 0$
	thickness(ft) = 0.0033
Orthotropic	$E'_{x'}(psf) = 25 \times 10^6$
	$E'_{y'} = 1$
	$G = 0$
	$v_{x'} = v_{y'} = 0$
	thickness (ft) = 0.0033

The shear interface model used is represented in Figure 82 and contains a shear stiffness given by k and an ultimate shear resistance given in terms of c and ϕ. These parameters were given the following values, which were set high to prevent pullout failure:

k= 15,000 lb/ft^2/ft

c = 500 psf

ϕ = 45 degrees

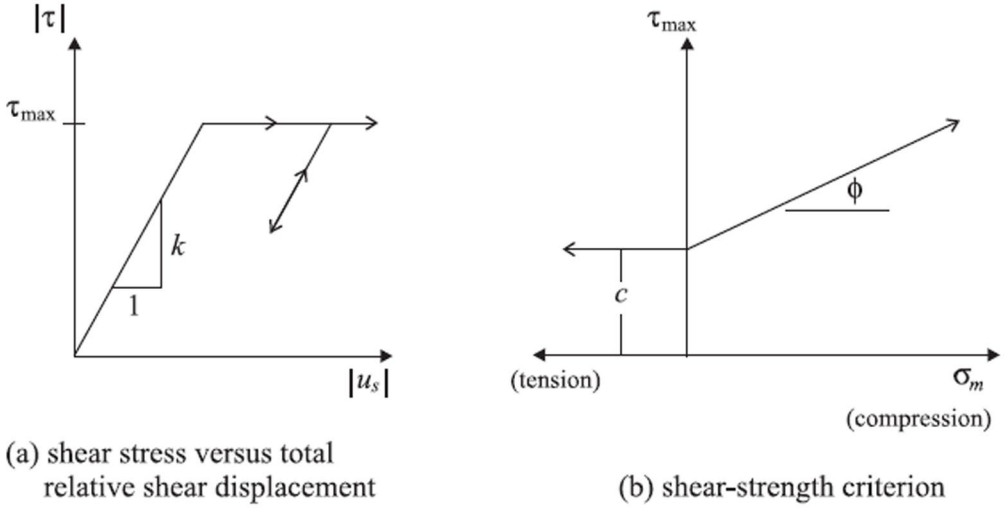

Figure 82: Shear behavior for geosynthetic-soil interfaces (FLAC, 2011).

7.2 SLOPE CONFIGURATION

A single slope geometry was analyzed and corresponds to Run 9, Case 8 (for rotational-type failure) or Run 9 (for wedge-type failures) of previously analyzed 2D slopes in Section 6.1. This slope has the following geometric properties:

H = 35 ft

β = 34°

α = 27.5°

X = 15.34 ft

A 3D model of this cross-section was given planar ends, resulting in the configuration shown in Figure 83. The z-direction of the model is vertical, the y-direction is along the

slope face and x is perpendicular to the y–z plane. The bottom of the model was fixed in the x, y and z directions. The two ends of the model were fixed in the y direction and the back of the model was fixed in the x direction. A cross-sectional view of the model for an unreinforced slope showing the weak soil unit in blue and the strong native soil in grey is shown in Figure 84. This configuration corresponds to a model used to analyze general (rotational) failures within the fill soil. A model used to analyze wedge-type failures, where a third soil type for the slip plane is added (in pink), is shown Figure 85.

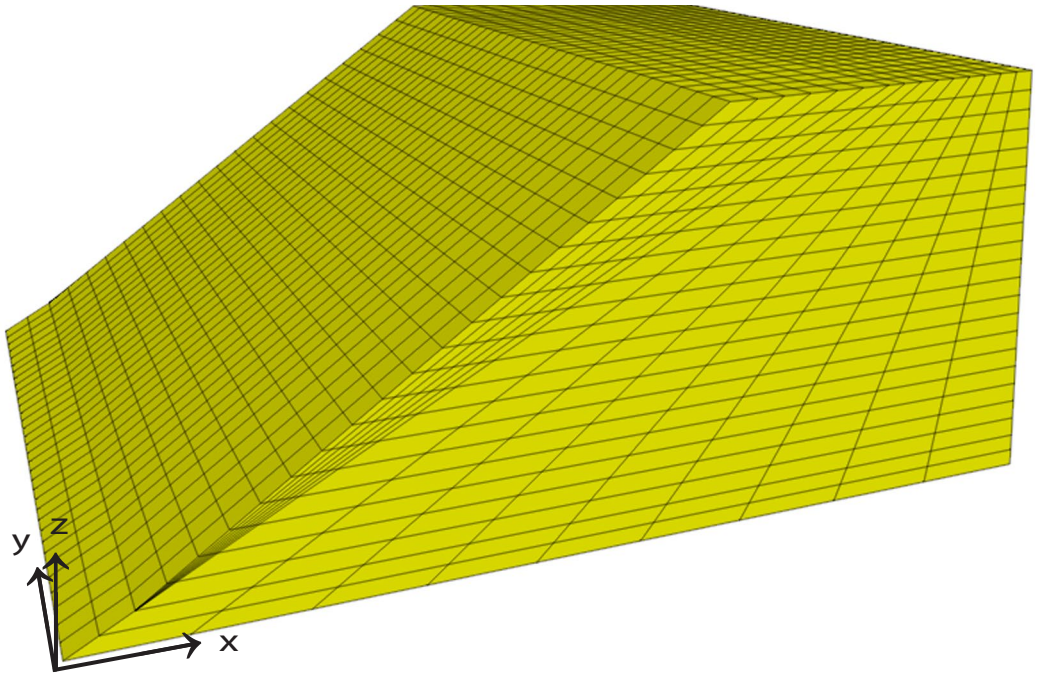

Figure 83: General configuration of 3D slope models.

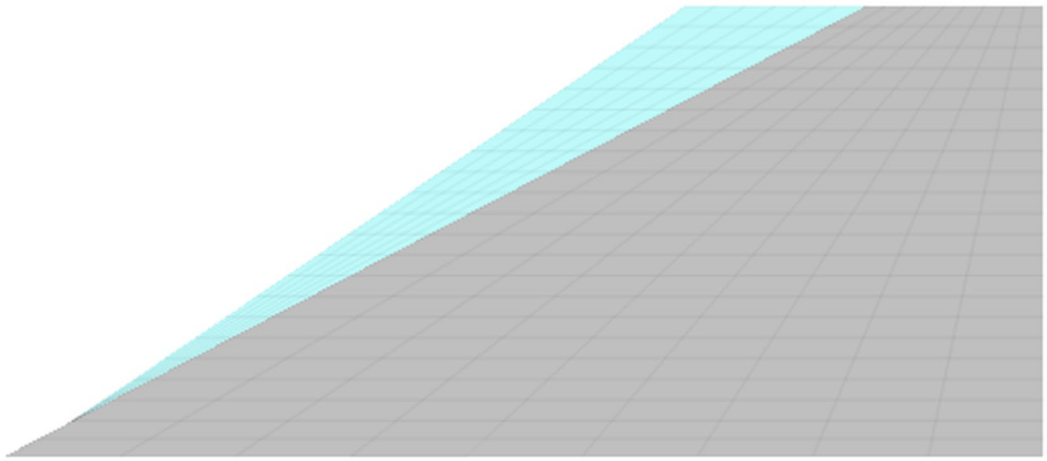

Figure 84: Cross section of an unreinforced 3D model for rotational failure.

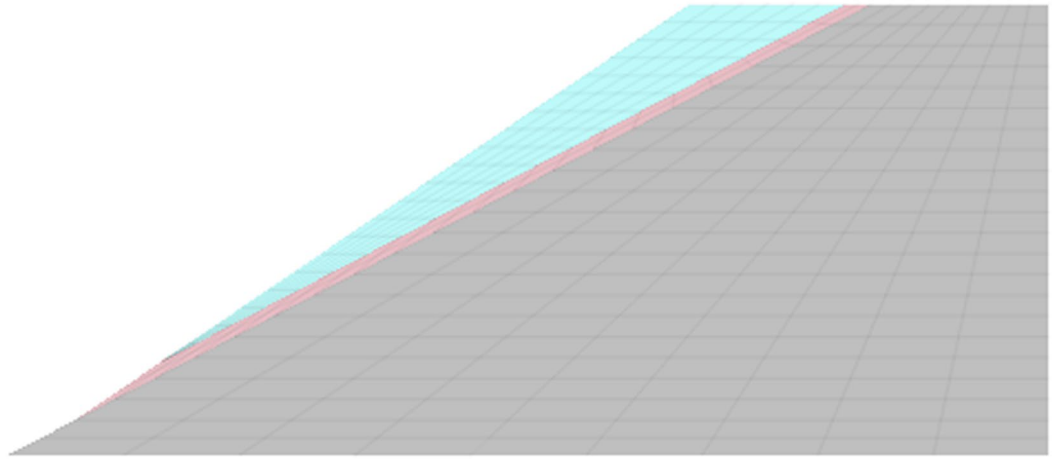

Figure 85: Cross section of an unreinforced 3D model for wedge failure.

To model three-dimensional effects, the ends of the model (in the y-direction) contained extended zones of strong native soil. A 3D view of an unreinforced model with the strong native soil at the ends is shown in Figure 86. Seven iterations of the model shown in Figure 86 were analyzed, corresponding to lengths (in the y-direction) of the weak soil of 10, 20, 30, 60, 120, 200 and 400 feet. The length of the extended zone at either end of strong native soil (in the y direction) was 15 feet for all seven models. The model shown in Figure 86 corresponds to a weak soil length of 60 feet.

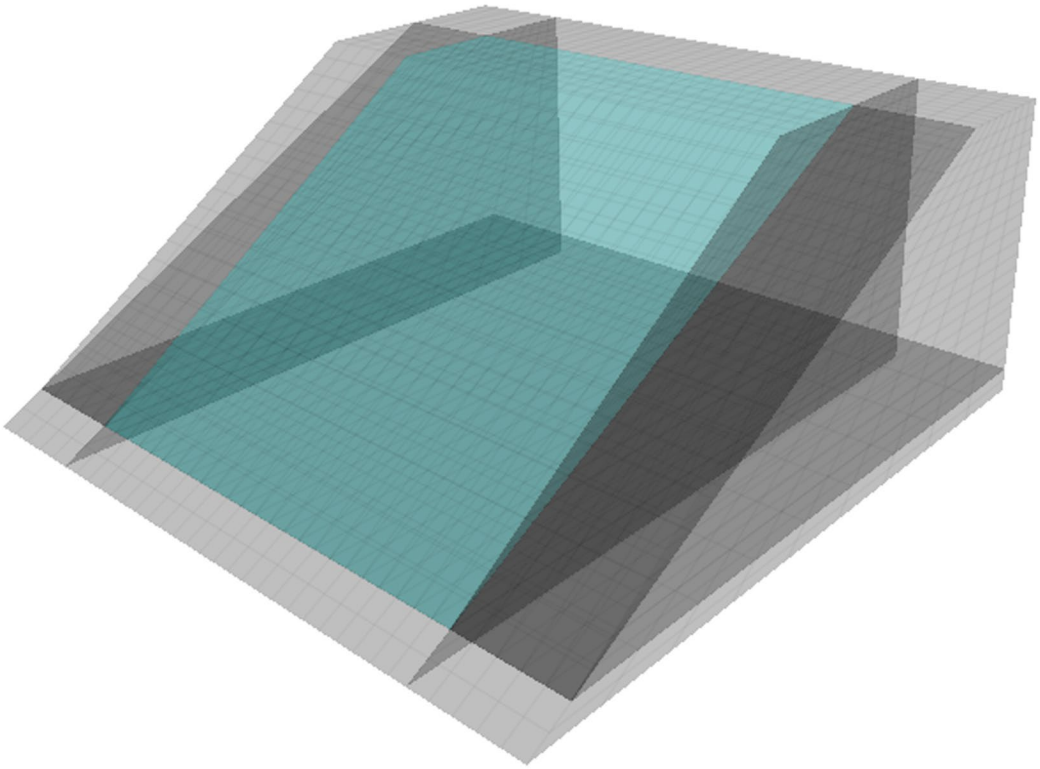

Figure 86: 3D view of an unreinforced model (weak soil length = 60 feet).

Reinforced models were created with 5 feet of reinforced soil and 5 layers of geosynthetic. A cross-section of a reinforced model is shown in Figure 87. The length of the reinforcement (in the y-direction) spanned the entire length of the model and was therefore anchored into the ends of the extended strong native soil. A list of the soil properties used for the soil layers associated with this modeling is provided in Table 30. The properties K and G are the elastic bulk modulus and shear modulus, respectively.

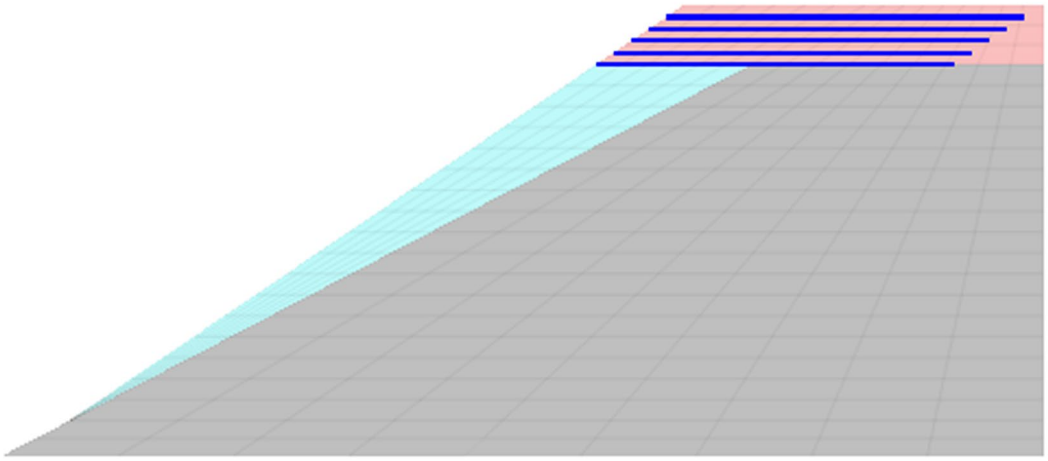

Figure 87: Cross-section of a 3D reinforced model for rotational failure.

Table 30: Soil Properties for 3D Models

Soil Layer	ϕ (degrees)	c (psf)	γ(pcf)	K(ksf)	G(ksf)
Strong/Native	50	0	125	840	388
Reinforced Mass	45	0	125	840	388
Weak (rotational failures)	24.5	55	125	420	194
Weak (wedge failures)	32	200	125	420	194
Slip Plane (wedge failures)	0	204	125	420	194

7.3 3D MODELING RESULTS

Models for unreinforced and reinforced cases were analyzed for both rotational and wedge-type failures. The reinforced models were analyzed using isotropic and orthotropic properties (corresponding to biaxial and uniaxial geogrid reinforcement, respectively). Each model type was analyzed for the seven different cases of weak soil length. This resulted in 42 models that were analyzed using FLAC3D.

Results from each model were summarized in terms of a factor of safety and contour plots of maximum shear strain increment and displacement magnitude. FLAC3D offers a greater number of results variables to view as compared to FLAC/Slope. Contours of displacement magnitude at failure were observed to be superior to velocity vectors, as previously used in FLAC/Slope, to provide a visual representation of material movement in the slope at failure.

The factor of safety for rotational and wedge failures as a function of weak soil length for the 14 cases analyzed is shown in Figure 88 for unreinforced slopes. It is observed that the factor of safety decreases as weak soil length increases. This is due to the resistance that is developed between the ends of the weak soil zone and the strong native ground. For short lengths of the weak soil zone, soil arching is also most likely appreciable and leads to a higher factor of safety. The additional resistance at the ends becomes negligible when the weak soil length is greater than approximately 150 ft. Contour plots show that failure surfaces and weak soil movement occurs up into the roadway bench for all of these unreinforced slopes, as illustrated in Figure 89 for a rotational failure with a weak soil length of 60 ft. The cross-section for this view is at the center of the weak soil length, as is the case for all remaining figures showing this information.

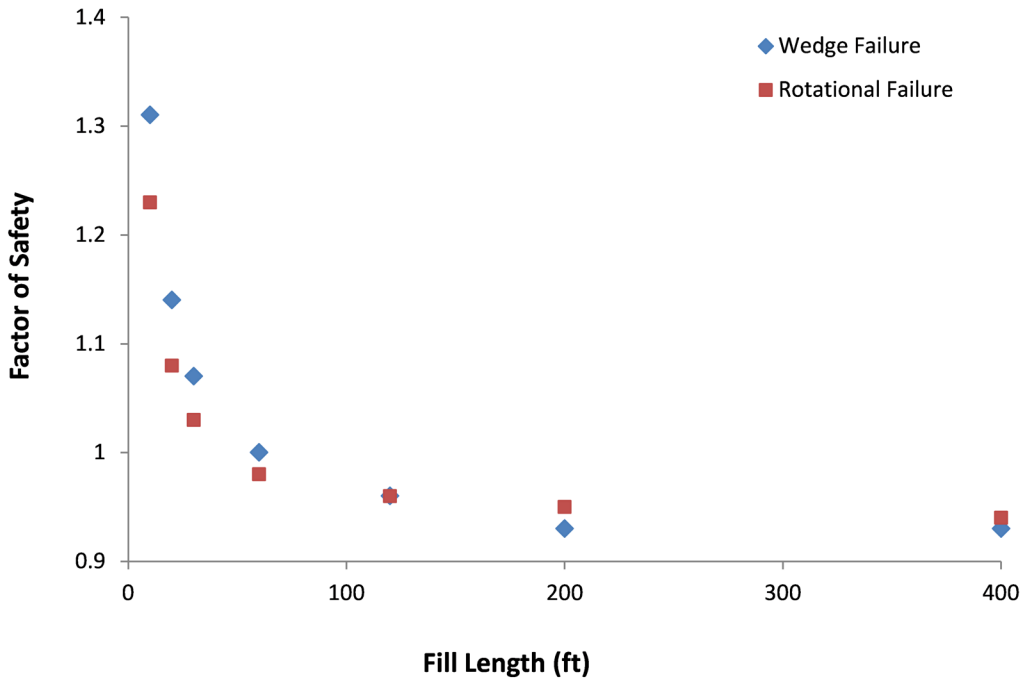

Figure 88: Factor of safety for unreinforced FLAC3D slopes versus weak soil length.

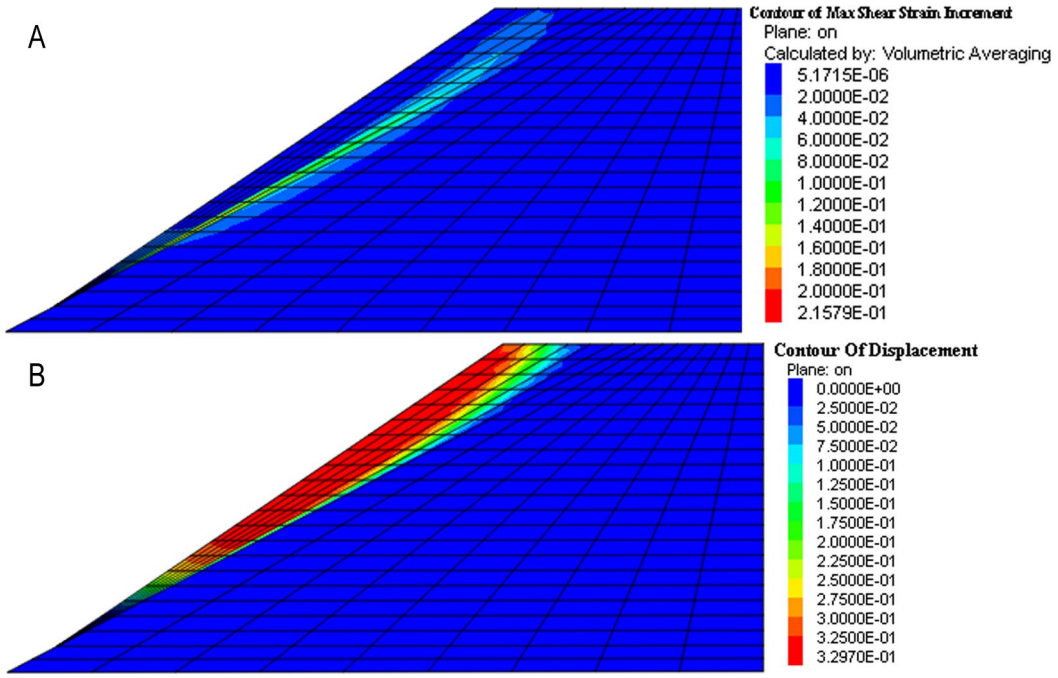

Figure 89: Contour plots, unreinforced 3D slope, rotational failure, 60 ft weak soil length, a) maximum shear strain increment, b) displacement magnitude.

Diagrams for a slope with a weak soil length of 60 ft reinforced with biaxial and uniaxial reinforcement are shown in Figure 90 and Figure 91, respectively, based on rotational failure. Both cases show improvement in terms of reducing the amount of movement on or below the roadway bench. The biaxial reinforcement case shows much better performance than the uniaxial material case, where the performance of the uniaxial case was unacceptable (movement observed on the road bench). A set of results for a wedge-type failure with a weak soil length of 60 ft for unreinforced, biaxial and uniaxial reinforced slopes is shown in Figure 92 through Figure 94 and shows the above conclusions even more strongly.

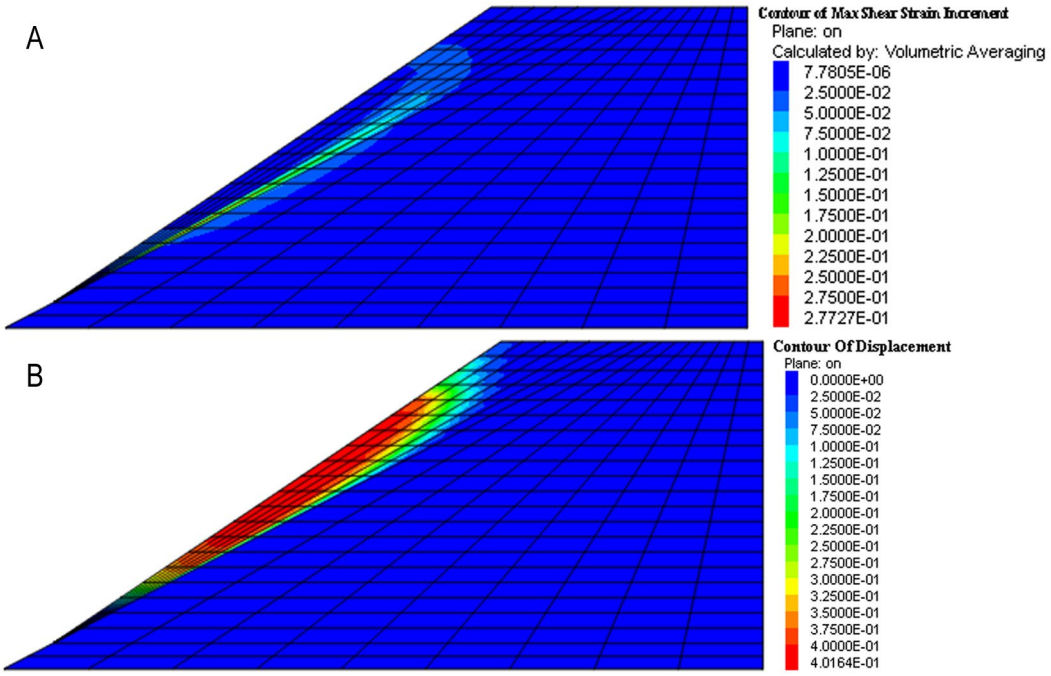

Figure 90: Contour plots, biaxial reinforced 3D slope, rotational failure, 60 ft weak soil length, a) maximum shear strain increment, b) displacement magnitude.

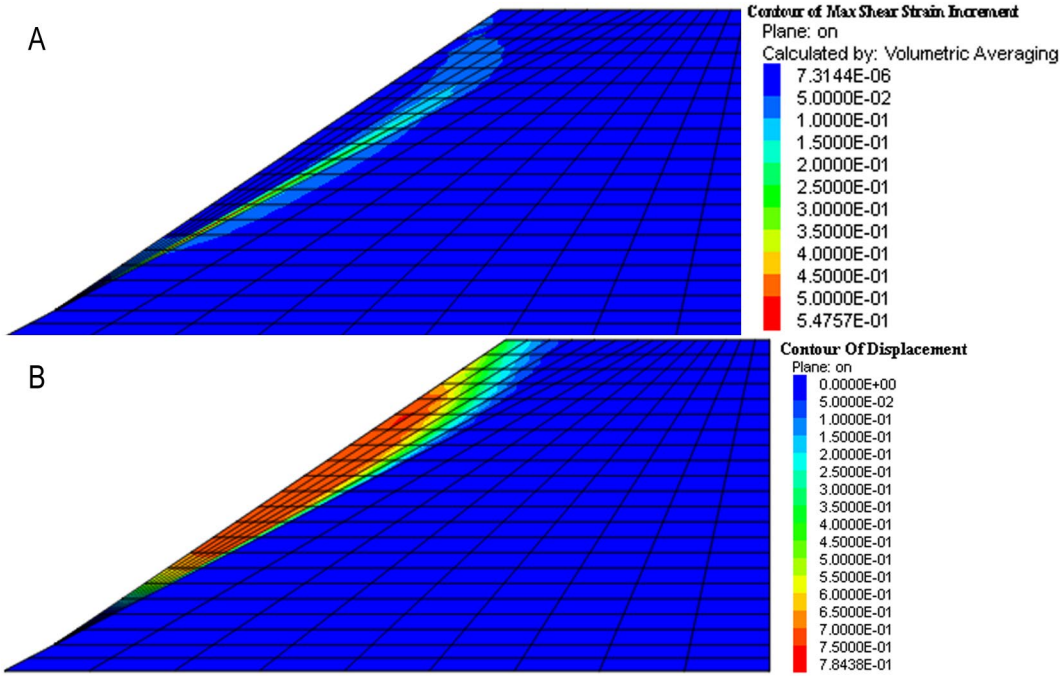

Figure 91: Contour plots, uniaxial reinforced 3D slope, rotational failure, 60 ft weak soil length, a) maximum shear strain increment, b) displacement magnitude.

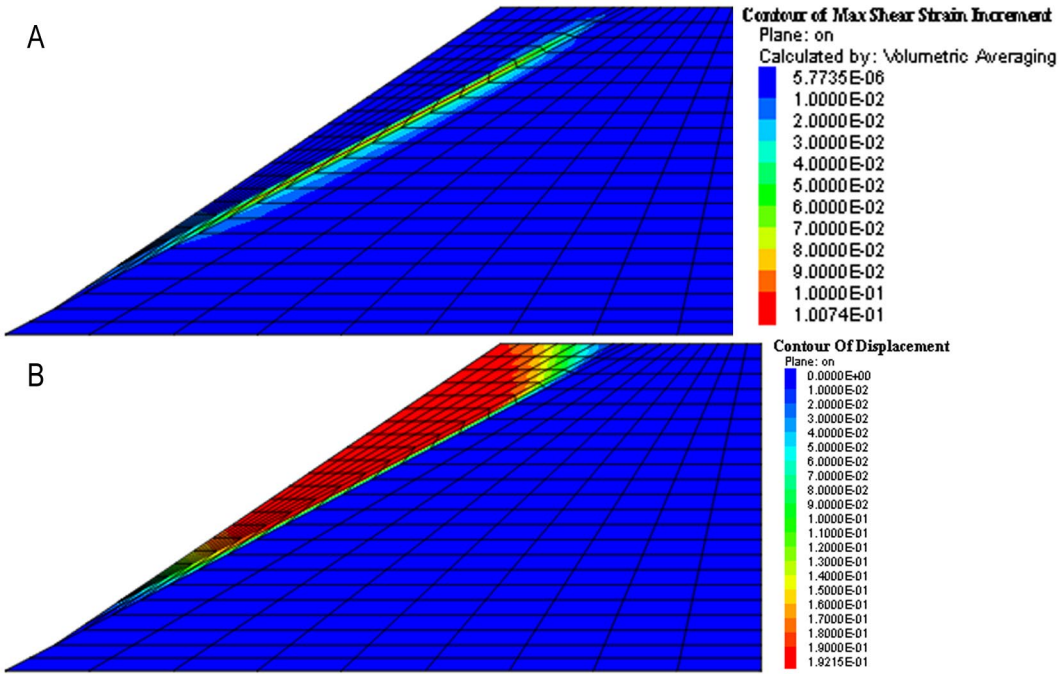

Figure 92: Contour plots, unreinforced 3D slope, wedge failure, 60 ft weak soil length, a) maximum shear strain increment, b) displacement magnitude.

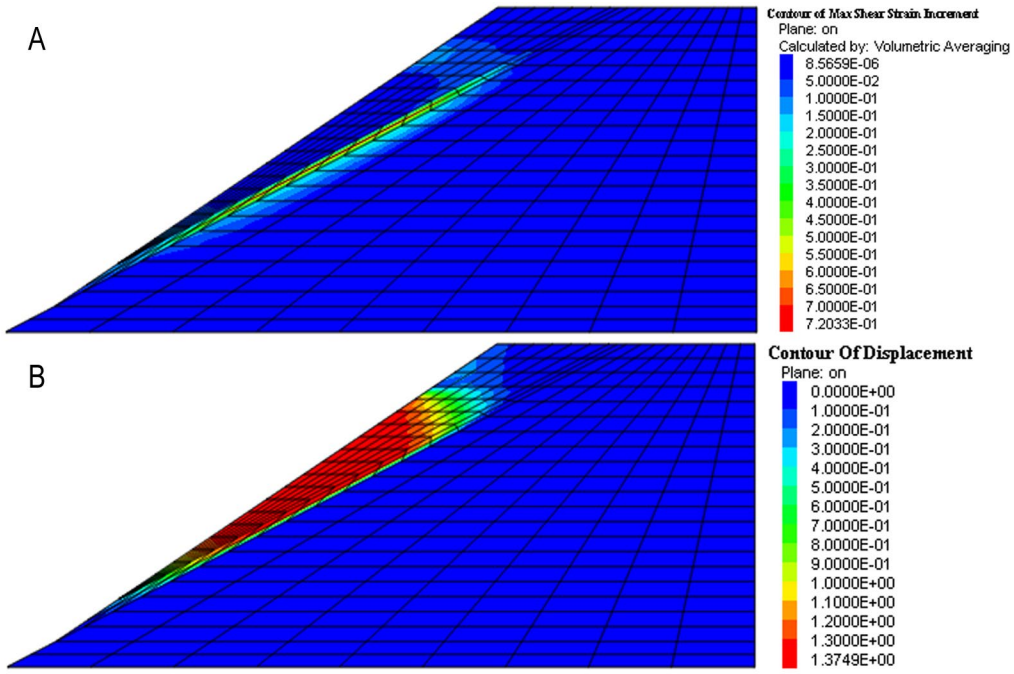

Figure 93: Contour plots, biaxial reinforced 3D slope, wedge failure, 60 ft weak soil length, a) maximum shear strain increment, b) displacement magnitude.

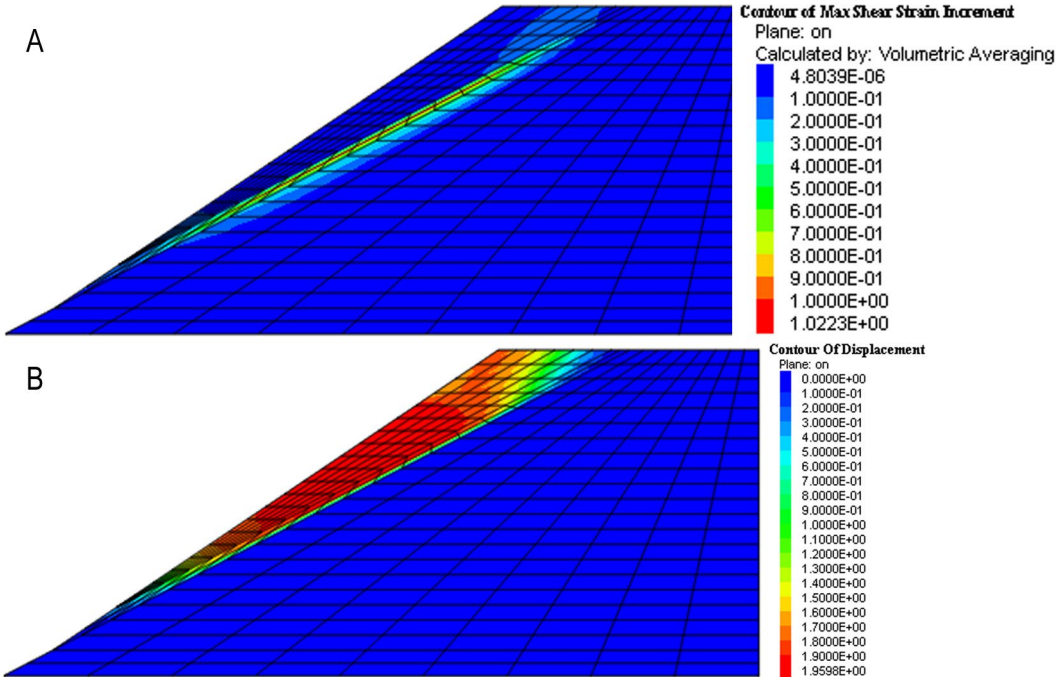

Figure 94: Contour plots, uniaxial reinforced 3D slope, wedge failure, 60 ft weak soil length, a) maximum shear strain increment, b) displacement magnitude.

Examination of sets of figures similar to Figure 89 through Figure 91 shows a similar pattern of improvement with reinforcement and significantly better performance with biaxial reinforcement (all of the contour plots for 3D analyses are shown in Appendix C). Differences in performance as a function of weak soil length were difficult to distinguish. In general, the above observations appear to hold true for any weak soil length and may be more significant for larger weak soil lengths.

To help define this better, a summary of the factor of safety obtained from each model run are provided in Table 31 and Table 32 for wedge and rotational failures, respectively. The percent improvement in the factor of safety for reinforced models with biaxial and uniaxial geosynthetics as compared to the corresponding unreinforced case versus the weak soil length of the model are shown in Figure 95 and Figure 96 for wedge and rotational failures, respectively. In viewing these results, it should be noted that the factors of safety for the reinforced models are relatively low because they correspond to critical failure surfaces that develop beneath the reinforced mass within the weak soil and tend to initiate along the face of the slope. As demonstrated previously with ReSSA, failure surfaces initiating along the roadway surface have higher factors of safety.

Table 31: Factor of Safety for Wedge Failures

Configuration	Weak Soil Length (ft)	Factor of Safety		
		Unreinforced	Biaxal Reinforced	Uniaxial Reinforced
1	10	1.31	1.38	1.36
2	20	1.14	1.30	1.24
3	30	1.07	1.25	1.17
4	60	1.00	1.20	1.10
5	120	0.96	1.17	1.06
6	200	0.93	1.15	1.04
7	400	0.93	1.14	1.03

Table 32: Factor of Safety for Rotational Failures

Configuration	Weak Soil Length (ft)	Factor of Safety		
		Unreinforced	Biaxal Reinforced	Uniaxial Reinforced
1	10	1.23	1.25	1.25
2	20	1.08	1.12	1.11
3	30	1.03	1.07	1.07
4	60	0.98	1.04	1.02
5	120	0.96	1.01	1.00
6	200	0.95	1.01	1.00
7	400	0.94	1.00	0.99

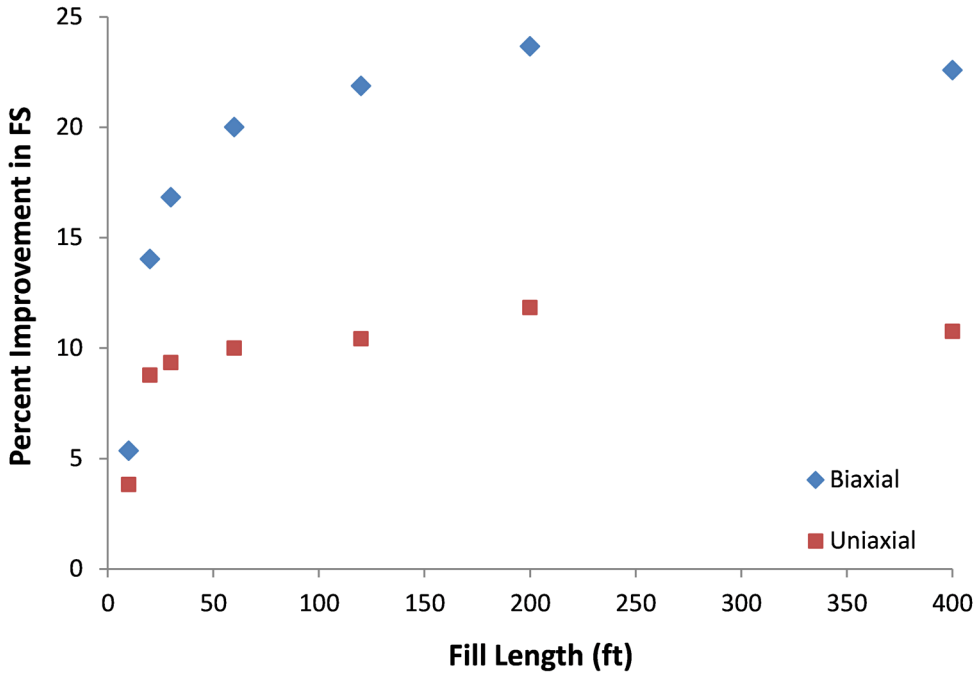

Figure 95: Percent improvement in factor of safety for biaxial and uniaxial geosynthetics for wedge failures.

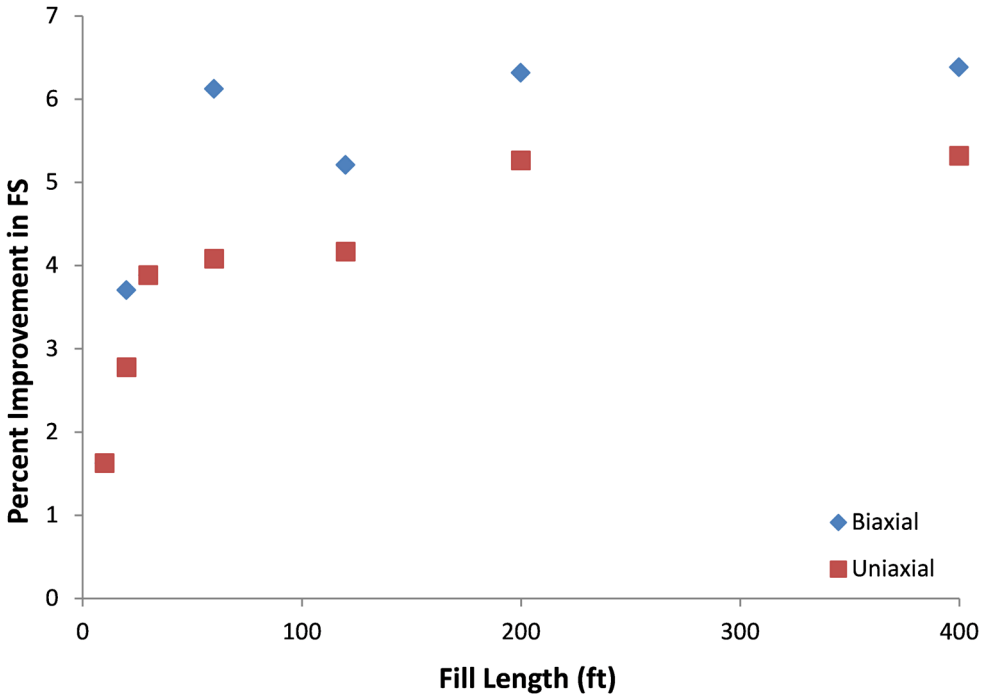

Figure 96: Percent improvement in factor of safety for biaxial and uniaxial geosynthetics for rotational failures.

These results show that both uniaxial and biaxial geosynthetics provide improvement to the factor of safety. Biaxial geosynthetics provide substantially more improvement for wedge failures as compared to uniaxial geosynthetics and nominally more improvement for rotational failures. The improvement in factor of safety tends to increase with increasing weak soil length up to a value of 150 to 200 feet, after which the improvement is nearly constant. This trend is most likely due to the fact that the factors of safety for unreinforced slopes with small values of weak soil length are relatively high and the addition of reinforcement does not have as significant of an effect on the stability of the slope. This data supports the trends seen in the contour plots discussed above. For all the cases examined, the maximum load in the geosynthetic was approximately 1,600 lb/ft.

The slope with a weak soil length of 60 ft was analyzed with 3, 2 and 1 equally spaced reinforcement layers within the 5 ft depth of reinforced soil for both rotational and wedge failures. In all cases, reducing the number of reinforcement layers from 5 resulted in poorer performance. The performance for all cases was viewed as unacceptable and supports the results from Chapters 5 and 6 showing the influence of reinforcement spacing on performance.

7.4 SUMMARY

A three-dimensional analysis program (FLAC3D) was used to examine the difference in slope performance when biaxial and uniaxial reinforcement was used. Results from the study were also used to evaluate the importance of anchoring at the ends of the patch. 3D models were set up for a single slope geometry with 7 different lengths of weak soil. Two sets of models allowed both rotational and wedge-type failures to be analyzed. Biaxial materials were modeled using isotropic material properties. Uniaxial materials were modeled using orthotropic material properties having negligible elastic modulus in the direction parallel with the slope face (i.e., in the direction of the weak soil length). Reinforced slopes contained 5 layers of reinforcement at a 1 ft spacing. Some additional models were examined with 3, 2 and 1 layers of reinforcement equally spaced within the 5 ft deep repair.

Results were expressed in terms of factor of safety and contour plots of maximum shear strain and displacement magnitude. The unreinforced slopes all showed factors of safety close to 1.0, and a pattern of failure extending up into the roadway bench. For a reinforcement spacing of 1 ft, the biaxial reinforcement resulted in considerable improvement and prevented material movement along and below the roadway bench for all cases examined. The uniaxial reinforcement resulted in improvement but also in unacceptable movement along the roadway bench. No clear differences in performance were noted as a function of weak soil length.

These results show the benefit of biaxial versus uniaxial reinforcement materials for a deep patch repair. The results obtained in the parametric study (Chapter 6) assume an isotropic reinforcement material for the 2D analysis and are therefore applicable to biaxial reinforcement. Given the appreciable reduction in performance with the use of uniaxial materials for the cases examined in this 3D study, it is recommended that biaxial materials be used in conjunction with the results from Chapter 6, and that the required strength be for the weakest direction of the biaxial material. Given the importance of strength in the direction parallel to the slope, the importance of anchoring the reinforcement in the strong native ground at the ends of the deep patch is apparent in order to develop tensile resistance in this direction.

Should uniaxial materials be specified for a deep patch, additional research is needed to make recommendations on the additional requirement placed on the reinforcement above those discussed in Chapter 6. These additional requirements could be in the form of a deeper depth of reinforcement, a reduced spacing and/or increased strength. Additional 3D analyses are required for a large number of cases backed by field testing to determine these additional requirements.

8 EFFECT OF NEGATIVE BATTER

Negative batter in deep patches is where the geosynthetic reinforced layers do not extend to the slope face and the width of the layers decreases with depth. Negative batter deep patches are most desirable on steep slopes where it may be difficult to operate construction equipment, particularly compaction equipment, near the slope face. Construction of a deep patch using negative batter involves the excavation of a trench which leaves the slope face undisturbed. The vegetated slope face provides stability and erosion control, which would need to be re-established if it was disturbed with a traditional deep patch. Thus, use of negative batter during deep patch construction can eliminate "environmental impacts" to the existing slope face. Because negative batter is more likely to be used on steep slopes, Slope II from Section 3.3, ($\beta = 39°$) was used to analyze several different negative batter deep patch configurations in FLAC/Slope. The purpose of this study was to examine any detrimental effects on slope performance by the use of negative batter. A specific negative batter deep patch from a WFLHD project in Idaho (shown in Figure 4 in Section 1.2) was also modeled in FLAC/Slope.

8.1 SLOPE II

Slope II consisted of the geometric and soil strength properties in Table 33 for both rotational and wedge analyses. FLAC/Slope estimated the factor of safety of the unreinforced slope to be 1.0 for rotational failure and 0.93 for wedge failure. In the parametric study summarized in Chapter 6, the resulting best deep patch configuration was found to be 5 ft deep with 5 layers of reinforcement for both rotational failure and wedge failure (Figure 97). Three configurations of negative batter geometry were modeled based on deviations from the "best" traditional deep patch geometry (Figure 98):

- Version 1—Top three layers of reinforcement extend to the slope face, the lower two layers terminate before the face at a 45° negative batter.
- Version 2—Top two layers of reinforcement extend to the slope face, three lower layers are at a negative batter.
- Version 3—Top two layers of reinforcement extend to the slope face. Third layer extends as far as the second layer (not quite to the slope face) to create a vertical portion. The two lower layers are at a negative batter.

Table 33: Slope Geometry and Soil Strength Properties for Slope II

		Rotational	Wedge
Slope Geometry			
	α(°)	29.8°	29.8°
	β(°)	39°	39°
	H(ft)	35	35
	X(ft)	18	18
	X_c(ft)	6.5	8.1
Soil Unit			
Weak	ϕ(°)	23	32
	c(lb/ft^2)	110	200
	γ(lb/ft^3)	125	125
Strong/Native	ϕ(°)	50	50
	c(lb/ft^2)	0	0
	γ(lb/ft^3)	125	125
Slip Plane	ϕ(°)	N/A	0
	c(lb/ft^2)	N/A	277
	γ(lb/ft^3)	N/A	125

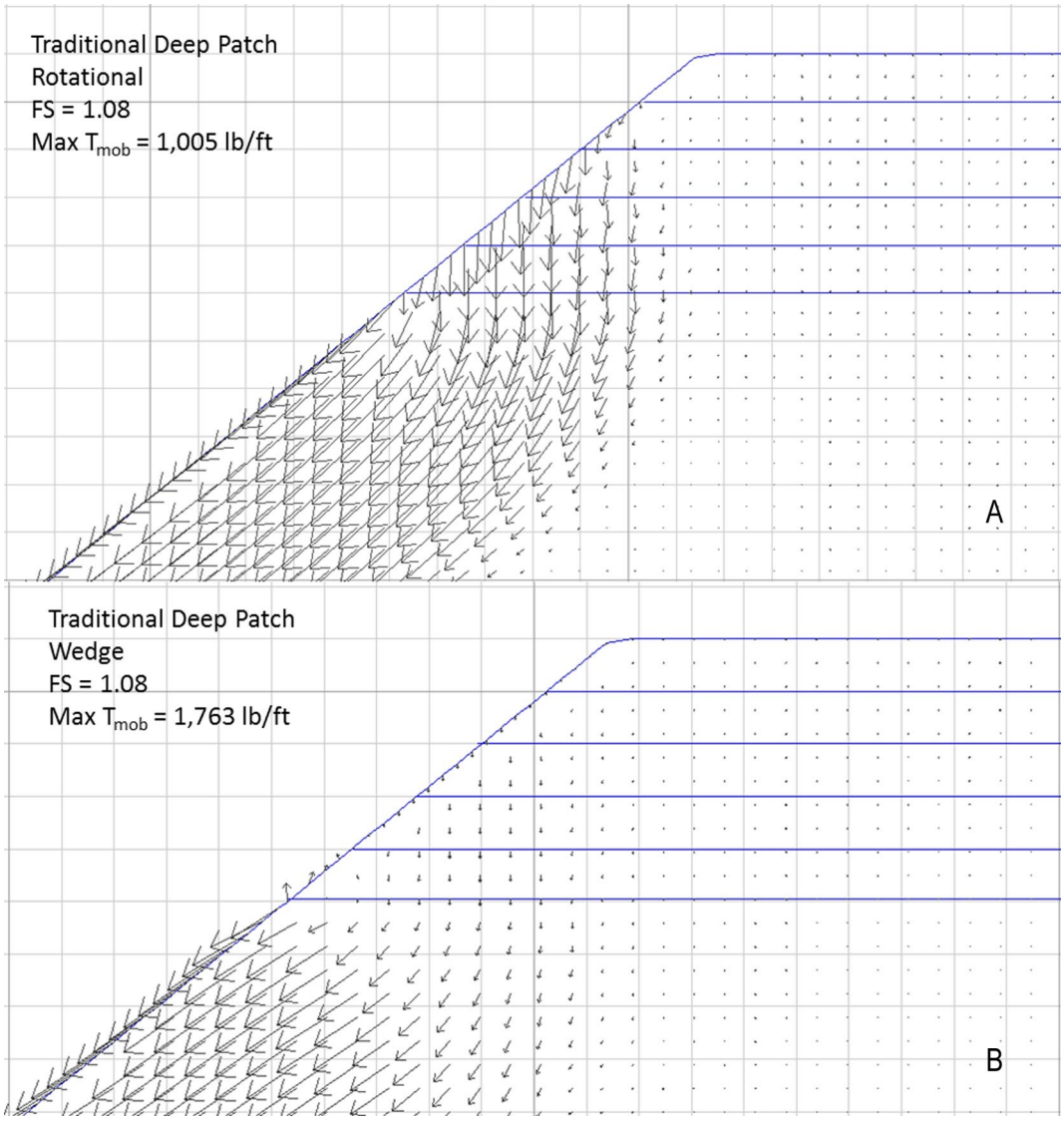

Figure 97: Velocity vector plots from FLAC/Slope for best traditional deep patch configuration: 5 ft deep, 5 layers of reinforcement for a) rotational failure and b) wedge failure.

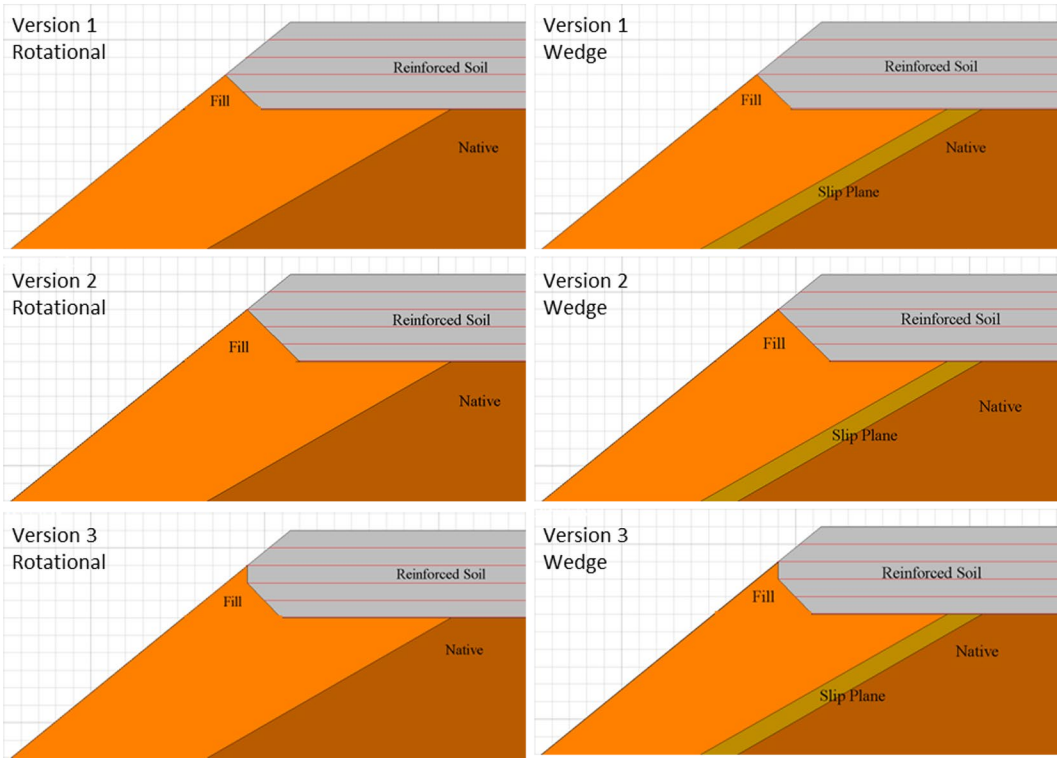

Figure 98: Close-up view of negative batter geometries for rotational and wedge models of Slope II.

The performance of the negative batter deep patches was ranked from 1 to 3 within each failure mode (Table 34) based on the velocity vector plots from FLAC/Slope (Figures 99 – 101). All negative batter deep patches modeled as part of this study (rotational and wedge) provided improvement compared to the unreinforced slope, although to a lesser degree than the traditional deep patch geometry. This is evident from the velocity vectors plots as well as the factors of safety computed by FLAC/Slope (Table 35). All of the negative batter versions for the wedge analyses appear acceptable, with little to no movement (arrows) located directly under the road bench. The rotational analyses indicate the negative batter geometry is not optimal and possibly unacceptable, although Version 3 may possibly be acceptable. While not shown here, negative batter versions were modeled with a similar geometry except with six layers of reinforcement and a total depth of 6 ft for the rotational failure mode and found to be more acceptable than the 5 ft deep patches. Thus, in some cases, the negative batter geometry may require a deeper repair than the traditional geometry. The maximum mobilized tensile force for the six 5 ft deep models was similar and varied between 817 and 965 lb/ft, which was less than the maximum mobilized tensile force in the traditional deep patch geometries. The wedge analyses showed a significant reduction in required tensile strength from 1,763 lb/ft for a traditional deep patch to 870 lb/ft for the preferred negative batter deep patch.

Table 34: Performance Rank for Negative Batter Analyses with Slope II

Negative Batter Geometry Version	Rotational	Wedge
1	2	2
2	3	3
3	1	1

Table 35: Factor of Safety for Negative Batter Analyses with Slope II

Model	Rotational		Wedge	
	FS	Percent Improvement	FS	Percent Improvement
Unreinforced	1.00	-	0.93	-
Traditional Deep Patch	1.08	8	1.08	16
Negative Batter Version 1	1.05	5	1.03	11
Negative Batter Version 2	1.04	4	1.01	9
Negative Batter Version 3	1.04	4	1.02	10

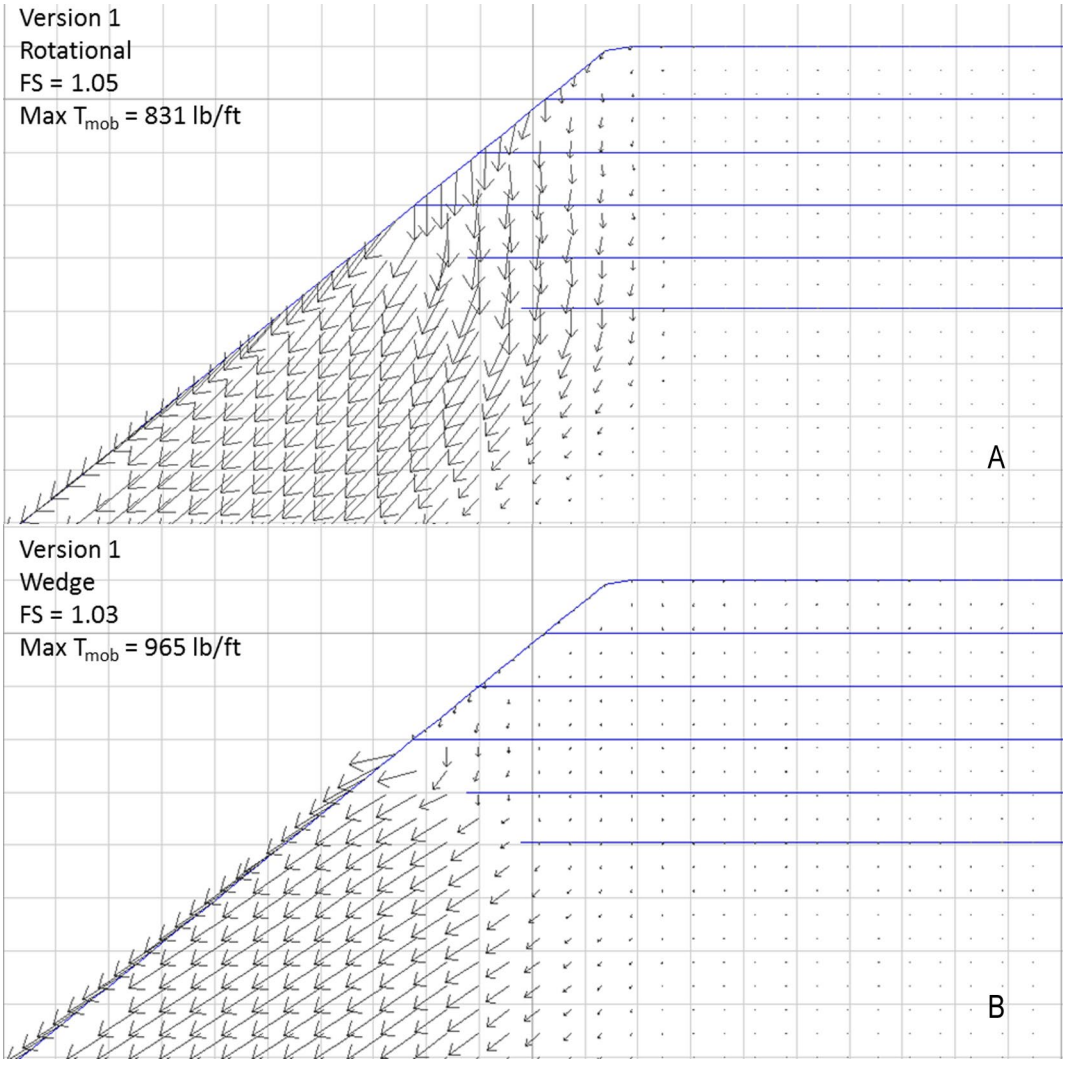

Figure 99: Velocity vector plot for negative batter Version 1 for a) rotational and b) wedge.

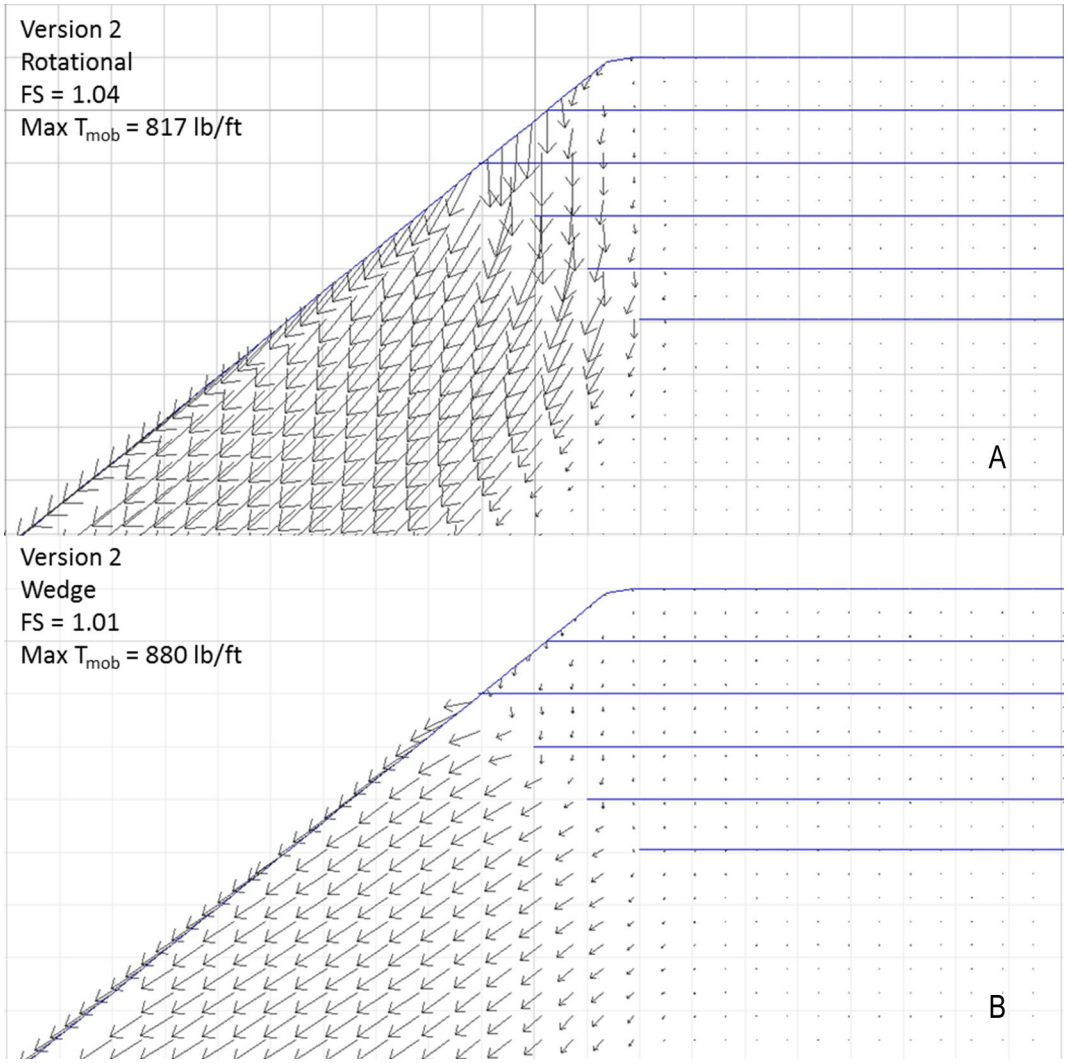

Figure 100: Velocity vector plot for negative batter Version 2 for a) rotational and b) wedge.

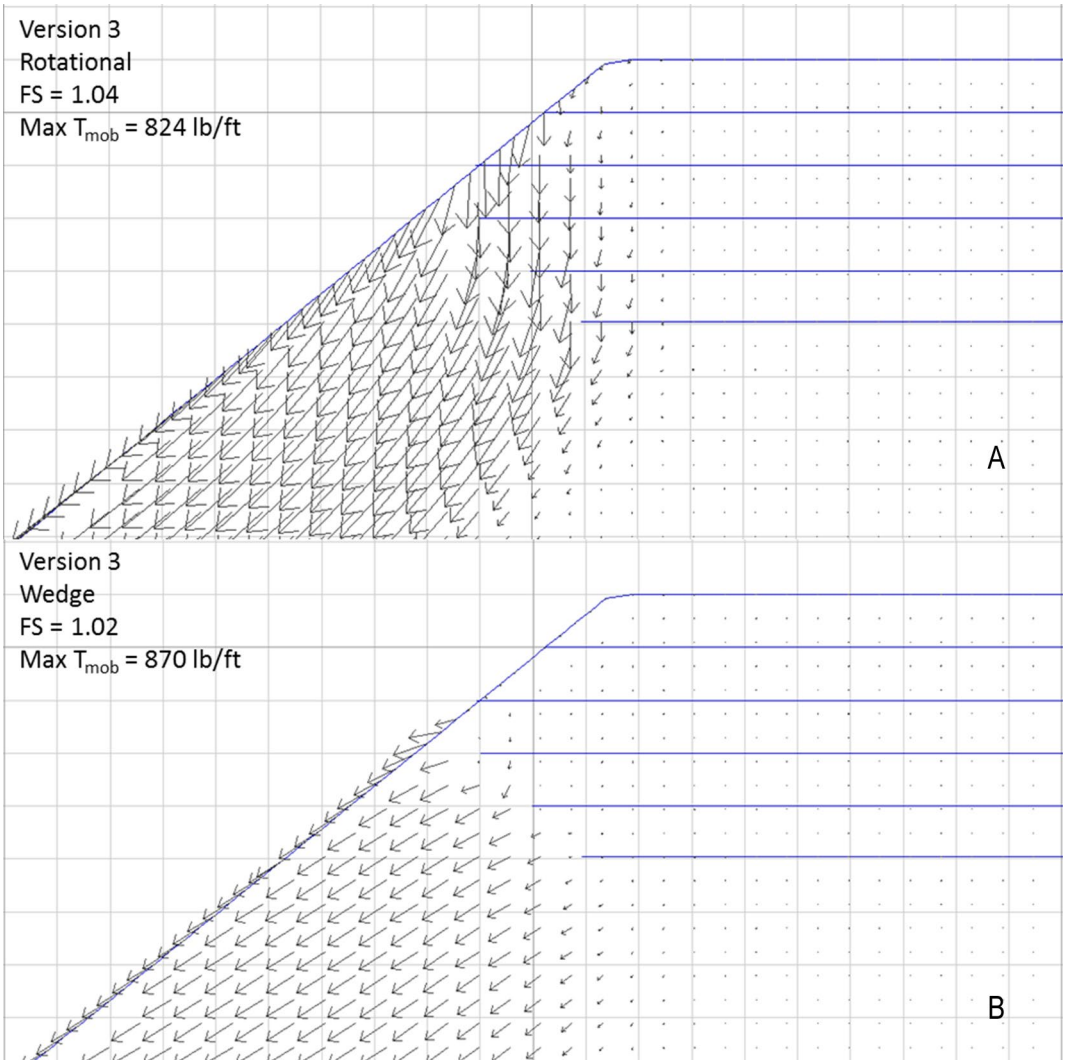

Figure 101: Velocity vector plot for negative batter Version 3 for a) rotational and b) wedge.

8.2 WFLHD DEEP PATCH

A negative batter deep patch designed by WFLHD for use in a project in Idaho consisted of six layers of wrapped geogrid with variable spacing and extending to a total depth of six feet. For purposes of evaluating the performance of this design for both rotational and wedge failure modes, slope geometry parameters were assumed (except $\beta = 45°$, which was known, and X_c, which was determined from unreinforced FLAC/Slope runs) and soil parameters were determined in a similar manner as the parametric study in Chapter 6. That is, for rotational analysis, ϕ and c for the weak soil were adjusted until ReSSA predicted FS = 1.0 for the unreinforced slope. For the wedge analysis, the weak soil was assumed to have $\phi = 32°$ and c = 200 psf, and the cohesion of the slip plane was determined from Equation 1 for FS = 1.0 (result: c = 243 psf). However, FLAC/Slope predicted the factors of safety for the unreinforced slopes to be 0.95 for rotational and 0.87 for wedge failure modes. The large deviation from 1.0 for the wedge analysis was not acceptable. Thus, Equation 1 was used to find a new value for cohesion corresponding to FS = 1.13 (result: c = 274 psf). For this new value of cohesion for the soil within the slip plane, FLAC/Slope predicted the factor of safety to be 0.95, which was considered acceptable. The slope geometry and soil strength properties for the negative batter analyses are shown in Table 36.

The deep patch schematic provided by WFLHD consisted of six layers of reinforcement, all wrapped across the face of the slope. In two of the layers, the wrapped portion extended to the back limit of excavation, essentially causing it to act as another layer of reinforcement. In the other four layers, the wrapped layer was shorter. In order to account for this unique geometry, the FLAC/Slope models were created using eight layers of reinforcement. A schematic of the FLAC/Slope model is shown in Figure 102 for rotational and wedge failure analyses.

Table 36: Slope Geometry and Soil Strength Properties for Slope with WFLHD Deep Patch

		Rotational	Wedge
Slope Geometry			
	α(°)	28°	28°
	β(°)	45°	45°
	H(ft)	20	20
	X(ft)	17.6	17.6
	X_c(ft)	5.8	7.1
Soil Segment			
Weak	ϕ(°)	18	32
	c(lb/ft^2)	145	200
	γ(lb/ft^3)	125	125
Strong/Native	ϕ(°)	50	50
	c(lb/ft^2)	0	0
	γ(lb/ft^3)	125	125
Slipe Plane	ϕ(°)	N/A	0
	c(lb/ft^2)	N/A	274
	γ(lb/ft^3)	N/A	125

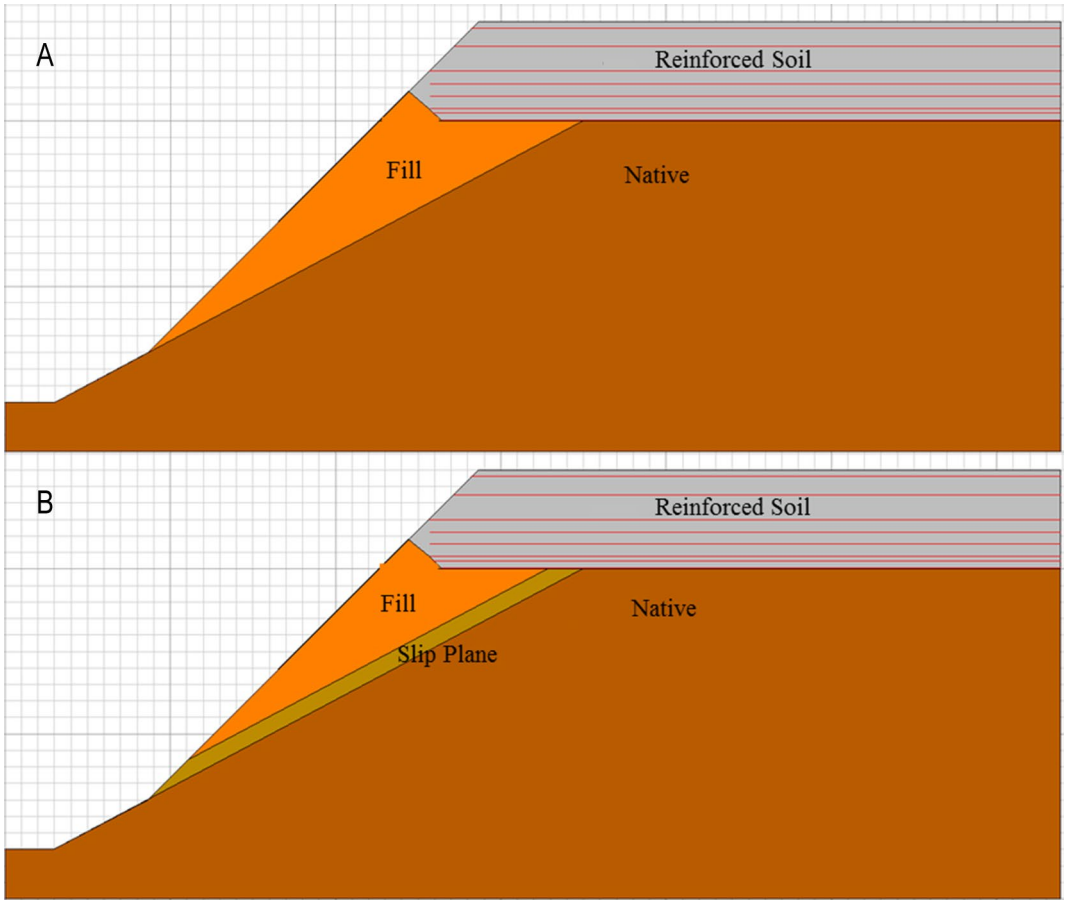

Figure 102: Schematic of slope with WFLHD deep patch for a) rotational failure and b) wedge failure.

The results of the FLAC/Slope models indicate that the WFLHD deep patch is acceptable for either rotational or wedge failure, although the wedge failure mode has a greater percent improvement in factor of safety (Figure 103 and Figure 104).

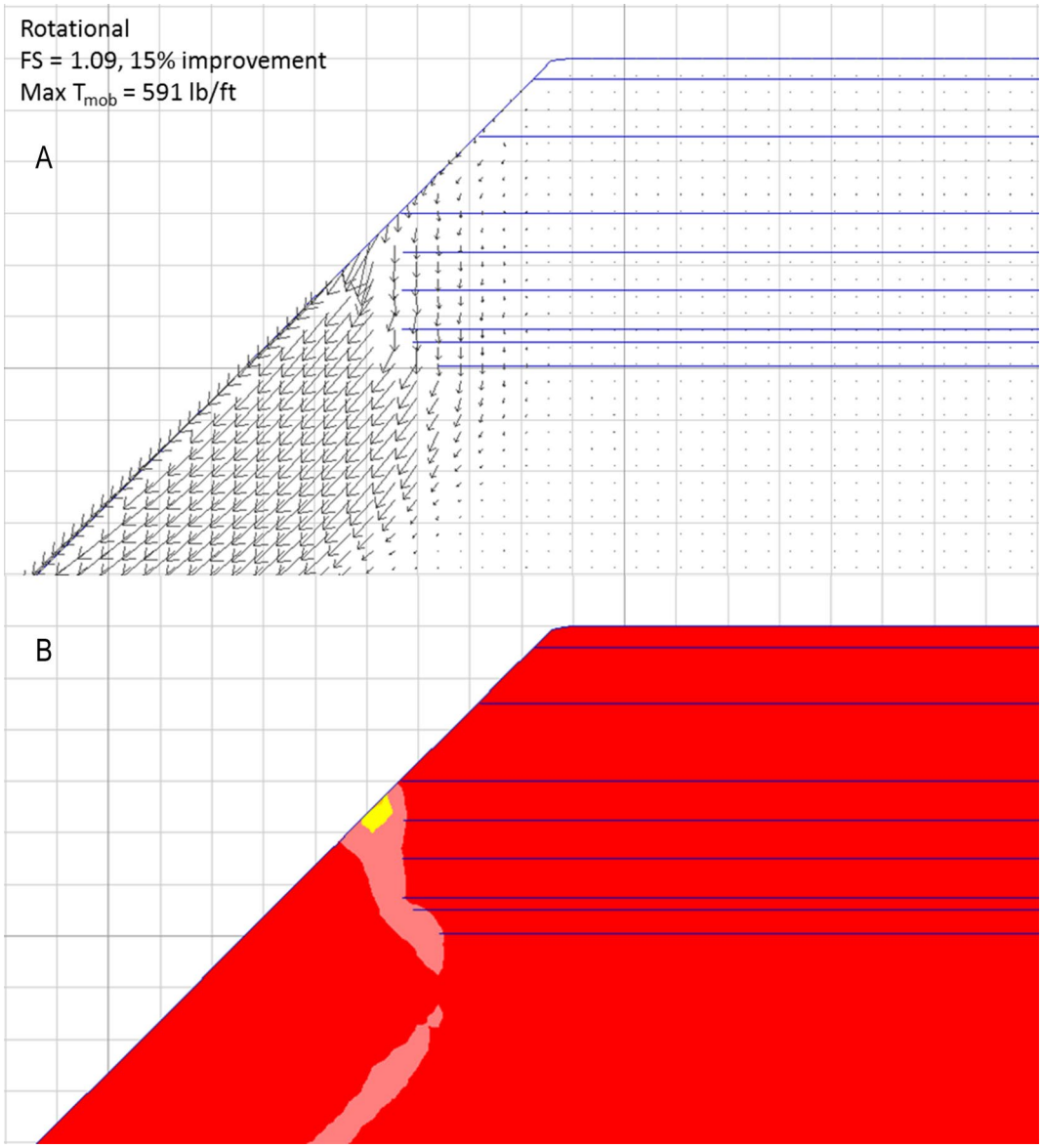

Figure 103: FLAC/Slope results for WFLHD deep patch rotational failure, a) velocity vector plot and b) shear strain rate contours.

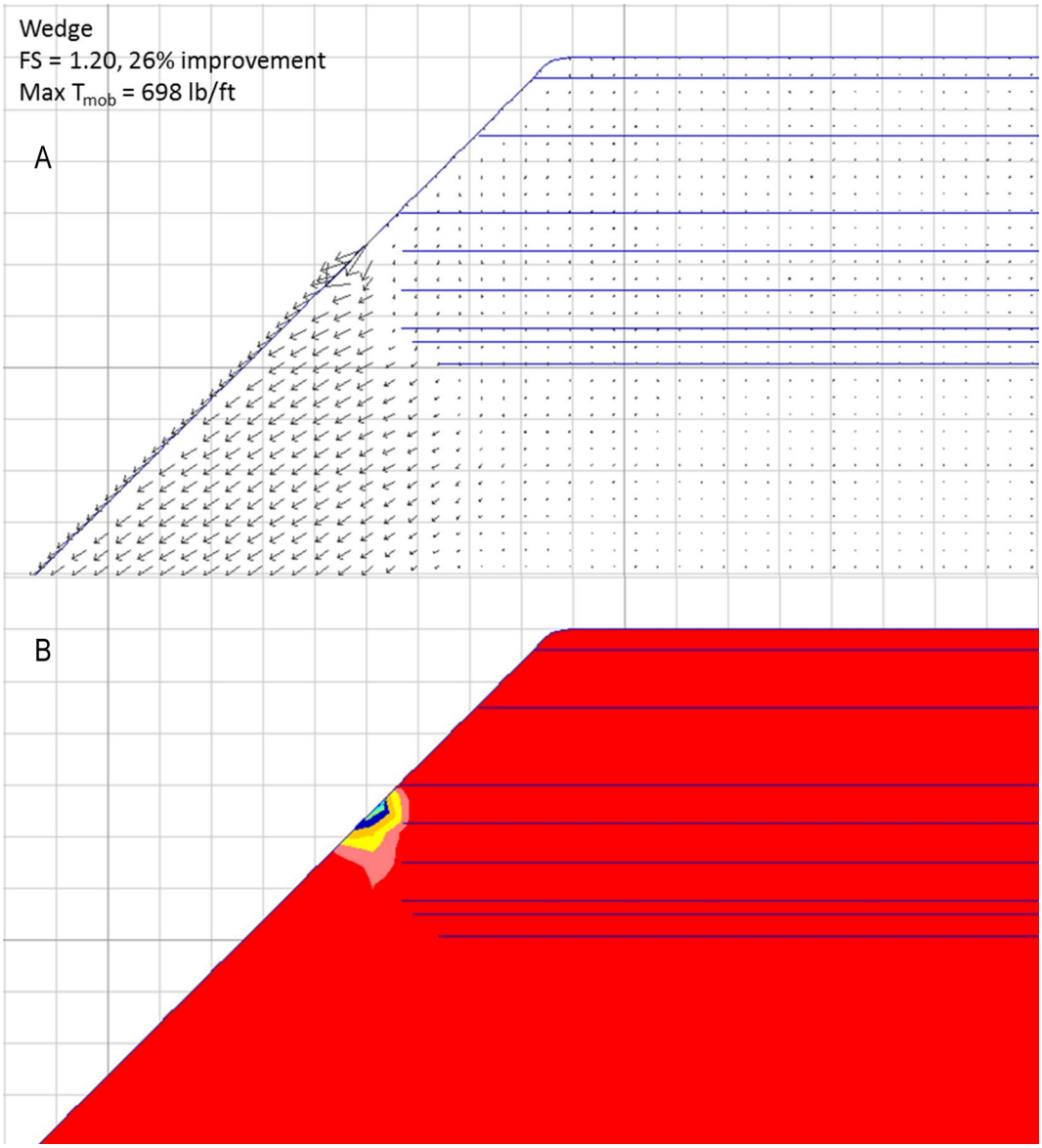

Figure 104: FLAC/Slope results for WFLHD deep patch wedge failure, a) velocity vector plot and b) shear strain rate contours.

8.3 SUMMARY

The performance of negative batter deep patches was investigated using FLAC/Slope for two slope geometries with various soil types (strengths) and failure mechanisms. The results indicated that negative batter deep patches were sometimes acceptable, and in some cases possibly required a deeper repair. Ultimately, the appropriateness of negative batter deep patches should be analyzed using a 2D finite difference or finite element analysis tool on a case-by-case basis using site-specific information.

9 DEEP PATCH DESIGN METHODOLOGY

9.1 BACKGROUND AND OVERVIEW

The deep patch method has been used for several decades as a mitigation technique for shallower subsidence of roadway embankments. The design procedure for this method has generally been based on limit equilibrium, slope stability analyses and/or rules of thumb. More recently, a simplified method for designing deep patches was created by the USDA Forest Service in cooperation with the FHWA Coordinated Federal Lands Highway Technology Improvement Program (Musser and Denning, 2005). A new method has been created based on the findings of research presented in Chapters 2 through 8 of this report. This new method was developed to have a well-documented analytical basis for conditions commonly occurring in slopes where a deep patch is appropriate.

9.2 IMPLEMENTATION CONSIDERATIONS

The deep patch repair method is primarily used to stabilize relatively shallow subsidence of the fill material associated with historic sidecast construction, or subsidence of a weaker, less competent wedge of material atop a more stable or natural deposit. Even though deep patches are generally limited to relatively shallow settlements they have also been used to repair larger global movements. These repairs, however, were typically employed as a short-term solution, and their long term performance has not been completely verified. The applicability of this method is generally limited to relatively narrow subsidence that occurs in the weaker embankment material and not in the stronger/natural slope (i.e., $X_c < X$, where X_c is the distance from the crest of the embankment to the furthest point of distress, and X is the distance from the slope crest to the estimated location of the strong/weak interface, as illustrated in Figure 105 (methods to estimate X in the field will be discussed in the next section). This method is intended for use on soils with higher friction angles and low cohesion, and not for low friction/high cohesion applications. The repair techniques developed as part of this research were developed for slope angles of $\beta = 34°$ and 39° (1½:1 and 1¼:1, respectively). These methods have been employed on steeper slopes (generally not greater than 1:1); however, development of the deep patch design at β angles greater than 1¼:1 was outside the scope of this project. General guidance to employ the deep patch repair technique is summarized in Table 37.

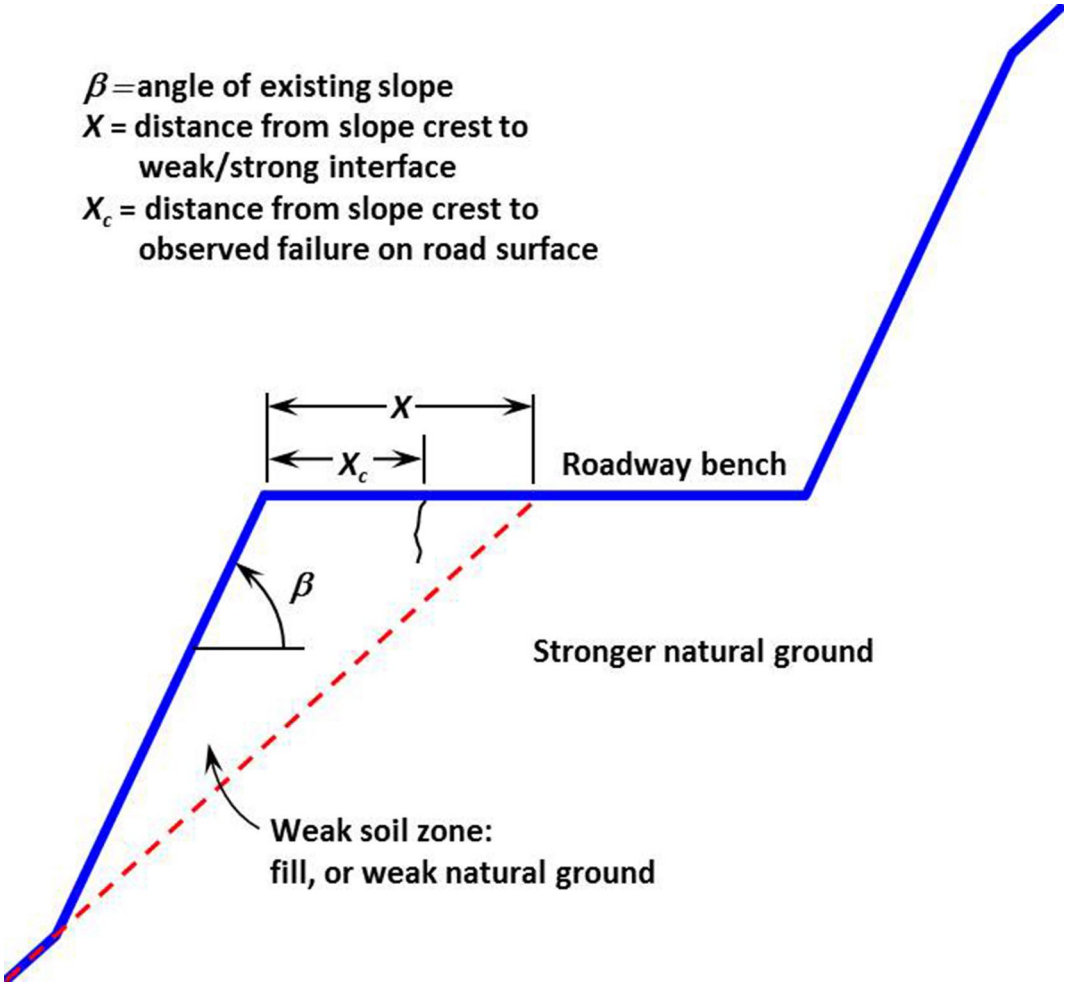

Figure 105: Illustration of slope geometry associated with deep patch repair.

Table 37: General Guidelines to Employ the Deep Patch Repair

Design Component	Guidance
Weak Soil Zone	granular materials (ϕ>15°) low cohesion (c<200psf)
Slope Geometry	34° < β < 39° 3 ft < X < 30ft 3 ft < X_c < 15ft
Distresses	shallow vertical deflection minimal slope creep

Road surface distresses typically addressed using the deep patch are generally arc-shaped resulting from continued or substantial movement of the weak soil material. The history of repair activity at a particular location may help locate a suitable site to employ the deep patch repair, but final selection mainly depends on the site topography and the extent of damage and/or subsidence. While the presence of water also has a direct influence on the performance of deep patches, providing adequate site drainage is assumed as part of the design and construction process, and is therefore not specifically addressed within.

9.3 DEEP PATCH DESIGN

The deep patch design methodology created as part of this research effort is based on the analytical work using limit equilibrium and numerical methods-based slope stability software, as described in Chapters 3 through 7. This method does not specifically require the use of limit equilibrium and/or finite difference analysis tools; however, these analytical methods can be used to verify and/or modify specific attributes of the design, if necessary or desired. The method is specific to addressing shallow rotational or wedge failures in the fill and/or weak material of road embankments by providing stability through geosynthetic reinforced soil layers in the upper part of the embankment beneath the road surface. It is assumed that routine slope design practices are incorporated as part of this process; for example, providing adequate drainage, designing an appropriate road surface, addressing potential erosion, managing vegetation, proper use of geosynthetic reinforcement (e.g., minimum embedment length, proper construction practices, etc.), compacting backfill material, etc. According to this method, there are generally three phases in the deep patch design process.

- **Site selection**—obtain preliminary field data to determine whether or not the deep patch repair technique is suitable.
- **Field data collection**—collect measurements of the extent of damage from slope instability as well as necessary design inputs.
- **Deep patch design**—Use design inputs to determine the depth, width, number of layers, layer spacing and tensile strength of the reinforcement, as detailed in the following subsections.

9.3.1 Step 1—Design Inputs

Assuming that the deep patch method is the most economical and feasible repair technique, the first step in the design process is to measure or estimate the specific design inputs. Beyond this, however, careful attention should be paid to other site characteristics such as vegetation, ground water levels and/or seepage, erosion, drainage, and any other site characteristic that may affect construction in order to make sure other repairs are included during construction. Groundwater is not specifically addressed in the design procedure. Future success of the deep patch repair depends

on these issues being addressed as part of the design process and during construction. Four parameters are needed to properly design a deep patch (illustrated in Figure 106):

L, the length of distress along the roadway at the embankment hinge point,

X_c, the horizontal distance from the embankment hinge point to the furthest point of distress as measured perpendicular to the centerline of the road,

X, the distance from the slope crest to the point at which the weak/strong or fill/native interface intersects the road surface, and

β, the angle of the embankment slope.

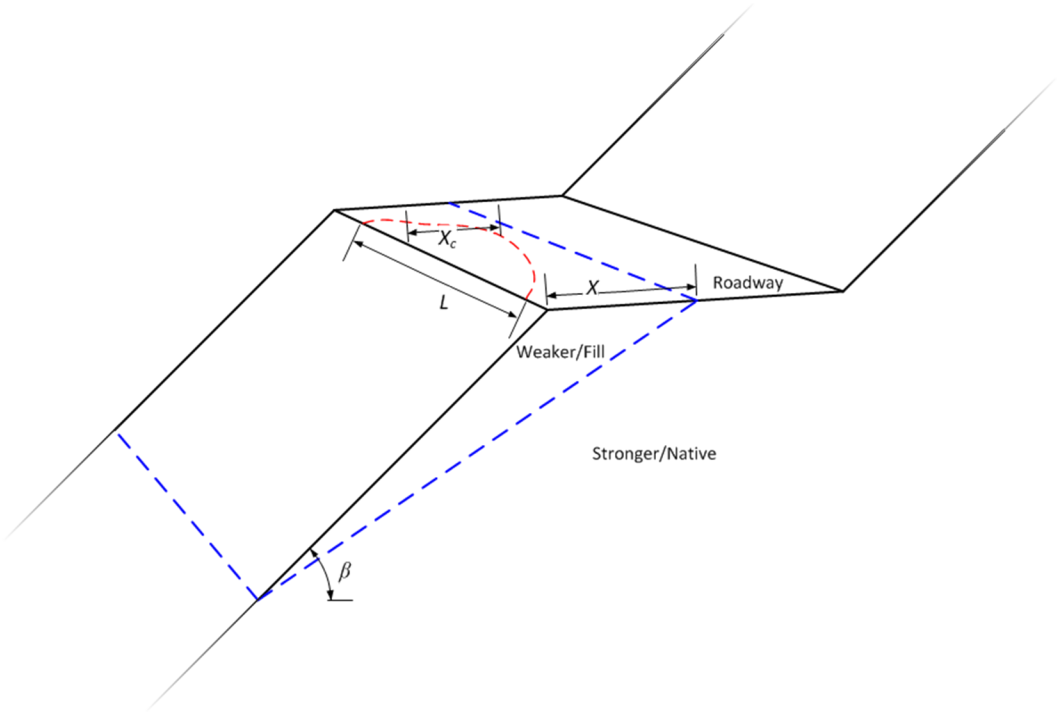

Figure 106: Illustration of parameters for deep patch design

Determining L is simple, and can be directly measured in the field using a standard tape measure. At times the arc-shaped distress in the road surface will extend into the road shoulder making it difficult to determine its extent, or it may terminate prior to reaching the edge. In either case, careful attention must be paid to ensure that the deep patch repair will be long enough to capture the entire affected area. Furthermore, an accurate measurement of the length is necessary to ensure sufficient embedment of the geosynthetic beyond the active zone (usually 5 to 15 ft, depending on site conditions).

The measurement of X_c is also simple, although determining where the crest is can sometimes be challenging depending on the road shoulder topography. In this study, X_c was limited to values greater than 3 ft since failure surfaces less than 3 ft usually initiate within the roadway shoulder and may not affect roadway performance. The analytical work described in Chapter 3 showed that X_c did not exceed 15 feet and was about half of X for the two slope geometries considered as part of this work (based on $\beta = 34°$ and 39°). **Therefore, design charts created as part of this project are limited to situations where X_c is greater than 3 ft, less than 15 ft, and is less than about half of the distance X.**

The distance X is not as easy to determine because there are no physical features that can be directly measured. Information from topographic surveys, borings, excavations or other subsurface investigations can be used to estimate this parameter; however, these methods tend to be expensive and time consuming, and may still not pinpoint its exact location. A reasonable estimate of X can be made based on topography and cut-and-cast balancing near the distressed location. Larger values of X tend to be associated with larger fills, while smaller values of X tend to be associated with larger cuts. Larger fills are generally over natural drainages, which are typically on an inside curve or on roads that are built entirely as an embankment. Conversely, larger cuts are typically on steeper natural slopes, on an outside curve, or are preceded or followed by an area needing fill. A summary of general criteria that can be used to estimate X is provided in Table 38. An estimate of X ±3 ft will generally lead to an appropriate and efficient design, based on the shape and layout of the design charts described in Step 2 and provided below. In cases where X is unknown, the depth of the deep patch will usually not vary by more than about 1 to 2 ft, but may vary by up to 4 ft in certain cases. **The design charts created as part of this project are limited to situations where X is greater than 3 ft and less than 30 ft, and generally more than twice as big as X_c.**

Table 38: Summary of General Criteria Used to Estimate X

X	General Criteria
Larger X	Wider Fill
	Inside Curve
	Natural drainage area or depression
	Shallower slopes/embankment
Smaller X	Wider cut into the hillside
	Outside corner
	Steeper natural slopes
	Preceded or followed by fill area

Design charts created as part of this effort were based on fill slopes of β = 34° and 39° only. Field measurements of β can be made using a clinometer, surveying equipment, or a plumb bob, level and tape measure. If the slope angle happens to be between 34° and 39°, the depth and tensile strength information can be interpolated.

9.3.2 Step 2—Determine Depth and Layer Spacing

The second step in the design process is to determine the depth of the deep patch and the spacing of the geosynthetic layers. Two sets of charts are used to determine the depth and layer spacing of the deep patch repair, based on X and X_c, one set for β = 34° (1½H:1V slope) and the other set for β = 39° (1¼H:1V slope). As described in detail in Chapter 3, limit equilibrium software was used to determine fill soil properties (ϕ and c) associated with a FS = 1.0. These parameters were used as inputs in FLAC/Slope to determine X_c for unreinforced slopes having various combinations of α (20–38°), H (10–60 ft), X (3–30 ft) and β (34 and 39°), as defined previously in Figure 48 in Chapter 3. Unreinforced slopes with both rotational and wedge type failures were analyzed. These slopes were then analyzed using FLAC/Slope with various configurations of reinforcement. The results were combined into single plots of X versus X_c for β = 34 and 39°, for repairs having 1-ft or 2-ft spacing between geosynthetic layers. Geosynthetic spacing less than 1 ft and greater than 2 ft were found to be either inefficient or ineffective. These plots were used as the basis of the graphics created in Figure 107 (β = 34°) and Figure 108 (β = 39°). Shaded areas on these charts are divided in several regions which indicate the depth of the deep patch. For β = 34°, deep patches range from 3 to 7 ft deep for 1-ft spacing and 4 to 10 ft deep for 2-ft spacing. For β = 39°, deep patches range from 3 to 9 ft deep for 1-ft spacing and 6 to 10 ft deep for 2-ft spacing. Depending on the fill slope angle, values of X and X_c are used to pinpoint a location on the 1-ft spacing and 2-ft spacing charts. Points that lie outside of the shaded area are invalid and indicate a situation where the deep patch design may not provide long term stability. The depth and spacing are recorded from Figure 107 or Figure 108 and the reinforcement tensile capacity is then determined in step 3.

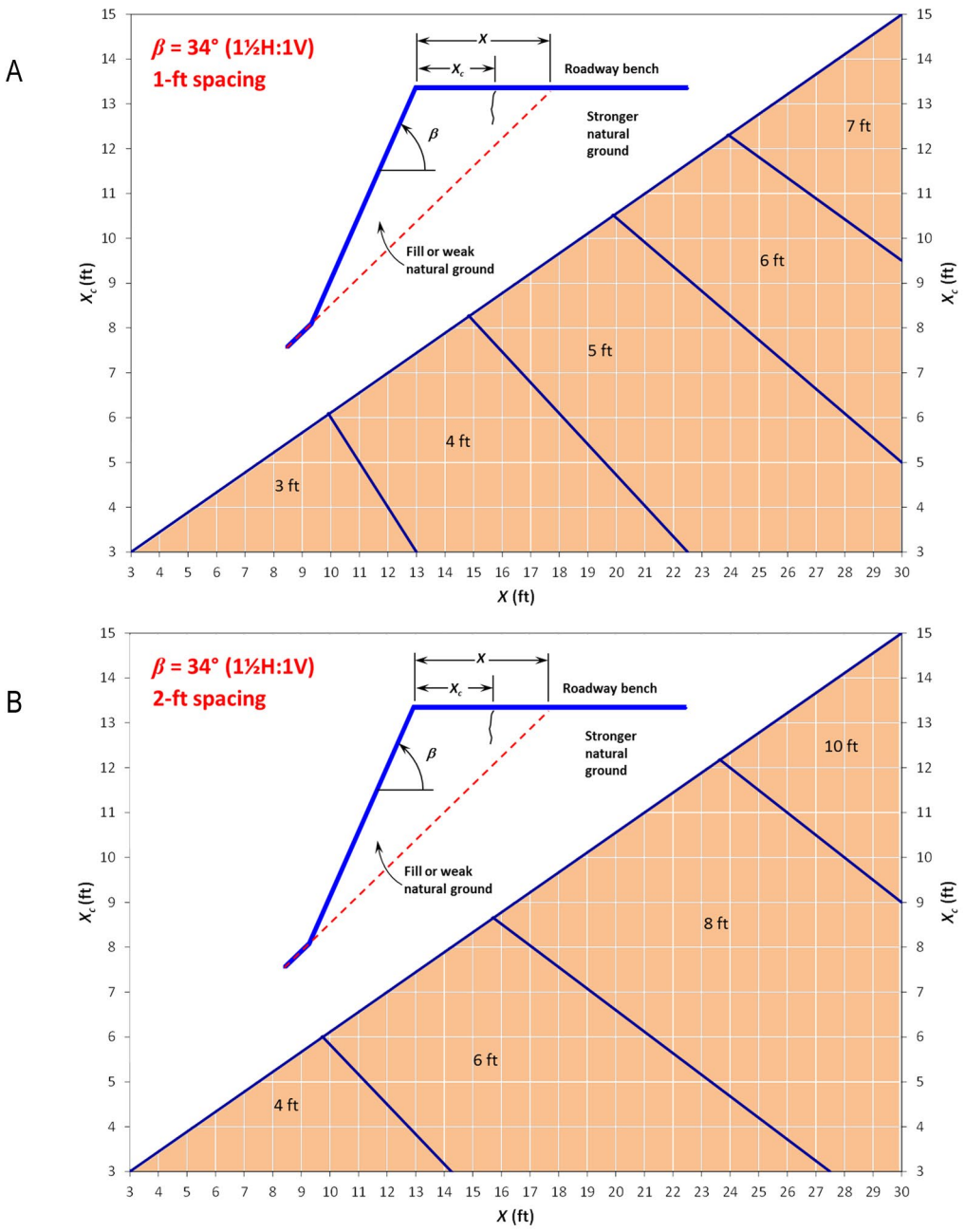

Figure 107: Design charts to determine depth and layer spacing for β = 34° (1½H:1V).

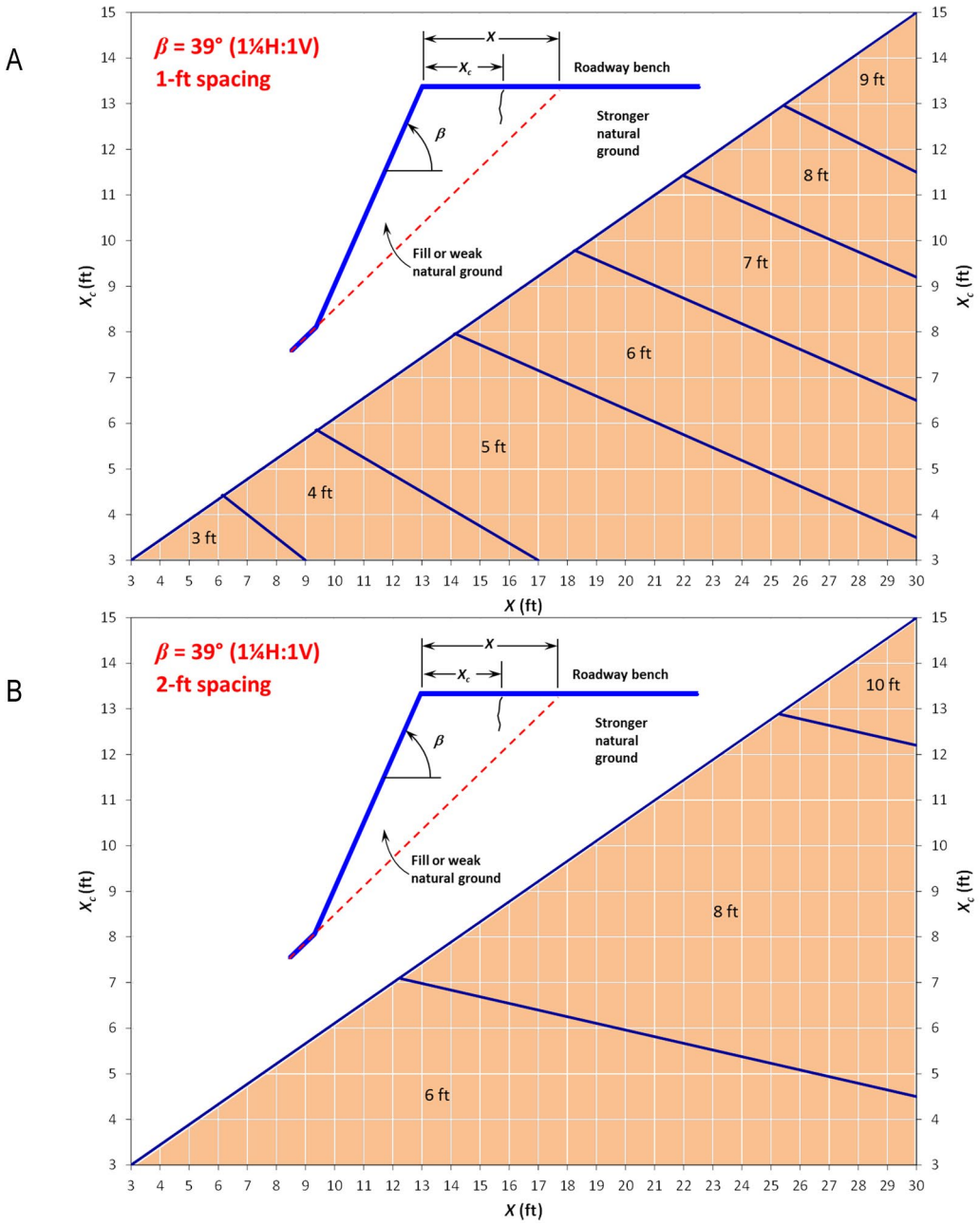

Figure 108: Design charts to determine depth and layer spacing for β = 39° (1¼H:1V).

9.3.3 Step 3—Determine Ultimate Total Tensile Capacity of Reinforcement

The four equations listed below can be used to determine the total required tensile capacity of the geosynthetic reinforcement (T_{req}) based solely on the distance X_c, where T_{req} has units of lb/ft and X_c has units of ft. The equations used to determine T_{req} were based on data from the numerical analysis discussed in Chapter 6. The equations for T_{req} were determined using a polynomial best fit line through the data presented in Figure 74 and Figure 75 for β = 34° (Equations 8 and 9, respectively) and Figure 80 and Figure 81 for β = 39° (Equations 10 and 11, respectively). This approach was shown to provide adequate estimates of tensile strength required for the various cases considered as part of this analysis, as discussed in Chapter 6.

β = 34°, 1-ft spacing: $T_{req} = 116X_c^2+144X_c$ **Equation 8**

β = 34°, 2-ft spacing: $T_{req} = 68X_c^2+269X_c$ **Equation 9**

β = 39°, 1-ft spacing: $T_{req} = 199X_c^2-262X_c$ **Equation 10**

β = 39°, 2-ft spacing: $T_{req} = 74X_c^2+287X_c$ **Equation 11**

where X_c has units of feet and T_{req} has units of lb/ft.

T_{req} is taken as the sum of the unfactored tensile strength of all geosynthetic layers in the deep patch. Strength values obtained using these equations are not factored, and may need to be adjusted based on expected installation damage, creep, and durability (chemical degradation, thermal oxidation, hydrolysis, environmental stress cracking and microorganisms), all of which are discussed in detail in Section 3.5 of the Design and Construction of Mechanically Stabilized Earth Walls and Reinforced Slopes (Berg et al., 2009a). The nominal, unfactored tensile strength of an individual layer of the geosynthetic (T_{nom}) is determined by dividing T_{req} by the number of geosynthetic layers (n) in the deep patch design (Equation 12). The ultimate tensile strength to be used to specify one geosynthetic layer can be determined using Equation 13.

$T_{nom} = T_{req}/n$ **Equation 12**

$T_{ult} = T_{nom} (RF_{ID} \cdot RF_{CR} \cdot RF_D)$ **Equation 13**

RF_{ID} is the installation damage reduction factor; see Table 3-9 in Section 3.5.2.b of Berg et al., 2009a.

RF_{CR} is the creep reduction factor which is a function of the geogrid polymer type; see range of typical values in Section 3.5.2.c of Berg et al., 2009a.

RF_{D} is the durability reduction factor which typically ranges from 1.1 to 2.0; see Section 3.5.2.d of Berg et al., 2009a.

The analysis and resulting design charts developed as part of this research utilized biaxial reinforcement properties. Using 3D modeling, it was shown that slope stabilization using biaxial geogrids was superior to uniaxial materials based on how well each type of material limited distresses in the road surface. Biaxial grids also showed better performance for longer repairs (i.e., greater L). However, biaxial grids are not available in the same magnitude of strengths as uniaxial grids or geotextiles. Additional research is needed to fully establish reinforcement requirements when uniaxial materials are used. Geotextiles are expected to perform similarly to biaxial geogrids as long as embedment length is adequate to prevent pullout (15 ft was found to be adequate, as described in Section 5.4). The 4th and final step is to optimize the design based on the T_{ult} calculated from these equations.

9.3.4 Step 4—Optimize and Finalize Design

The most efficient design can be determined using information collected from steps 1–3; however, the most economical design will also depend on several external factors such as cost, availability of construction materials (e.g., geogrids, structural fill), topography, site layout, anticipated traffic levels, etc. In general, using the 2-ft spacing uses less geosynthetic, but increases the depth of the deep patch. Conversely, using a 1-ft spacing is generally shallower, but uses more reinforcement. Consideration of the depth, number of layers and required tensile force is necessary to determine the most efficient design. The required geogrid strength per layer must be factored based on expected installation damage, creep, durability, chemical degradation, and/or biological degradation to specify a particular geosynthetic.

The length and width of the deep patch is the final step in the design process. Based on the analysis described in Chapter 5, **the embedded length of the geosynthetic is assumed to be 10 feet beyond X_c for geogrids and 15 feet beyond X_c for geotextiles.** Mohney et al. (1994) recommends that the geogrid be embedded by at least a distance of X_c beyond the innermost crack. Limit equilibrium-based analytical tools that use site-specific characteristics can be used to optimize geosynthetic embedment length necessary to provide adequate pullout resistance. **The length of the deep patch (i.e., parallel to the direction of traffic) is generally 10 to 15 ft beyond the ends of the deep patch.**

9.3.5 Design Flow Chart

The flowchart in Figure 109 summarizes the deep patch design steps described above.

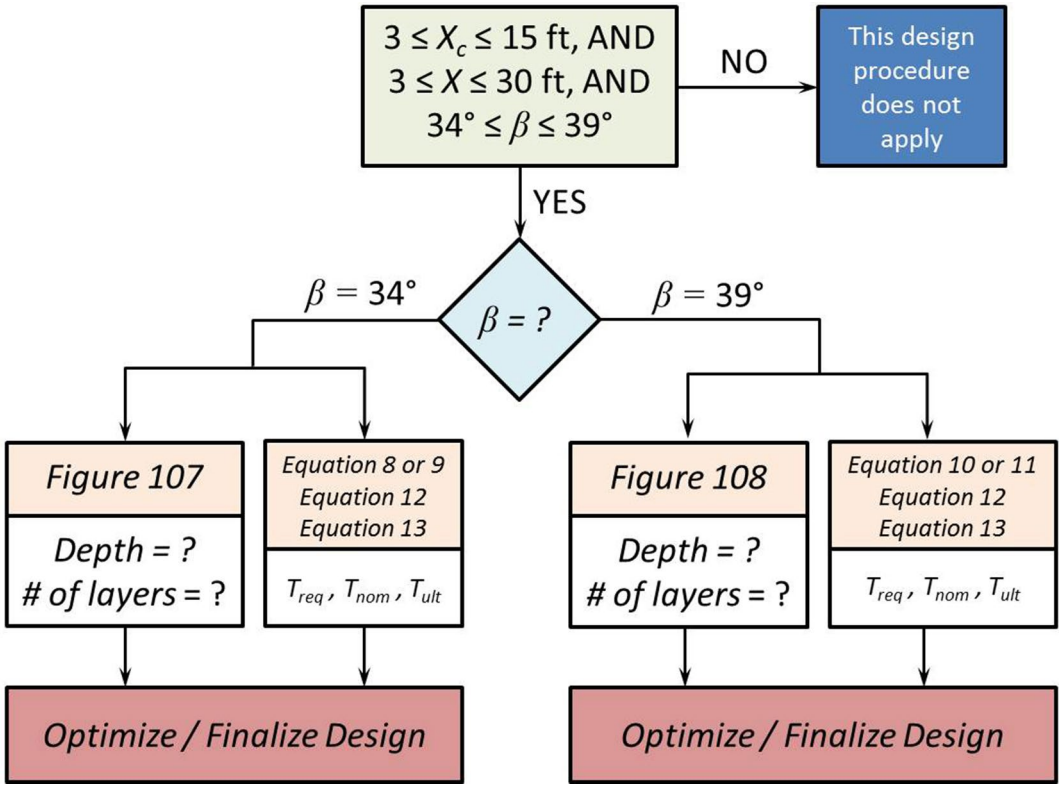

Figure 109: Flowchart of deep patch design method.

9.4 DESIGN EXAMPLE

General description—the site is located on a curved section of road near an intersection with a natural drainage. The arc-shaped distresses in the pavement are in line with the drainage and were repaired using an asphalt patch two years prior to a recent site visit. Differential displacement since then shows about 0.5 inches of movement.

Step 1—Field data indicates that the length of the distress is 60 ft, X_c is 7 ft, and the fill slope angle, β, is 39° (1¼H:1V). The width of the road bench is 24 feet, and because the roadway crosses a natural drainage at this location, it is assumed that the road bench is

mostly fill material. This is further substantiated by the cuts on either end of the affected area. Therefore, X was estimated to be between 18 and 24 ft (i.e., 21 ± 3 ft).

Check: $3 \le X_c \le 15$ ft $\quad 3 \le 7 \le 15$ ✓ **okay**

Check: $3 \le X \le 30$ ft $\quad 3 \le 21 \le 30$ ✓ **okay**

Check $34° \le \beta \le 39°$ $\quad \beta = 39°$ ✓ **okay**

Step 2—Determine the depth and spacing of the deep patch using the $\beta = 39°$ design charts using X_c and X, as illustrated in Figure 110 below.

A

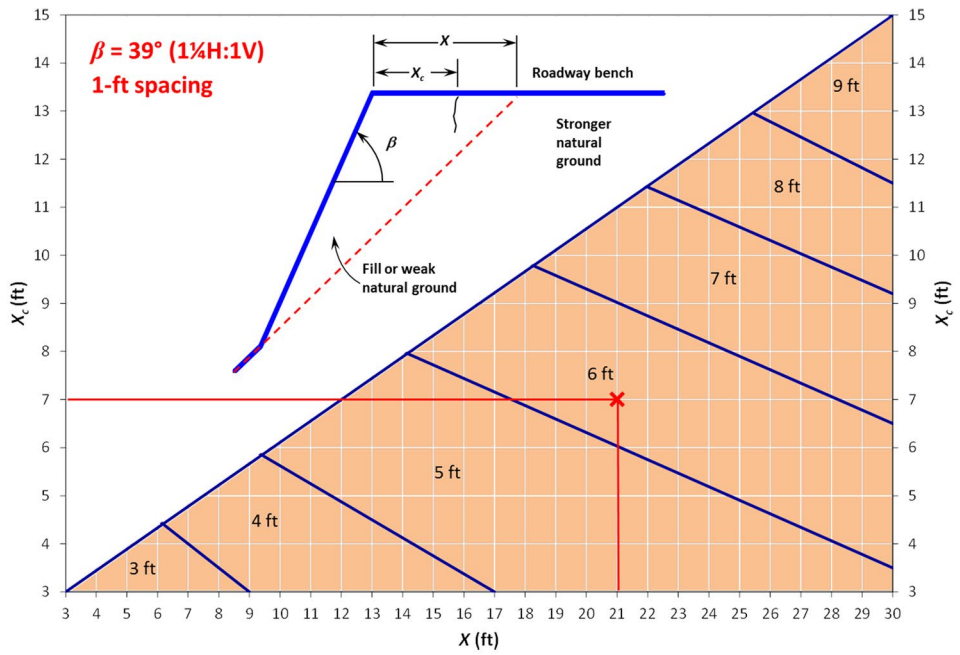

B

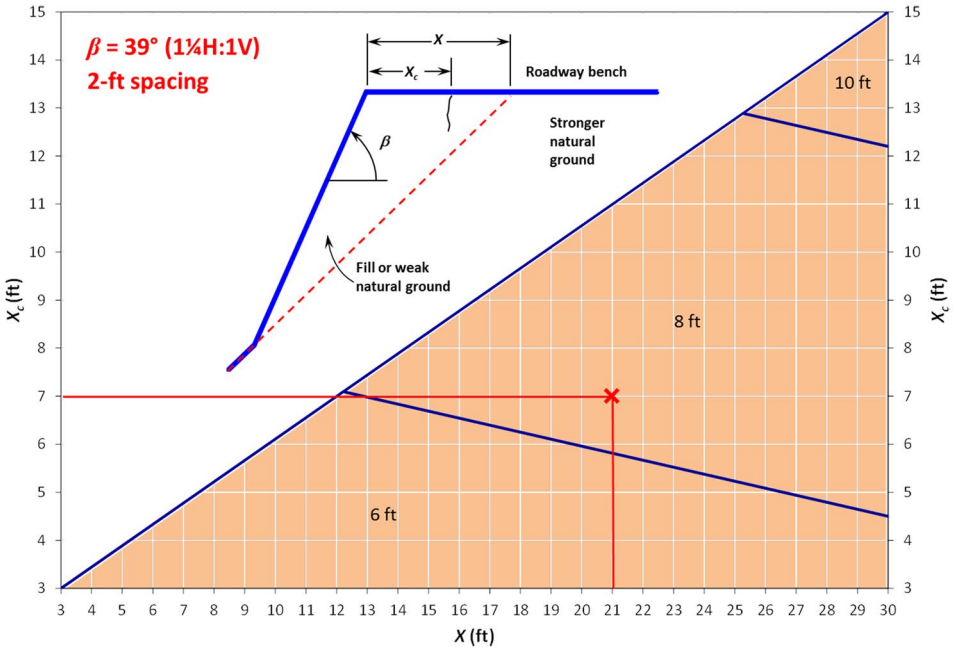

Figure 110: Illustration of depth and layer spacing determination from new design charts.

Results indicate that a 6 ft deep repair with 6 layers (Option 1) or an 8 ft deep repair with 4 layers (Option 2) will work. Schematics of the site layout for each of these options are presented in Figure 111, assuming a 10-foot embedment length of a geogrid.

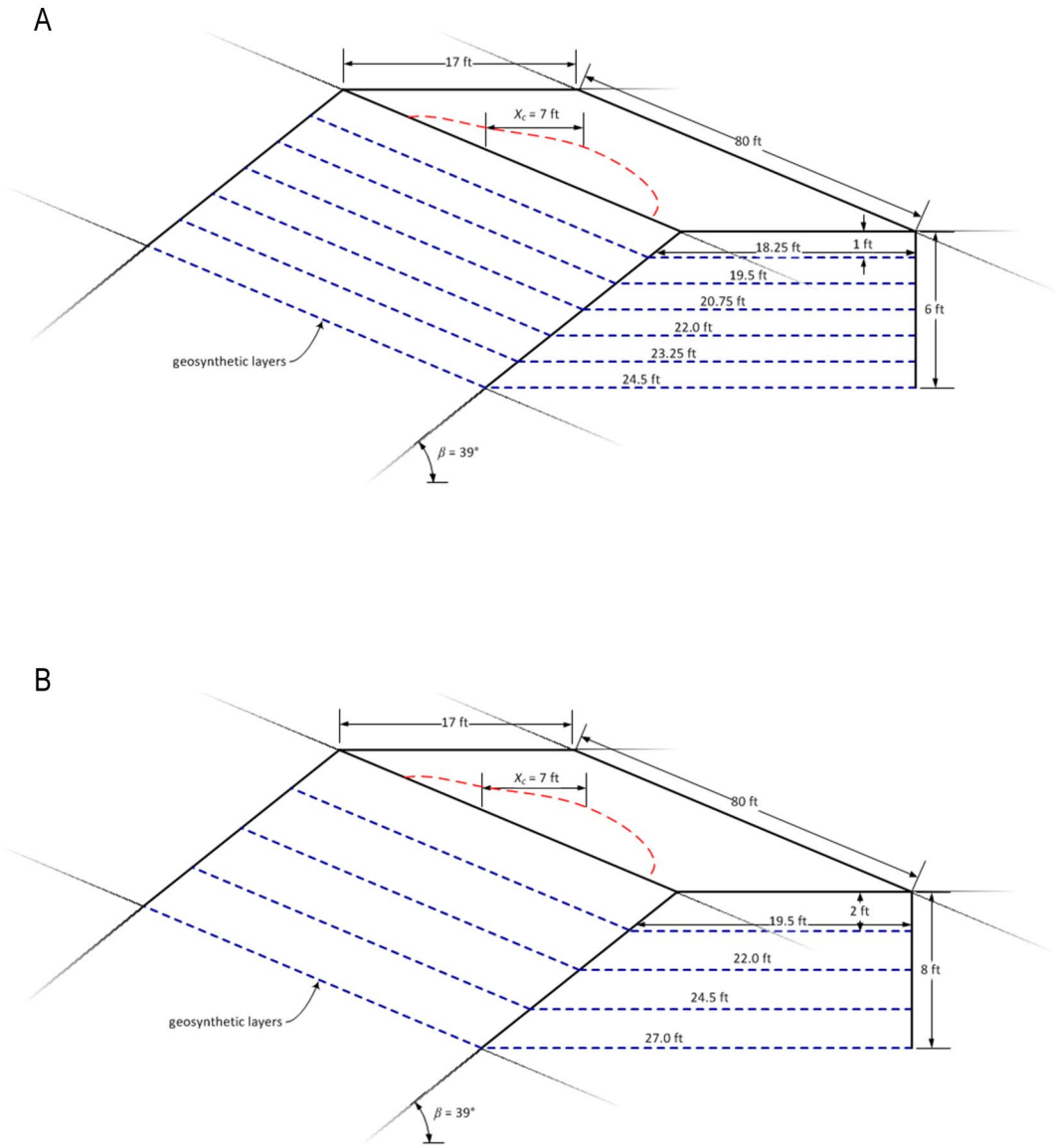

Figure 111: Illustrations of design options: a) Option 1 – 6 ft deep, 6 layers and b) Option 2 – 8 ft deep, 4 layers.

Step 3—Determine the total required tensile capacity of the geogrid reinforcement using X_c and Equation 10 and Equation 11.

$\beta = 39°$, 1-ft spacing: $T_{req1} = 199X_c^2 - 262X_c$ $T_{req1} = 199(7)^2 - 262(7)$ $T_{req1} = 7917$ lb/ft

$\beta = 39°$, 2-ft spacing: $T_{req2} = 74X_c^2 + 287X_c$ $T_{req2} = 74(7)^2 + 287(7)$ $T_{req2} = 5635$ lb/ft

The nominal strength needed for each individual layer can be determined by dividing the total tensile strength required by the number of layers. For 1-ft spacing, 7,917 lb/ft of tensile force is needed, divided by 6 layers; T_{nom1} = 1,320 lb/ft per layer. For 2-ft spacing, 5,635 lb/ft of tensile force is needed, divided by 4 layers; T_{nom2} = 1,409 lb/ft per layer. Equation 13 can be used to calculate the ultimate tensile capacity of the reinforcement. From Table 3-9 (Berg et al., 2009a), an RF_{ID} of 1.4 seems reasonable for most geogrids. Assuming a polyester geogrid was going to be used on this project, then a RF_{CR} of about 2.0 is reasonable. RF_D ranges between 1.1 and 2, so a middle value of 1.5 was chosen for this example.

For $\beta = 39°$, 1-ft spacing: $T_{ult1} = 1{,}320(1.4*2.0*1.5)$ $T_{ult1} = 5{,}544$ lb/ft

For $\beta = 39°$, 2-ft spacing: $T_{ult2} = 1{,}409(1.4*2.0*1.5)$ $T_{ult2} = 5{,}918$ lb/ft

Step 4—The cost comparison is based solely on the cost of excavation and placement of embankment fill, and the purchase of the geogrids. The following five assumptions were made to facilitate a direct comparison between the two available options.

1. A single product was selected that would work for either option. In that case, the cost comparison is based solely on the amount of geogrid needed for each option and not directly the required strength. Cost per square yard of geogrid was assumed to be \$5/yd^2.
2. The cost of excavation is \$20/yd^3 and \$50/yd^3 for materials and placement; \$70/yd^3 combined.
3. The geogrid is embedded 10 ft beyond X_c.
4. The geogrid is extended 10 ft beyond both ends of the excavation parallel to the road; total excavation = 80 ft. Construction ramps on each end are not included in the analysis.
5. Geogrids terminate at the slope face (i.e., no wrapped face).

Construction Quantities

Calculate the total area of geosynthetics for each option:

Area 1 = 80 (18.25 + 19.5 + 20.75 + 22 + 23.25 + 24.5) = 10,260 ft^2 = 1,140 yd^2

Area 2 = 80 (19.5 + 22 + 24.5 + 27) = 7,440 ft^2 = 827 yd^2

Calculate the volume of excavation for each option:

Volume 1 = 80 [(6*17) + (0.5*6*7.5)] = 9,960 ft^3 = 369 yd^3

Volume 2 = 80 [(8*17) + (0.5*8*10)] = 14,080 ft^3 = 521 yd^3

Cost Calculations

Determine the total cost of the geogrids for each option:

Geogrid-cost 1 = \$5/yd^2 * 1,140 yd^2 = \$5,700

Geogrid-cost 2 = \$5/yd^2 * 827 yd^2 = \$4,135

Determine the total cost of excavation for each option:

Ex-cost 1 = \$70/yd^3 * 369 yd^3 = \$25,830

Ex-cost 2 = \$70/yd^3 * 521 yd^3 = \$36,470

Determine total costs of excavation and geosynthetics for each option:

Total 1 = \$25,830 + \$5,700 = \$31,530 ✓ **best option**

Total 2 = \$36,470 + \$4,135 = \$40,605

In conclusion, the 6 ft, 6 layer option is the best based solely on geosynthetic and construction costs. From this example, the cost of deep patch repairs is affected more by the excavation and material placement than the geosynthetics. In these examples, the cost of the geosynthetic was much less than the cost of the earthwork; therefore, it is anticipated that in most cases it will be more cost effective to select the shallower option.

9.5 COMPARISON OF DESIGN EXAMPLE TO A RESSA DESIGN

The new design method presented in this report was compared to a more general method of design with ReSSA using the same parameters from the design example provided above. An infinite number of slopes can be created by adjusting H (slope

height) and α (original slope angle or angle of strong, native ground). A slope height of 60 ft was assumed for this comparison, which represents the greatest slope height likely to exist in the field. Several ReSSA analyses were run to back-calculate the soil strength parameters such that 1) the factor of safety of the critical slip circle was 1.0, and 2) the failure surface intersected the road bench 7 feet from the crest (X_c = 7 ft, as in the design example). The weak soil properties were found to be ϕ = 22°, c = 172 psf; the strong/native soil properties were ϕ = 50°, c = 0 psf.

With the unreinforced slope calibrated to the design example, the next step was to determine the tensile strength required to reinforce the slope to a factor of safety of 1.3. It was demonstrated in Section 4.2 that different deep patch configurations (based on depth and reinforcement spacing) behaved similarly as long as they all contained the same total resistance as provided by the geosynthetics, meaning that a single layer of reinforcement could be used to determine the tensile strength of the reinforcement needed to provide a factor of safety of 1.3 just as well as multiple layers. Using this information, a single layer of geosynthetic reinforcement having T_{req} = 8,500 lb/ft was necessary. Using the allowable tensile strength limitations based on pullout, the following configurations provide the required 8,500 lb/ft of reinforcement:

- 6 ft depth, 6 layers of reinforcement at 1-ft spacing,
- 7 ft depth, 4 layers of reinforcement at 1.75-ft spacing, and
- 8 ft depth, 4 layers of reinforcement at 2-ft spacing.

Pullout considerations limit the amount of tensile strength that is mobilized in each layer of reinforcement (refer to Figure 67 in Section 5.4). Using this information, the nominal tensile strength needed for each layer of the three configurations is 1,734 lb/ft, 2,807 lb/ft, and 2,600 lb/ft, respectively, based on a 10-foot embedment length, L_e = 10 ft (Table 39). Applying the same reduction factors from the design example (RF_{ID} = 1.4, RF_{CR} = 2.0, and RF_D = 1.5), the T_{ult} needed for each configuration is 7,279 lb/ft, 11,789 lb/ft, and 10,920 lb/ft, respectively.

Table 39: Tensile Strength for ReSSA Design Configurations

Configuration	Depth (ft)	Available Pullout Resistance (lb/ft)	Assigned Tensile Strength (lb/ft)	Cumulative Tensile Strength (ft/lb)
6 ft, 6 layers	1	550	550	550
	2	1100	1100	1650
	3	1650	1650	3300
	4	2200	1733	5033
	5	2750	1733	6766
	6	3300	T_{nom} =1734	8500
7 ft, 4 layers	1.75	962	962	962
	3.5	1925	1925	2887
	5.25	2888	2806	5693
	7	3850	T_{nom} =2807	8500
8 ft, 4 layers	2	1100	1100	1100
	4	2200	2200	3300
	6	3300	2600	5900
	8	4400	T_{nom} = 2600	8500

These three deep patch configurations were modeled using ReSSA to verify the design factor of safety. The results from this analysis indicated that the factors of safety were lower than expected (FS = 1.2 instead of 1.3). In order to increase the factor of safety to 1.3, the embedment length of the geosynthetic was increased from 10 ft to 12 ft. The greater embedment length allowed greater mobilization of tensile strength in upper layers of reinforcement thereby reducing the nominal tensile strengths required for each configuration, the final results of which are summarized in Table 40.

Table 40: Summary of Comparison between New Design and ReSSA

Design Tool	Deep Patch Configuration	T_{req}(lb/ft)	T_{nom}(lb/ft)	T_{ult}(lb/ft)	L_e(ft)
New Design	6 ft deep, 6 layers	7917	1320	5544	10
	8 ft deep, 4 layers	5635	1409	5918	10
ReSSA	6 ft deep, 6 layers	8500	1638	6880	12
	7 ft deep, 4 layers	8500	2544	10,685	12
	8 ft deep, 4 layers	8500	2400	10,080	12

Overall, these results indicate that the tensile strength requirements based on the ReSSA analysis were slightly greater than the new design method. However, for shorter slopes (H = 40 or 20 ft), the depth, number of layers and reinforcement tensile strength requirements are greater for new design method than for the ReSSA. For example, for H = 40 ft, T_{req} = 6,000 lb/ft and a 5 ft, 5 layer or 6 ft, 3 layer are the recommended deep patch configurations. Shallower deep patches with less reinforcement are adequate for shorter slopes because less soil mass is involved in the original failure.

This ReSSA design example indicates that general limit equilibrium theory may be used to design deep patches, and it will generally provide results similar to the new design method developed as part of this project. Practical design knowledge (e.g., from previous experience or the design charts within this report) is necessary to determine depth of the deep patch, the number of geosynthetic layers, and the embedment length of the geosynthetic. The designer may then use ReSSA iteratively to evaluate multiple design configurations to determine the most practical and economical approach. If soil strength parameters or more specific information about geosynthetic–soil interaction properties are known, it is recommended to check the deep patch design using a general limit equilibrium method.

9.6 COMPARISON OF DESIGN EXAMPLE TO MUSSER AND DENNING (2005)

The method discussed in this report was compared to the method developed by Musser and Denning (2005) using the same parameters from the design example provided above. The pertinent parameters associated with this method are X_c, X, SD, ϕ, β and L_2, which are defined below.

- X_c is measured in the field, and is defined as 7 ft for this example.
- X, which is limited to between 3 and 12 ft on the design charts, can be set to X_c if unknown. X was set equal to X_c for this example; $X = X_c = 7$ft.
- SD, the slope distance from the crest of the fill to the lower limit of the sliding mass (i.e., toe of failure), can be calculated in terms of H (the height of the fill) and β using Equation 14, which is based on the geometry of the slope. Values for H ranged between 10 and 60 ft for the analytical work described in Chapter 3. Using an H of 10 ft yields a SD of 15.9 ft, and an H of 60 ft yields a SD of about 95 ft. The maximum SD that can be accommodated using Musser and Denning's charts, however, is 80 ft (mislabeled as 79 ft on the design charts), which corresponds to an H of about 50 ft. For this design example, SD values of 15.9 and 80 were used for the deep patch design, to evaluate the effect SD has on the design.
- $SD = \frac{H}{\sin\beta}$ **Equation 14**

- The friction angle of the fill, ϕ, is limited to 25, 30 or 35° based on the available design charts from Musser and Denning. All of these values were used to evaluate their effect on the results, specifically, the required tensile force for the geogrids.
- β is defined as 39°, based on the slope angle provided in Example 1 above.
- L_2 = 60 ft, based on the length provided in Example 1 above.

The design chart labeled as Figure 10 in Musser and Denning (2005) was used to determine the depth of the deep patch repair, as illustrated in Figure 112. For a SD of 15.9, the depth is 3.6 ft (shown in red) and for a SD of 80 ft, the suggested depth is 5 ft (shown in blue).

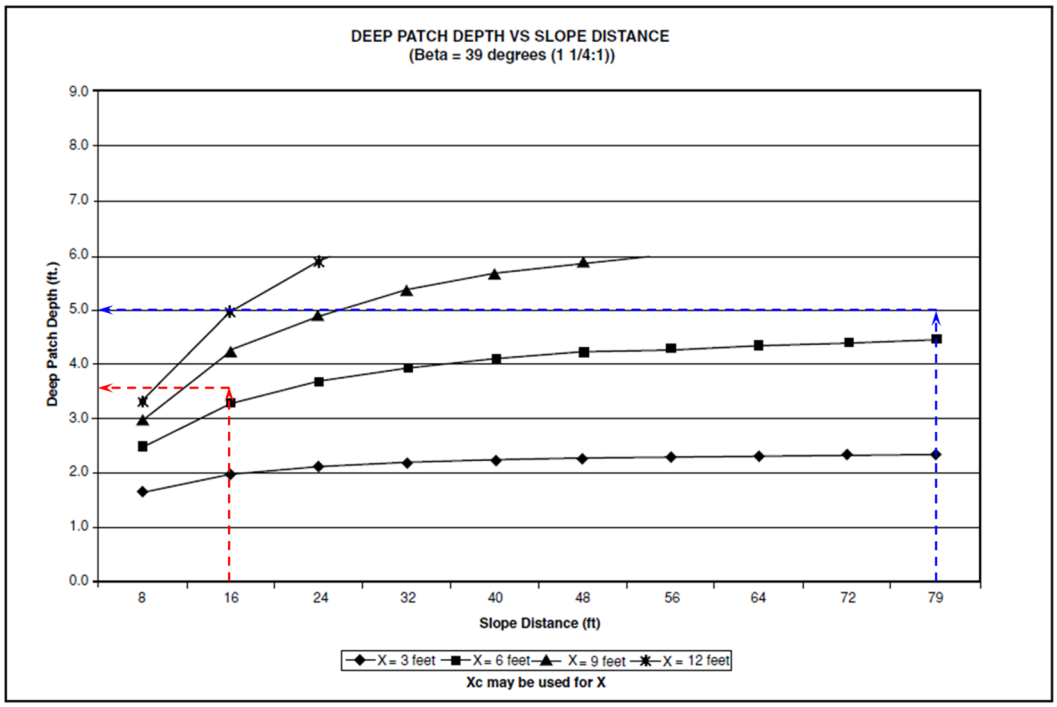

Figure 112: Illustration of depth determination from Musser and Denning (2005) design charts.

The required total tensile force can be calculated using one of three different design charts based on a friction angle of 25, 30 or 35°. Since the friction angle of the soil is not known in the design example above, the required force was determined using all three design charts (Figures 11, 15[5] and 13 from Musser and Denning, 2005), as illustrated in Figure 113 through Figure 115, and tabulated in Table 41.

[5]Figure 12 in Musser and Denning (2005), which was intended by the authors to be used for ϕ= 30° and β= 39°, was not correct. Figure 15 from their design example contained the correct information and was used instead.

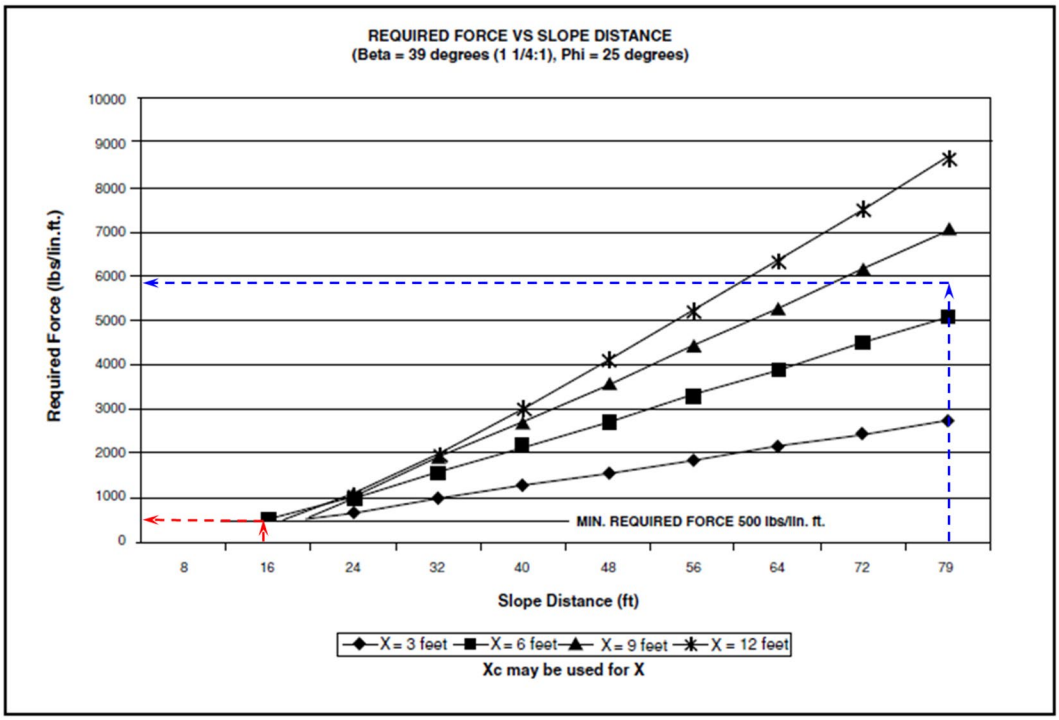

Figure 113: Illustration of required force determination from Musser and Denning (2005) design charts for $\phi = 25°$.

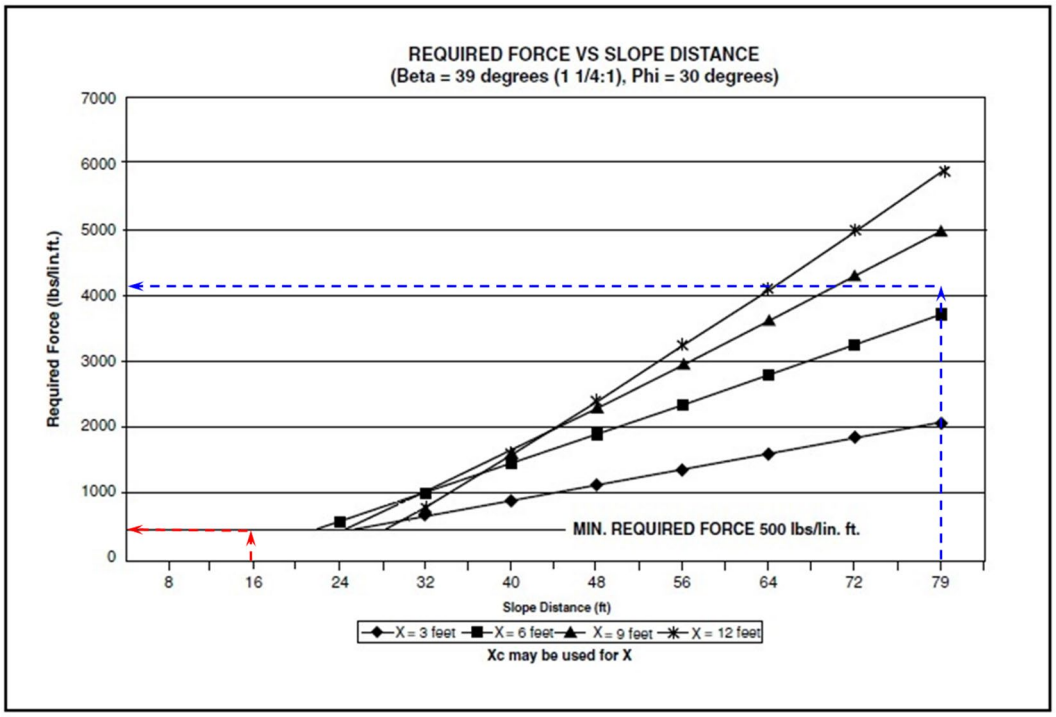

Figure 114: Illustration of required force determination from Musser and Denning (2005) design charts for $\phi = 30°$.

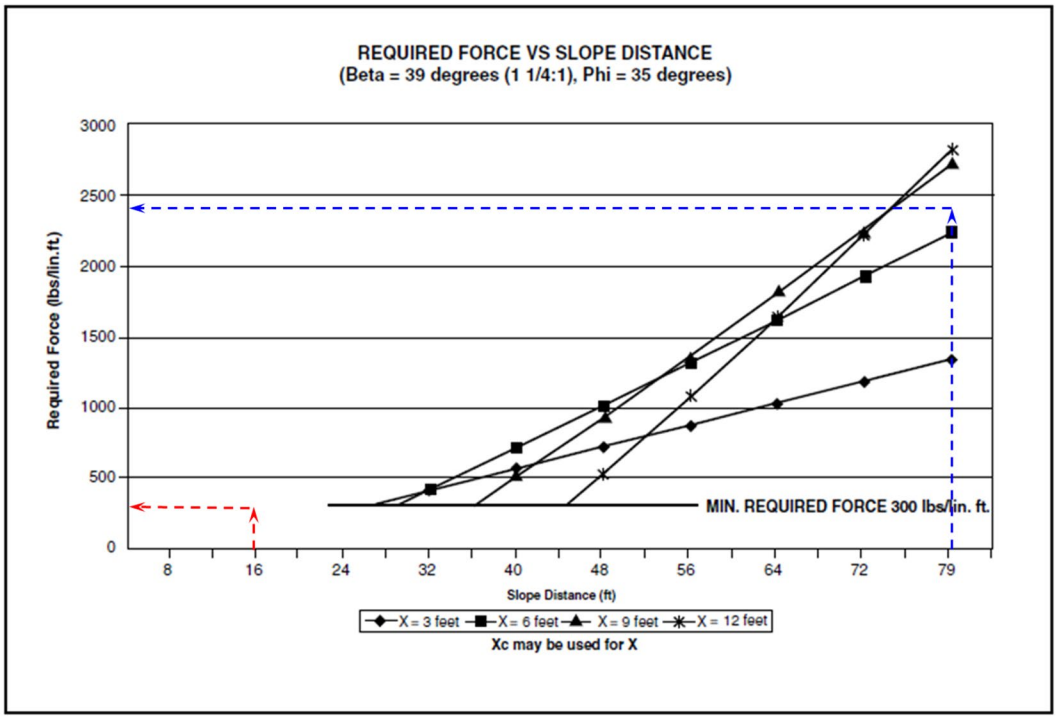

Figure 115: Illustration of required force determination from Musser and Denning (2005) design charts for $\phi = 35°$.

Table 41: Summary of Tensile Force Requirements from Musser and Denning (2005) Design Charts

SD	Required Geogrid Total Load Capacity (lb/ft)		
	$\phi = 25$	$\phi = 30$	$\phi = 35$
15.9 ft	500	500	300
80 ft	5900	4200	2400

Considering all of this information, there are essentially two configuration options based on the design parameters: a 4 ft deep patch (rounded up from 3.6 ft) or a 5 ft deep patch. To determine geogrid spacing, Musser and Denning (2005) make the following recommendations:

1. One to four layers of geogrid are usually used (e.g., one layer for 1.5-ft-deep excavation, and two to four layers for deeper patches, up to 6 feet deep).
2. Bottom layer usually placed 0.5 feet above bottom of excavation on top of leveling course.
3. Uppermost layer should be placed at least 1 ft below road surface.

4. Geogrid layers should be spaced evenly.
5. Geogrid spacing should coincide with backfill layer thicknesses, and should typically be greater than 1 ft.

Taking these suggestions into consideration, it is recommended that 2 layers of geogrid be used for the 4-ft-deep repair (located at 2 ft and 4 ft depths), and 3 layers of geogrid be used for the 5-ft-deep repair (located at 1 ft, 3 ft and 5 ft depths). The maximum and minimum reinforcement strength requirements based on the friction angle of the soil were used to calculate the amount of force needed per layer of geogrid, as summarized in Table 42. Average values were calculated as the midpoint of the range to facilitate a more direct comparison of the various options. Values ranged considerably, from 100 lb/ft to 2,950 lb/ft, based on the depth of the deep patch, the number of layers and the slope distance, SD. Values of load capacity are pre-factored using a FS = 1.2 (Musser and Denning, 2005). In addition, the same reduction factors from Example 1 were used to adjust the required tensile strengths (RF_{ID} = 1.40, RF_{CR} = 2.0, and RF_{D} = 1.5), as shown in Table 42.

Table 42: Summary of Tensile Force Requirements per Layer

	Deep Patch Depth	Required Load Capacity per Layer (lb/ft)		
		$\phi = 25$	$\phi = 30$	$\phi = 35$
Range of Values	4 ft	250-2950	250-2100	150-1200
	5 ft	170-1970	170-1400	100-800
Average Unfactored Values	4 ft	1600	1175	675
	5 ft	1070	785	450
Average Factored Values	4 ft	6720	4935	2835
	5 ft	4494	3297	1890

The tensile strength requirements are similar between the three friction angles, ranging from about 1,900 lb/ft to about 6700 lb/ft, so a single value of $5/yd^2 is a reasonable estimate of the cost of the geosynthetic for each of these three options. Additionally, using this unit cost will facilitate a direct comparison between the two design examples. Beyond this, four additional assumptions were made to facilitate a direct comparison between the two available options, as well as between the two design techniques. The cost comparisons are based solely on the cost of excavation and placement of embankment fill, and the purchase of the geogrids. The construction quantities and associated costs were calculated for each option (Option 1 is the 4-foot deep patch and Option 2 is the 5-foot deep patch).

1. The cost of excavation is \$20/yd^3 and \$50/yd^3 for materials and placement; \$70/yd^3 combined.
2. Musser and Denning recommend that the geogrid be embedded distance X_c (i.e., $L_e = X_c$), so L_e = 7 ft for this design example.
3. The geogrid is extended 10 ft beyond both ends of the excavation parallel to the road; total excavation = 80 ft. Construction ramps on each end are not included in the analysis.
4. Geogrids terminate at the slope face (i.e., no wrapped face).

Construction Quantities

Calculate the total area of geosynthetics for each option:

Area 1 = 80 (16.5 + 19) = 2,840 ft^2 = 316 yd^2

Area 2 = 80 (15.25 + 17.75 + 20.25) = 4,260 ft^2 = 473 yd^2

Calculate the volume of excavation for each option:

Volume 1 = 80 [(4*14) + (0.5*4*5)] = 5,280 ft^3 = 195 yd^3

Volume 2 = 80 [(5*14) + (0.5*5*6.25)] = 6,850 ft^3 = 254 yd^3

Cost Calculations

Determine the total cost of the geogrids for each option:

Geogrid-cost 1 = \$5/yd^2 * 316 yd^2 = \$1,580

Geogrid-cost 2 = \$5/yd^2 * 473 yd^2 = \$2,365

Determine the total cost of excavation for each option:

Ex-cost 1 = \$70/yd^3 * 195 yd^3 = \$13,650

Ex-cost 2 = \$70/yd^3 * 254 yd^3 = \$17,780

Determine total costs of excavation and geosynthetics for each option:

Total 1 = \$13,650 + \$1,580 = \$15,230 ✓ **best option**

Total 2 = \$17,780 + \$2,365 = \$20,145

As noted in the previous example, the cost of the geosynthetics is much lower than the earthwork, so using the most efficient design will most often be the shallower repair. Based on the results of the design example using the Musser and Denning approach, the shallower, 4-ft-deep repair is more cost effective than the 5 ft repair, being about $5,000 less expensive.

9.7 SUMMARY

A new design method for deep patch repair was formulated based on limit-equilibrium and numerical modeling results. A design example based on this new approach indicated that a deep patch 6 ft deep having 6 layers of geogrid was the most efficient design. The same parameters were used to determine a deep patch design based on the methodology proposed by Musser and Denning (2005), where the most efficient design was a deep patch 4 ft deep with 2 layers of geogrid. In conclusion, the results from the design example using Musser and Denning's method were less conservative than the newly developed method, being 2 ft shallower and having 4 less layers of geogrid. The new method required similar tensile strength in the geosynthetic to adequately stabilize the slope failure. In conclusion, it is recommended that the new method be used to design deep patches in the future. The new method uses design inputs from the field (X_c, X, β and L) that are relatively easy to determine during a routine site visit.

10 SUMMARY, CONCLUSIONS AND RECOMMENDATIONS

10.1 SUMMARY

The objective of this research was to evaluate the deep patch slope repair methodology by analytical methods and field observations for the purpose of developing a simple design method suitable for use by Federal Lands Highway and Forest Service personnel. Literature was reviewed, current design methodologies were documented and site visits were conducted to better understand how the deep patch methodology has been used in the past, to evaluate the performance of in-service deep patch sites and to help authenticate the newly proposed design method.

An analytical study was conducted to model the effects of various slope configurations, failure mechanisms, deep patch design geometries, and type of geosynthetics using 2D and 3D computer modeling software. Deep patch repairs were analyzed using a limit equilibrium and a numerical method. The program ReSSA was used for limit equilibrium and FLAC/Slope and FLAC3D was the finite difference numerical method used. Cut and fill slopes requiring a deep patch repair were idealized by modeling the weak soil as a wedge with a horizontal top and sitting on strong native ground hillside. Failure by rotational slippage occurring within the weak soil and wedge-type movements occurring along a separate layer of soil referred to as a slip plane located between the contact of the weak soil and strong native ground, were considered. Limits to slope geometry parameters were established and were used to establish the bounds of the parametric study conducted.

A parametric study was conducted using the methodology established for choosing an optimal reinforcement configuration. This study resulted in potential design charts for the necessary deep patch configuration and required reinforcement tensile strength for a given site based on X and X_c. In general, as X and X_c increase, the depth of the deep patch and the required reinforcement tensile strength increase. Reinforcement requirements are slightly greater for $\beta = 39°$ slopes than $\beta = 34°$.

The effects of depth and vertical spacing of the reinforcement on the performance of the deep patch was analyzed in addition to the geometry of the reinforcement at the face of the slope. From these efforts, a new design method for deep patch repair was formulated based on limit-equilibrium and numerical modeling results.

10.2 CONCLUSIONS

Following is a list of significant outcomes from this research.

- Overall, the 48 deep patch-repaired sites that were visited in November 2010 and May 2011 were performing well, with the exception of a single site in the Siuslaw National Forest.
- For unreinforced slopes and rotational failures, FLAC/Slope and ReSSA produced similar factors of safety; however, FLAC/Slope produced slightly different failure surfaces with different values of X_c. For wedge failures, FLAC/Slope produced smaller yet comparable factors of safety as compared to an equation for sliding of a wedge along a planar failure surface. The smaller factor of safety is most likely due to a critical failure surface involving the development of a tension crack, which is not taken into account by the sliding wedge equation. Values of X_c were larger for wedge failures as compared to rotational failures.
- FLAC/Slope provided results expressed in terms of shear strain rate contours and velocity vector plots, which give information on patterns of slope movement and location of failure surfaces. This information was used to determine the performance of a reinforced slope when the goal was to limit movement along and below the roadway bench.
- Use of ReSSA for unreinforced slopes showed that for rotational failures having a factor of safety of 1.0, large values of X_c are possible only for a combination of weak soil friction angle and cohesion using unrealistically low values of friction angle. Since a ground water table and subsequent seepage forces were not included in these analyses, this observation may be due in part to the absence of these destabilizing elements.
- ReSSA was used to show that for a deep patch, a satisfactory factor of safety (1.3) could be obtained when the critical failure surface was forced to initiate along the roadway bench while a more general failure circle search resulted in a lower factor of safety (about 1.0), which generally corresponded to a failure circle initiating along the slope face and confined to soil below the reinforcement. This information was used to establish a design philosophy for a deep patch repair, which is to provide for stability of the roadway bench while not necessarily ensuring stability for the overall slope as a whole. In particular, the deep patch should limit movement and failure to the weak soil along the slope face and below the reinforcement. Movement and failure should not extend up to or involve soil below the roadway bench.
- Limit equilibrium methods have limitations for evaluating the influence of reinforcement spacing and depth of the reinforced mass for slopes reinforced with a deep patch. In particular, limit equilibrium methods show that an adequate factor of safety can be obtained with one layer of strong reinforcement or with multiple layers of weaker reinforcement having the same total reinforcement tensile capacity. The limit equilibrium method, however, does not provide information on the movement of weak soil as failure occurs, and cannot be used to determine whether soil within the area of the roadway bench experiences excessive movement for a given reinforcement configuration.
- Velocity vector and shear strain rate contour results from FLAC/Slope allow examination of patterns of movement and failure within the context of the design philosophy for a deep patch repair. The methodology for deciding upon an optimal reinforcement configuration (involving a depth of the reinforced mass,

number of reinforcement layers and reinforcement spacing) was established by evaluating velocity vector and shear strain rate contour results from FLAC/Slope. This subjective methodology resulted in clear bounds in terms of depth of the reinforced mass and number of reinforcement layers of acceptable and unacceptable performance. For a given slope geometry, several reinforcement configurations can result in acceptable performance.

- Wedge failures are associated with greater reinforcement requirements than rotational failures.
- Using FLAC/Slope, an evaluation of tensile force mobilized in reinforcement layers showed that the maximum tensile force mobilized was as much as 180 percent above the average tensile force mobilized for all layers. Since most designs will use the same geosynthetic type for all layers and be chosen to carry the maximum tensile force expected, there will be greater excess capacity for those cases showing greater differences between the maximum and average reinforcement tensile forces. FLAC/Slope and ReSSA showed a discrepancy in the required tensile force and it was suggested that FLAC/Slope provided the more realistic reinforcement strength requirement for the deep patch repair configuration.
- Reinforcement capacities for upper layers of geosynthetic are limited by pullout considerations because of low confining pressures. The design charts developed for this project assume embedment lengths of 10 ft for geogrids and 15 ft for geotextiles.
- A three-dimensional analysis program (FLAC3D) was used to examine the difference in slope performance when biaxial and uniaxial reinforcement were used. Results were expressed in terms of factor of safety and contour plots of maximum shear strain and displacement magnitude. Slopes with different lengths of weak soil confined by ends adjacent to strong native ground all showed factors of safety close to 1.0, and a pattern of failure extending up into the roadway bench when unreinforced. For a reinforcement spacing of 1 ft and a depth of reinforcement of 5 ft, biaxial reinforcement resulted in considerable improvement and prevented material movement along and below the roadway bench. The uniaxial reinforcement resulted in improvement but also in unacceptable movement along the roadway bench. No clear differences in performance were noted as a function of weak soil length.
- The results obtained in the parametric study (Chapter 6) assume an isotropic reinforcement material for the 2D analysis and are therefore applicable to biaxial reinforcement. Given the appreciable reduction in performance with the use of uniaxial materials for the cases examined in this study, it is recommended that biaxial materials be used in conjunction with the results from Chapter 6, and that the required strength be for the weakest direction of the biaxial material. Given the importance of strength in the direction parallel to the slope, the importance of anchoring the reinforcement in the strong native ground at the ends of the deep patch is apparent in order to develop tensile resistance in this direction.
- Should uniaxial materials be specified for a deep patch, additional research is needed to make recommendations on the additional requirement placed on the reinforcement above those shown in Chapter 6. These additional requirements could be in the form of a deeper depth of reinforcement, a reduced spacing and/or increased strength. Additional 3D analyses are required for a large number of cases backed by field testing to determine these additional requirements.

- In a traditional deep patch, the reinforcement extends to the slope face. Two slopes were modeled with a portion of the reinforcement terminating behind the slope face at a vertical and negative batter. These deep patches showed improvement compared to the unreinforced case, but to a lesser extent than a traditional deep patch. In some cases, a deeper repair may be needed if vertical or negative batter geometry is desired.
- Results from the comparison between ReSSA and the new design method indicated that the tensile strength requirements based on the ReSSA analysis were slightly greater than the new design method. However, for shorter slopes (H < 60 ft), the depth, number of layers and reinforcement tensile strength requirements are likely to be somewhat greater for new design method than for ReSSA.
- Compared to the design method created by Musser and Denning (2005), the new method required similar tensile strength, but the final design was 2 feet deeper and required 4 additional layers of geosynthetic to adequately stabilize the slope failure.

10.3 RECOMMENDATIONS

In conclusion, it is recommended that the new method be considered for future deep patch applications and for comparison to other methods (designs based on past experience, limit equilibrium computer models, Musser and Denning (2005) charts, etc.). The new method is simple to apply and uses design inputs from the field (X_c, X, β and L) that are relatively easy to determine during a routine site visit. Nevertheless, full-scale models, multiple deep patch installations in the field, and additional numerical modeling are needed to validate and refine this method and findings to further ensure a safe and economical design for these low-volume road applications. Laboratory and field tests should include, 1) centrifuge testing, 2) several full scale models of a deep patch installation in a controlled area, and 3) several fully instrumented deep patch installations in the field. The expected outcome of these tests is a better understanding of the load distribution in the various geosynthetic layers, which can be used to refine the suggested deep patch design method. More extensive numerical modeling is also recommended to address topics not fully studied in this project, including 1) the behavior of uniaxial geogrids, and 2) the performance of vertical and negative batter deep patches using more slope and soil conditions. Finally, it is recommended that design charts with a slope angle β = 45° be developed to augment the β = 34 and β = 39° design charts.

10.3.1 Centrifuge Testing

Controlled testing in the laboratory is an efficient means to understand the basic behavior of geotechnical systems. Therefore, it is recommended that a series of centrifuge tests of deep patch and control embankments be studied to better understand how the deep patch system performs in a variety of conditions. Centrifuge tests are an efficient means to study several deep patch configurations relatively quickly and easily. Some

of the variables that should be tested include the depth of the deep patch, the number of geosynthetic layers and the slope angle. Instrumentation would mainly be used to monitor the strains and displacements of the soil and geosynthetic. This information is useful to better understand the behavior of deep patches, as well as to help design and testing of the full-scale laboratory deep patches.

10.3.2 Full-Scale Deep Patch in Laboratory

While centrifuge testing is an efficient means to study several variables quickly, the results from scaled models may not fully represent a full-scale deep patch application. Nevertheless, the design of the full-scale, controlled deep patch models should be based, in part, on the results of the centrifuge testing. Multiple deep patches should be constructed in a controlled area so that the traveling public will not be inconvenienced during construction, testing and loading. Similar to the centrifuge tests, the main variables that should be studied as part of this effort include the depth of the deep patch, the number of geosynthetic layers, and the slope angle. The preferred method to create failure stresses in the deep patch is to introduce water to the slope system, but this may also be accomplished using collapsible layers. Instrumentation should be installed to monitor the deep patch repair during construction and loading. Tiltmeters will be used to monitor the global movement of the slope, displacement sensors mounted to the geosynthetics will be used to monitor load/strain responses in each of the layers, and strain gauges may be placed in strategic locations to monitor localized strain in the geosynthetic. Traditional survey equipment should be used to monitor global movements of the deep patch embankment. The expected outcome from this testing is to better understand the tensile load distribution in the geosynthetic and the general failure mechanism associated with the deep patch system.

10.3.3 Monitored Deep Patch Field Installations

It is recommended that three deep patch installations on paved roads be monitored in the field at slope angles of 1:1, 1.25:1 and 1.5:1. Once candidate sites are confirmed, an extensive review of the site conditions should be made prior to construction. In addition to a full site characterization, drill equipment is suggested to extract soil samples and/or characterize the soil profile prior to excavation. Computer models and deep patch designs will be generated using this and other pertinent data collected from the site. A careful and thorough assessment of these sites using soil samples, photographs, survey measurements, etc. should also be made during excavation to further substantiate pre-construction information. Instrumentation should be installed on the geosynthetics and surrounding soils as the deep patches are being constructed. Similar to the full-scale models, displacement gauges should be strategically placed on the geosynthetic to evaluate strain at specific locations. These measurements can be used to back-calculate

load in the geosynthetic layers over time and under a variety of loading conditions. Computer models of these slopes will be generated based on this information, and along with the information from the centrifuge and full-scale models, will be used to refine the deep patch design methodology. Long term monitoring of these deep patch installations should continue for many years to gain a full appreciation for their behavior over time.

11 REFERENCES

Adams, M., Nicks, J., Stabile, T., Wu, J., Schlatter, W., and Hartmann, J. (2011a). Geosynthetic Reinforced Integrated Bridge System: Synthesis Report. Federal Highway Administration, FHWA-HRT-11-026, 64p.

Adams, M., Nicks, J., Stabile, T., Wu, J., Schlatter, W., and Hartmann, J. (2011b). Geosynthetic Reinforced Integrated Bridge System: Implementation Guide. Federal Highway Administration, FHWA-HRT-11-026, 169p.

Barret, R.K. and Ruckman, A.C. (2007). "GRS—A New Era in Reinforced Soil Technology" In Gabr, M.A. and Bowders, J.J. (Eds), Proceedings of Sessions of Geo-Denver 2007, February 18–21, 2007, Denver, CO, ASCE Geotechnical Special Publication No. 165.

Berg, R., Christopher, B.R. and Samtani, N.C. (2009a). Design of Mechanically Stabilized Earth Walls and Reinforced Slopes – Volume I, Federal Highway Administration, FHWA-NHI-10-024, FHWA GEC 011-Vol I, 306p.

Berg, R., Christopher, B.R. and Samtani, N.C. (2009b). Design of Mechanically Stabilized Earth Walls and Reinforced Slopes – Volume II, Federal Highway Administration, FHWA-NHI-10-025, FHWA GEC 011-Vol II, 378p.

Bishop, A.W. (1955). "The Use of the Slip Circle in Stability Analysis of Slopes" Geotechnique, Vol. 5, pp. 7-17.

Bussert, F. and Cavanaugh, J. (2010). "Recent Research and Future Implications of the Actual Behavior of Geogrids in Reinforced Soil" In Finno, R., Hashash, Y.M., and Arduino, P. (Eds), Proceedings of the 2010 Earth Retention Conference, August 1–4, 2010, Bellevue, WA, ASCE Geotechnical Special Publication No. 208, 943p., pp. 460–477.

Christopher, B.R., Gill, S.A., Juran, I. and Mitchell, J.K. (1989). Reinforced Soil Structures, Design and Construction Guidelines. Federal Highway Administration, FHWA-RD-89-043, 306p.

Elias, V., Christopher, B.R. and Berg, R.R. (2001). Mechanically Stabilized Earth Walls and Reinforced Soil Slopes, Design and Construction Guidelines. Federal Highway Administration, FHWA-NHI-00-043, 394p.

Griffiths, D.V. and Lane, P.A. (1999). "Slope Stability Analysis by Finite Elements" Geotechnique, Vol. 49, No. 3, pp. 387-403.

Hatami, K. and Bathurst, R.J. (2005). "Development and Verification of a Numerical Model for the Analysis of Geosynthetic-Reinforced Soil Segmental Walls

Under Working Stress Conditions" Canadian Geotechnical Journal, Vol. 42, pp. 1066-1085.

Helwany, M.B. (1994). The Deep Patch Technique for Landslide Repair. Colorado Transportation Institute, Final Report No. CTI-UCD-2-94, 118p.

Holtz, R.D. and Schuster, R.L. (1996). Chapter 17: Stabilization of Soil slopes. In Turner, A.K. and Schuster, R.L. (Eds), Landslides: Investigation and Mitigation. Transportation Research Board Special Report 247. National Research Council, 673p.

Huang, B., Bathurst, R.J. and Hatami, K. (2009). "Numerical Study of Reinforced Soil Segmental Walls Using Three Different Constitutive Soil Models" Journal of Geotechnical and Geoenvironmental Engineering, ASCE, Vol. 135, No. 10, pp. 1486-1498.

Mitchell, J.K. and Villet, W.C.B. (1987). Reinforcement of Earth Slopes and Embankments. NCHRP Report 290. Transportation Research Board, National Research Council. 330p.

Mohney, J. et al. (1994). Retaining Wall Design Guide. Federal Highway Administration, FHWA-FLP-94-006, 535p.

Musser, S.W. and Denning, C. (2005). Deep Patch Road Embankment Repair Application Guide. USDA Forest Service and Federal Highway Administration, Report No. 0577 1204–SDTDC, 32p.

Powell, W., Keller, G.R., and Brunette, B. (1999). "Applications for Geosynthetics on Forest Service Low-Volume Roads" Transportation Research Record No. 1652, pp. 113–120.

San, K-C, Leshchinsky, D. and Matsui, T. (1994). "Geosynthetic Reinforced Slopes: Limit Equilibrium and Finite Element Analyses" Soils and Foundations, Vol. 34, No. 2, pp. 78-85.

Spencer, A. (1967). "A Method of Analysis for Stability of Embankments Using Parallel Inter-Slice Forces" Geotechnique, Vol. 17, pp. 11-26.

Tanchaisawat, T., Bergado, D.T. and Voottipruex, P. (2009). "2D and 3D Simulation of Geogrid-Reinforced Geocomposite Material Embankment on Soft Bangkok Clay" Geosynthetics International, Vol. 16, No. 6, pp. 420-432.

VanBuskirk, C. (2010) "Adoption and Implementation of GRS Design Concepts: A Consultant's Perspective" GCS Wall Website. [Online] Available http://gcswall.com/pdf/calvingcsgrspaper2010.pdf

Vulova, C. and Leshchinsky, D. (2003). Effects of Geosynthetic Reinforcement Spacing on the Performance of Mechanically Stabilized Earth Walls. Federal Highway Administration, Report No. FHWA-RD-03-048, 226p.

Wu, J.T.H. and Helwany, S.M.B. (2001). "Examining the Effects of Reinforcement in U.S. Forest Service Deep-Patch Landslide Repair Technique: Full-Scale Model Tests." Transportation Research Record 1772, pp.203–210.

Wu, J.T.H., Lee, K.Z.Z., Helwany, S.B., and Ketchart, K. (2006). Design and Construction Guidelines for Geosynthetic-Reinforced Soil Bridge Abutments with a Flexible Facing. NCHRP Report 556. Transportation Research Board, National Research Council. 152p.

Yang, K.-H., Zornberg, J.G., and Bathurst, R.J. (2010). "Mobilization of Reinforcement Tension within Geosynthetic Reinforced Soil Structure" In Finno, R., Hashash, Y.M., and Arduino, P. (Eds), Proceedings of the 2010 Earth Retention Conference, August 1–4, 2010, Bellevue, WA, ASCE Geotechnical Special Publication No. 208, 943p., pp. 494–501.

APPENDIX A: VELOCITY VECTOR PLOTS FROM FLAC/SLOPE FOR SLOPE I ROTATIONAL ANALYSES

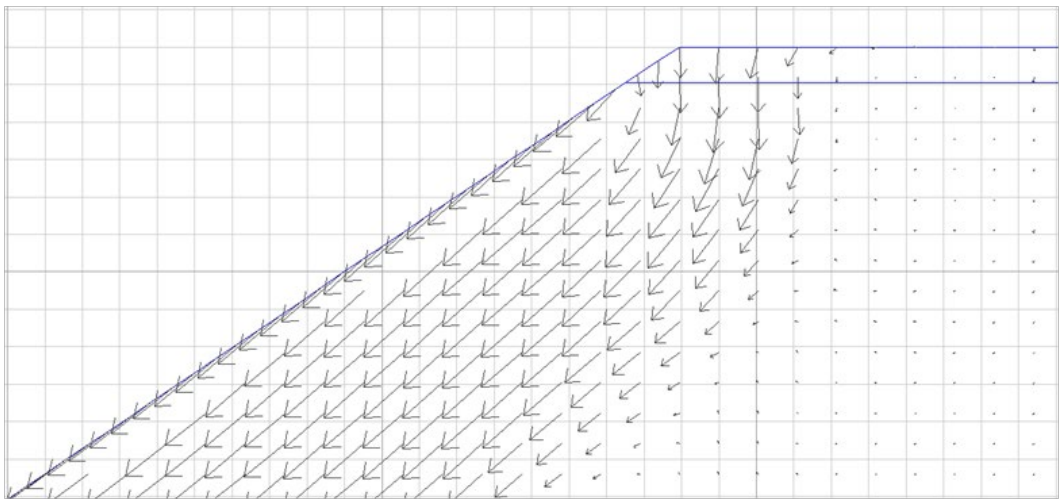

Figure A1: Velocity vector plot for 1 layer of reinforcement at 1 ft spacing.

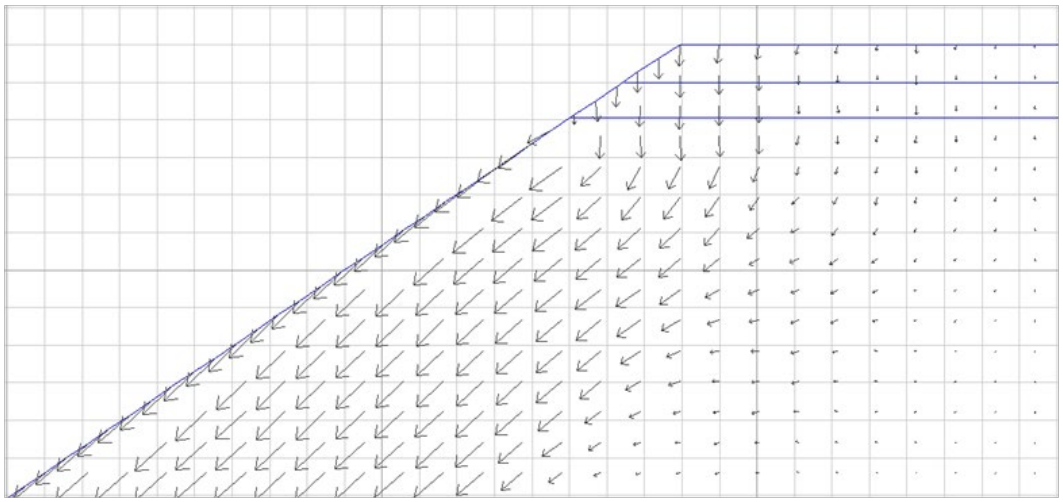

Figure A2: Velocity vector plot for 2 layers of reinforcement at 1 ft spacing.

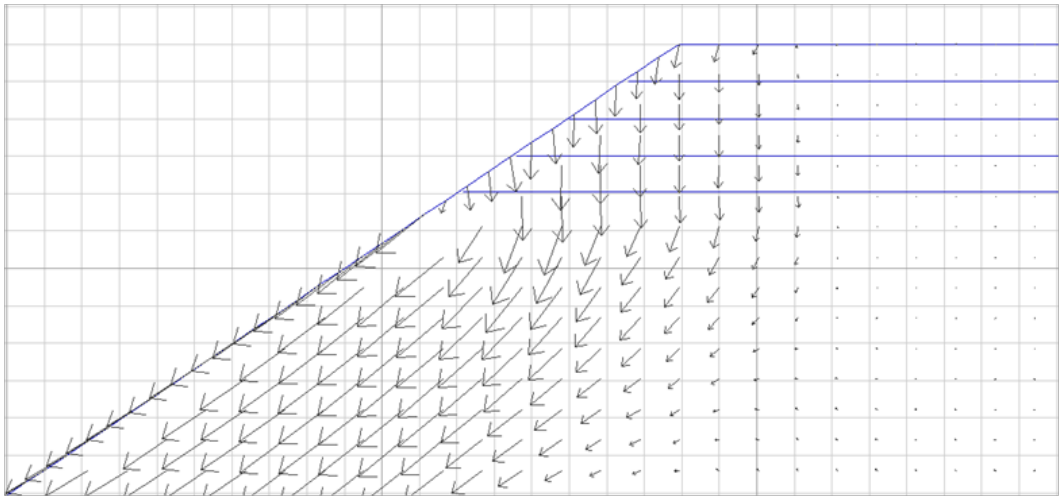

Figure A3: Velocity vector plot for 4 layers of reinforcement at 1 ft spacing.

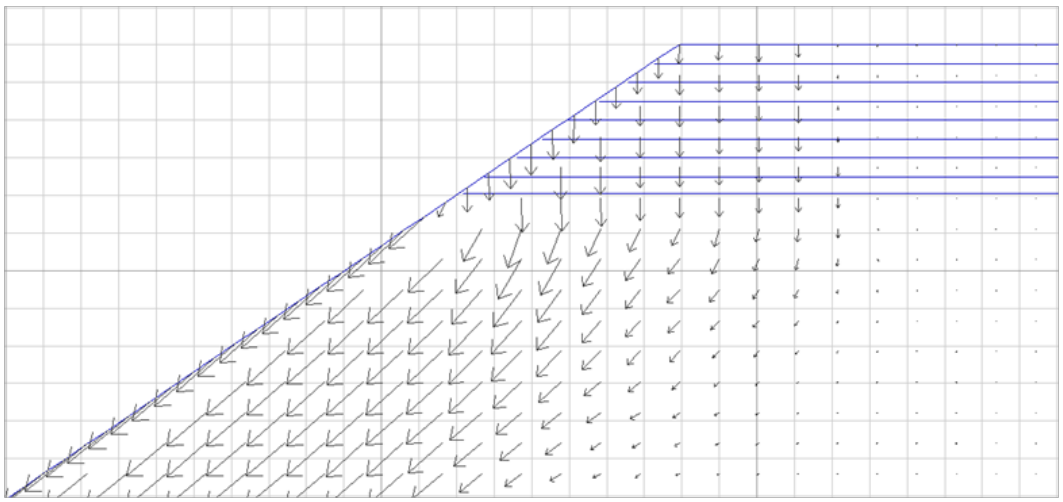

Figure A4: Velocity vector plot for 8 layers of reinforcement at 0.5 ft spacing.

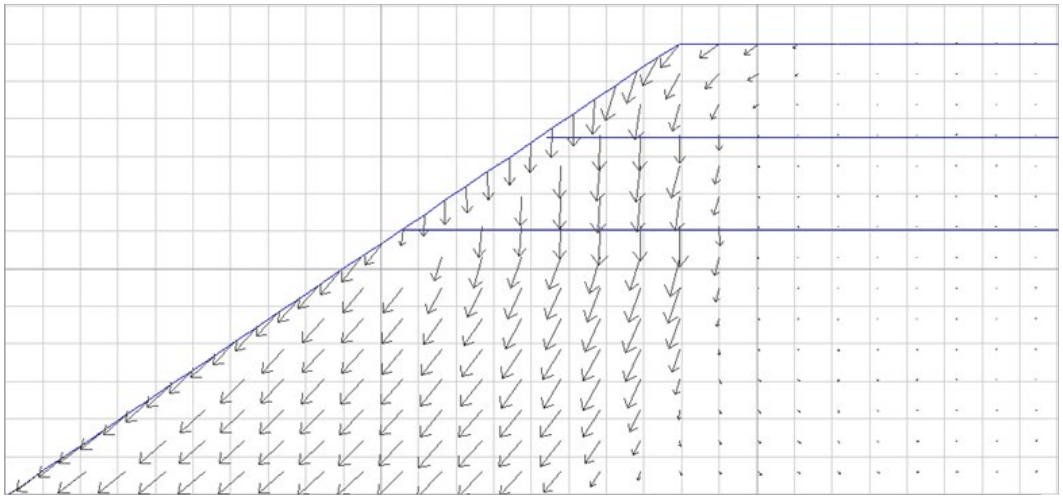

Figure A5: Velocity vector plot for 2 layers of reinforcement at 2.5 ft spacing.

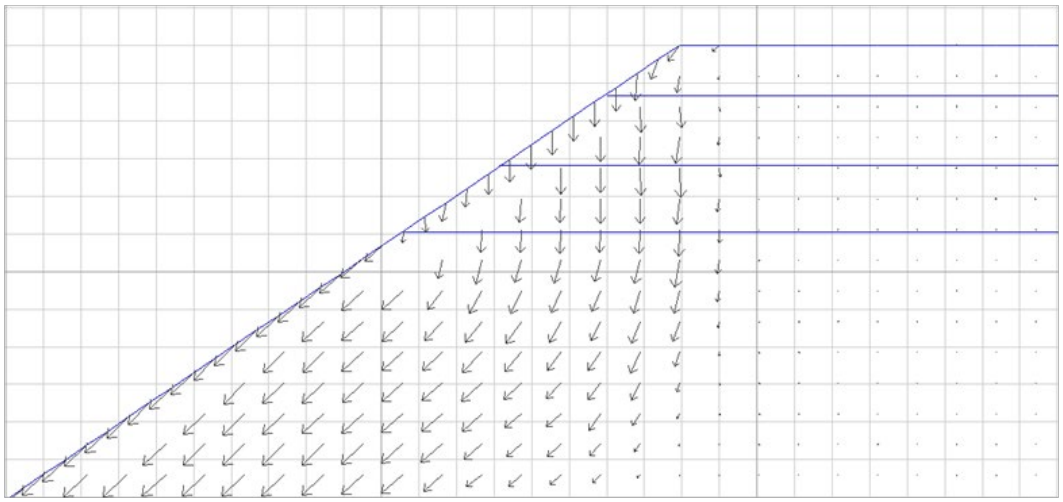

Figure A6: Velocity vector plot for 3 layers of reinforcement at 1.83 ft spacing.

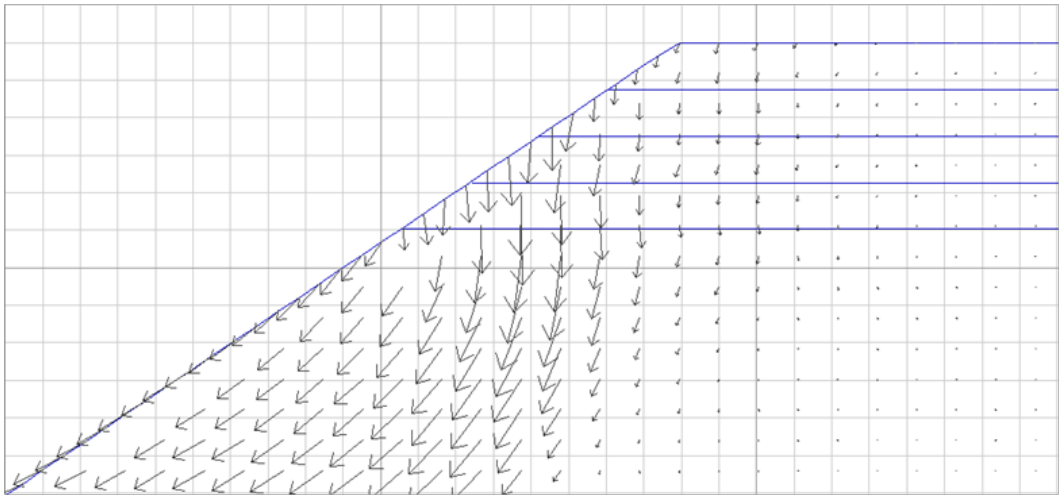

Figure A7: Velocity vector plot for 4 layers of reinforcement at 1.25 ft spacing.

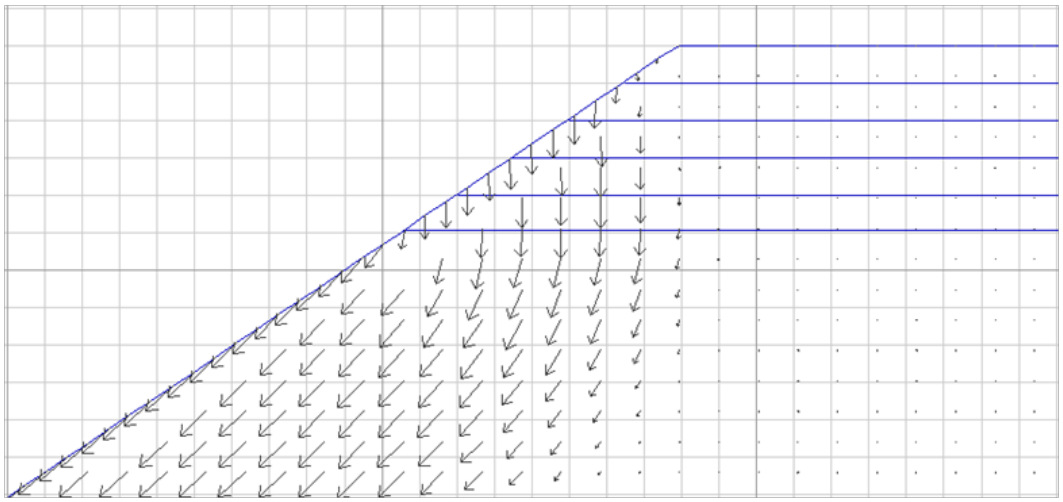

Figure A8: Velocity vector plot for 5 layers of reinforcement at 1 ft spacing.

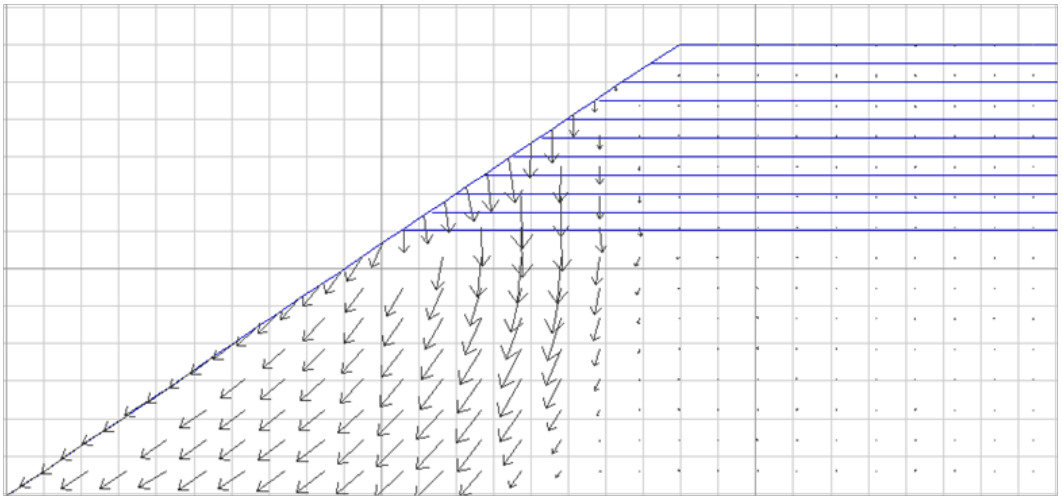

Figure A9: Velocity vector plot for 10 layers of reinforcement at 0.5 ft spacing.

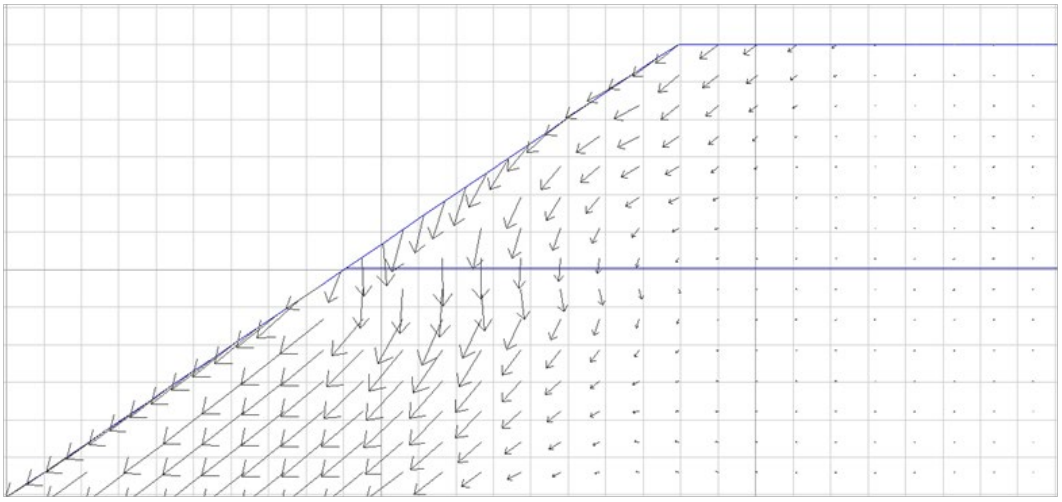

Figure A10: Velocity vector plot for 1 layer of reinforcement at 6 ft spacing.

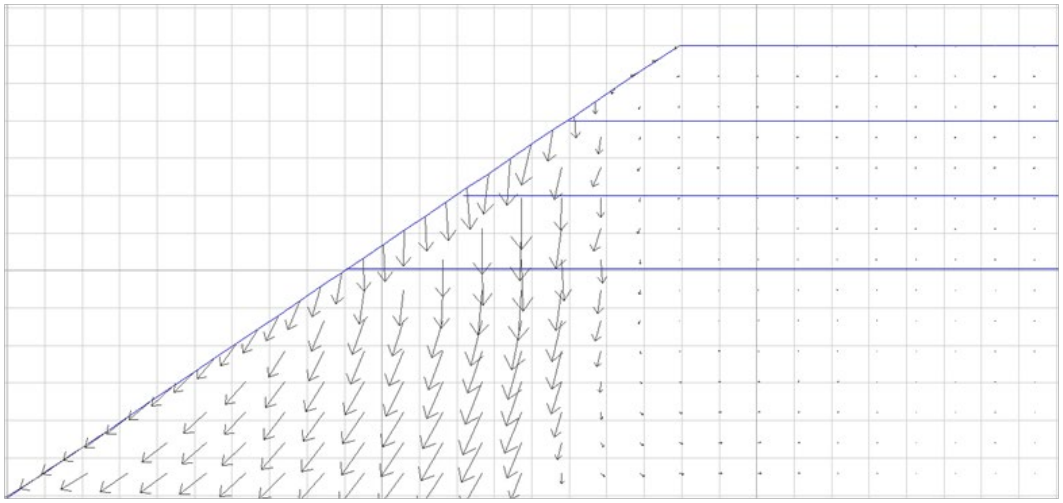

Figure A11: Velocity vector plot for 3 layers of reinforcement at 2 ft spacing.

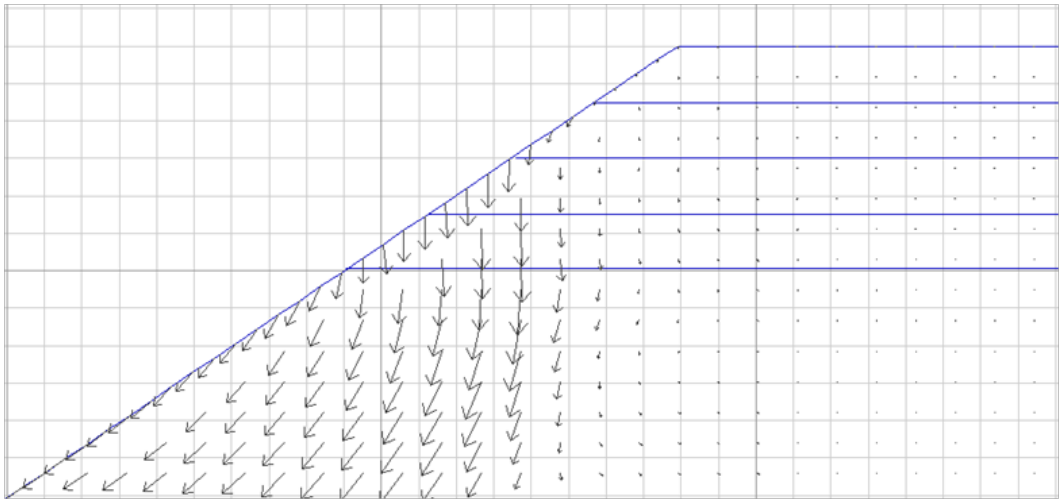

Figure A12: Velocity vector plot for 4 layers of reinforcement at 1.5 ft spacing.

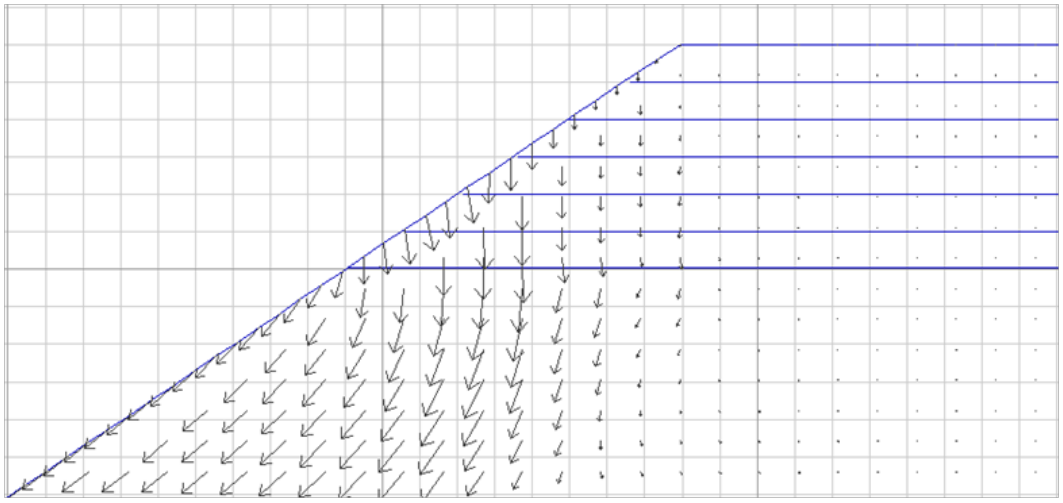

Figure A13: Velocity vector plot for 6 layers of reinforcement at 1 ft spacing.

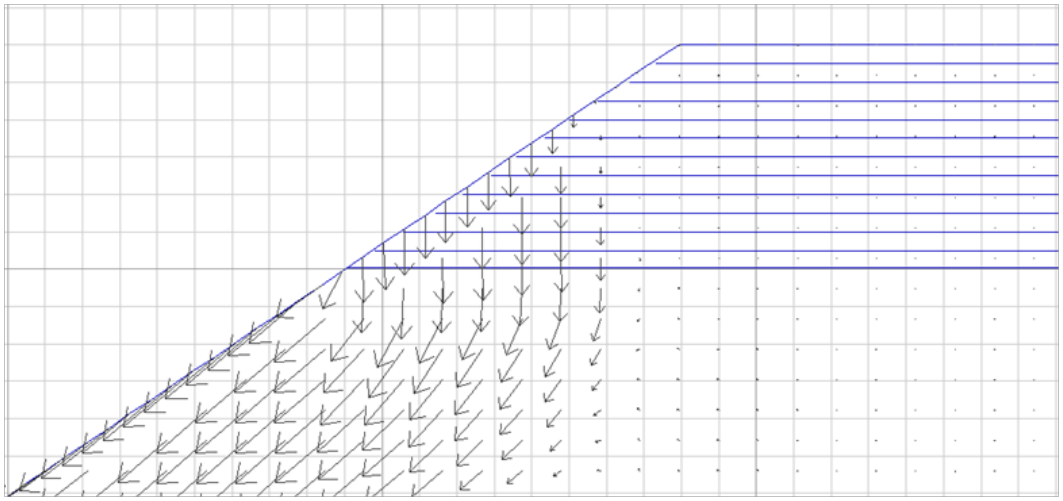

Figure A14: Velocity vector plot for 12 layers of reinforcement at 0.5 ft spacing.

APPENDIX B: VELOCITY VECTOR PLOTS FROM FLAC/SLOPE FOR SLOPE I WEDGE ANALYSES

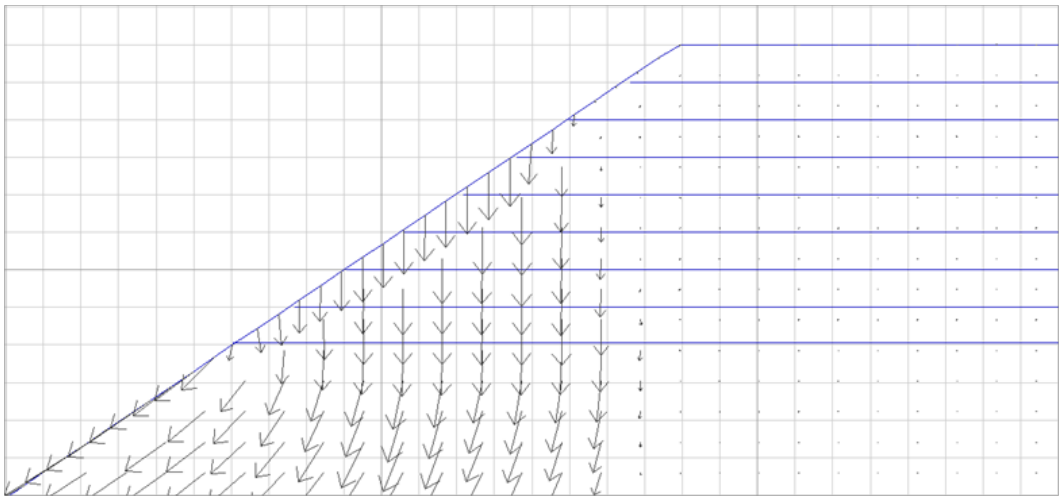

Figure B1: Velocity vector plot for 8 layers of reinforcement at 1 ft spacing.

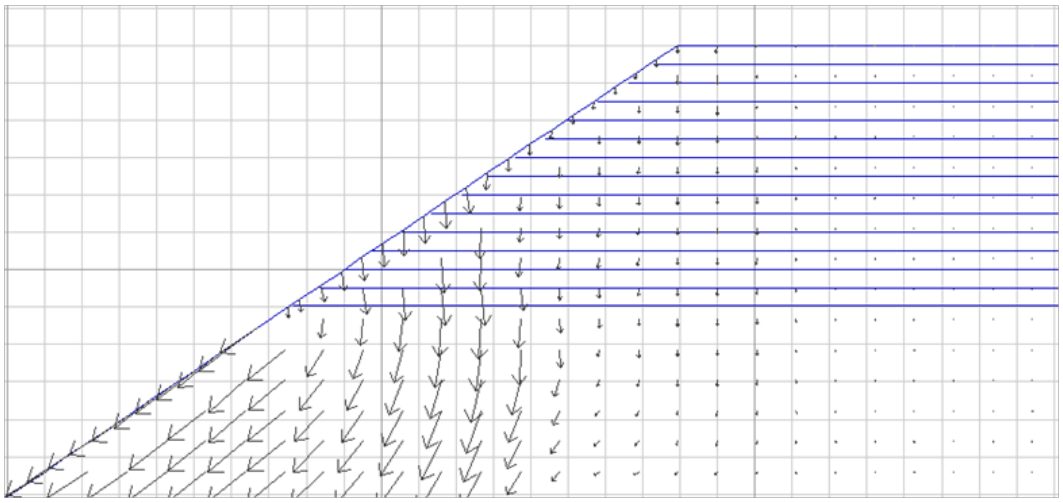

Figure B2: Velocity vector plot for 14 layers of reinforcement at 0.5 ft spacing.

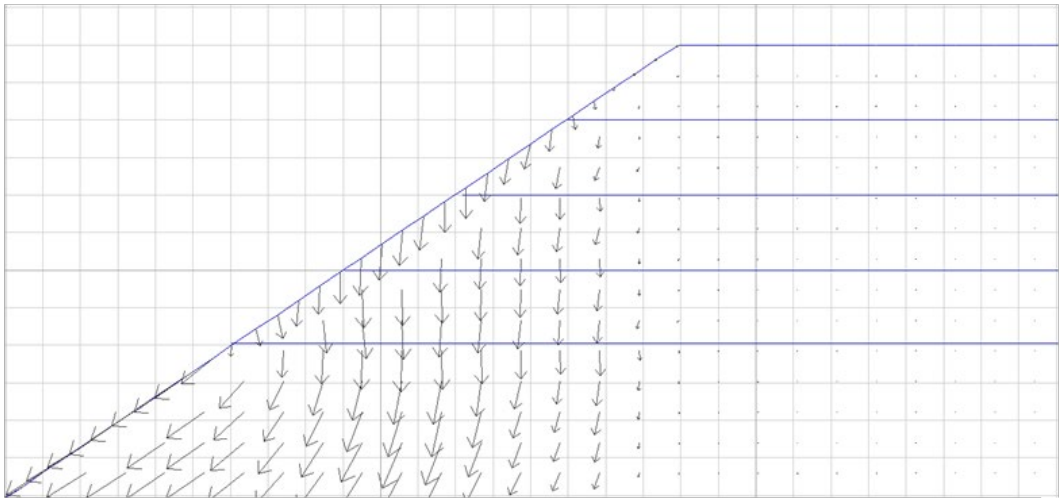

Figure B3: Velocity vector plot for 4 layers of reinforcement at 2 ft spacing.

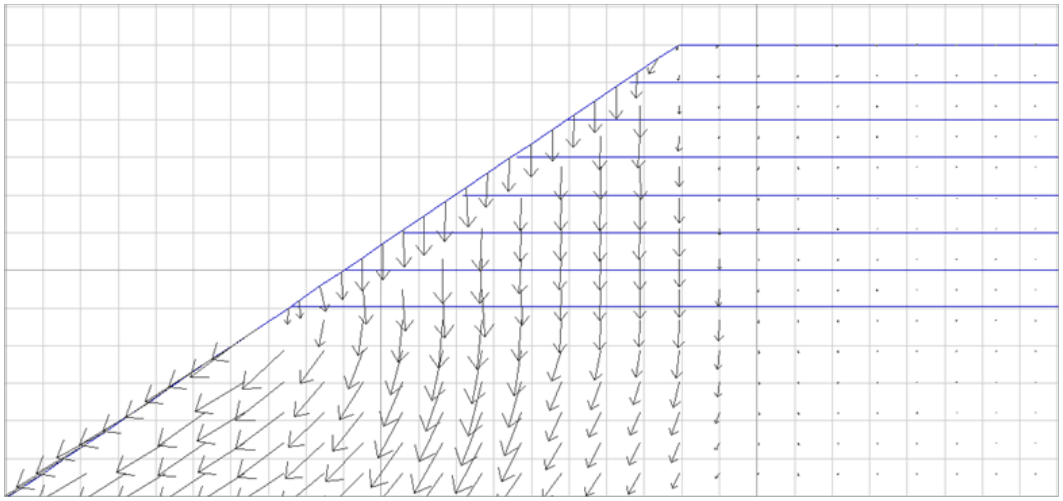

Figure B4: Velocity vector plot for 7 layers of reinforcement at 1 ft spacing.

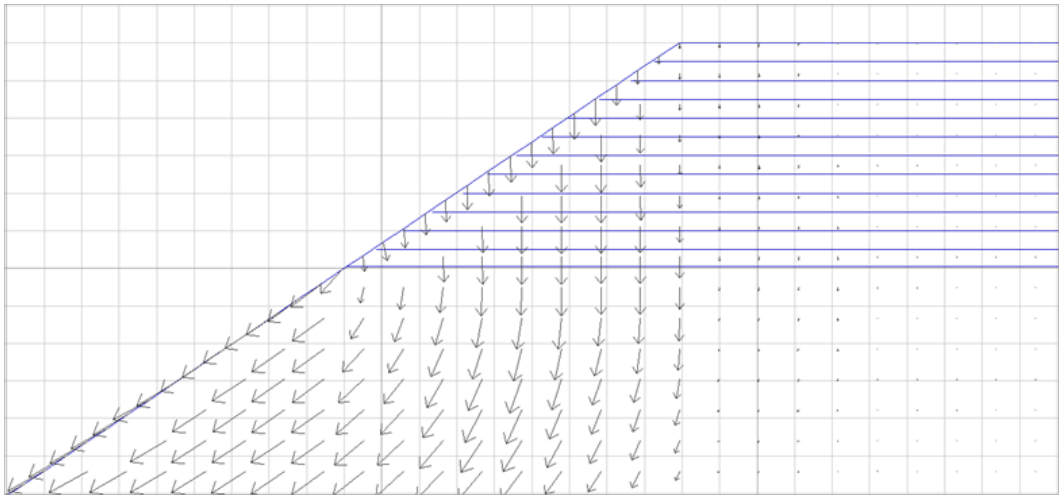

Figure B5: Velocity vector plot for 12 layers of reinforcement at 0.5 ft spacing.

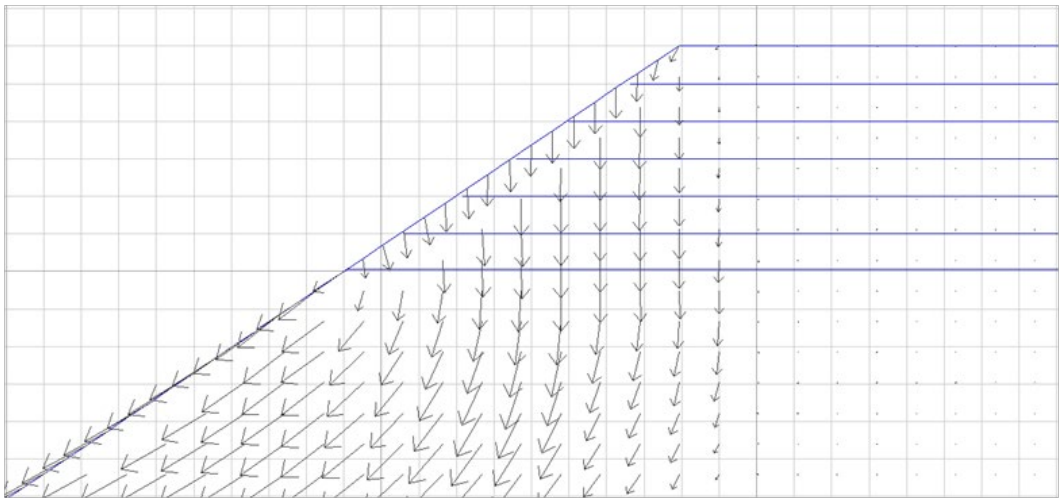

Figure B6: Velocity vector plot for 6 layers of reinforcement at 1 ft spacing.

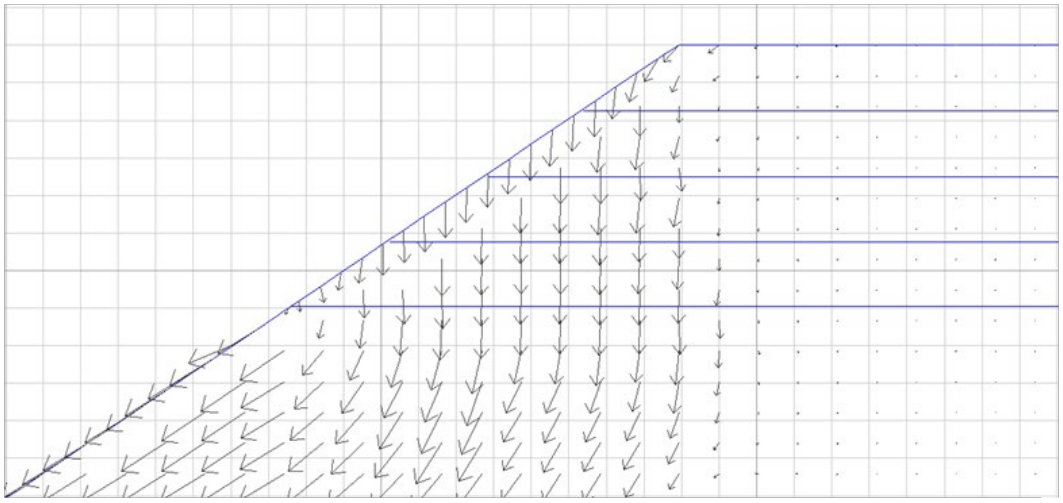

Figure B7: Velocity vector plot for 4 layers of reinforcement at 1.75 ft spacing.

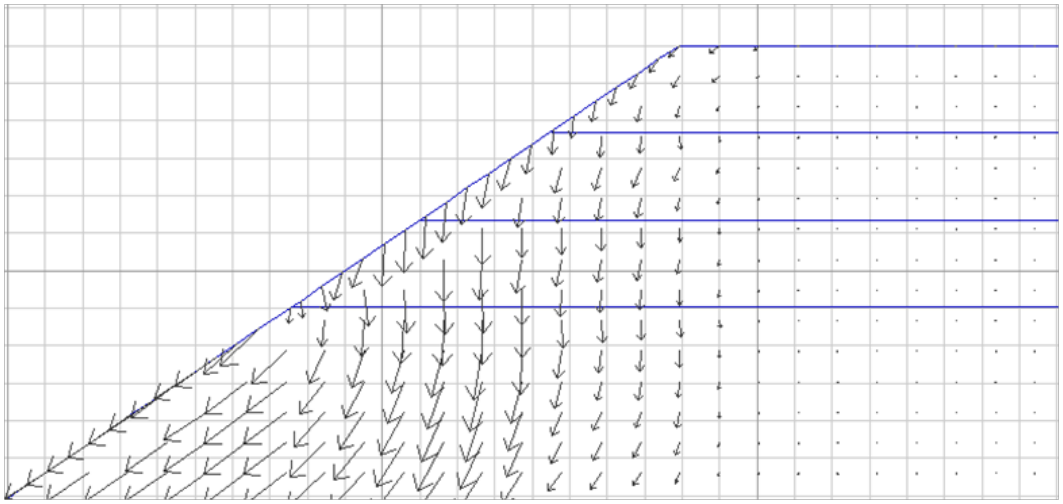

Figure B8: Velocity vector plot for 3 layers of reinforcement at 2.33 ft spacing.

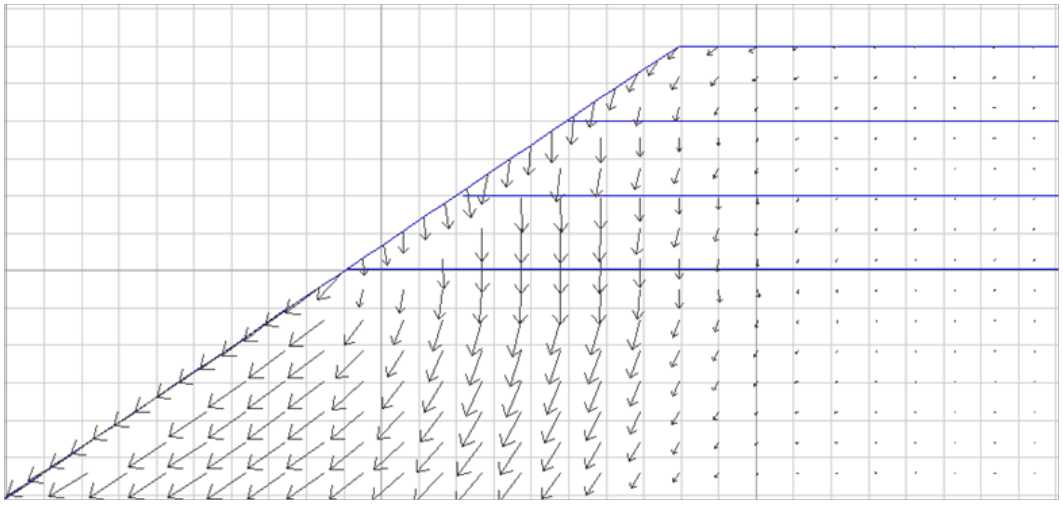

Figure B9: Velocity vector plot for 3 layers of reinforcement at 2 ft spacing.

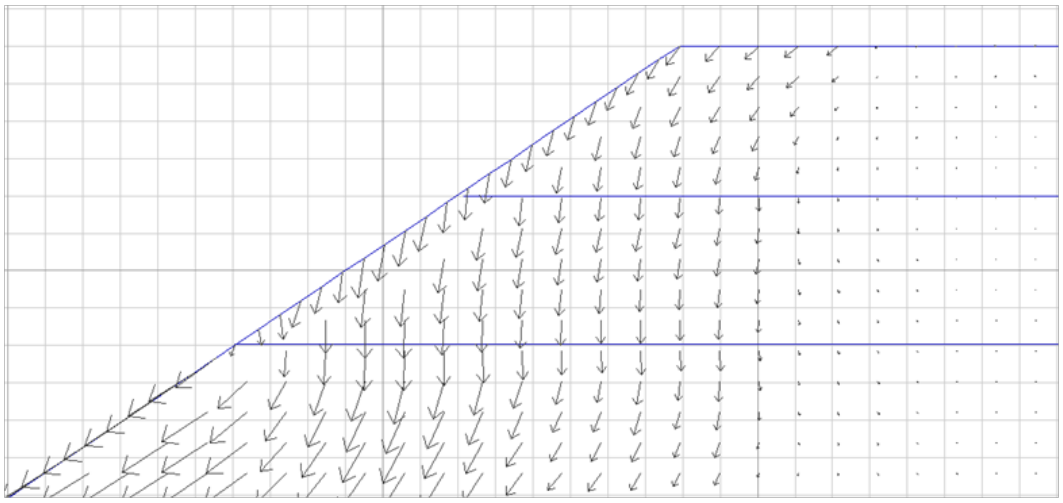

Figure B10: Velocity vector plot for 2 layers of reinforcement at 4 ft spacing.

APPENDIX C: CONTOUR PLOTS FROM FLAC3D

UNREINFORCED ROTATIONAL

a)

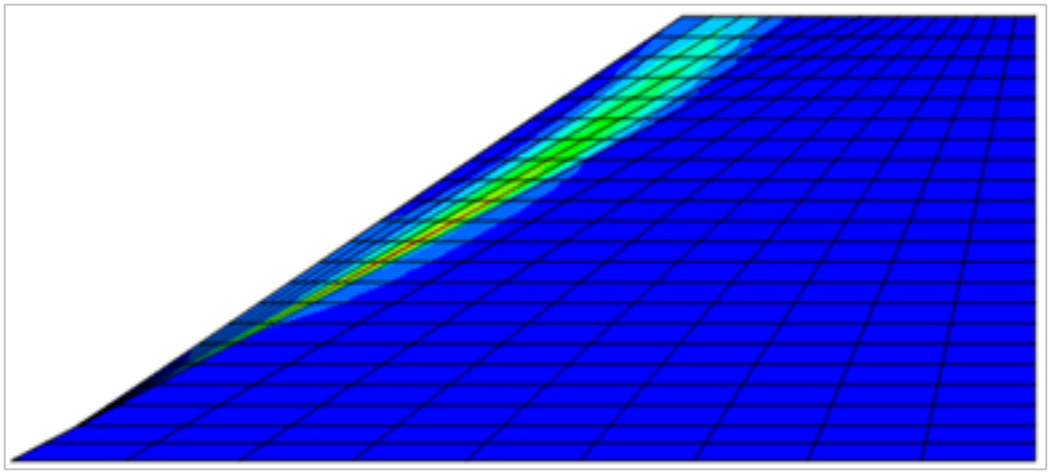

b)

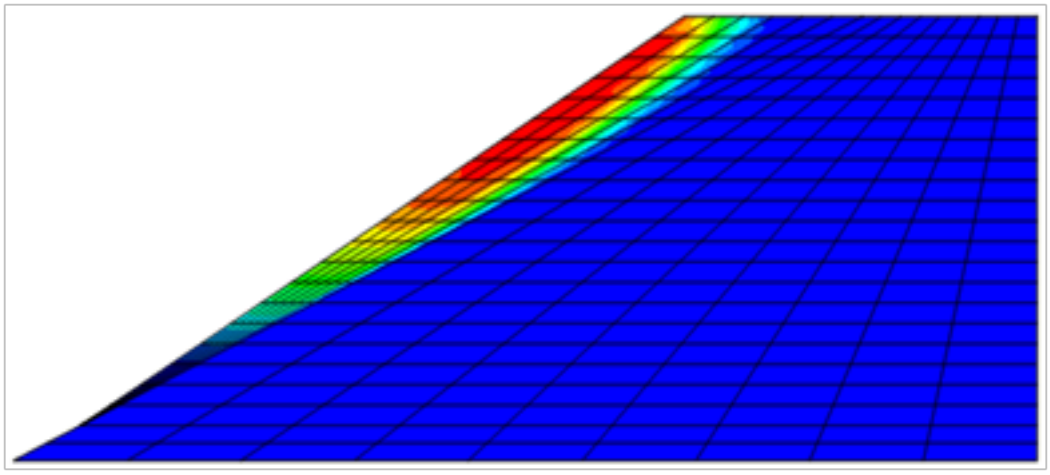

Figure C1: 10 ft fill length, a) maximum shear strain increment, b) displacement magnitude.

a)

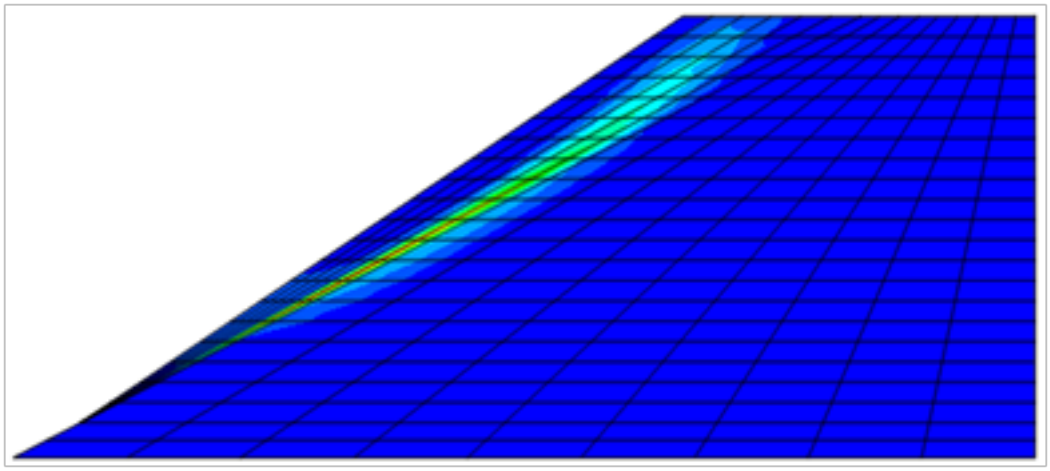

b)

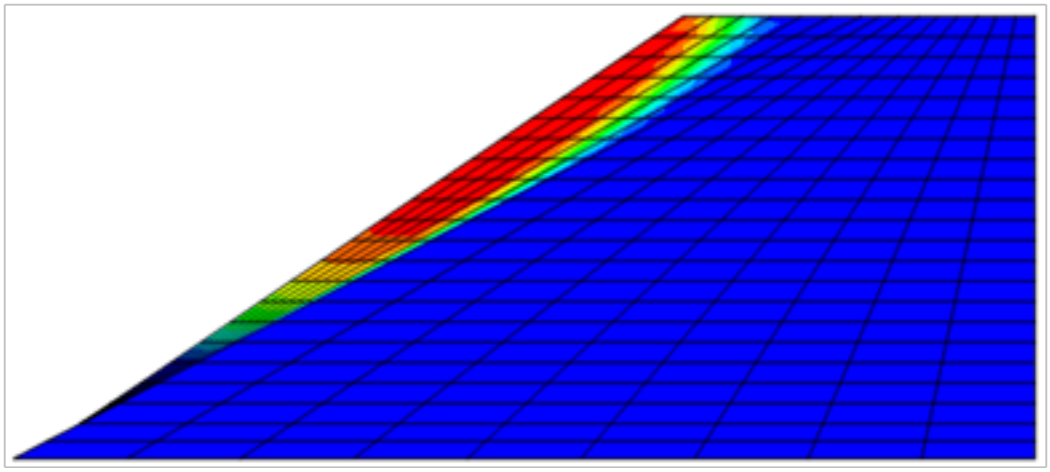

Figure C2: 20 ft fill length, a) maximum shear strain increment, b) displacement magnitude.

a)

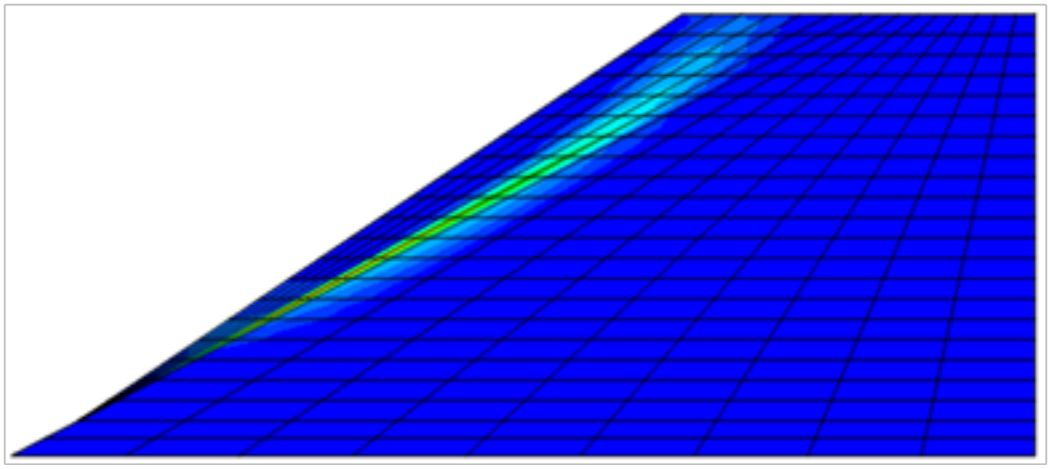

b)

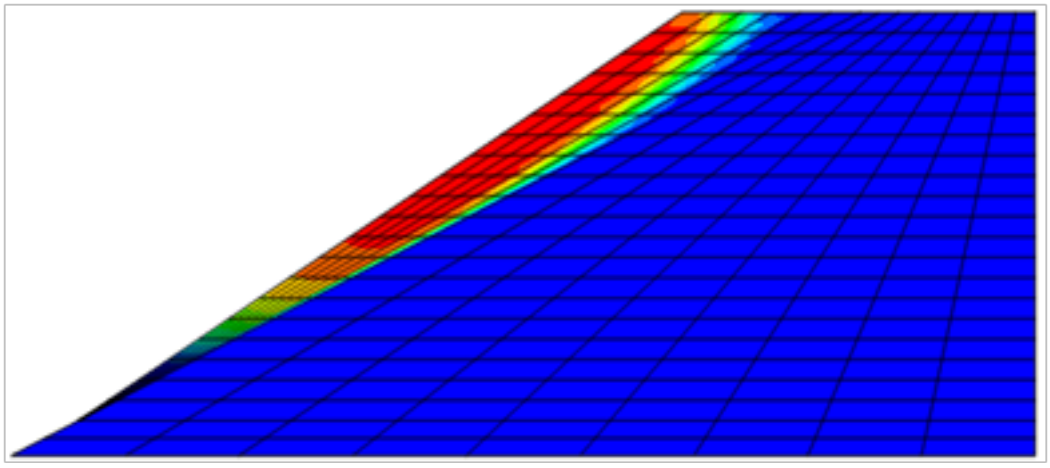

Figure C3: 30 ft fill length, a) maximum shear strain increment, b) displacement magnitude.

a)

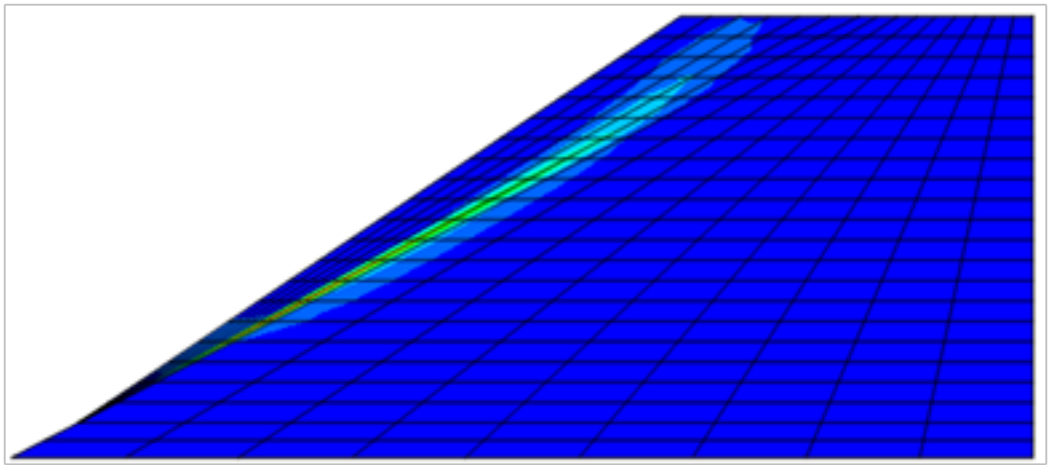

b)

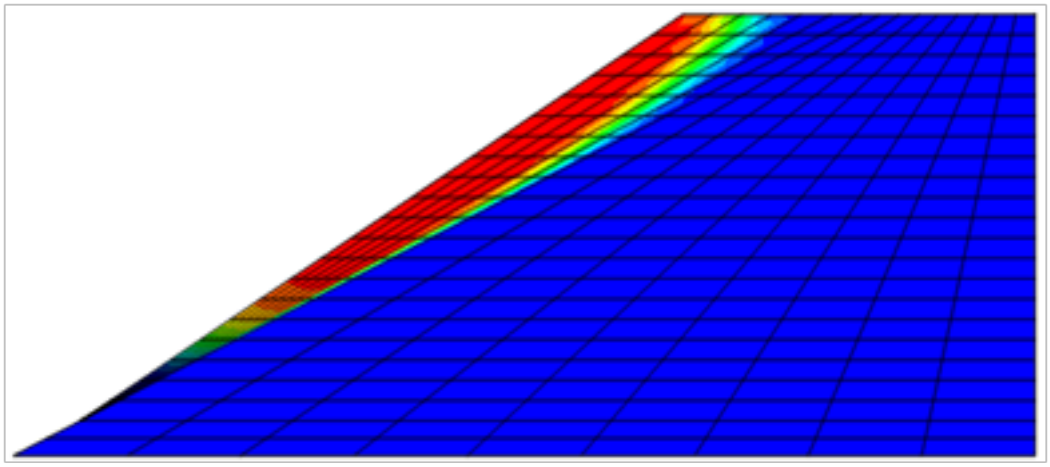

Figure C4: 60 ft fill length, a) maximum shear strain increment, b) displacement magnitude.

a)

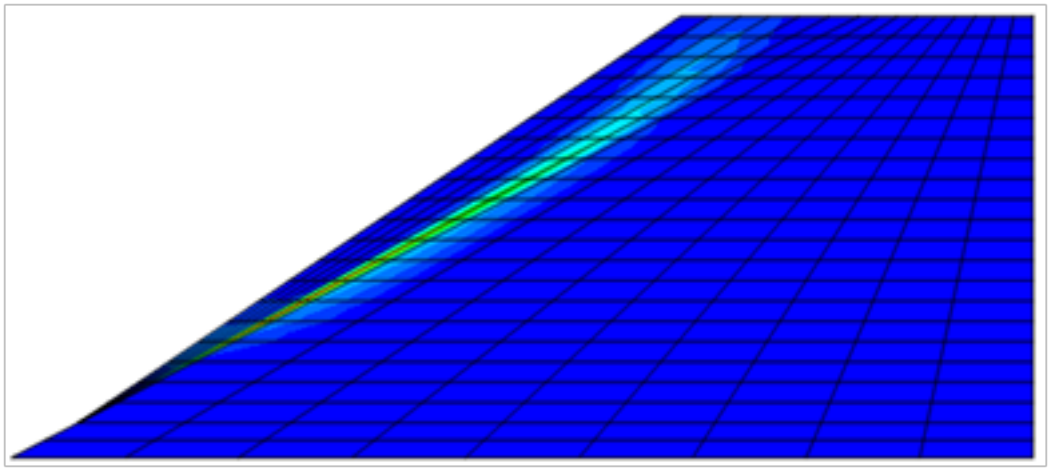

b)

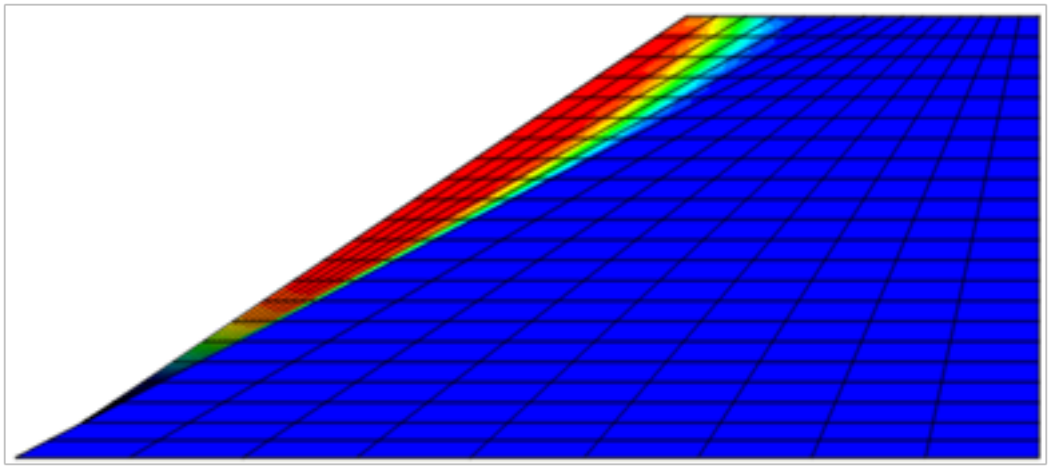

Figure C5: 120 ft fill length, a) maximum shear strain increment, b) displacement magnitude.

a)

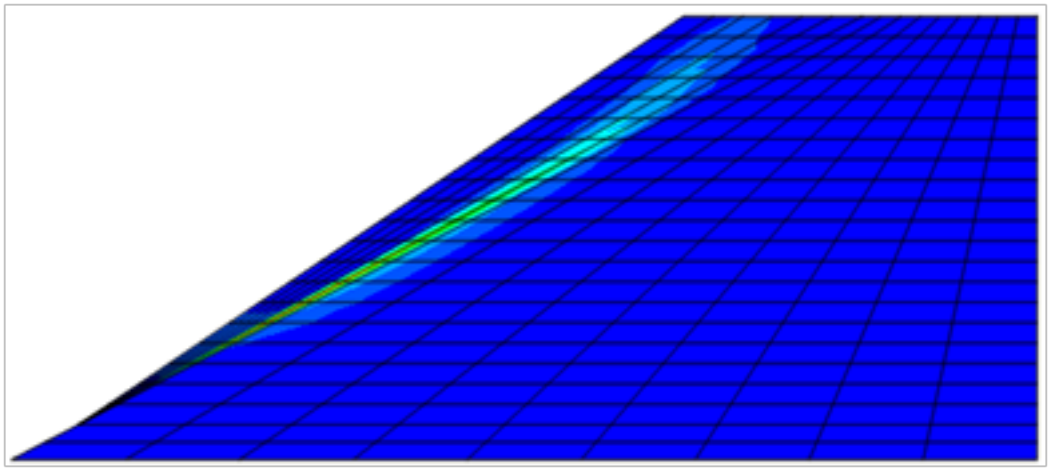

b)

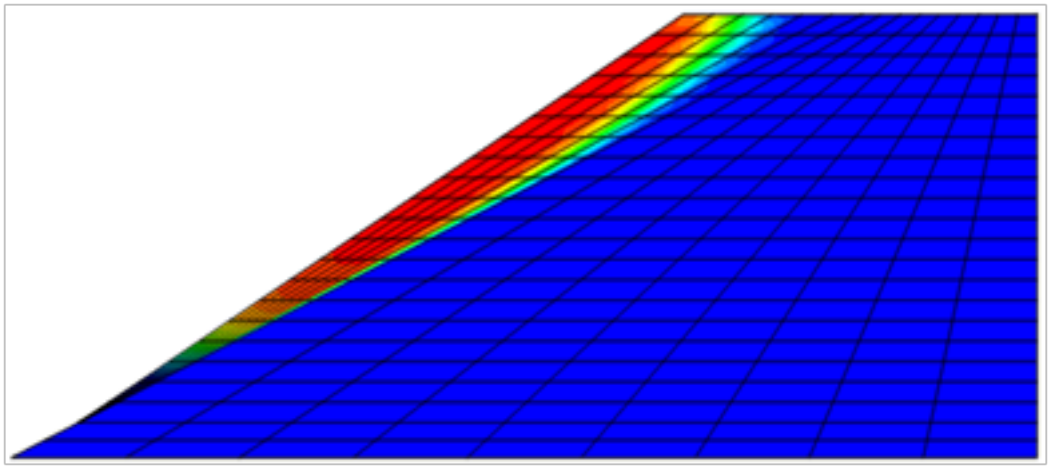

Figure C6: 200 ft fill length, a) maximum shear strain increment, b) displacement magnitude.

a)

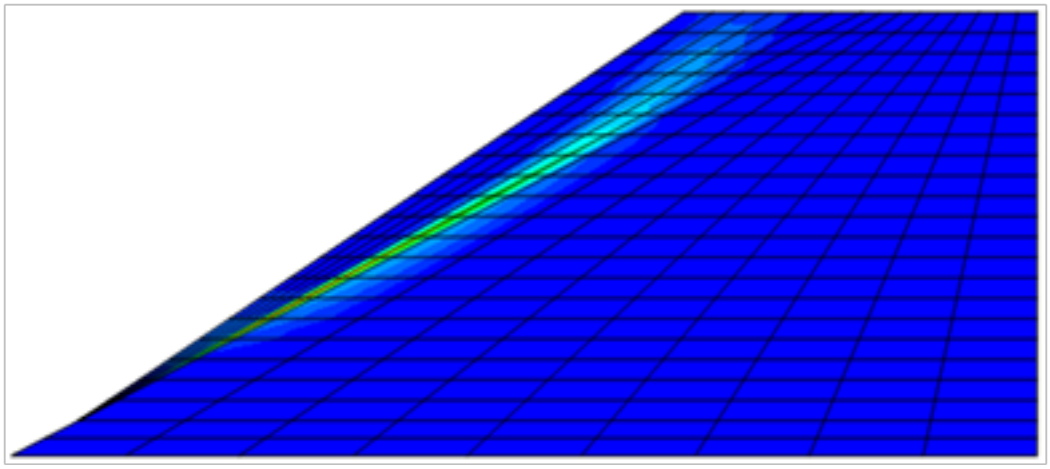

b)

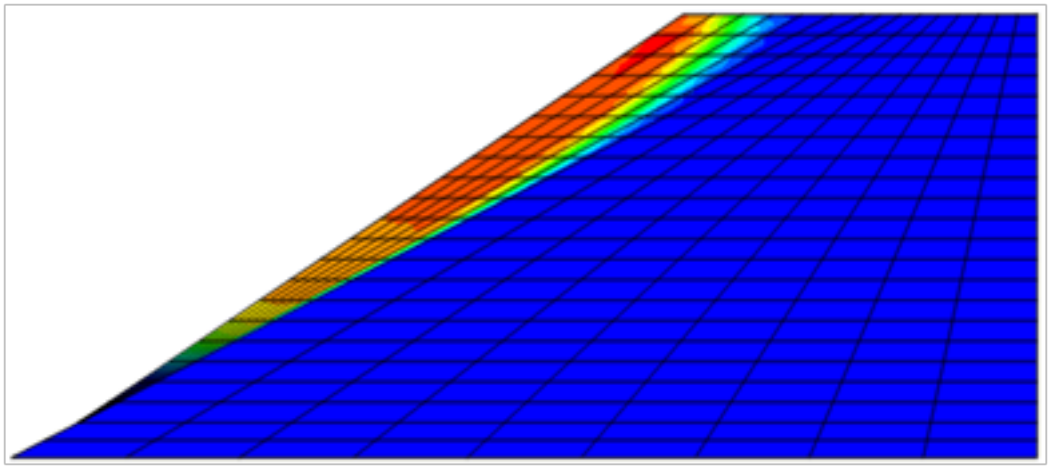

Figure C7: 400 ft fill length, a) maximum shear strain increment, b) displacement magnitude.

UNREINFORCED WEDGE

a)

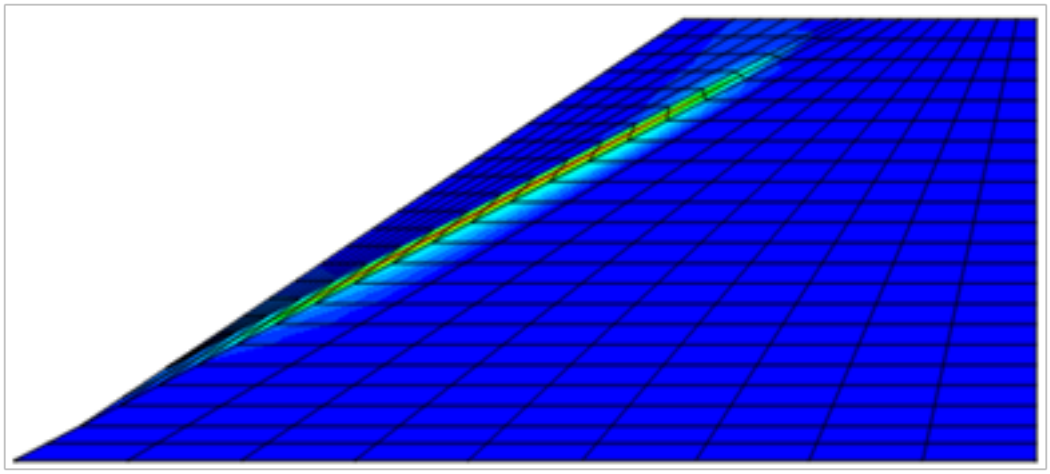

b)

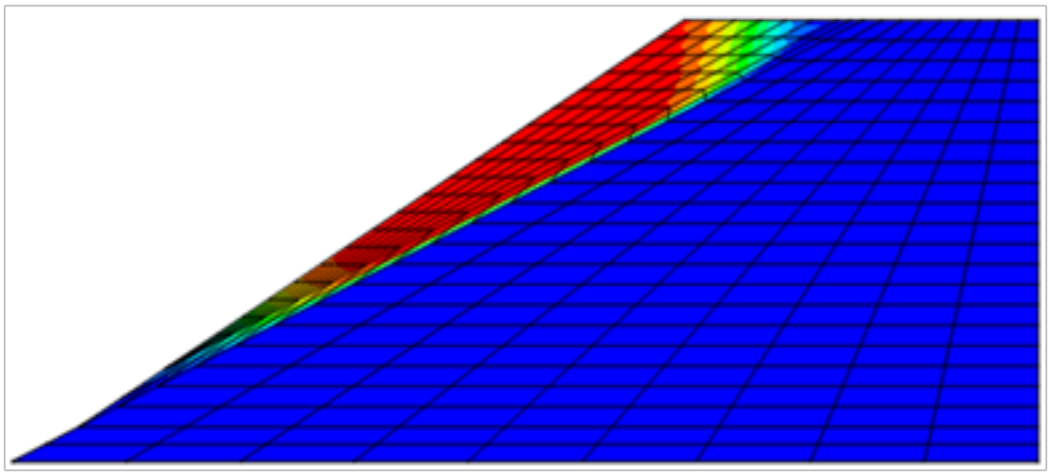

Figure C8: 10 ft fill length, a) maximum shear strain increment, b) displacement magnitude.

a)

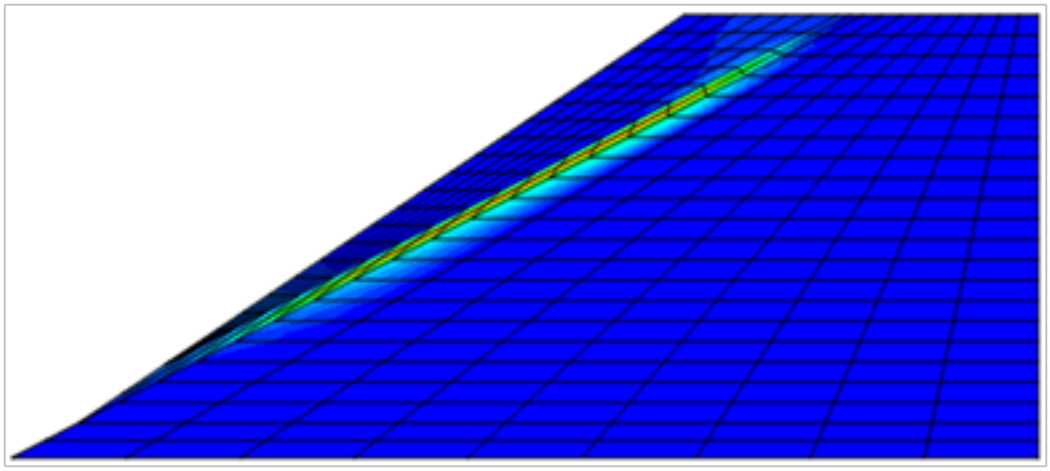

b)

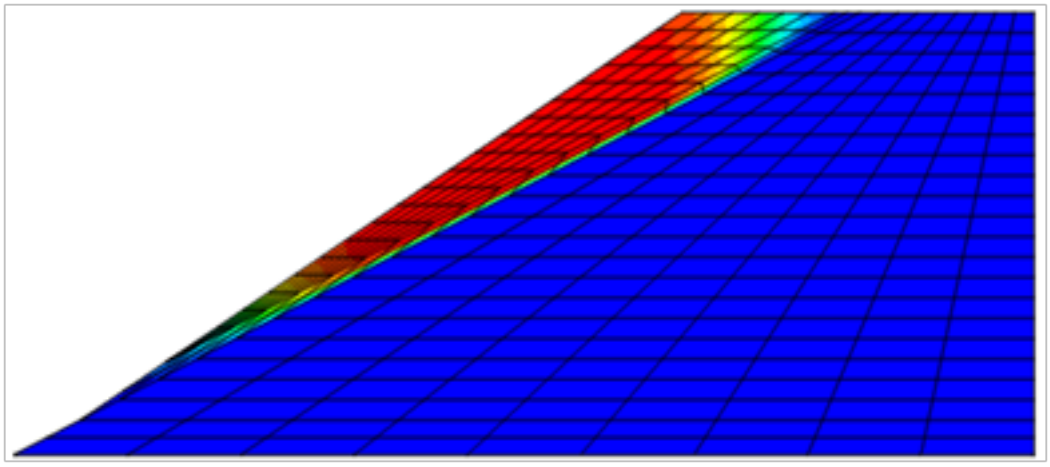

Figure C9: 20 ft fill length, a) maximum shear strain increment, b) displacement magnitude.

a)

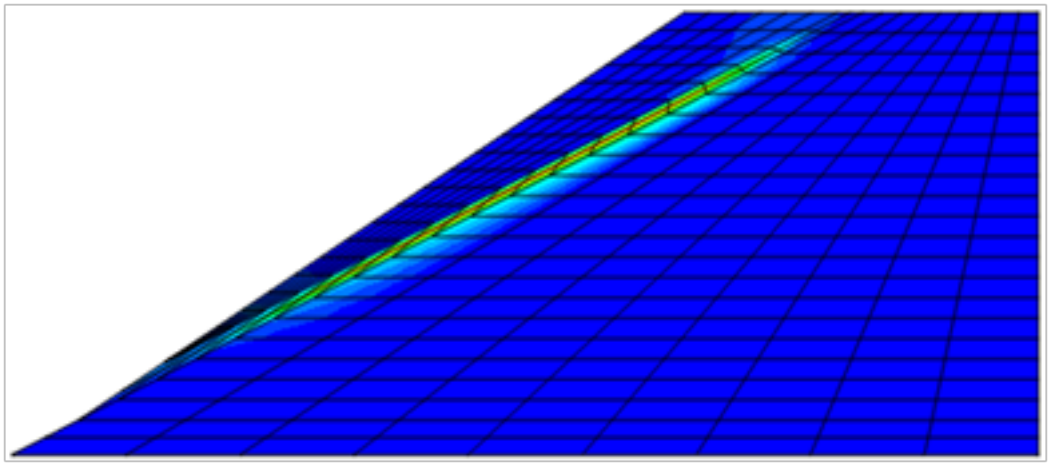

b)

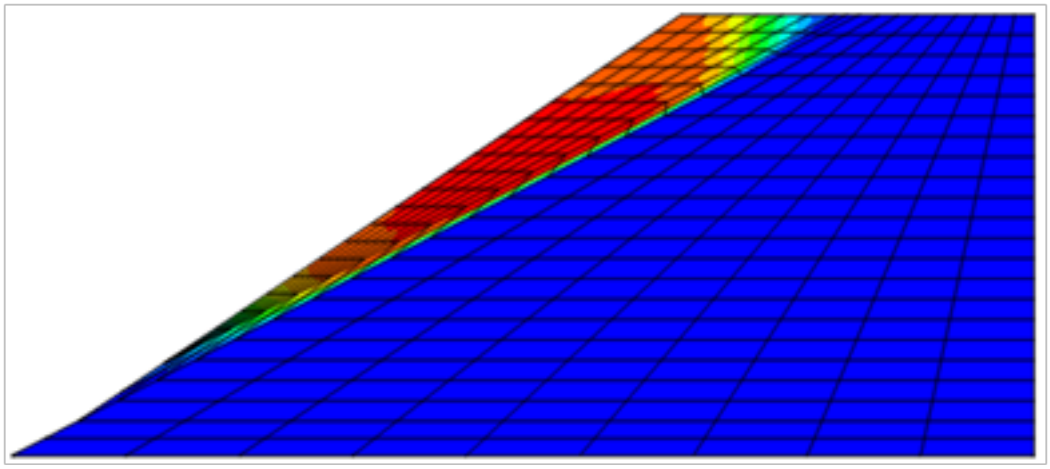

Figure C10: 30 ft fill length, a) maximum shear strain increment, b) displacement magnitude.

a)

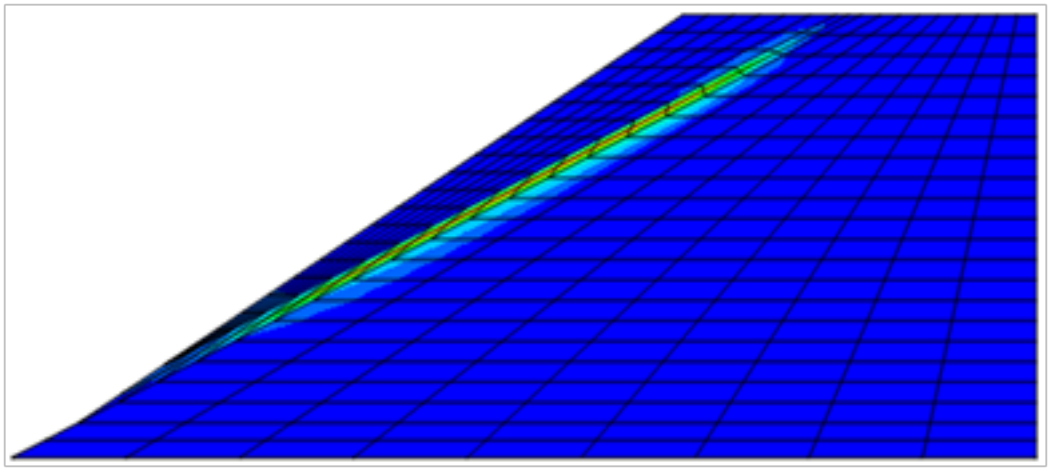

b)

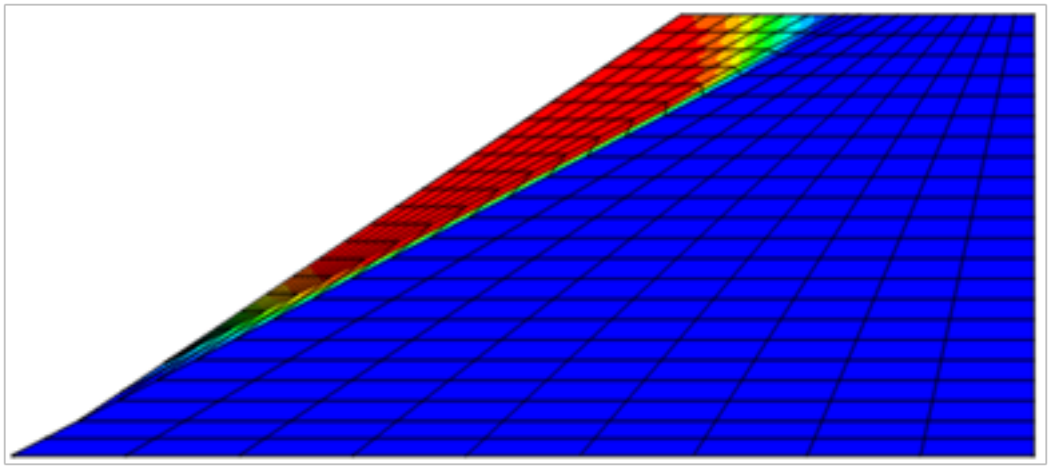

Figure C11: 60 ft fill length, a) maximum shear strain increment, b) displacement magnitude.

a)

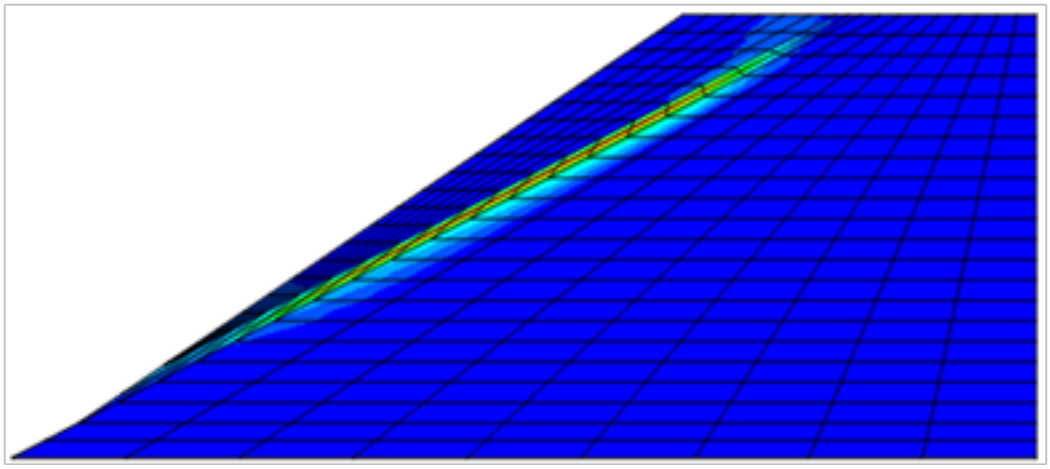

b)

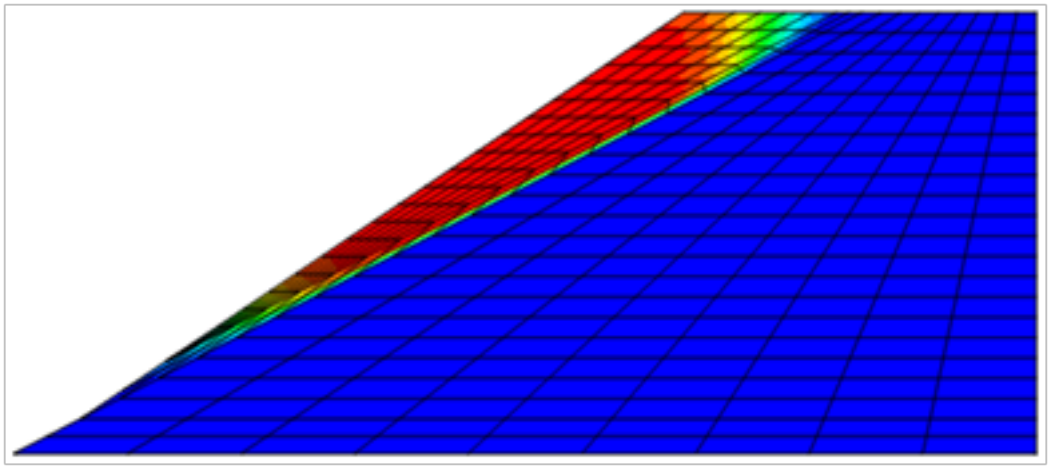

Figure C12: 120 ft fill length, a) maximum shear strain increment, b) displacement magnitude.

a)

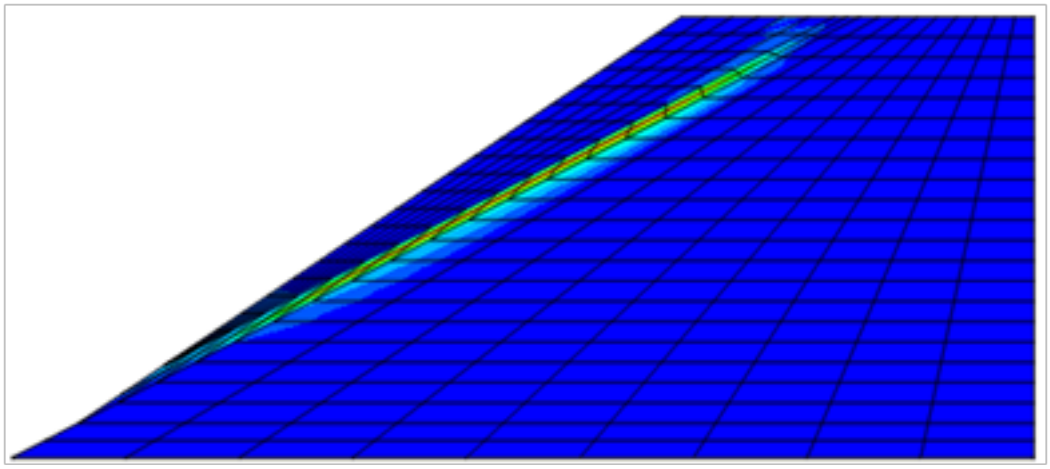

b)

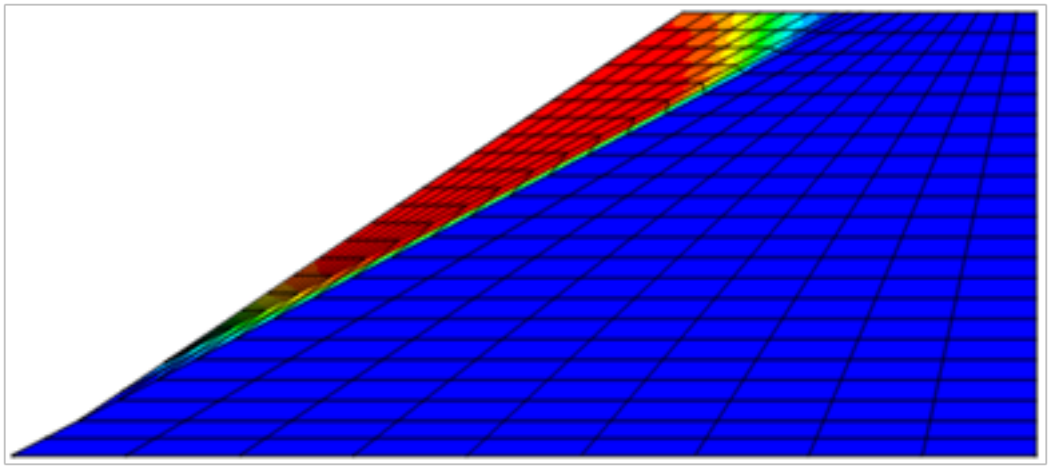

Figure C13: 200 ft fill length, a) maximum shear strain increment, b) displacement magnitude.

a)

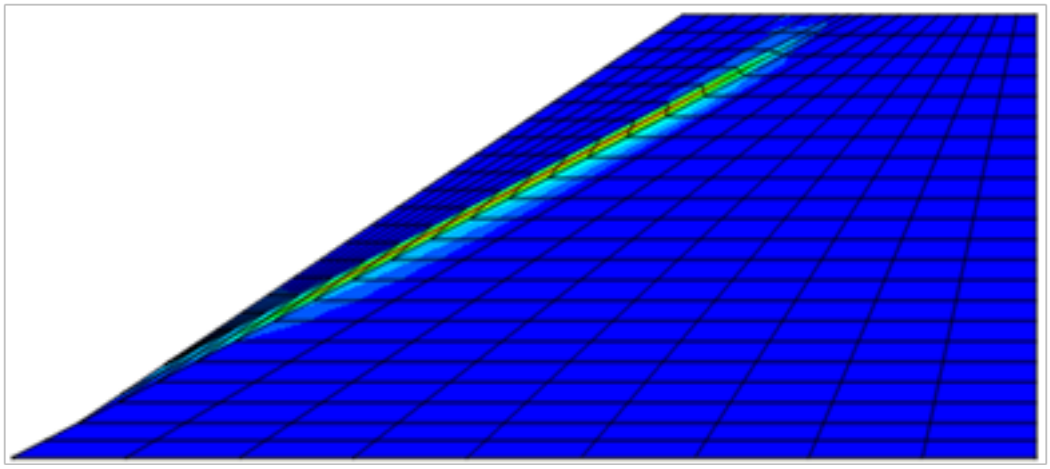

b)

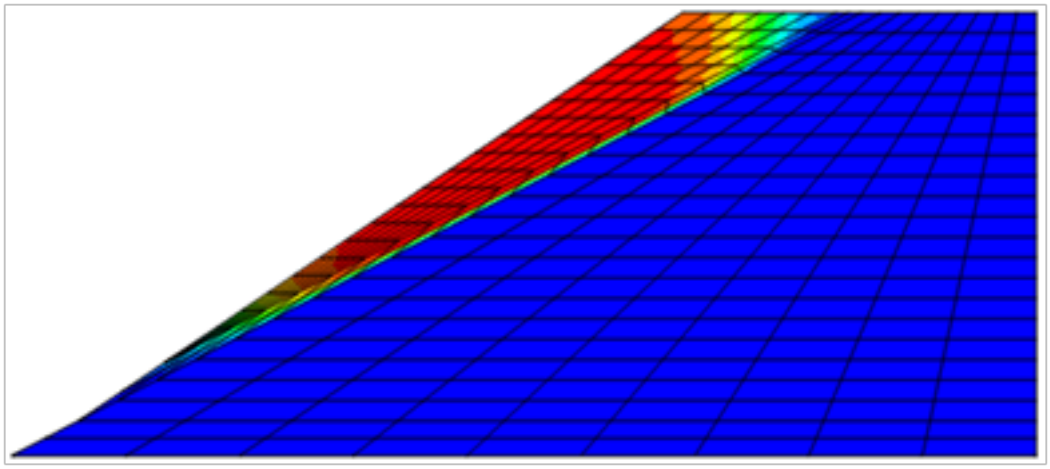

Figure C14: 400 ft fill length, a) maximum shear strain increment, b) displacement magnitude.

REINFORCED (5’ 5 LAYERS) ROTATIONAL UNIAXIAL

a)

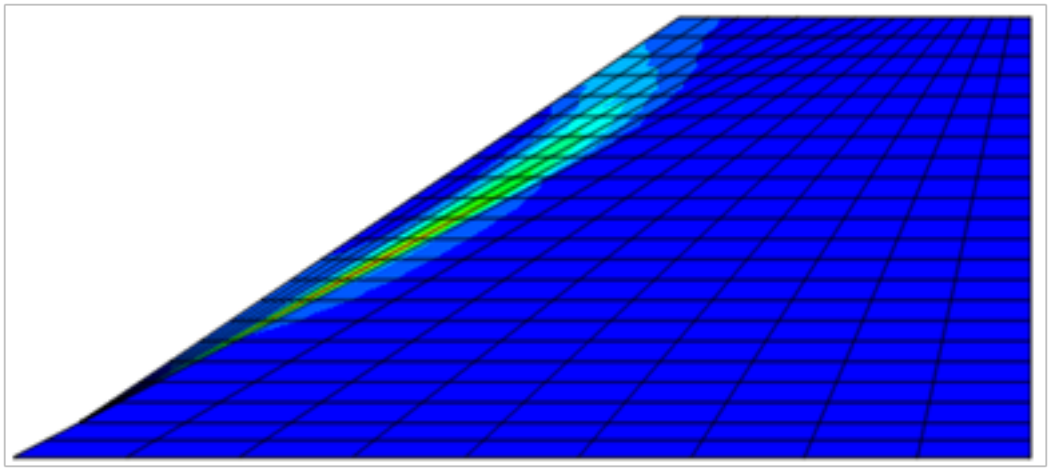

b)

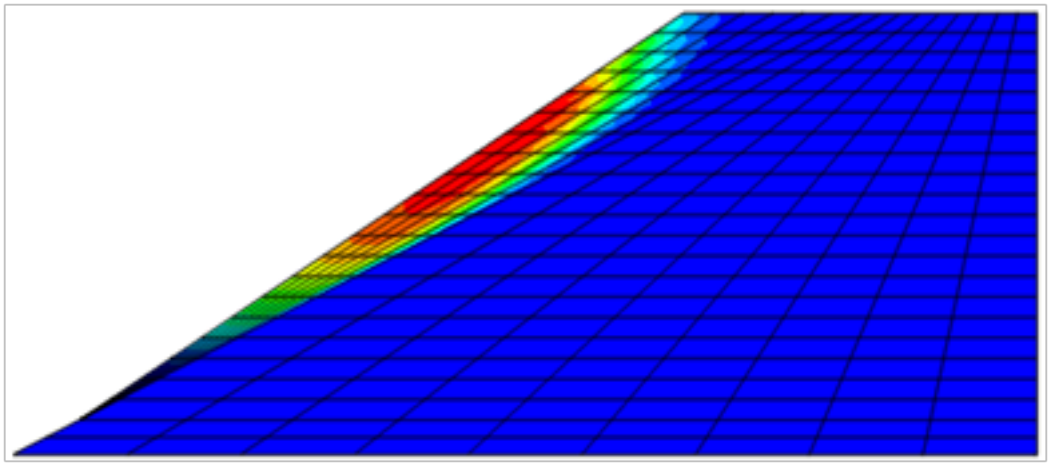

Figure C15: 10 ft fill length, a) maximum shear strain increment, b) displacement magnitude.

a)

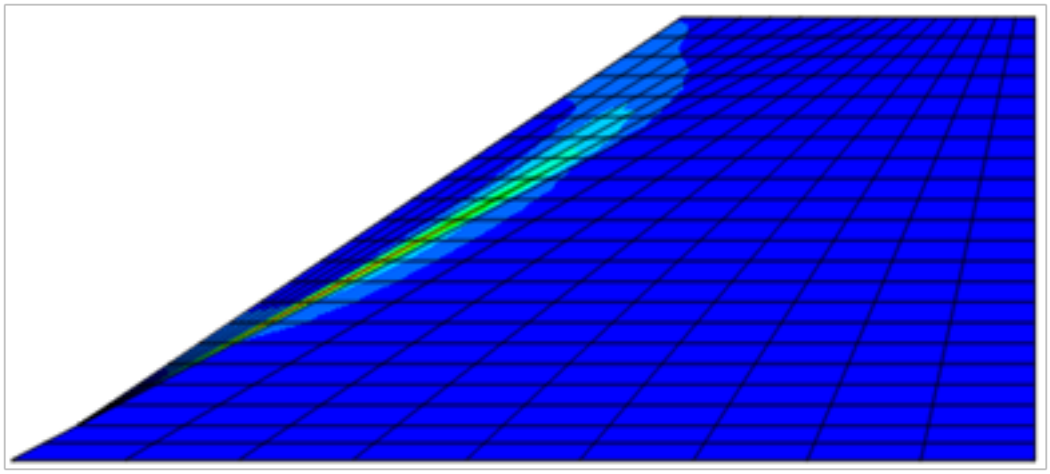

b)

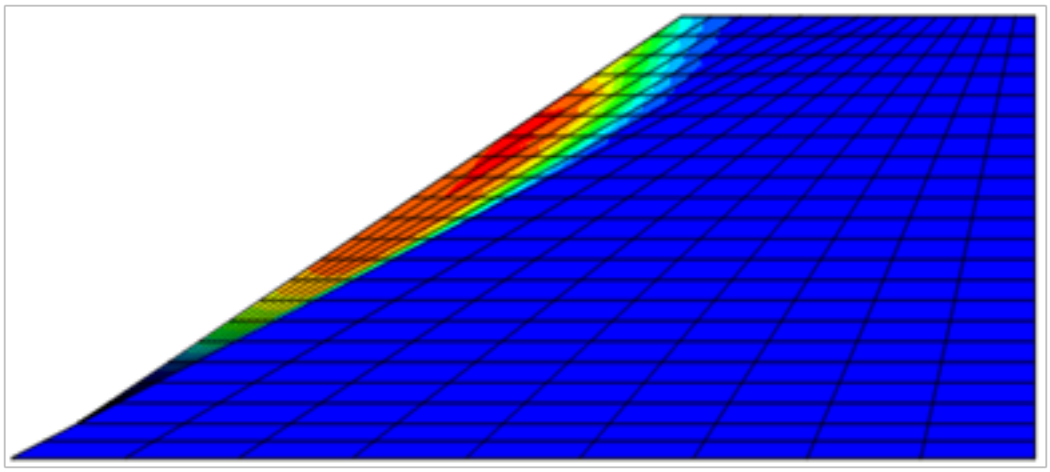

Figure C16: 20 ft fill length, a) maximum shear strain increment, b) displacement magnitude.

a)

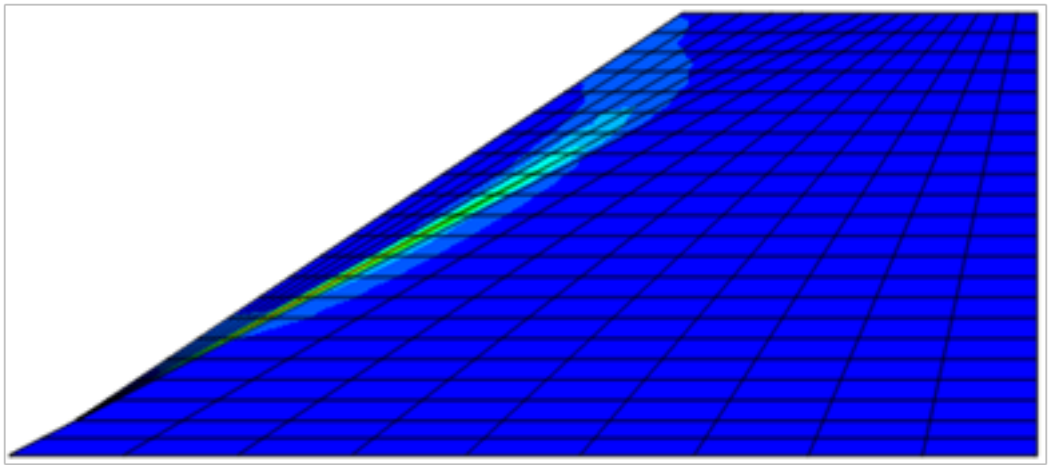

b)

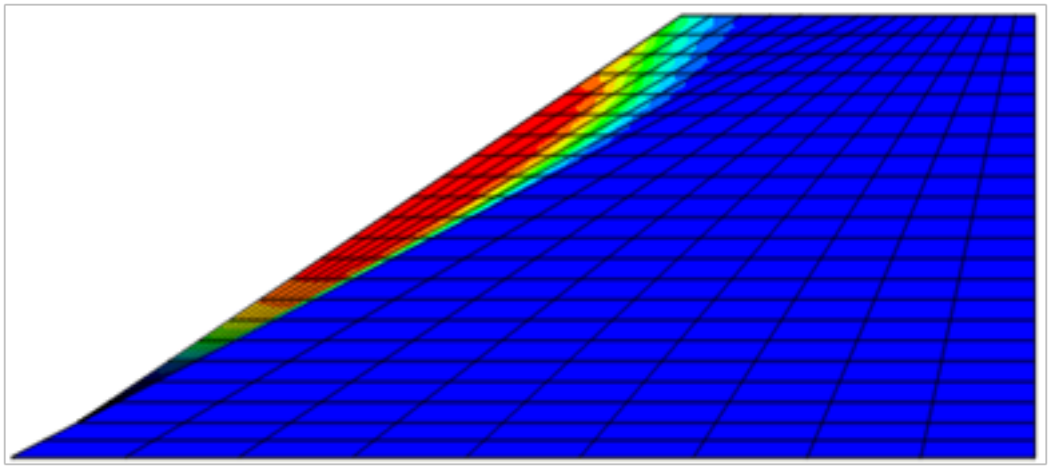

Figure C17: 30 ft fill length, a) maximum shear strain increment, b) displacement magnitude.

a)

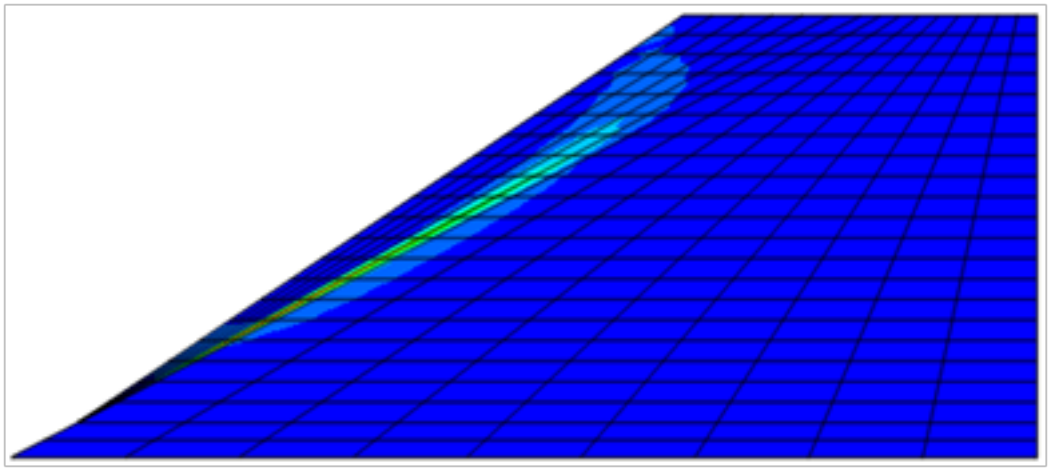

b)

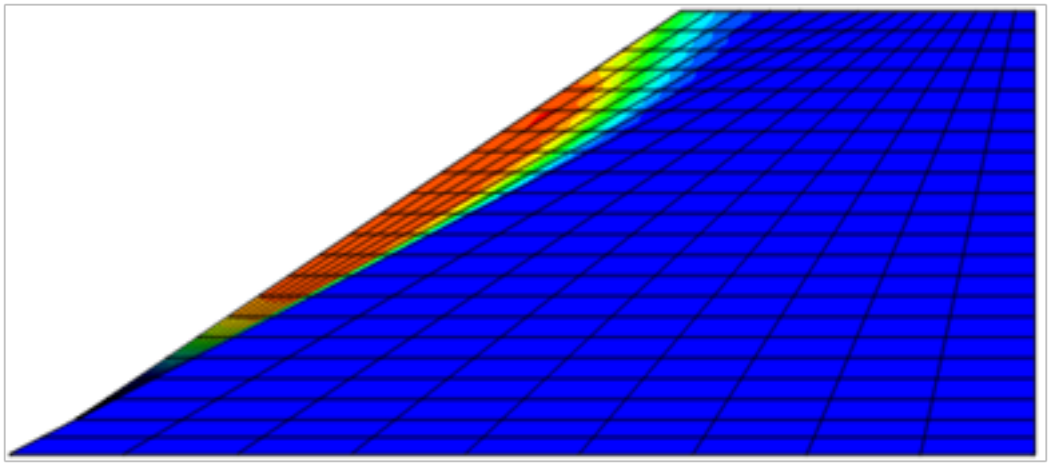

Figure C18: 60 ft fill length, a) maximum shear strain increment, b) displacement magnitude.

a)

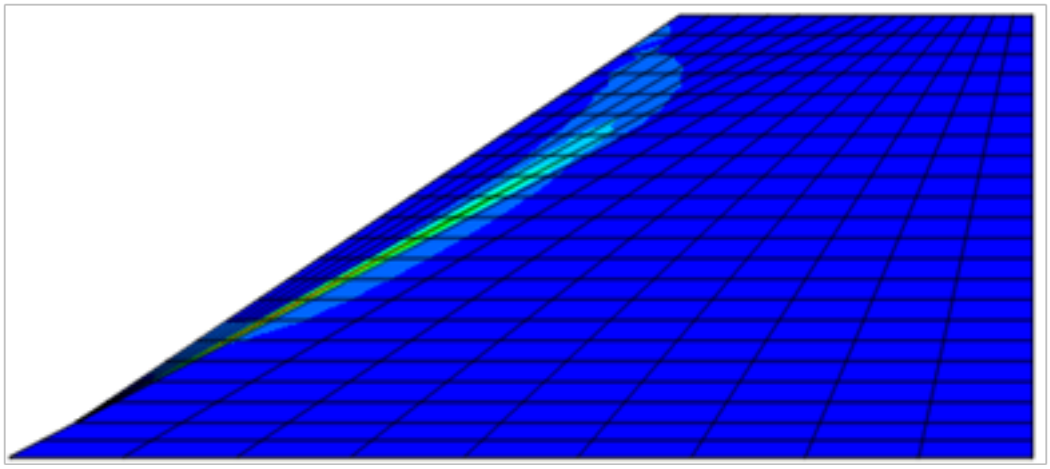

b)

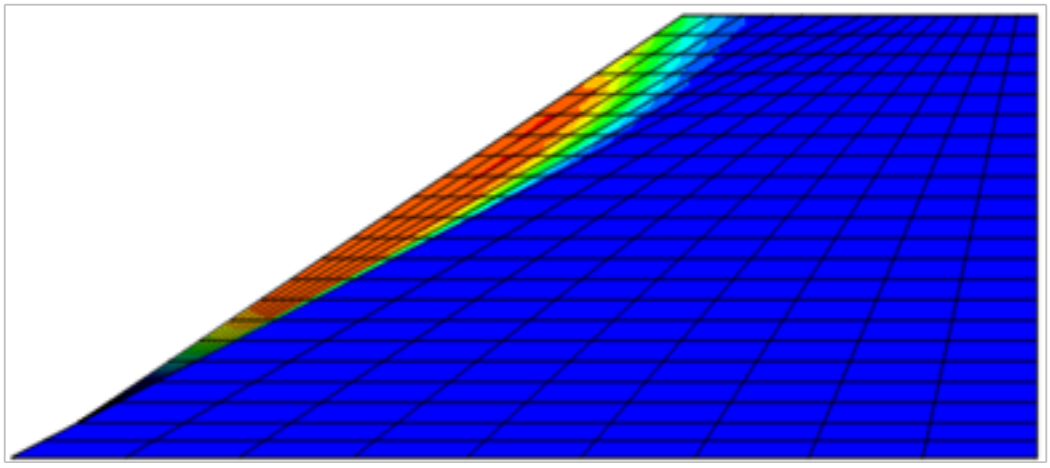

Figure C19: 120 ft fill length, a) maximum shear strain increment, b) displacement magnitude.

a)

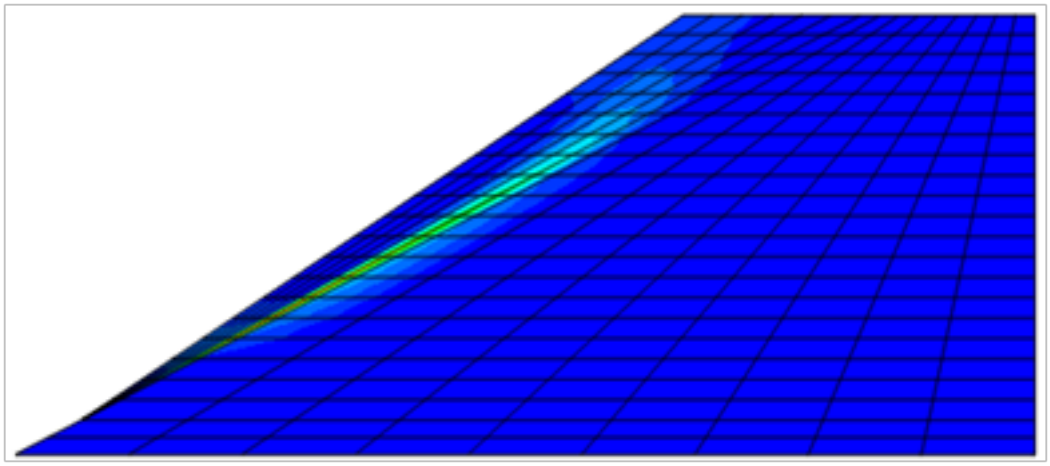

b)

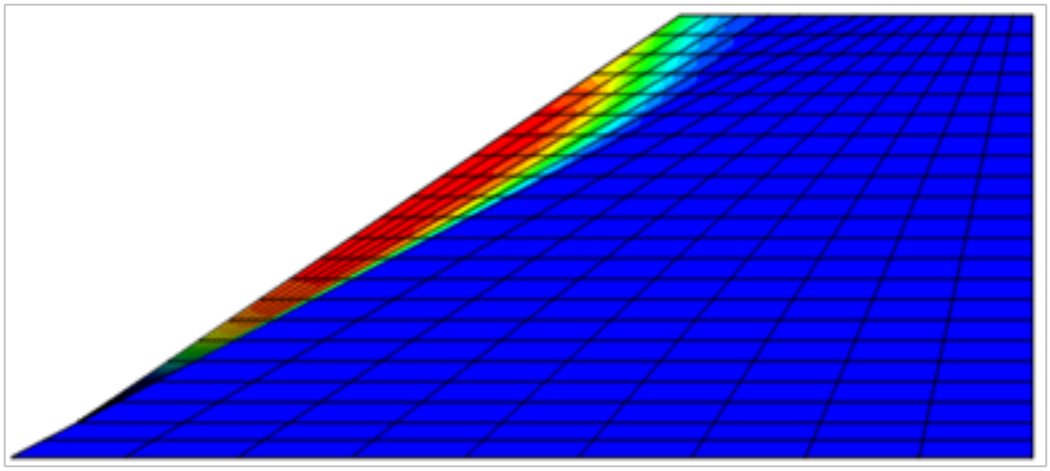

Figure C20: 200 ft fill length, a) maximum shear strain increment, b) displacement magnitude.

a)

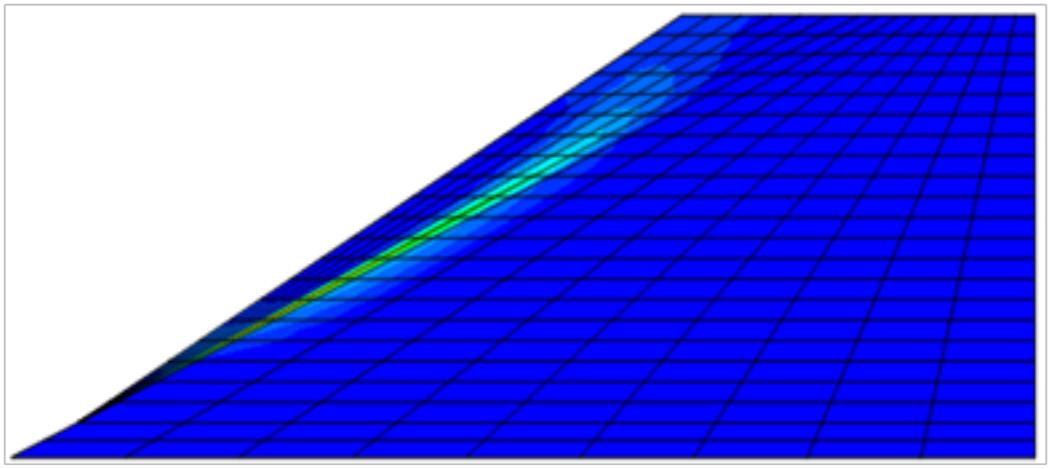

b)

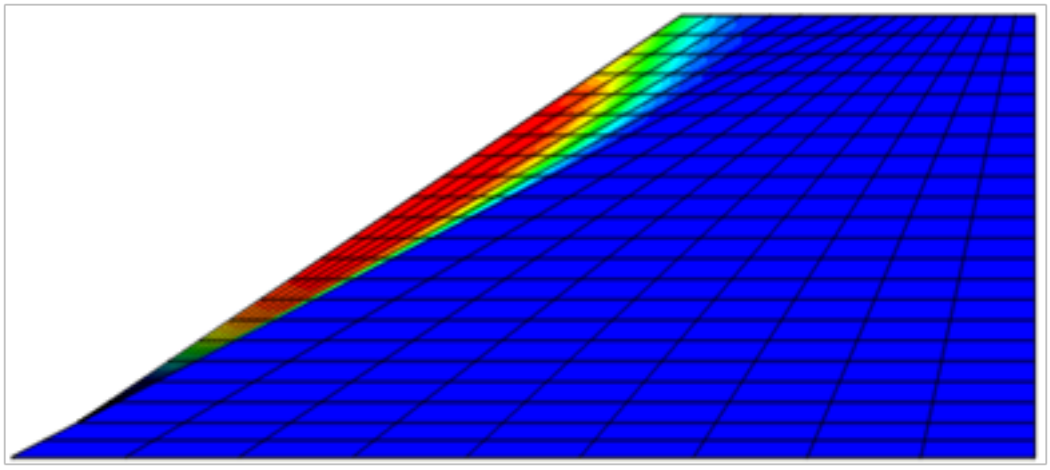

Figure C21: 400 ft fill length, a) maximum shear strain increment, b) displacement magnitude.

REINFORCED (5' 5 LAYERS) ROTATIONAL BIAXIAL

a)

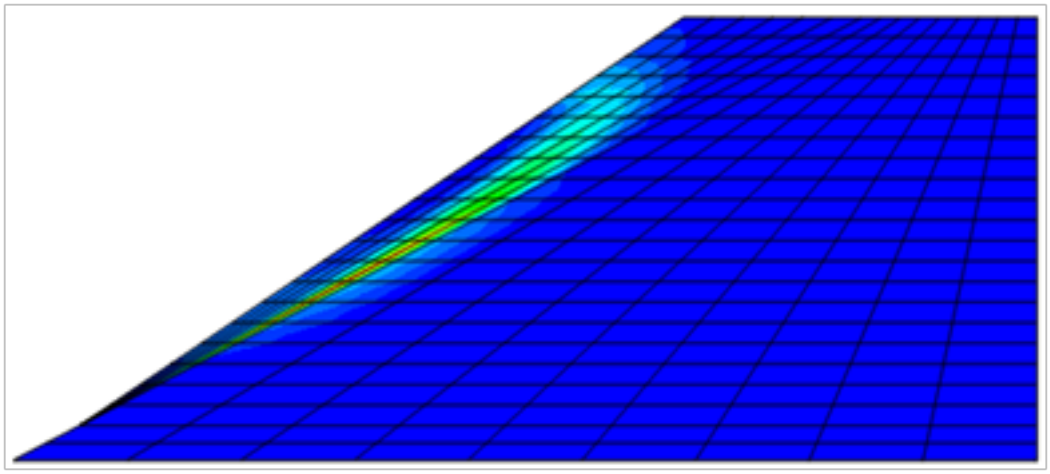

b)

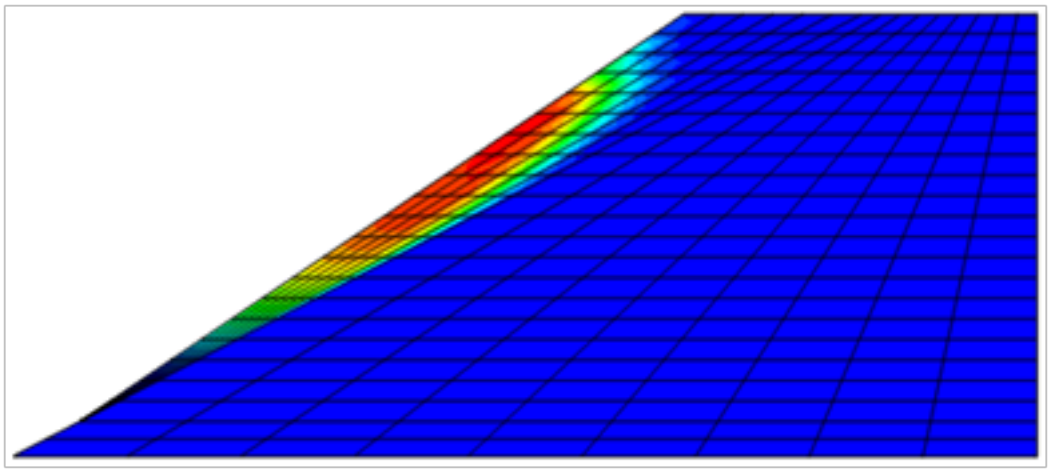

Figure C22: 10 ft fill length, a) maximum shear strain increment, b) displacement magnitude.

a)

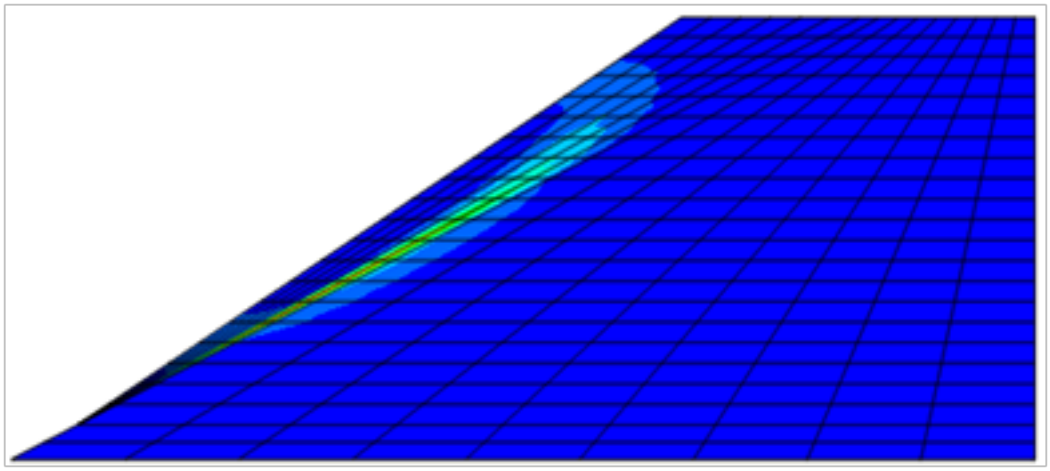

b)

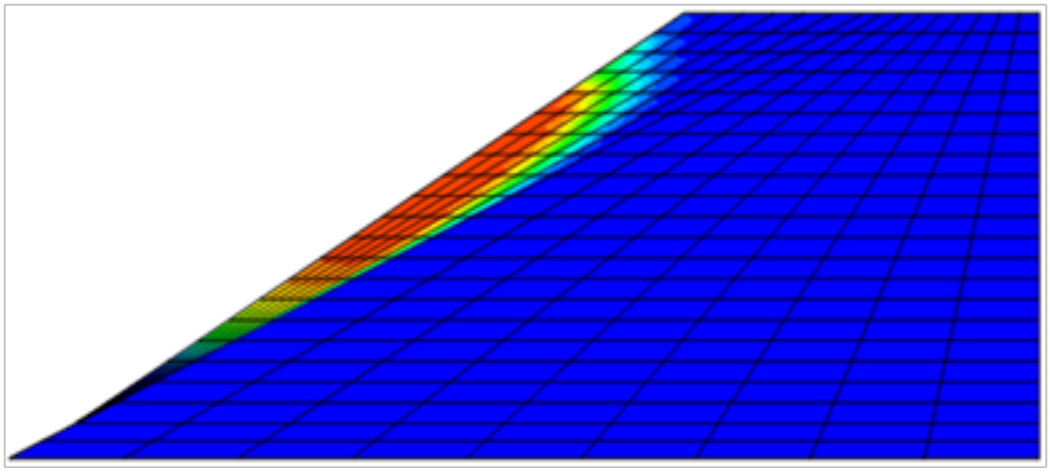

Figure C23: 20 ft fill length, a) maximum shear strain increment, b) displacement magnitude.

a)

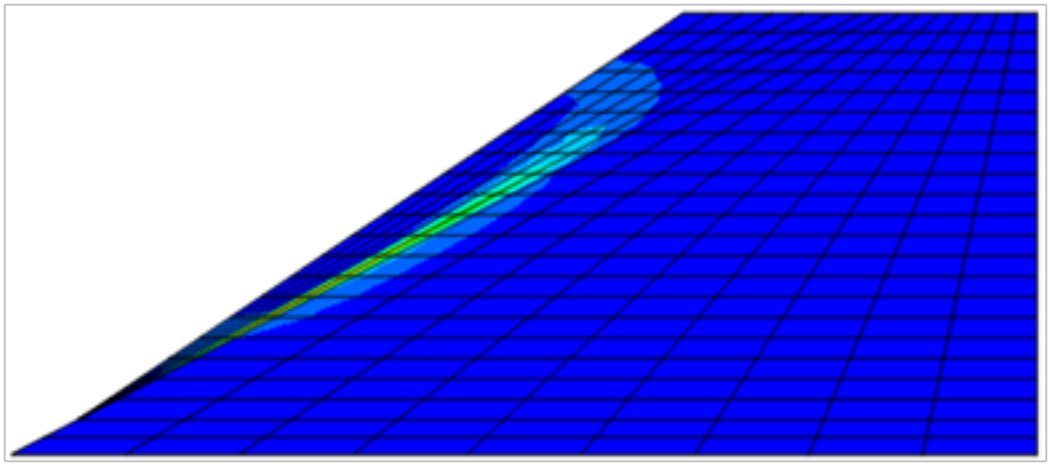

b)

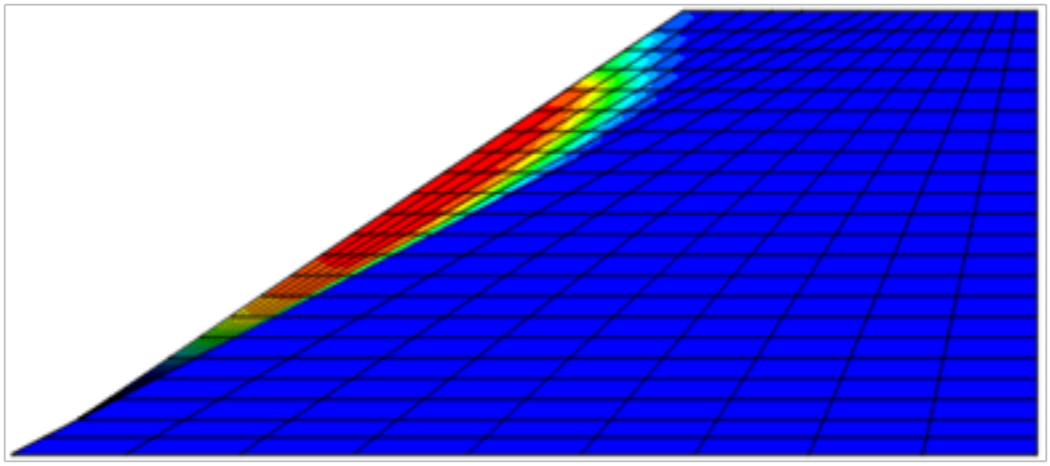

Figure C24: 30 ft fill length, a) maximum shear strain increment, b) displacement magnitude.

a)

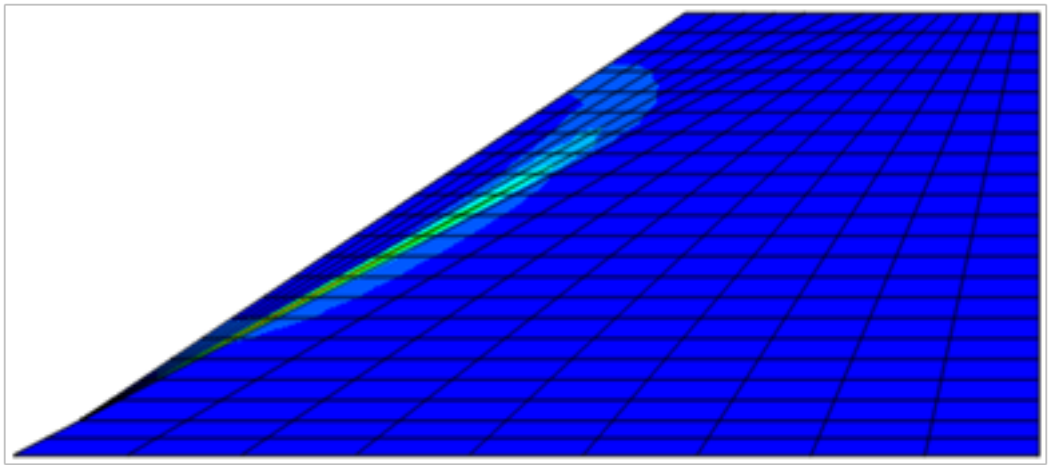

b)

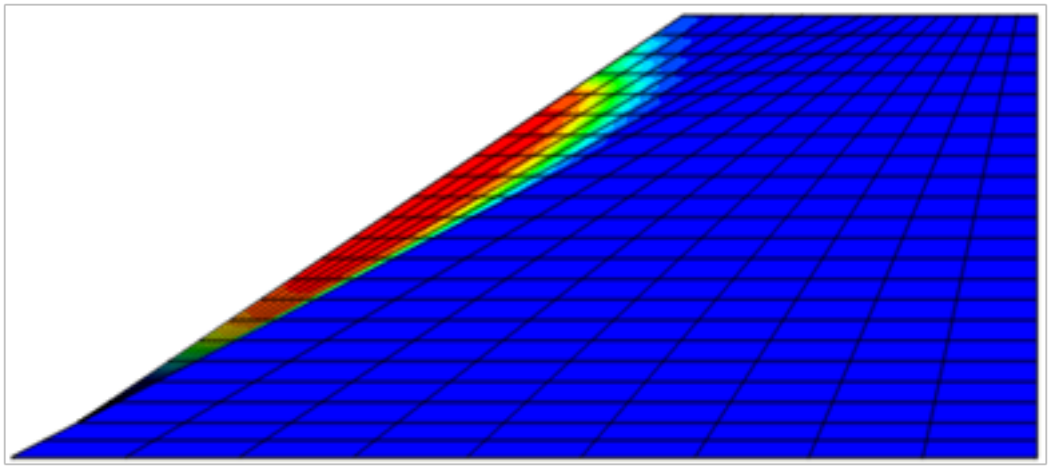

Figure C25: 60 ft fill length, a) maximum shear strain increment, b) displacement magnitude.

a)

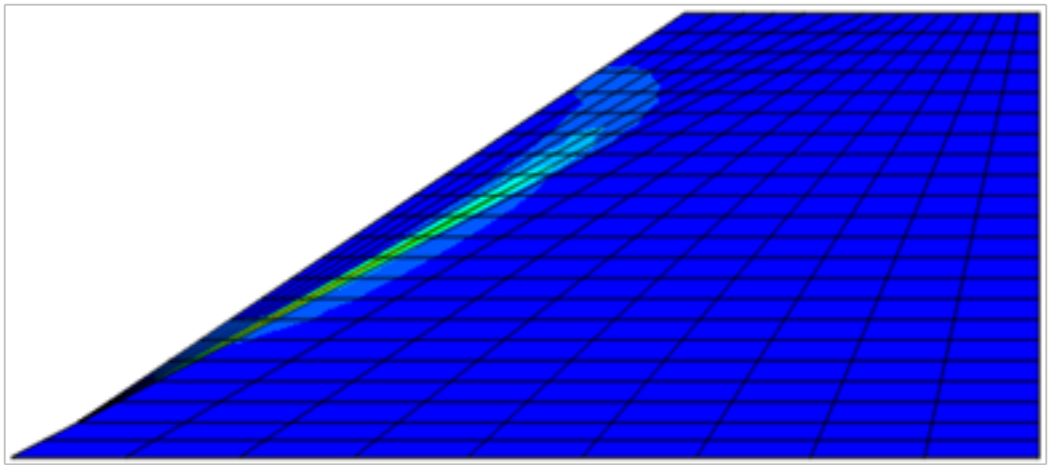

b)

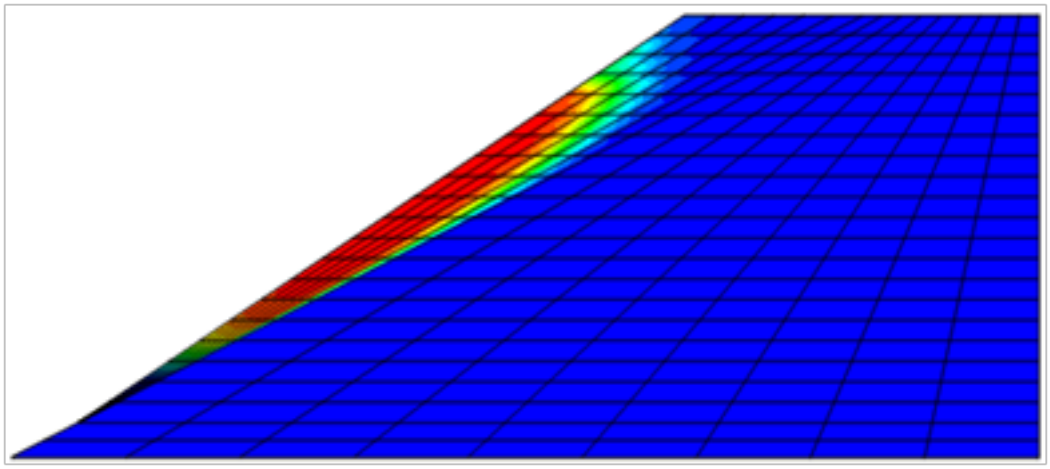

Figure C26: 120 ft fill length, a) maximum shear strain increment, b) displacement magnitude.

a)

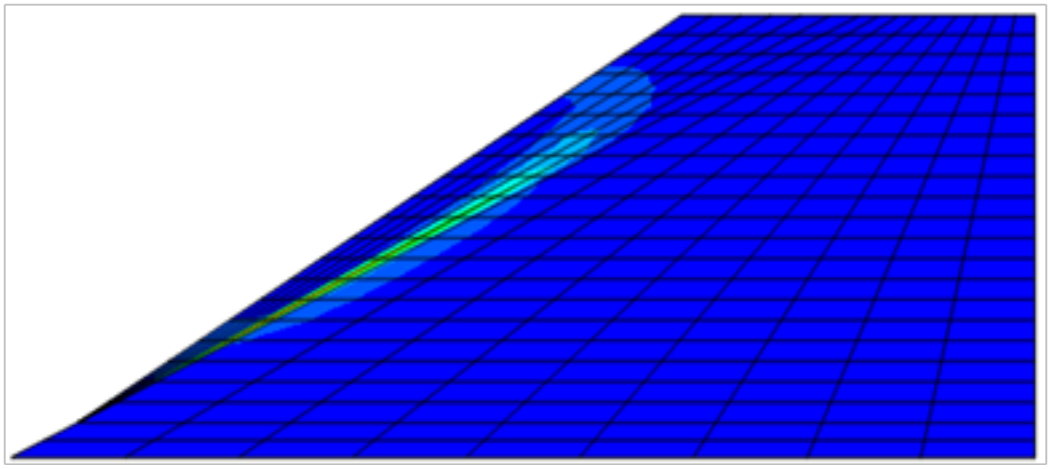

b)

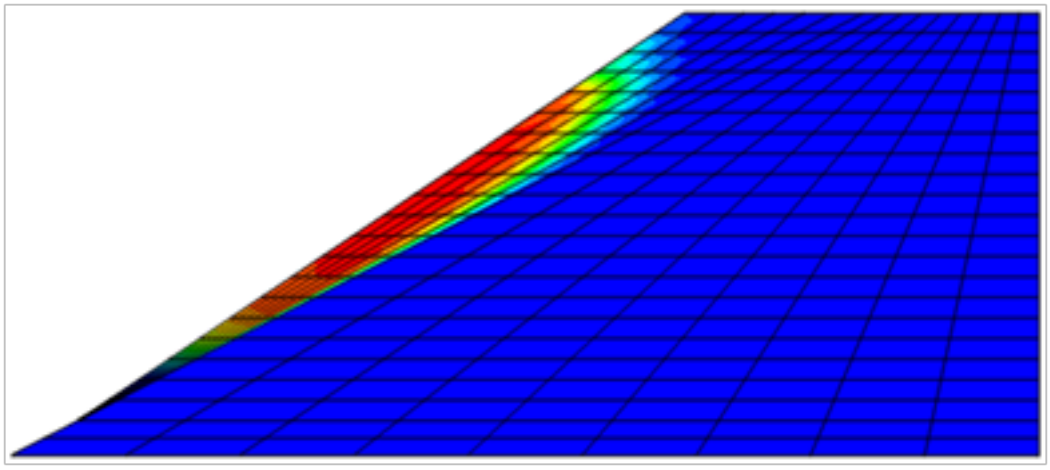

Figure C27: 200 ft fill length, a) maximum shear strain increment, b) displacement magnitude.

a)

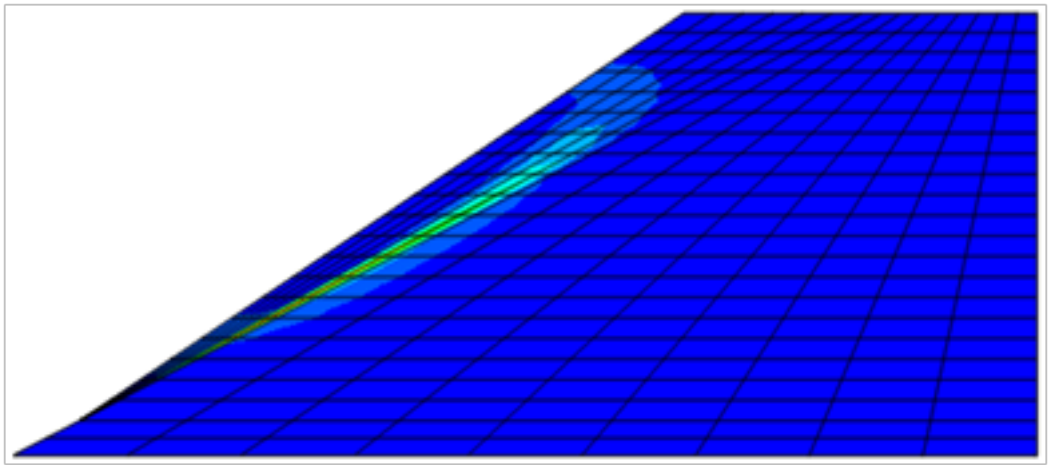

b)

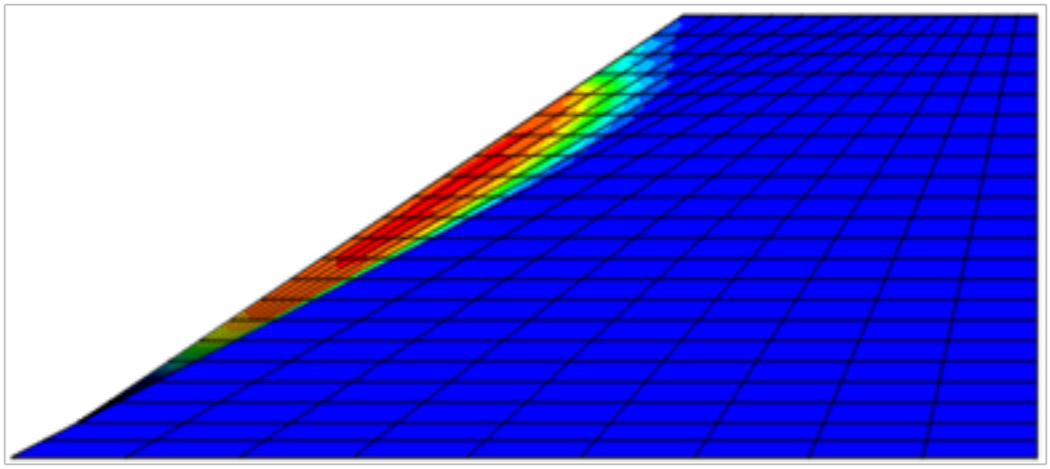

Figure C28: 400 ft fill length, a) maximum shear strain increment, b) displacement magnitude.

REINFORCED (5’ 5 LAYERS) WEDGE UNIAXIAL

a)

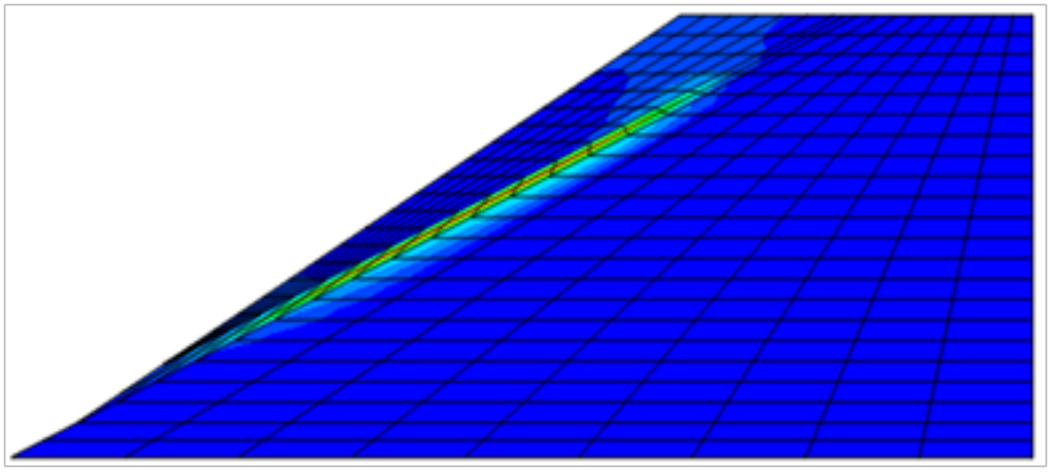

b)

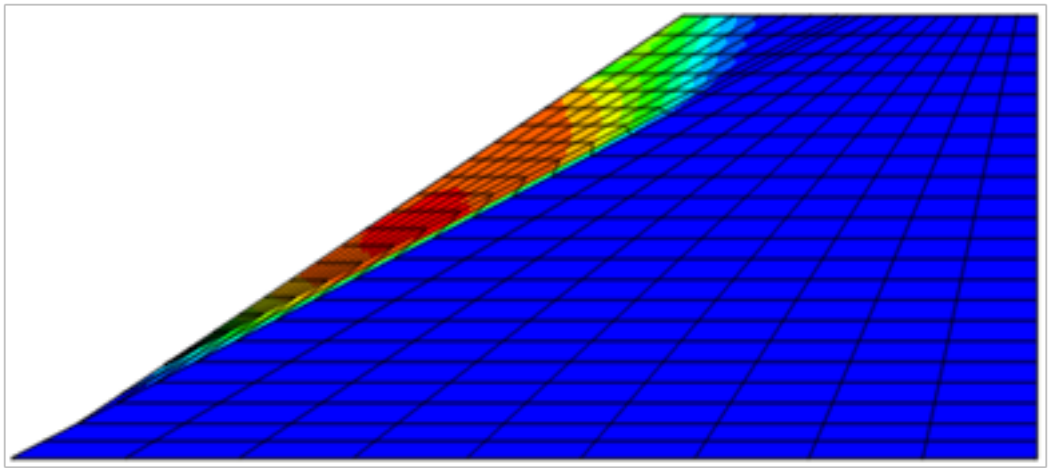

Figure C29: 10 ft fill length, a) maximum shear strain increment, b) displacement magnitude.

a)

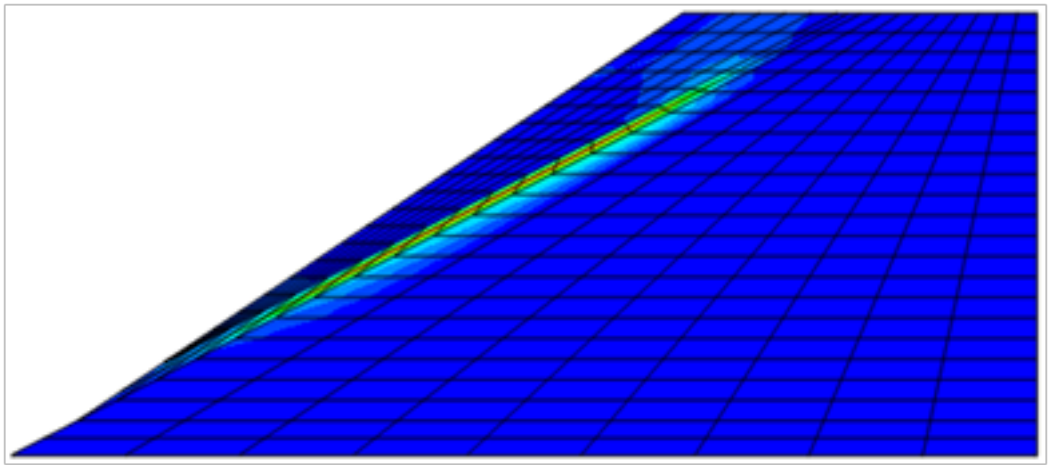

b)

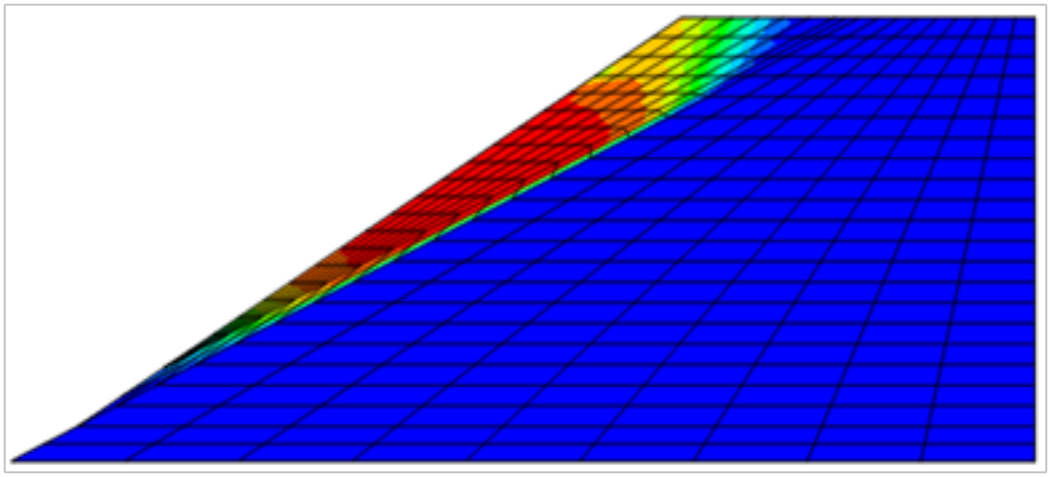

Figure C30: 20 ft fill length, a) maximum shear strain increment, b) displacement magnitude.

a)

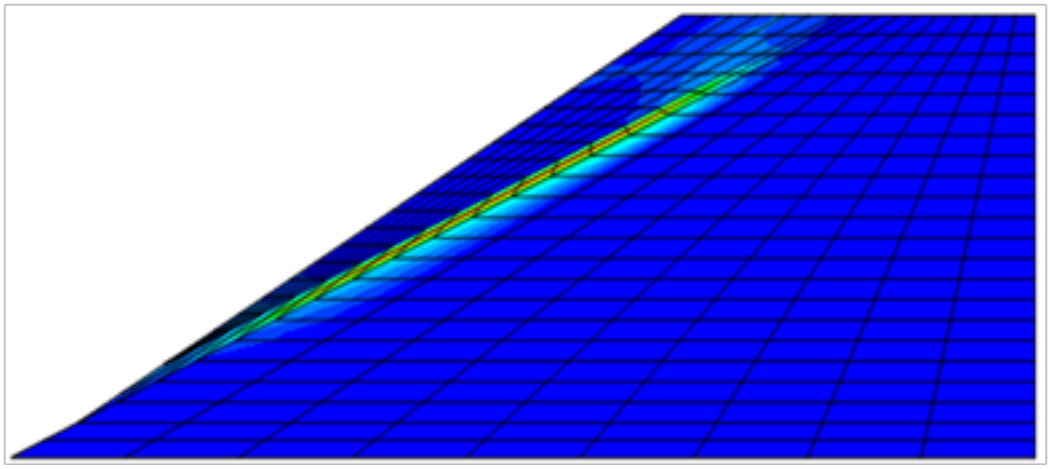

b)

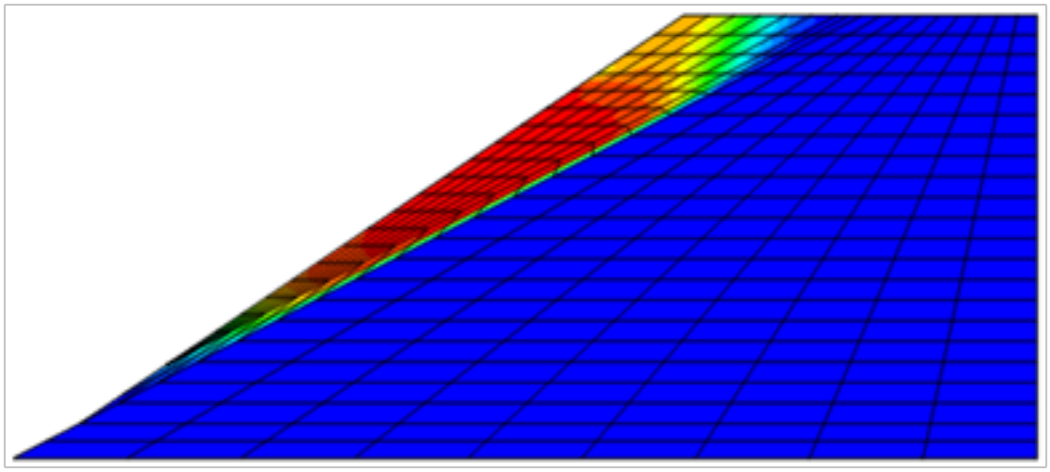

Figure C31: 30 ft fill length, a) maximum shear strain increment, b) displacement magnitude.

a)

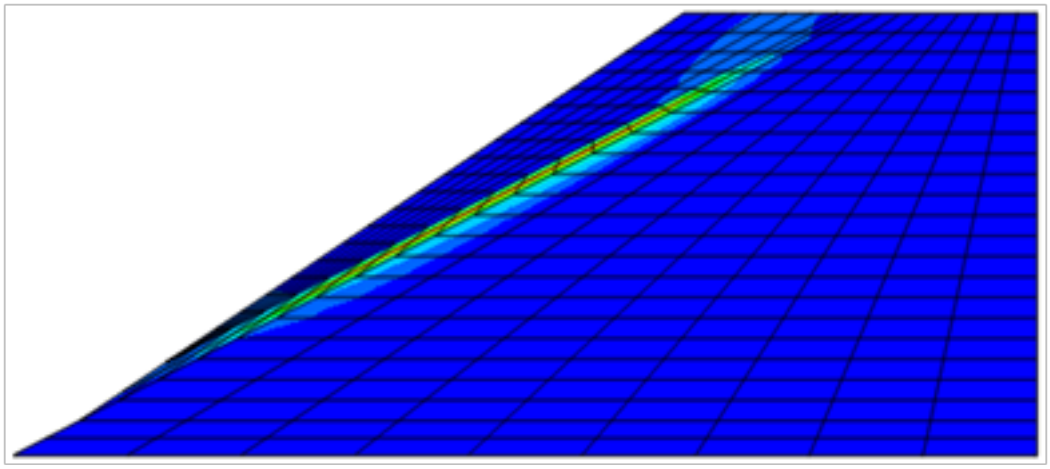

b)

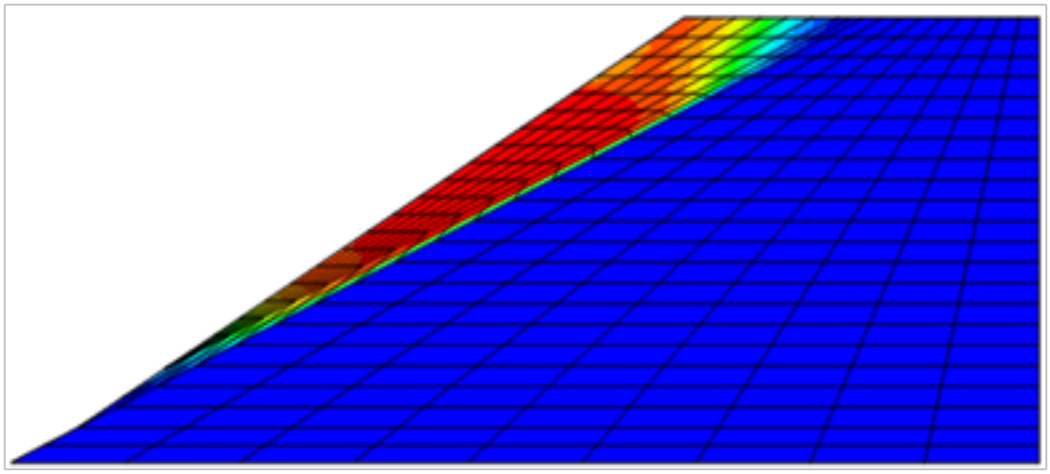

Figure C32: 60 ft fill length, a) maximum shear strain increment, b) displacement magnitude.

a)

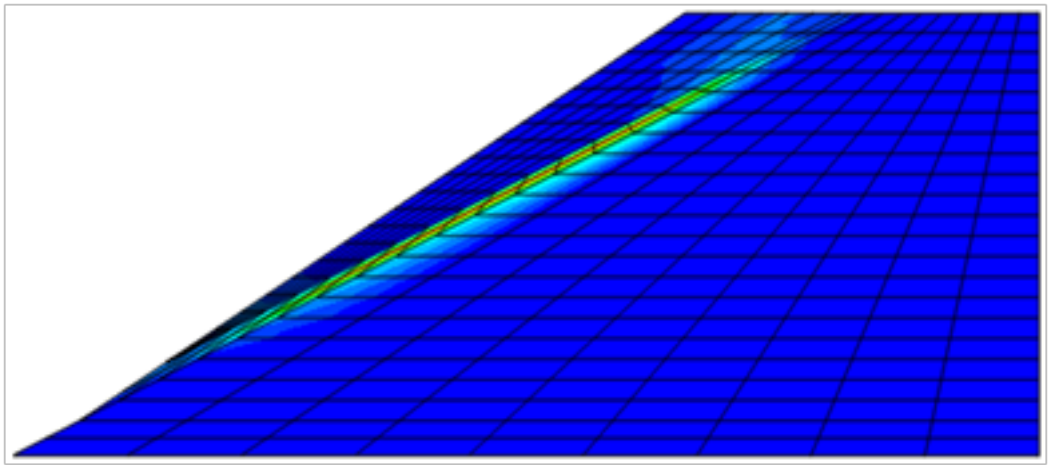

b)

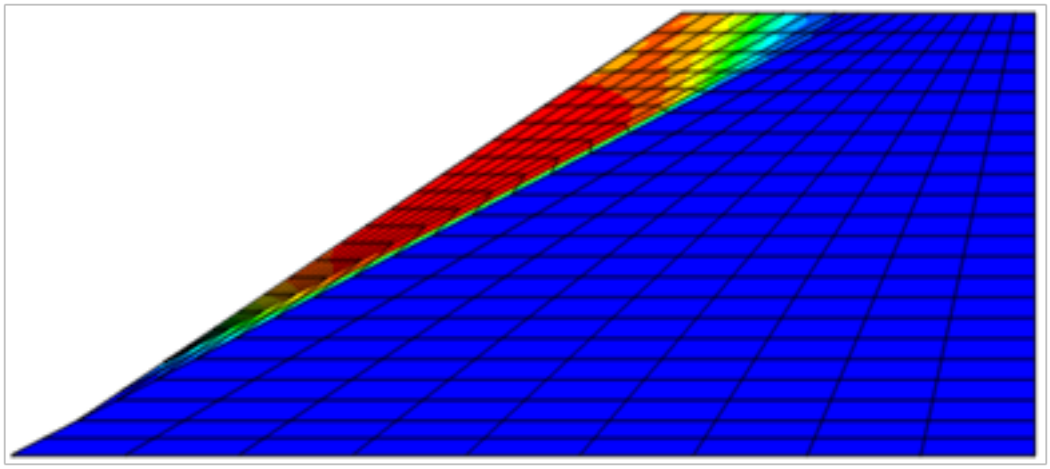

Figure C33: 120 ft fill length, a) maximum shear strain increment, b) displacement magnitude.

a)

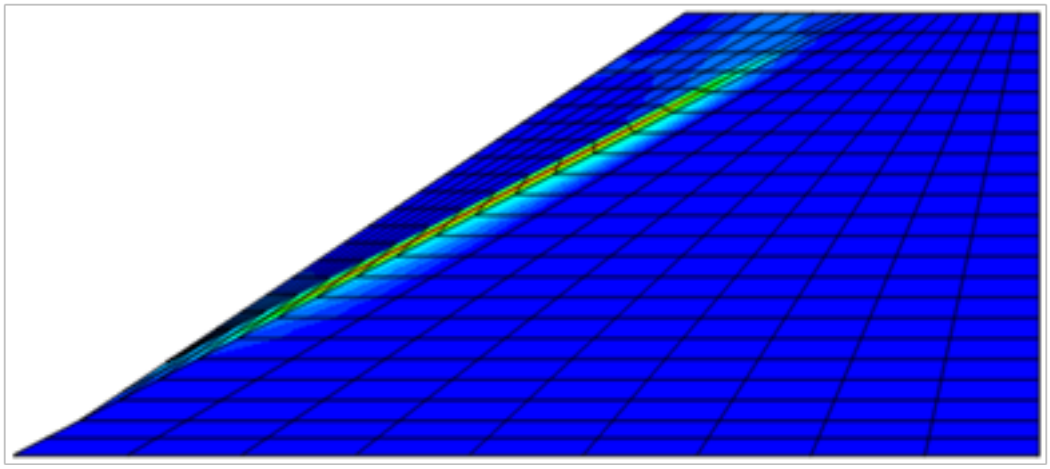

b)

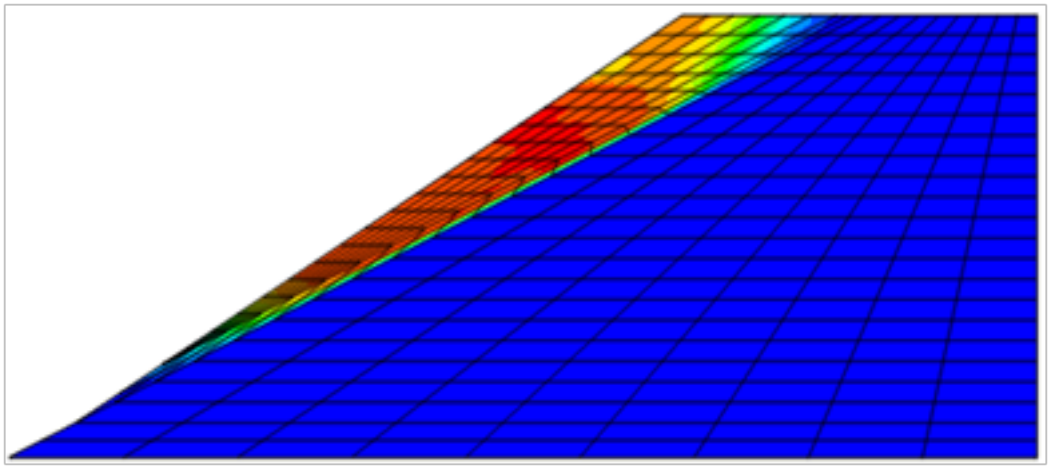

Figure C34: 200 ft fill length, a) maximum shear strain increment, b) displacement magnitude.

a)

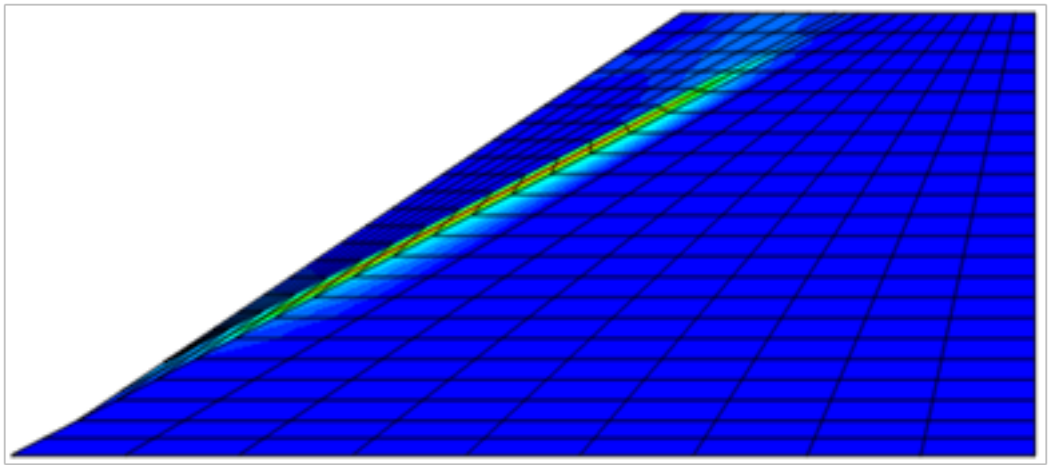

b)

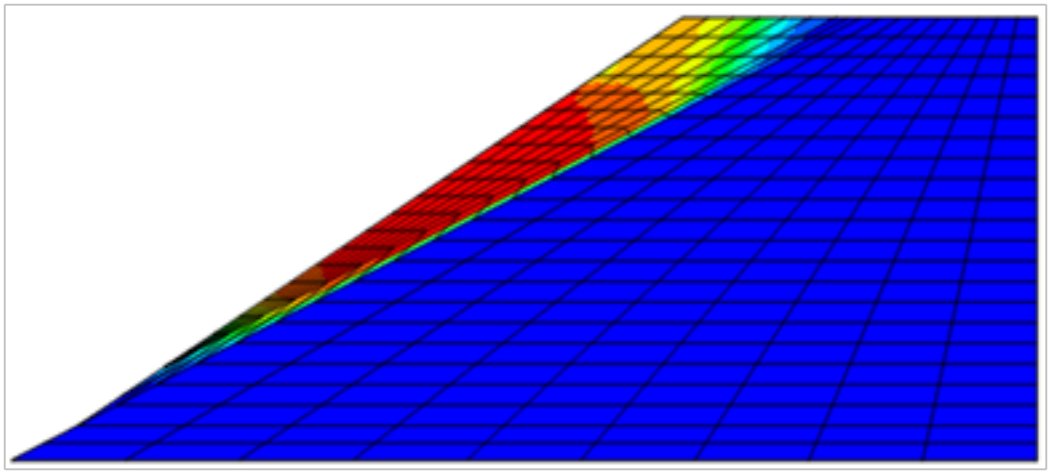

Figure C35: 400 ft fill length, a) maximum shear strain increment, b) displacement magnitude.

REINFORCED (5' 5 LAYERS) WEDGE BIAXIAL

a)

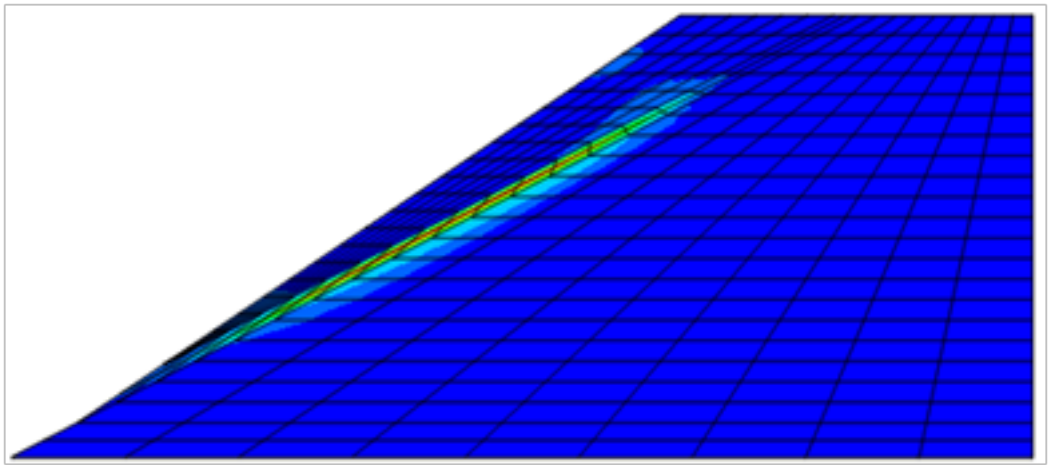

b)

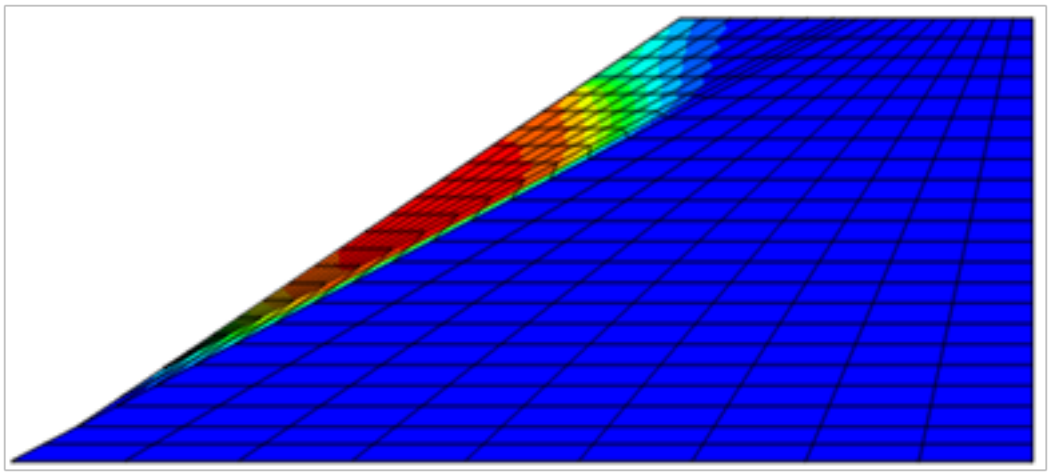

Figure C36: 10 ft fill length, a) maximum shear strain increment, b) displacement magnitude.

a)

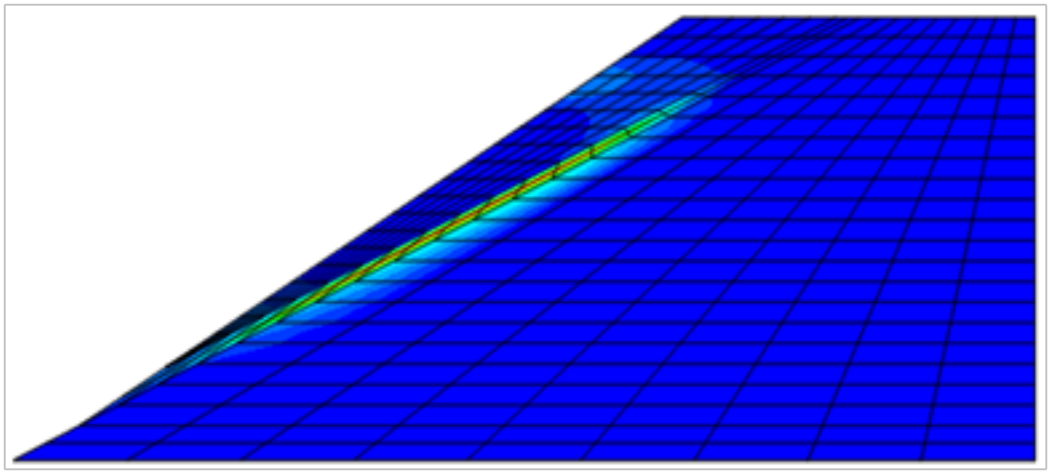

b)

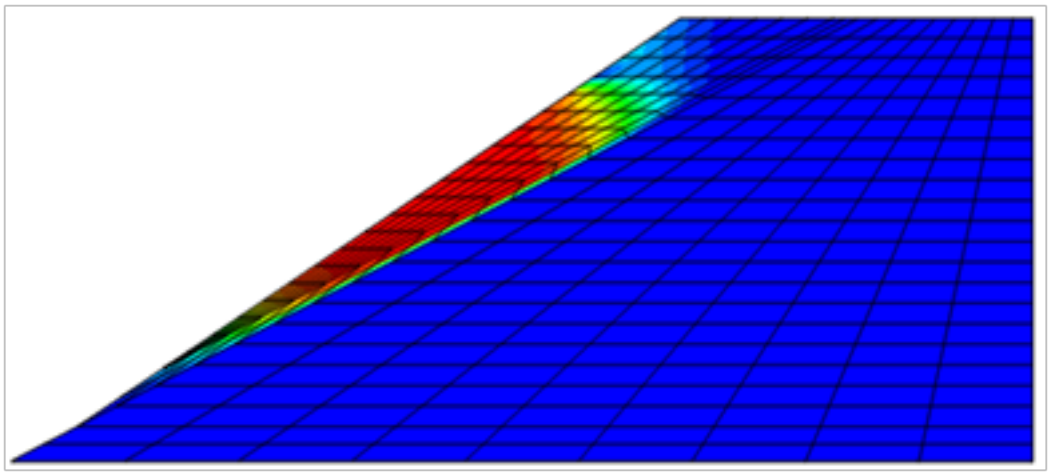

Figure C37: 20 ft fill length, a) maximum shear strain increment, b) displacement magnitude.

a)

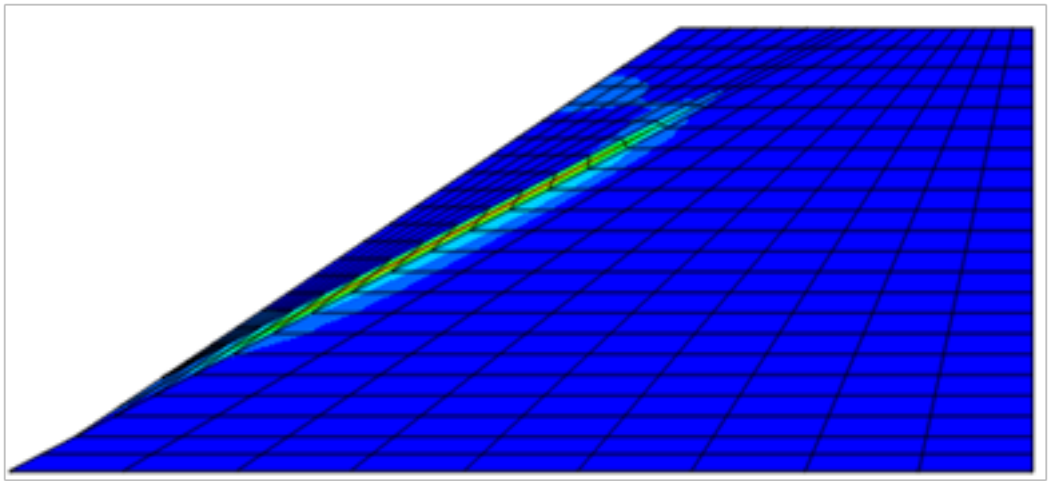

b)

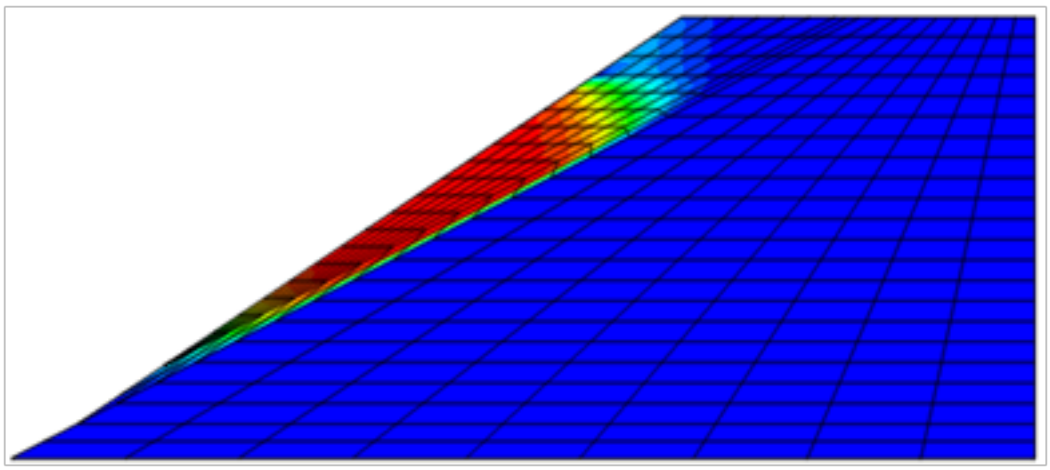

Figure C38: 30 ft fill length, a) maximum shear strain increment, b) displacement magnitude.

a)

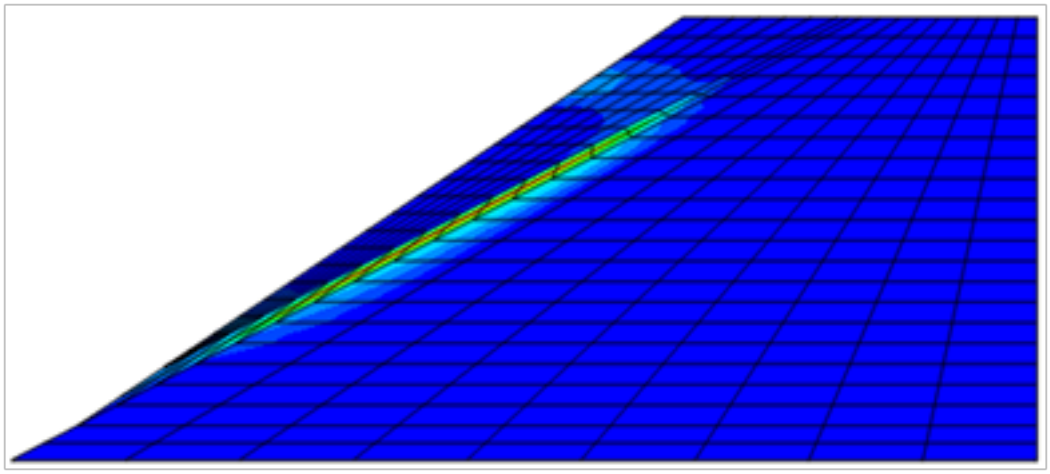

b)

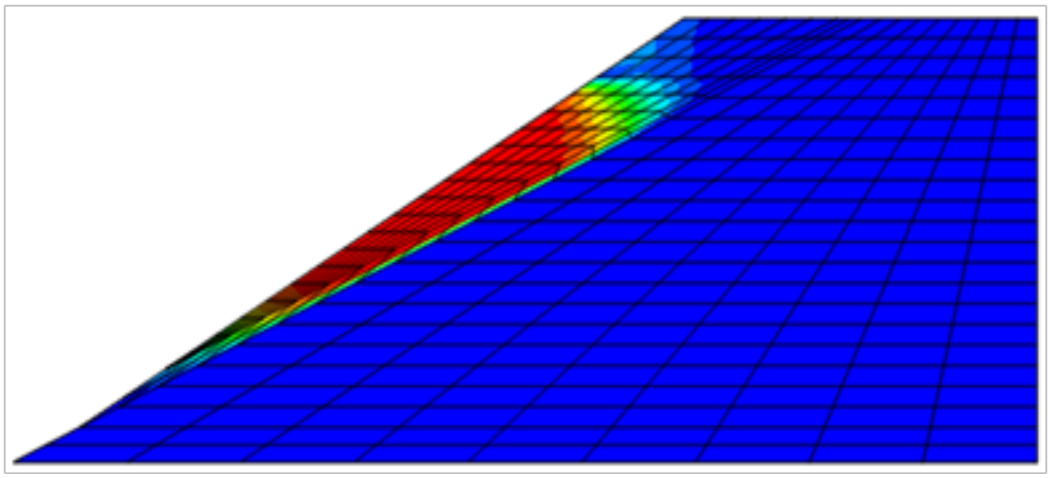

Figure C39: 60 ft fill length, a) maximum shear strain increment, b) displacement magnitude.

a)

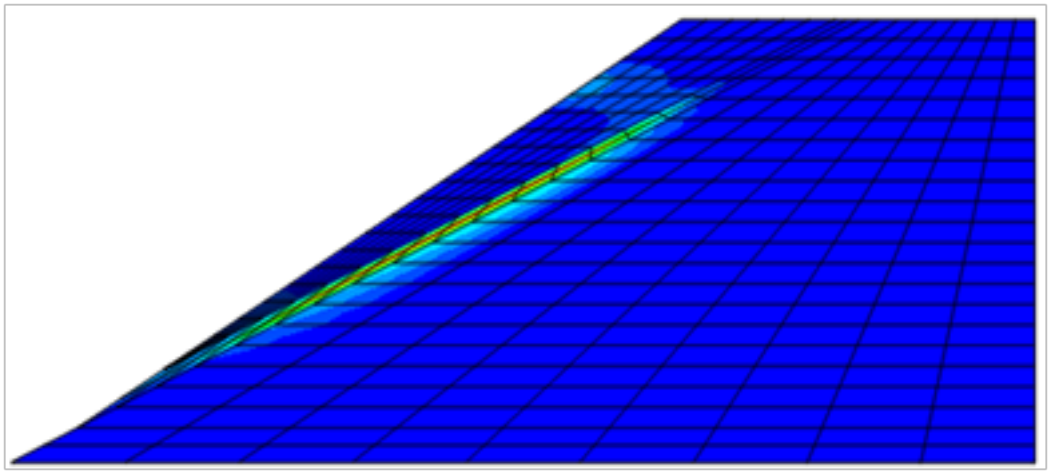

b)

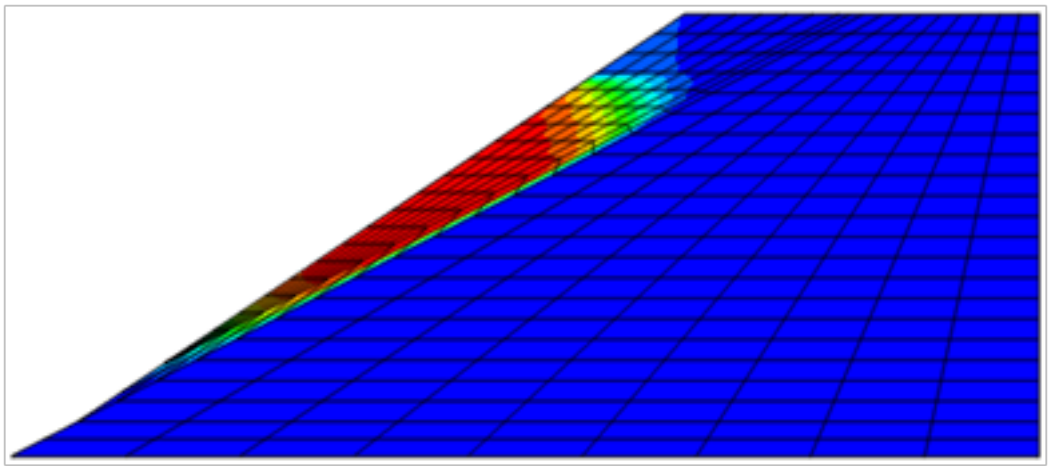

Figure C40: 120 ft fill length, a) maximum shear strain increment, b) displacement magnitude.

a)

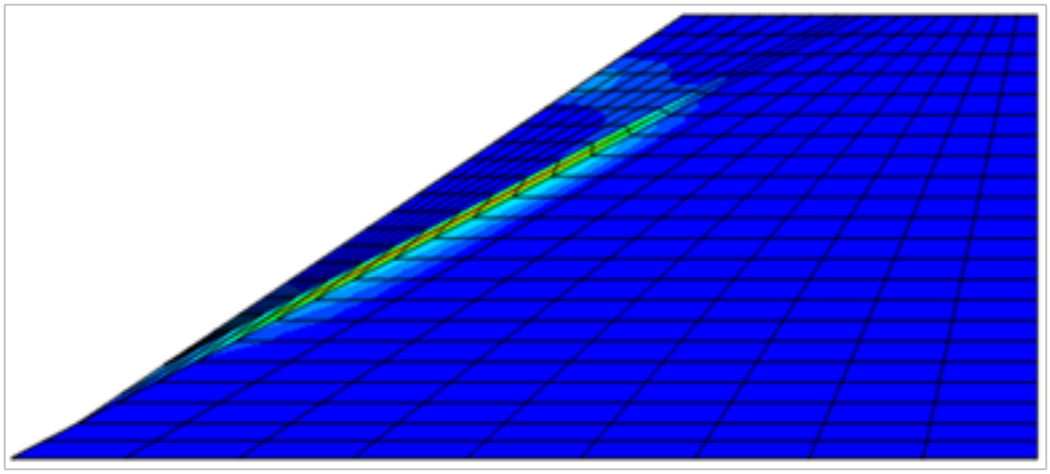

b)

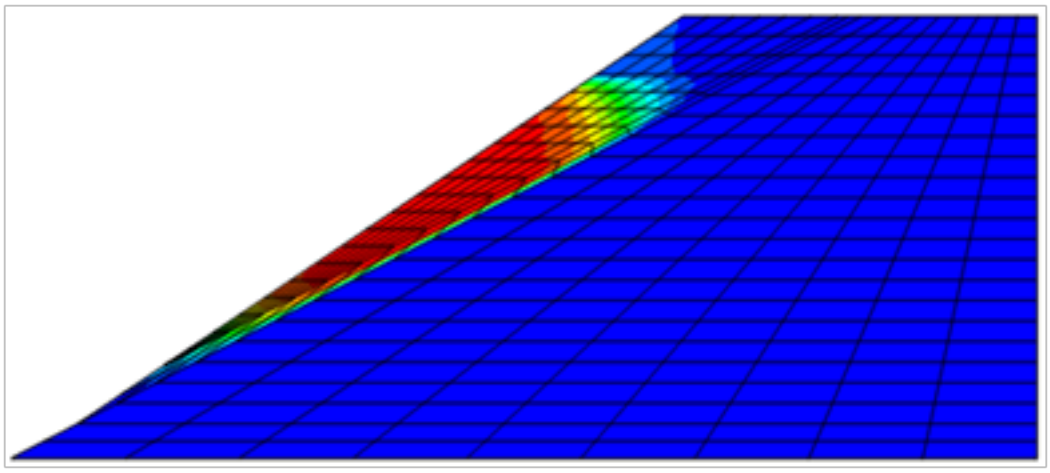

Figure C41: 200 ft fill length, a) maximum shear strain increment, b) displacement magnitude.

a)

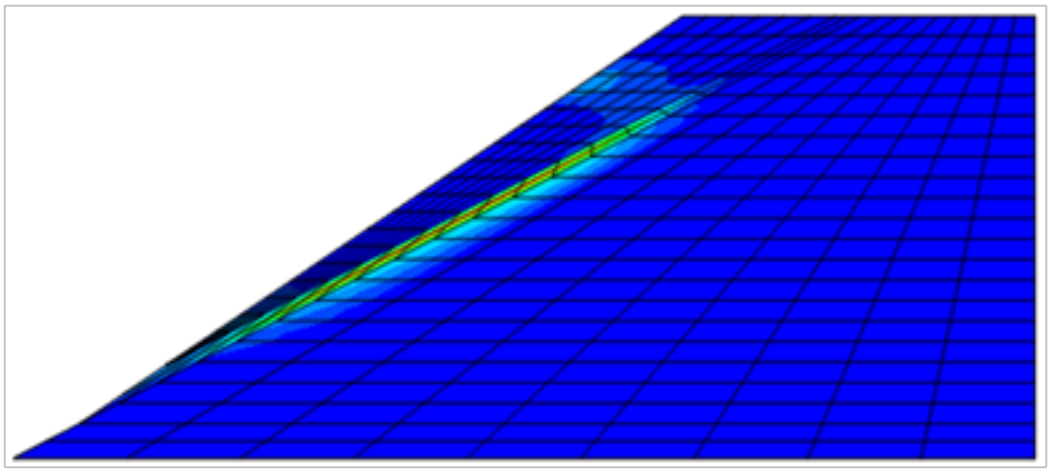

b)

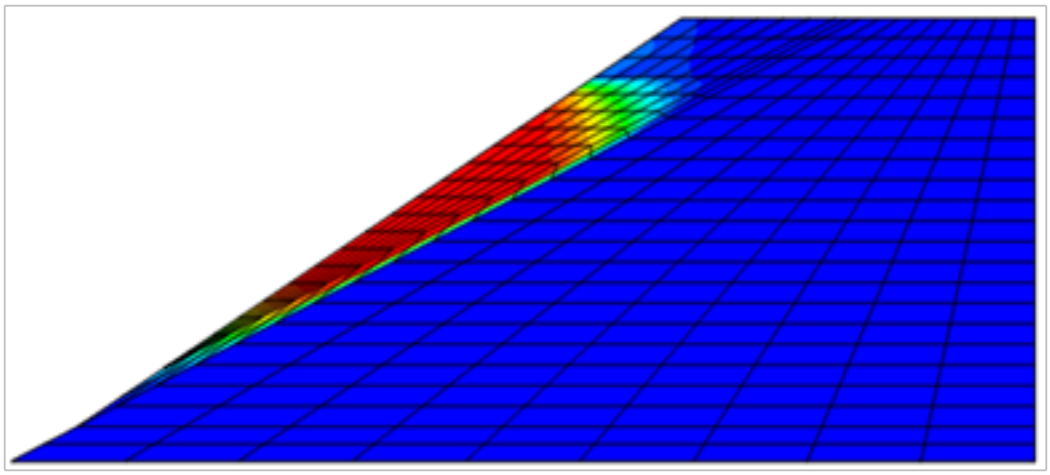

Figure C42: 400 ft fill length, a) maximum shear strain increment, b) displacement magnitude.

REINFORCED (5’ 3, 2, 1 LAYERS) ROTATIONAL UNIAXIAL

a)

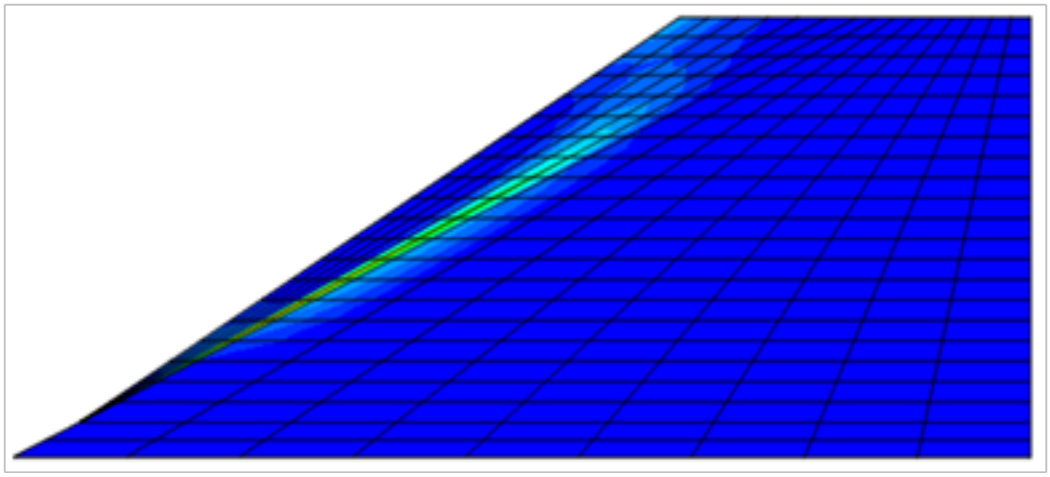

b)

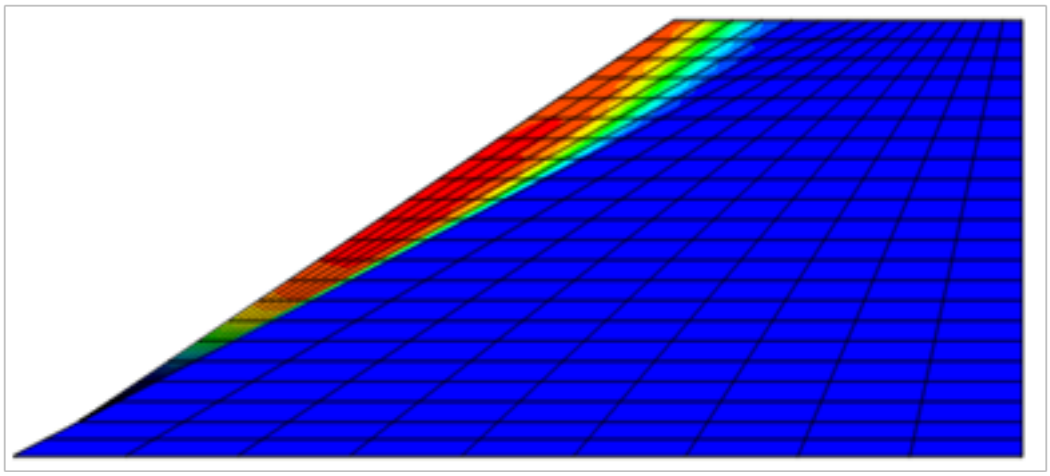

Figure C43: 60 ft fill length, 5’3L, a) maximum shear strain increment, b) displacement magnitude.

a)

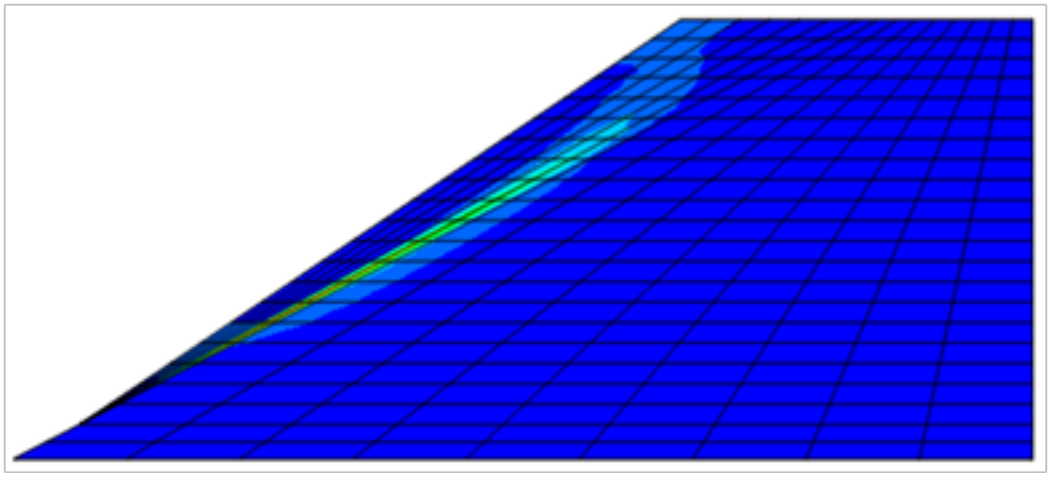

b)

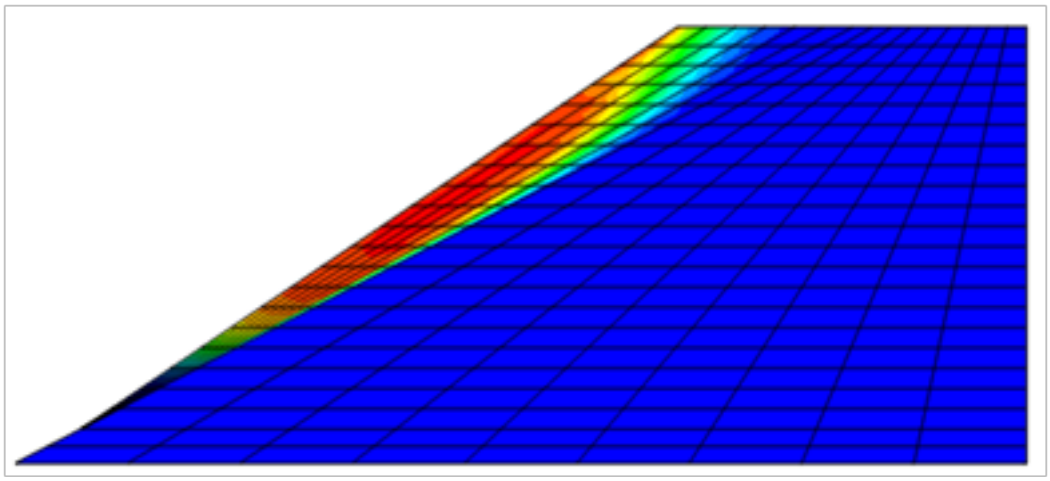

Figure C44: 60 ft fill length, 5'2L, a) maximum shear strain increment, b) displacement magnitude.

a)

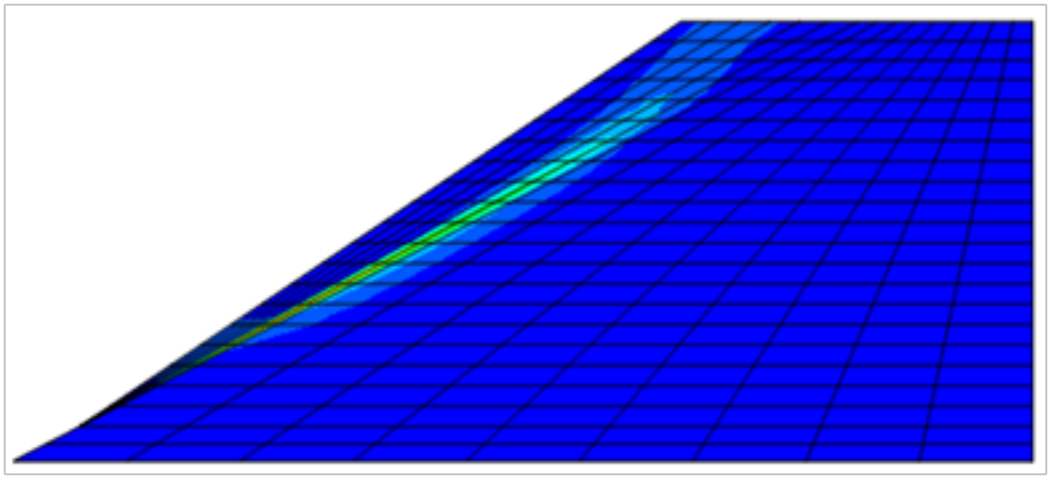

b)

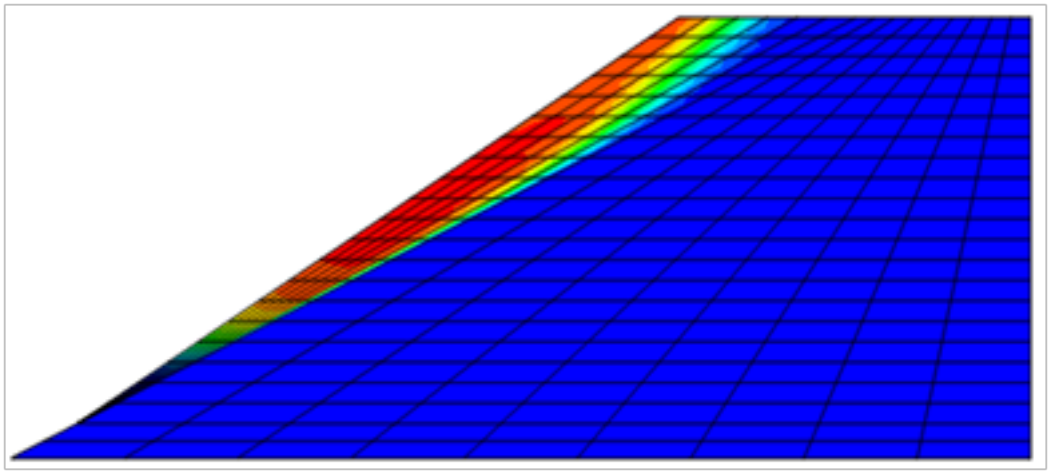

Figure C45: 60 ft fill length, 5'1L, a) maximum shear strain increment, b) displacement magnitude.

REINFORCED (5’3, 2, 1 LAYERS) ROTATIONAL BIAXIAL

a)

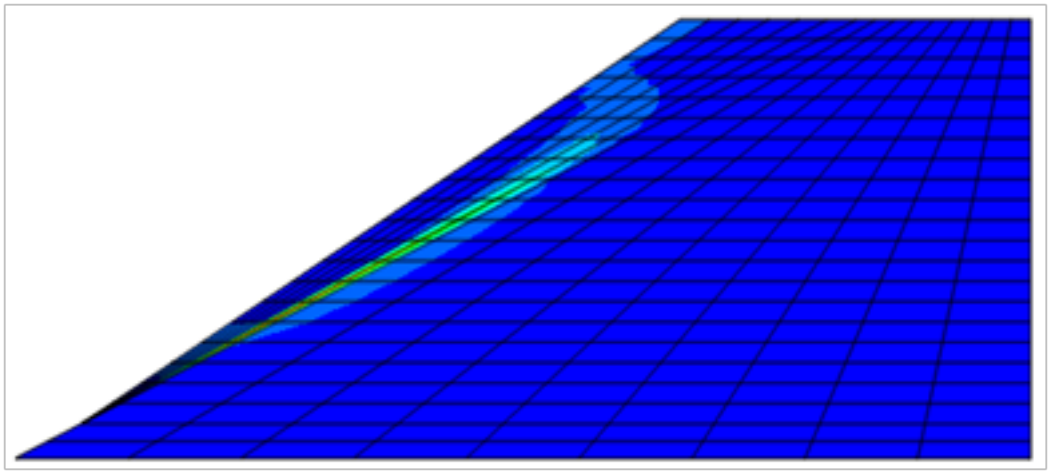

b)

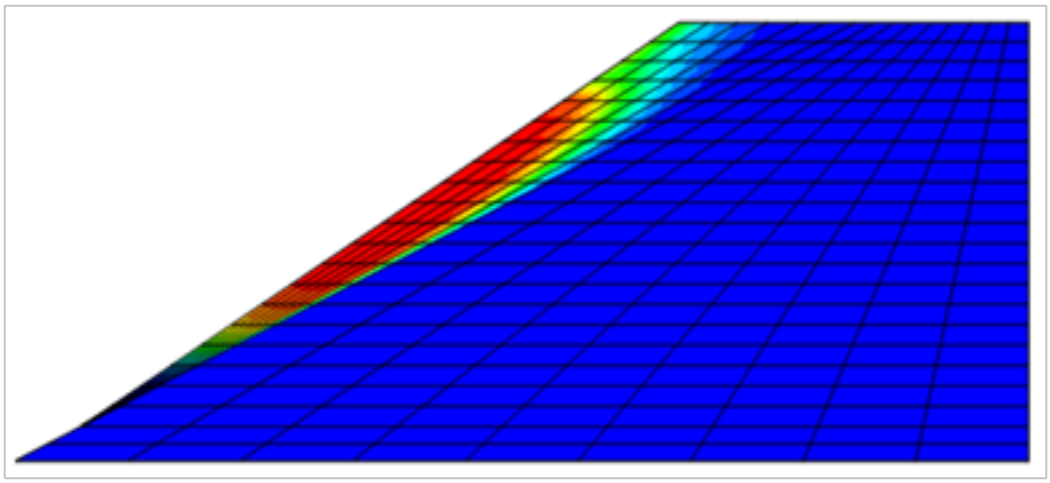

Figure C46: 60 ft fill length, 5’3L, a) maximum shear strain increment, b) displacement magnitude.

a)

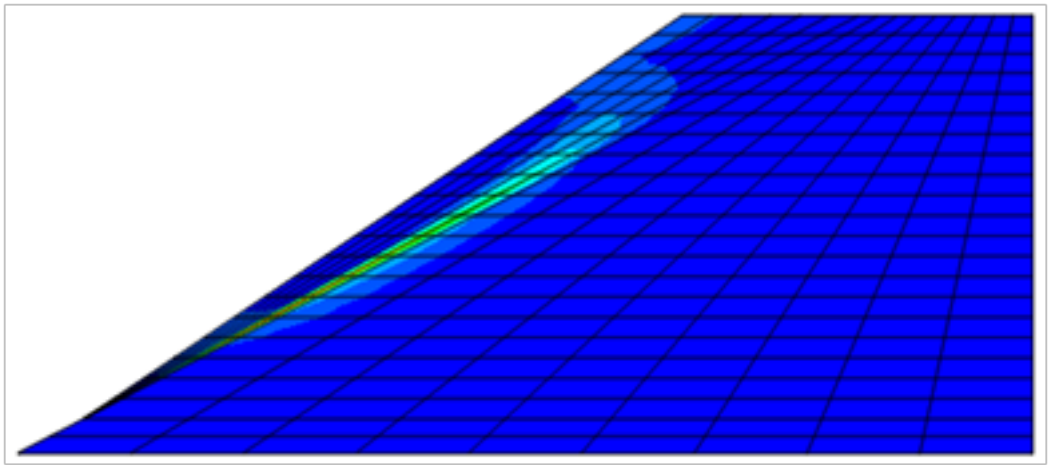

b)

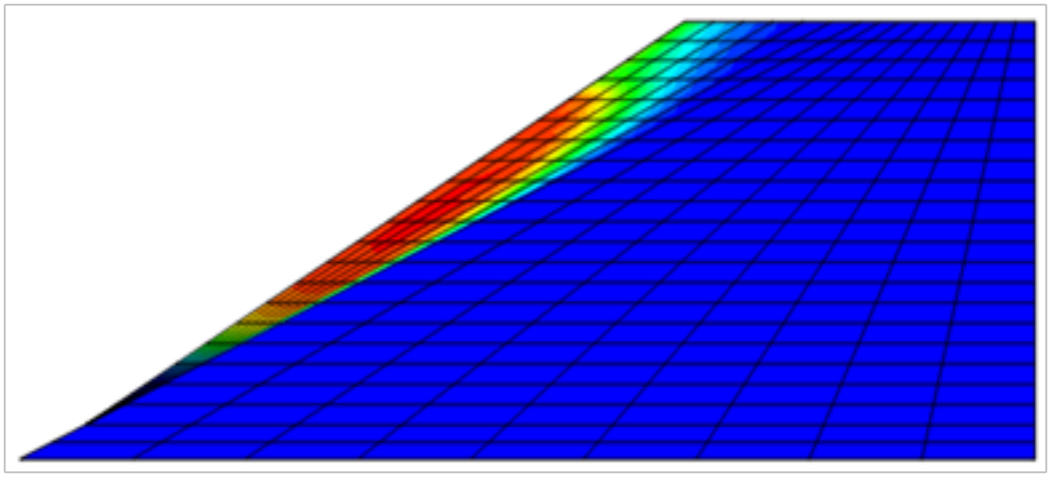

Figure C47: 60 ft fill length, 5'2L, a) maximum shear strain increment, b) displacement magnitude.

a)

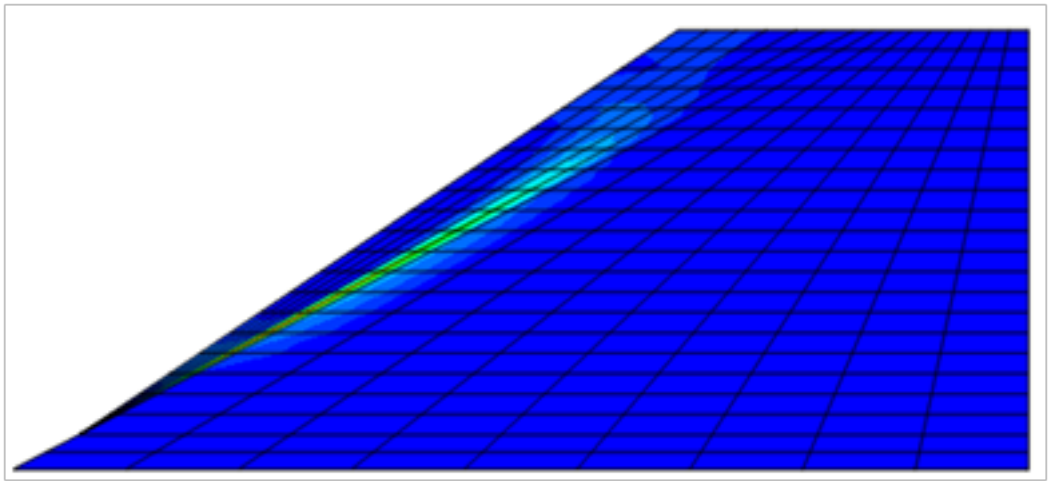

b)

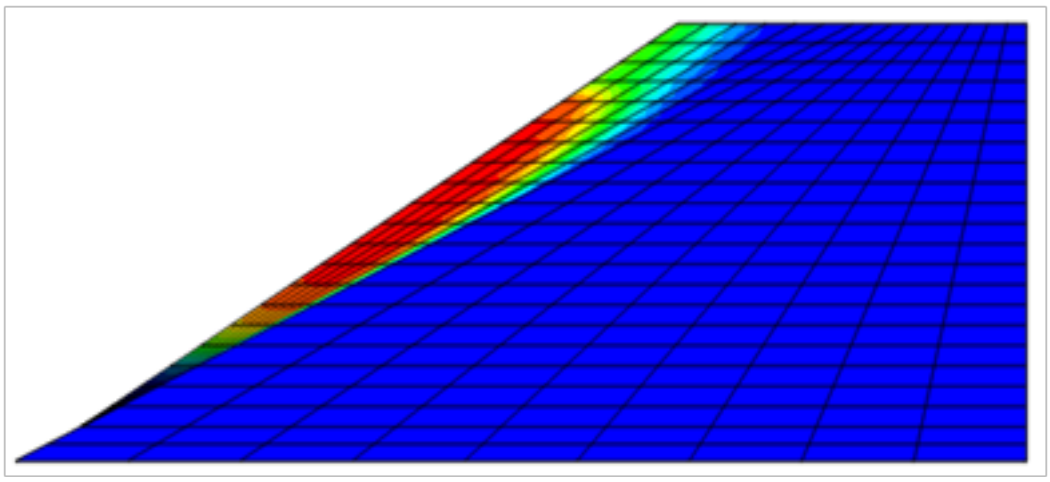

Figure C48: 60 ft fill length, 5'1L, a) maximum shear strain increment, b) displacement magnitude.

REINFORCED (5’3, 2, 1 LAYERS) WEDGE UNIAXIAL

a)

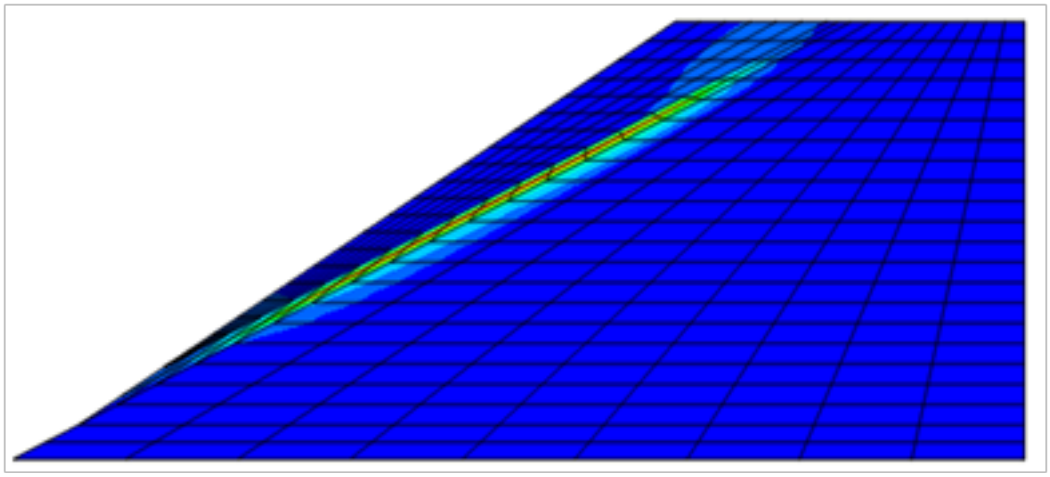

b)

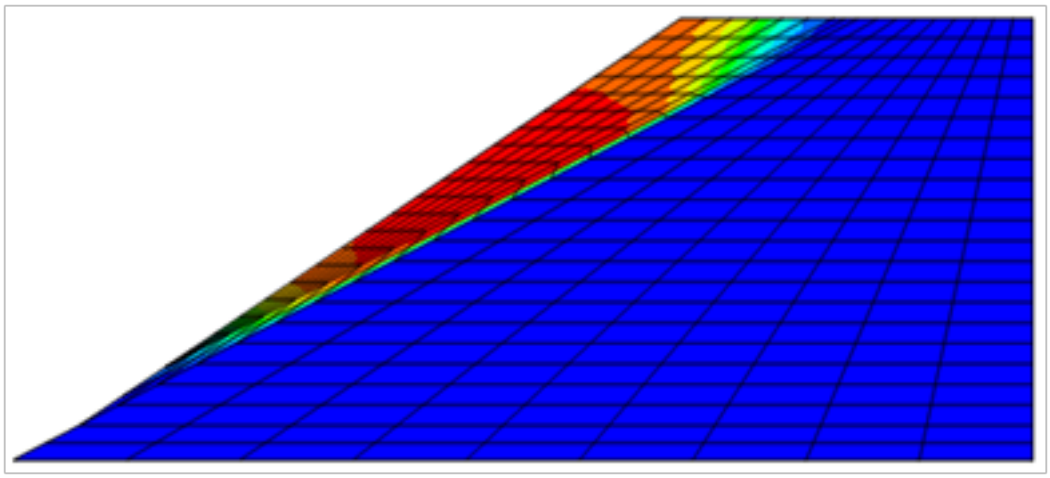

Figure C49: 60 ft fill length, 5’3L, a) maximum shear strain increment, b) displacement magnitude.

a)

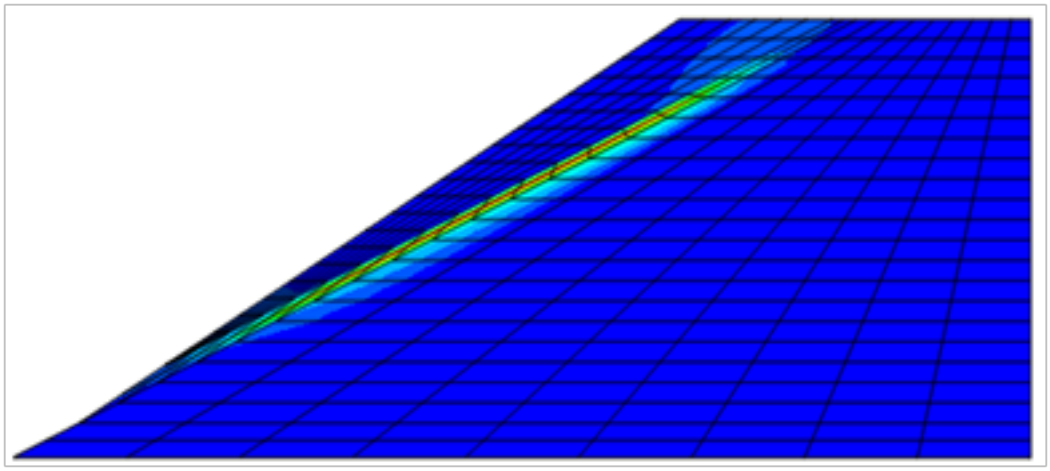

b)

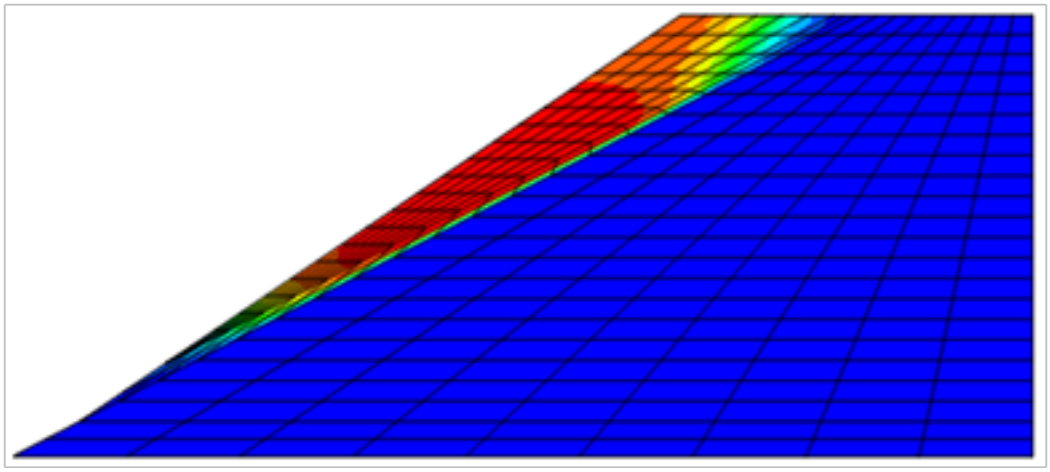

Figure C50: 60 ft fill length, 5'2L, a) maximum shear strain increment, b) displacement magnitude.

a)

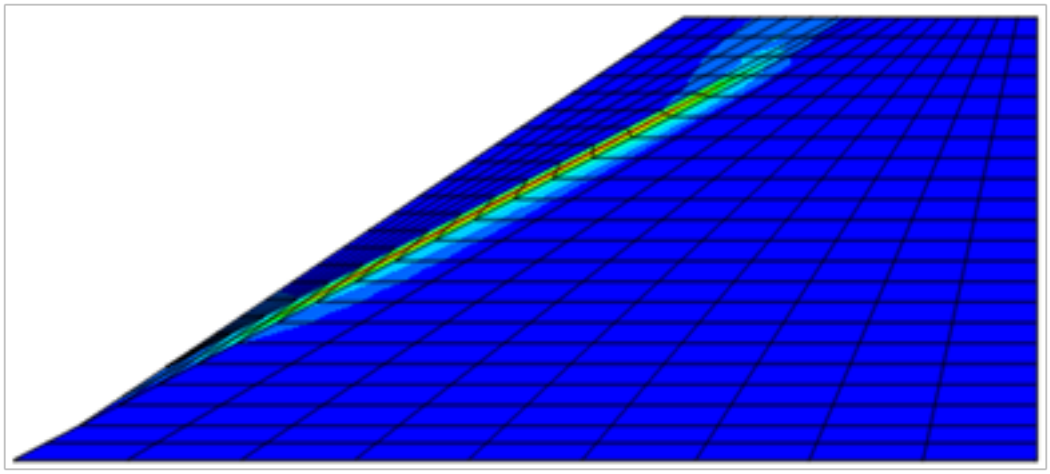

b)

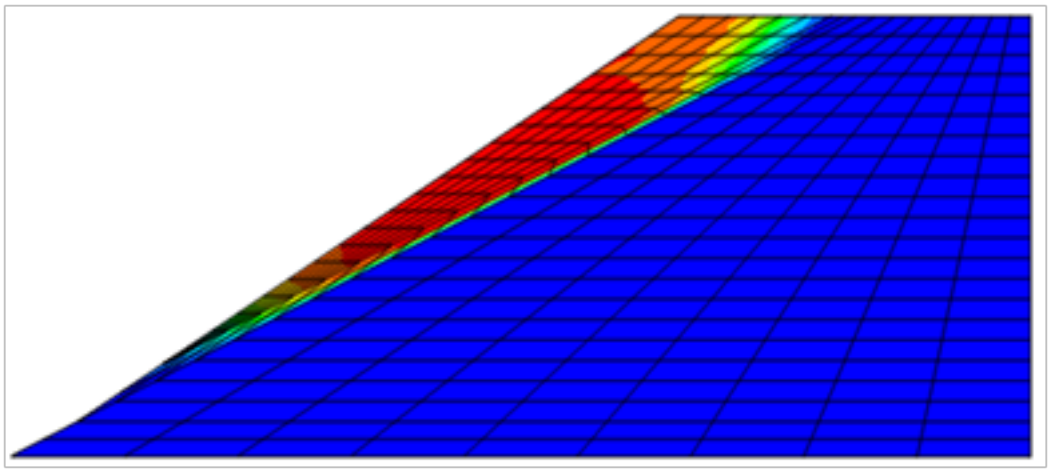

Figure C51: 60 ft fill length, 5'1L, a) maximum shear strain increment, b) displacement magnitude.

REINFORCED (5’ 3, 2, 1 LAYERS) WEDGE BIAXIAL

a)

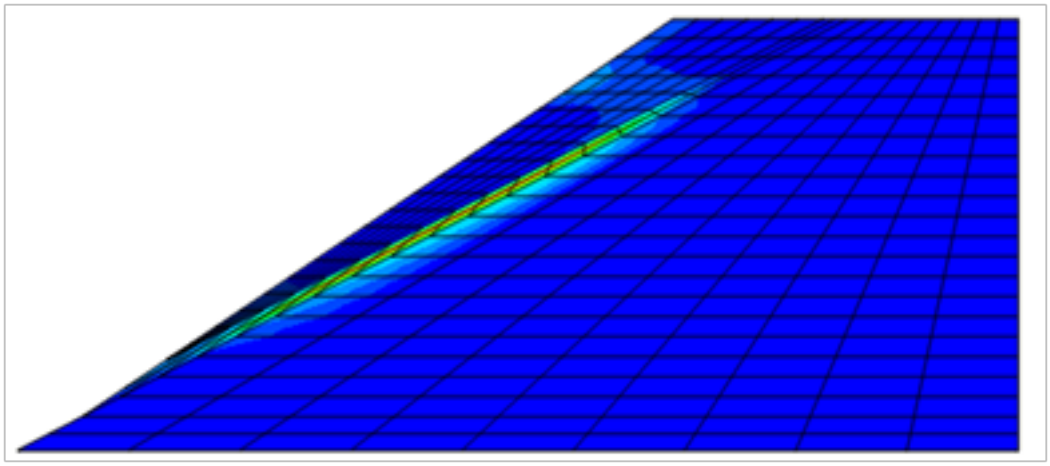

b)

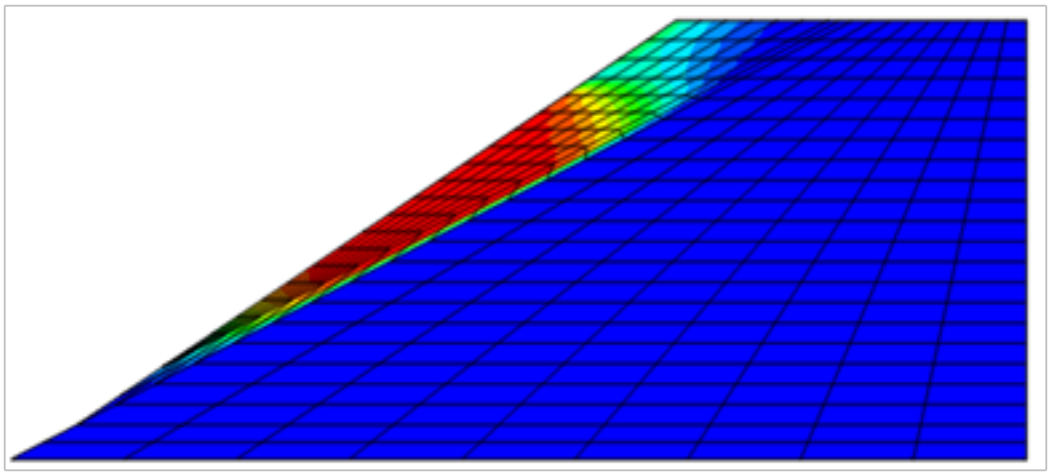

Figure C52: 60 ft fill length, 5’3L, a) maximum shear strain increment, b) displacement magnitude.

a)

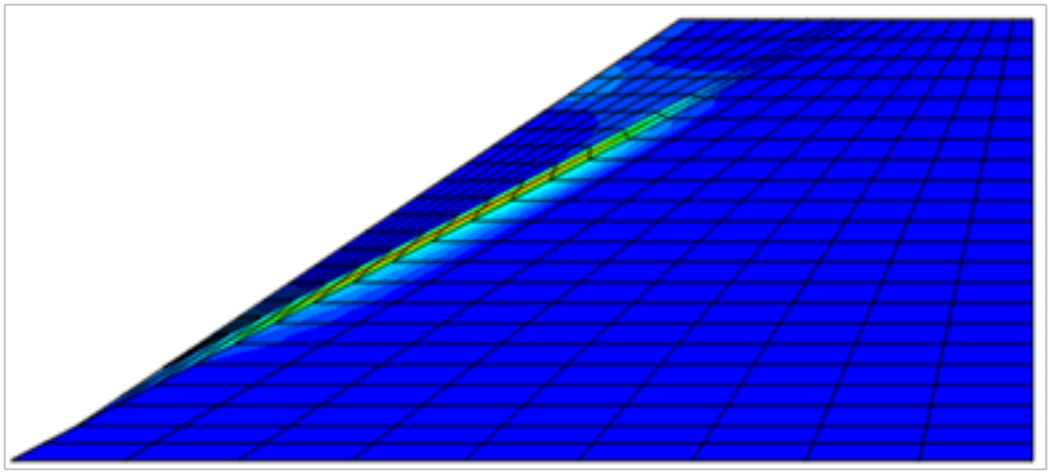

b)

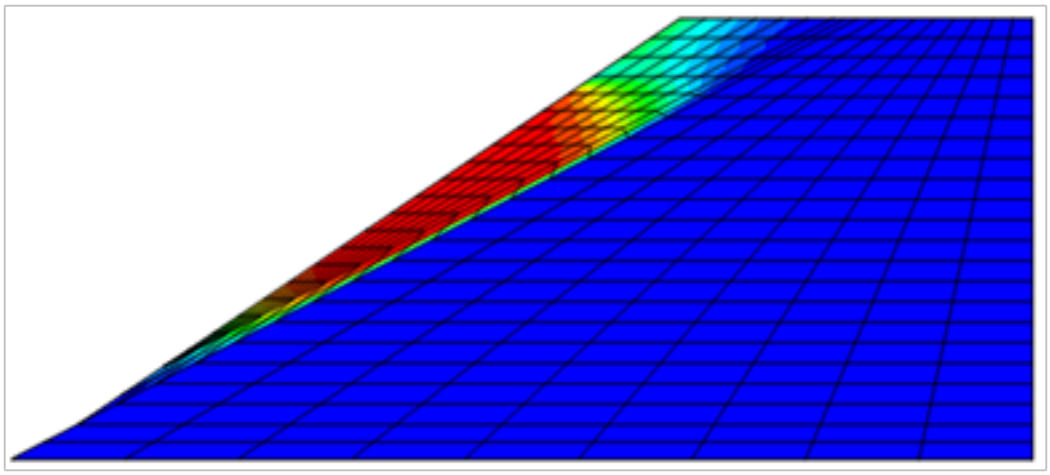

Figure C53: 60 ft fill length, 5'2L, a) maximum shear strain increment, b) displacement magnitude.

a)

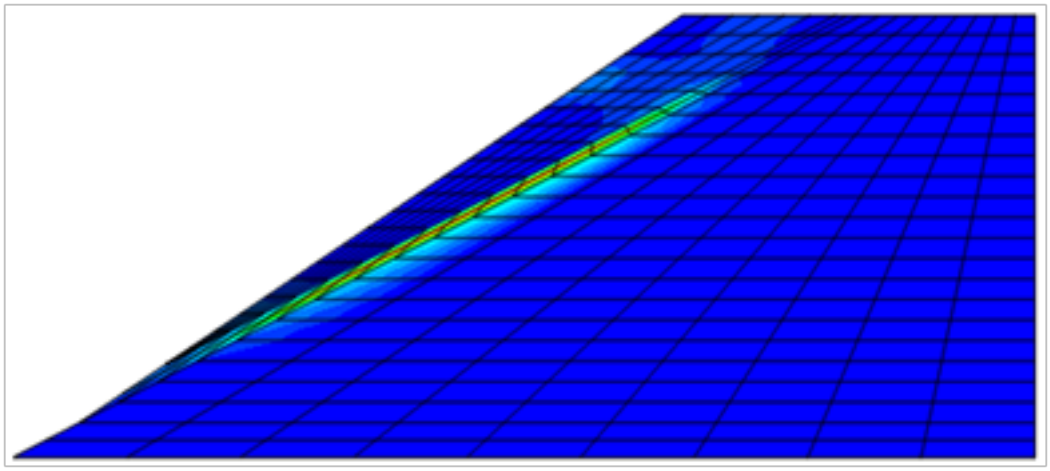

b)

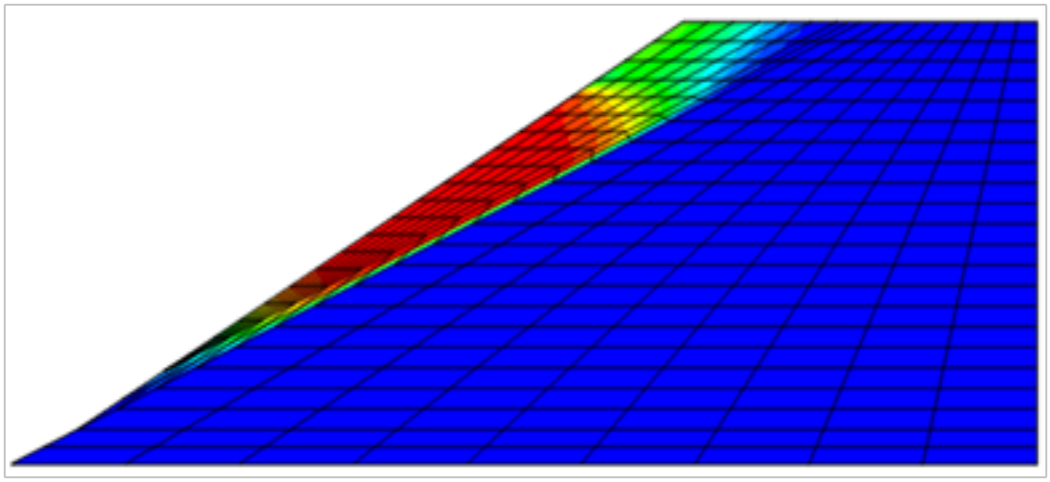

Figure C54: 60 ft fill length, 5'1L, a) maximum shear strain increment, b) displacement magnitude.

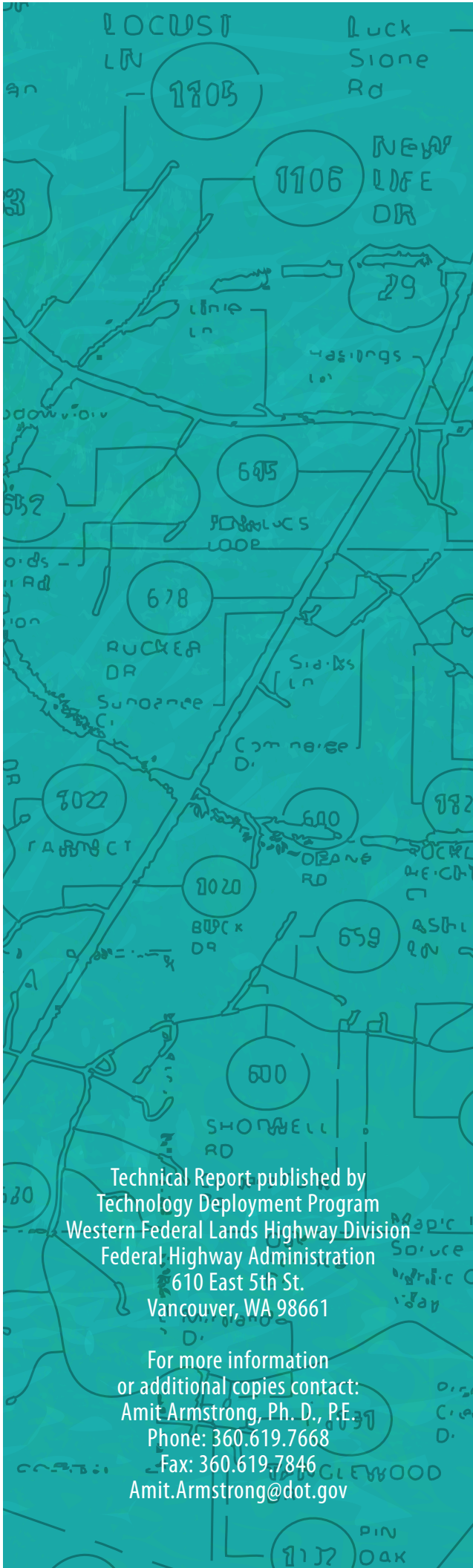

Technical Report published by
Technology Deployment Program
Western Federal Lands Highway Division
Federal Highway Administration
610 East 5th St.
Vancouver, WA 98661

For more information
or additional copies contact:
Amit Armstrong, Ph. D., P.E.
Phone: 360.619.7668
Fax: 360.619.7846
Amit.Armstrong@dot.gov